Jeunes & Chercheurs

Livret des **posters**

LA LIGUE CONTRE LE CANCER

NBR1, UN NOUVEAU GÈNE DE PRÉDISPOSITION AUX CANCERS DU REIN FAMILIAUX IMPLIQUÉ DANS L'AUTOPHAGIE

Florine Adolphe[1,2], Sophie Ferlicot[2,3,4], Virginie Verkarre[4,5], Flore Renaud[1,2], Sophie Couvé[1,2], Pauline Garnier[1,2], Betty Gardie[1,6], Stéphane Richard[1,2,4] & Sophie Gad[1,2]

[1]EPHE, PSL, Paris ; [2]CNRS U9019, Gustave Roussy, Université Paris-Saclay, Villejuif ; [3]Service d'Anatomie Pathologique, Hôpital de Bicêtre, Le Kremlin-Bicêtre ; [4]Réseau National de Référence pour Cancers Rares de l'Adulte PREDIR, Hôpital de Bicêtre, AP-HP, et Service d'Urologie, Le Kremlin-Bicêtre ; [5]Service d'Anatomie Pathologique, HEGP, AP-HP, Paris ; [6]L'Institut du Thorax, INSERM, CNRS, Université de Nantes, Nantes.

Contact : florine.adolphe@gustaveroussy.fr

CONTEXTE

Le cancer du rein représente le 6ème cancer le plus fréquent chez l'adulte en France. La majorité des cancers du rein est d'origine sporadique et 30% des patients ont des métastases lors du diagnostic. Dans 6 à 8% des cancers du rein sont d'origine héréditaire.

La connaissance du gène en cause est cruciale afin d'identifier les individus à risque dans une famille.

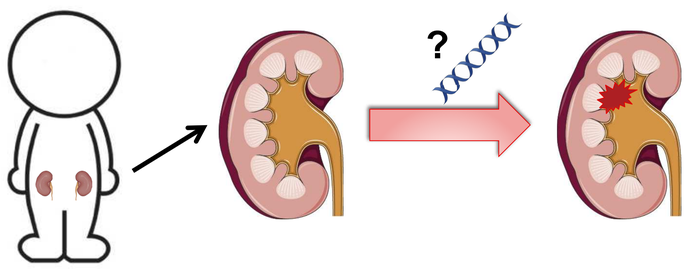

Grâce au séquençage d'exome, nous avons identifié une mutation de type décalage du cadre de lecture dans le gène *NBR1* dans une famille atteinte de cancers du rein héréditaires.

L'AUTOPHAGIE

NBR1 est une protéine récepteur cargo impliquée dans l'autophagie.

Avec son partenaire p62, elles acheminent les composants cellulaires endommagés au niveau des phagophores où ils seront séquestrés, puis dégradés, suite à la fusion avec des lysosomes.

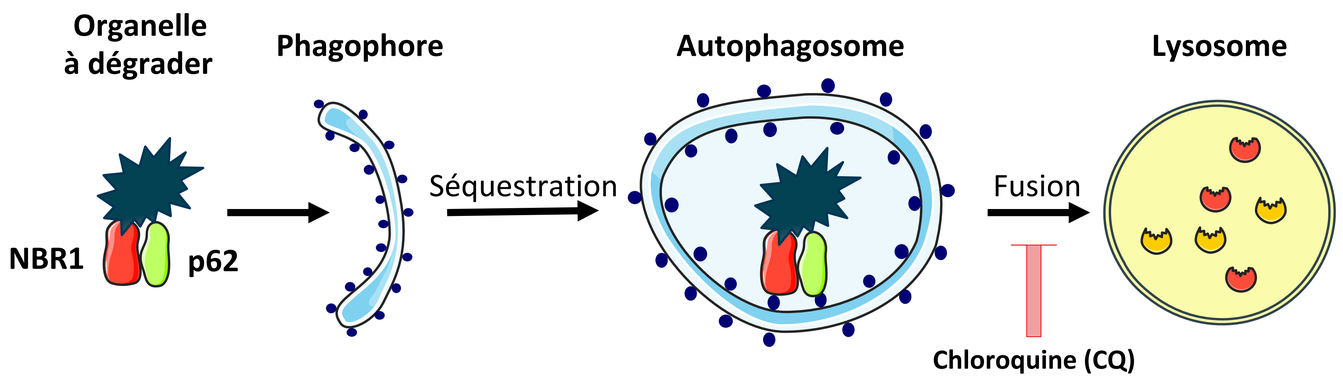

OBJECTIF : Etude fonctionnelle de la mutation de *NBR1*, basée sur l'hypothèse d'un effet dominant négatif

ETUDE DE LA STABILITE DES TRANSCRITS DE *NBR1*

Analyse des ARN de *NBR1* dans la tumeur d'un patient par RT-PCR :

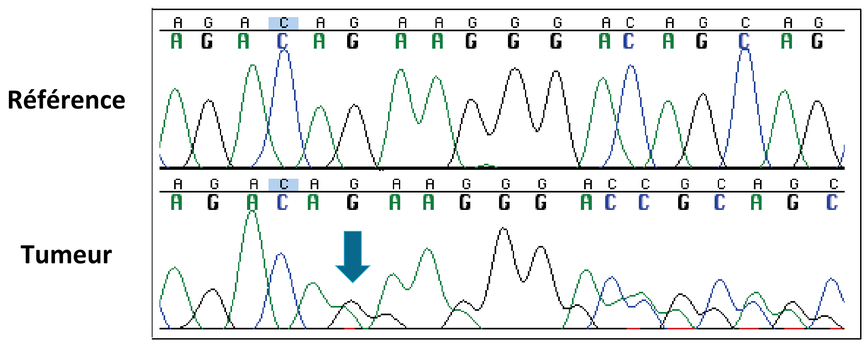

Les transcrits mutés de *NBR1* sont stabilisés dans la tumeur, dû à l'inefficacité du NMD (*Nonsense-Mediated mRNA Decay*), mécanisme de contrôle qualité des ARN qui prévient la production de protéines anormales.

CARACTERISATION DU MODE D'ACTION DE NBR1 MUTEE

Analyse de la capacité de NBR1 à interagir et à co-localiser avec ses partenaires :

Immunoprécipitation

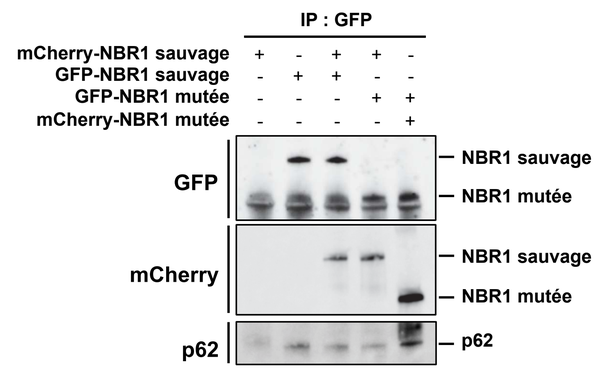

Immunofluorescence

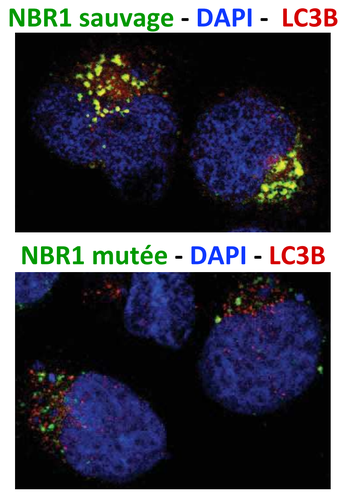

NBR1 mutée est capable d'interagir avec son partenaire p62, mais ne co-localise pas avec LC3B à la surface des phagophores.

IMPACT DE NBR1 MUTEE SUR L'AUTOPHAGIE

Etude de l'activation de l'autophagie suite à des carences nutritives (HBSS) :

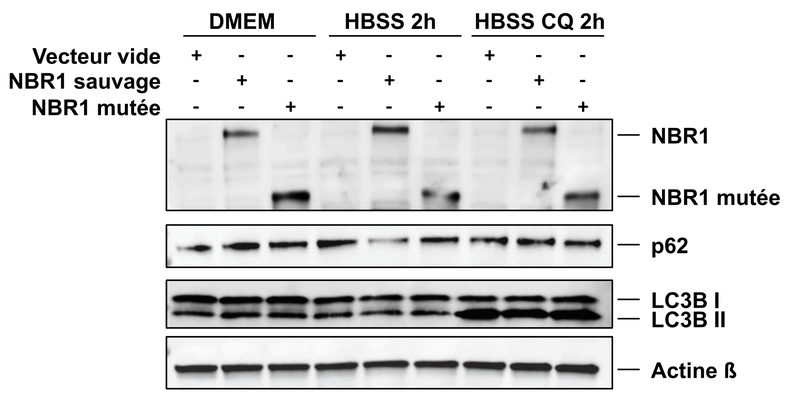

Le manque en nutriments induit une dégradation des acteurs de l'autophagie, qui est bloquée par l'ajout de Chloroquine (CQ).

En présence de NBR1 mutée, cette dégradation est inhibée.

AVANTAGE PROLIFERATIF DE NBR1 MUTEE

Etude de la prolifération d'une lignée cellulaire de rein tumoral par test de formation de colonies:

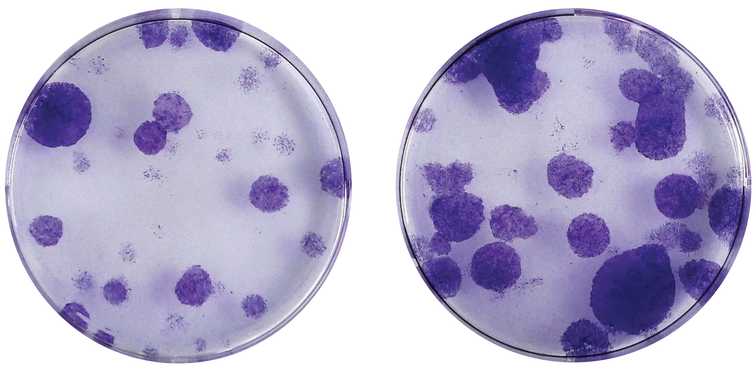

NBR1 sauvage — NBR1 mutée

La surexpression de NBR1 mutée confère un avantage prolifératif aux cellules par rapport à la surexpression de NBR1 sauvage.

CONCLUSION & PERSPECTIVES

Nous avons identifié une mutation dans un nouveau gène impliqué dans l'autophagie. Les expériences réalisées suggèrent que la protéine NBR1 mutée impacte la fonction de ses partenaires et le processus d'autophagie. **NBR1 semble donc être un bon candidat comme gène de prédisposition aux cancers du rein dans cette famille.**

Des expériences complémentaires permettront de caractériser l'implication de NBR1 et de l'autophagie dans la carcinogenèse rénale.

Enfin, l'identification du gène à l'origine des cancers du rein dans cette famille permettra la mise en place d'un test génétique afin de distinguer les individus à risque de développer un cancer et de leur proposer une prise en charge adaptée.

REMERCIEMENTS

Nous remercions les patients et les familles.

Merci aux cliniciens et généticiens qui nous ont fourni les ADN constitutionnels, ainsi qu'aux pathologistes pour les tumeurs congelés ou fixées.

Ce travail est réalisé avec le soutien de la Ligue contre le Cancer (Nationale ; Comités des Yvelines, du Cher, de l'Allier et de l'Indre), de l'Association pour la Recherche sur les Tumeurs du Rein (Artur) et de l'Institut National du Cancer (INCa).

Développement d'un peptide thérapeutique ciblant l'interaction pro-cathepsine D/LRP-1 dans le cancer mammaire

AL KHALIFA Tesnim[1], BAUD Stéphanie[2], CHAZEE Lise[1], LING Claude[3], KIEFFER Bruno[3], DEDIEU Stéphane[1], ETIQUE Nicolas[1]

1 – UMR CNRS 7369 MEDyC, Équipe "Matrice Extracellulaire, Cancer et Cibles thérapeutiques », Université Reims Champagne-Ardenne, Campus Moulin de la Housse, BP 1039, 51687 Reims Cedex 2
2 – UMR CNRS 7369 MEDyC, Équipe « Modélisation moléculaire et Imagerie Multi-Echelle», Université Reims Champagne-Ardenne, Campus Moulin de la Housse, BP 1039, 51687 Reims Cedex 2
3 - UMR CNRS 7104 - Inserm U 1258, Équipe "Structure et Dynamique des polymères biologiques par Résonance Magnétique Nucléaire" IGBMC, 1 Rue Laurent Fries 67400 Illkirch-Graffenstaden

Introduction

La pro-cathepsine D est une protéase aspartique surexprimée et secrétée abondamment par les cellules cancéreuses mammaires dans le micro-environnement tumoral. Elle constitue un marqueur de mauvais pronostic reconnu dans le cancer du sein[1]. La pro-cathepsine D est en effet capable de stimuler l'angiogenèse, la formation de métastases ainsi que la croissance des fibroblastes. Cet effet sur les fibroblastes passe par sa liaison au récepteur LRP-1, un récepteur d'endocytose de la famille des récepteurs au LDL, et notamment au niveau de la partie extracellulaire de sa chaîne β (résidus 349-394)[2]. Les fibroblastes du microenvironnement tumoral jouant un rôle essentiel dans la progression tumorale, notre objectif est de concevoir des peptides originaux dérivés de LRP-1 capables de bloquer sélectivement l'interaction pro-cathepsine D/LRP-1 et ses effets délétères dans le cancer du sein.

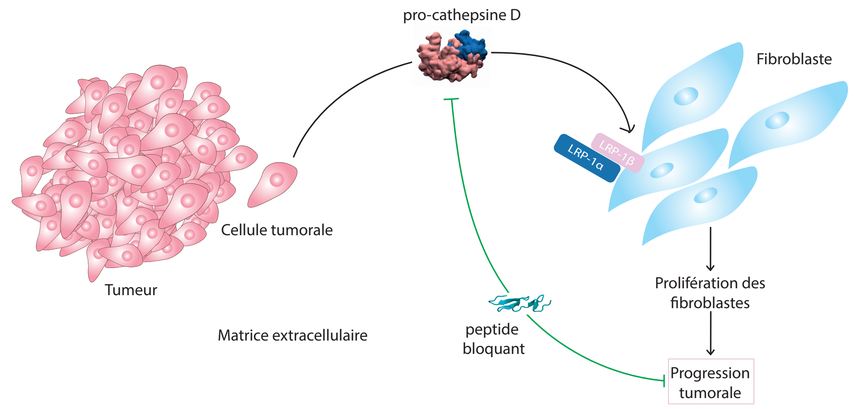

Schéma résumant l'objectif principal de ce projet : Concevoir et valider des peptides dérivés de la chaine β de LRP-1 capables d'inhiber les effets délétères de l'interaction pro-cathepsine D/ LRP-1 dans la tumorogenèse mammaire.

Résultats

I. Etude de l'interaction pro-cathepsine D/LRP-1β par modélisation moléculaire *in silico*

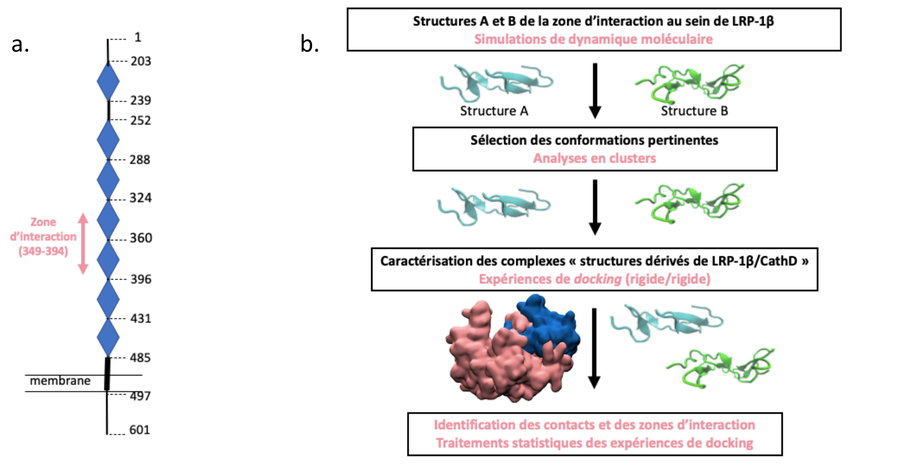

(**a**) Schéma de la chaine β du récepteur LRP-1[3] dont la structure reste encore indéterminée. La présence de séquences EGF-Like (losange bleu) et la zone d'interaction (349-394)[2] avec la pro-cathepsine D sont indiquées sur la partie extracellulaire. **(b)** A l'aide de la séquence primaire et du serveur de prédiction de structure par homologie I-TASSER, deux modèles de structures de la zone d'interaction (A et B) ont pu être obtenus. Ces deux modèles ont été soumis à une simulation de dynamique moléculaire en solvant aqueux explicite (logiciel GROMACS) et les meilleures conformations obtenues ont été soumis à un protocole de *docking* rigide/rigide (logiciel HEX) sur la structure de la pro-cathepsine D (disponible sur le serveur de la PDB, Ref : 1LYW). Différents réglages inhérents aux objets biologiques utilisés ont été testés puis validés lors de ce protocole. Au final, 100 expériences de *docking* ont été réalisées pour chaque couple structure LRP-1/pro-cathepsine D étudié.

II. Identification des résidus clés de l'interaction pro-cathepsine D/LRP-1β

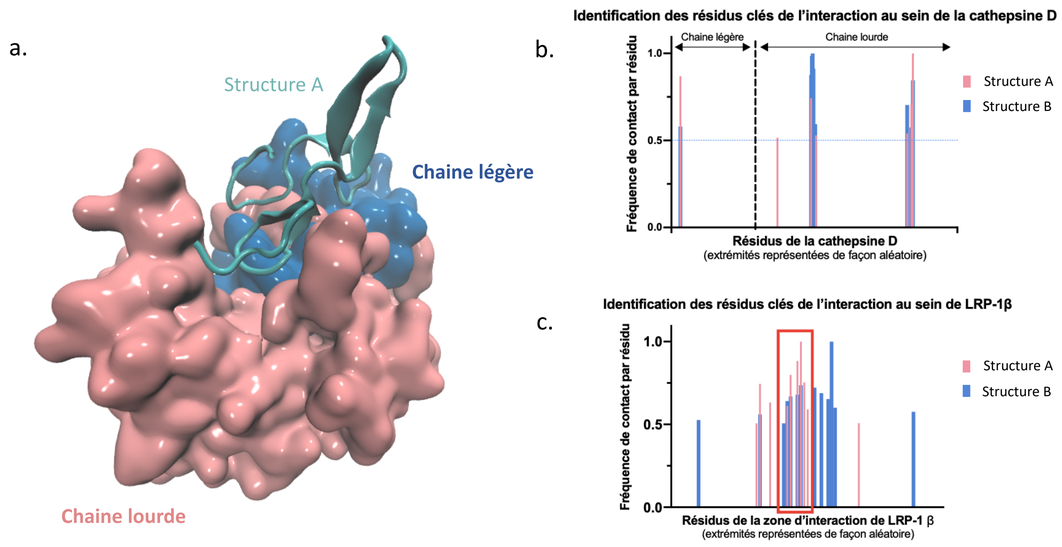

(a) Modèle d'interaction entre la cathepsine D (chaine lourde et chaine légère) et la zone d'interaction de LRP1-β (structure A) obtenu lors de nos expériences de *docking* moléculaire selon le protocole spécifique décrit dans la partie I **(b)** Étude des fréquences de contact des résidus de la cathepsine D avec les structures A (rose) et B (bleu) issus de LRP-1 sur l'ensemble des expériences de *docking*. 3 zones d'interaction potentielles ont été identifiées. Une zone localisée sur la chaine légère et deux sur la chaine lourde. 5 résidus à forte probabilité de contact ont pu être identifiés. (c) Étude des fréquences de contact des résidus issus des structures A (rose) et B (bleu) de LRP-1 avec la cathepsine D sur l'ensemble des expériences de *docking*. Un « hot spot » commun aux 2 structures A et B a pu être identifié (cadre rouge).

III. Design de peptides bloquant l'interaction pro-cathepsine D/LRP-1β

	pI	Net charge	Hydrophilicité	Structure prédite (I-TASSER)
Peptide 1	8,74	1,9	Basique	
Peptide 2	7,83	0,8	Basique	
Peptide 3	8,1	0,9	Basique	
Peptide 4	8,78	0,9	Basique	
Peptide 5	8,13	0,9	Basique	
Peptide 6	5,97	-0,2	Neutre	

A partir des résidus identifiés sur la chaine β de LRP-1, 6 peptides (numérotés 1 à 6) ont été proposés puis synthétisés. Le tableau ci-dessus présente les propriétés physico-chimiques de ces peptides ainsi que leur structure prédite par le serveur I-TASSER et représentées en mode *new cartoon* sous VMD. Ces différents peptides sont solubles en solvant aqueux (eau, NaCl 0,9%).

IV. Détermination de l'affinité des peptides pour la pro-cathepsine D par Thermophorèse micro-échelle (MST)

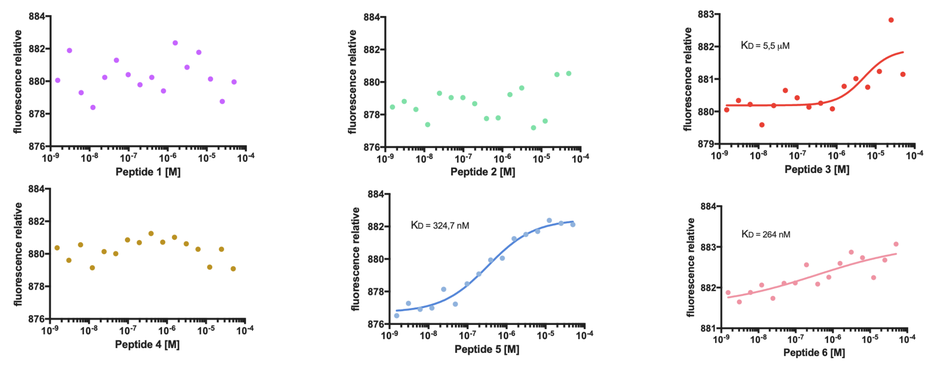

La pro-cathepsine D a été marquée avec le Kit His-Tag labelling kit Red-Tris NTA (Nanotemper) puis mélangée avec les différents peptides (1 à 6) en utilisant une série de dilution allant de 50 µM à 1.5 nM. Les 16 mélanges ont ensuite été analysés par un Monolith NT.115 (NanoTemper) à 26°C. Les paramètres de l'instrument étaient les suivants : 20% LED power, 40% MST power, and 5/30/5 laser off/on/off, (n=3). Les données ont été analysées avec le logiciel NT MO Affinity Analysis v2.1.3 (NanoTemper). Les K_D sont précisés pour les peptides ayant interagit avec la pro-cathepsine D.

V. Etude par immunoprécipitation du pouvoir bloquant des peptides sur l'interaction pro-cathepsine D/LRP-1β

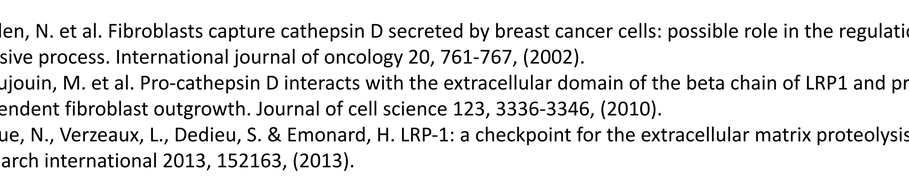

(a) Etude de l'effet des peptides ayant de l'affinité pour la pro-cathepsine D 3, 5 et 6 (100µM) sur l'interaction pro-cathepsine D/LRP-1β par immunoprécipitation. La pro-cathepsine D couplée à un Tag 6-His a été incubée avec un fragment de la chaine β (Frag LRP1β) ou α (Frag LRP1α, ctrl) de LRP-1 couplé à un épitope myc en absence ou en présence de chacun des peptides (Pep3, 5 et 6, 100µM). Les mélanges ont ensuite été purifiés sur colonne Ni-Nta puis analysés après électrophorèse par immunoempreinte. **(b)** Histogramme représentant la quantité de fragment de la chaine β de LRP-1 ayant interagit avec la pro-cathepsine D. Les résultats ont été normalisés par rapport au mélange Frag LRP-1β /pro-cathepsine D en absence de peptide.

Conclusions

Nos analyses *in sillico* ont permis d'obtenir un modèle de l'interaction pro-cathepsine D/LRP-1 et d'identifier pour la première fois des résidus susceptibles d'être impliqués dans cette interaction. Nous avons notamment identifié, au sein de LRP-1, une région qui semble contenir une séquence clef dictant l'interaction moléculaire avec la pro-cathepsine D. A partir de cette séquence, nous avons proposé une série de 6 peptides dont les premières analyses ont permis de montrer la capacité de certains peptides à lier la pro-cathepsine D et à bloquer son interaction avec LRP-1 (peptide 3, 5 et 6). Ces résultats devront être confirmés puis complétés par d'autre méthodes *in vitro* (spectroscopie RMN) et *in cellulo* (co-culture cellules cancéreuses mammaires/fibroblastes, PLA,…).

Contact :

Tesnim AL KHALIFA
UMR CNRS 7369 MEDyC, Équipe "Matrice Extracellulaire, Cancer et Cibles thérapeutiques », Université Reims Champagne-Ardenne
Email: tesnim.al-khalifa@univ-reims.fr

References :

1. Heylen, N. et al. Fibroblasts capture cathepsin D secreted by breast cancer cells: possible role in the regulation of the invasive process. International journal of oncology 20, 761-767, (2002).
2. Beaujouin, M. et al. Pro-cathepsin D interacts with the extracellular domain of the beta chain of LRP1 and promotes LRP1-dependent fibroblast outgrowth. Journal of cell science 123, 3336-3346, (2010).
3. Etique, N., Verzeaux, L., Dedieu, S. & Emonard, H. LRP-1: a checkpoint for the extracellular matrix proteolysis. BioMed research international 2013, 152163, (2013).

Remerciements :

Tous mes remerciements vont à la cancéropôle Grand-Est ainsi qu'à la Ligue Nationale contre le Cancer et ses donateurs qui ont permis de financer ce projet.

TLR3: UN RECEPTEUR DE MORT A ACTIVER DANS LES NEUROBLASTOMES ?

Joseph Bisaccia[1], Séverine Fagault[1], Juliette Geoffray[1], Kathrin Weber[1], Marie Castets[1]

[1]Cancer Research Center of Lyon, Université Claude Bernard Lyon 1, INSERM 1052, CNRS 5286, Centre Léon Bérard

Neuroblastome

Tumeur extra-crâniale la plus fréquente chez l'enfant: 150 nouveaux cas diagnostiqués chaque année en France.

Constitué de cellules tumorales appelées neuroblastes, qui dérivent d'une population de cellules embryonnaires appelées cellules des crêtes neurales.

50% des patients avec une amplification du gène *N-MYC* et/ou un neuroblastome de stade 4 ne peuvent être guéris avec les thérapies actuelles.

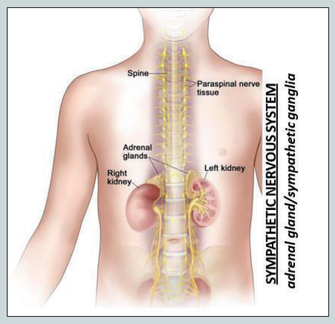

L'échec des traitements et les rechutes s'expliquent notamment par l'apparition de résistance à l'activation des voies de mort cellulaire, dans les cellules tumorales, dont les mécanismes restent mal compris.

TLR3

Toll-like receptor 3 : récepteur présent à la surface de vésicules à l'intérieur de la cellule (endosome).

Dans les cellules normales, TLR3 déclenche une réponse immunitaire innée par reconnaissance notamment de molécules d'origine virale : les ARN double brin (ARNdb ou dsRNA).

Dans les cellules tumorales, TLR3 déclenche la mort des cellules en activant différentes voies de signalisation.

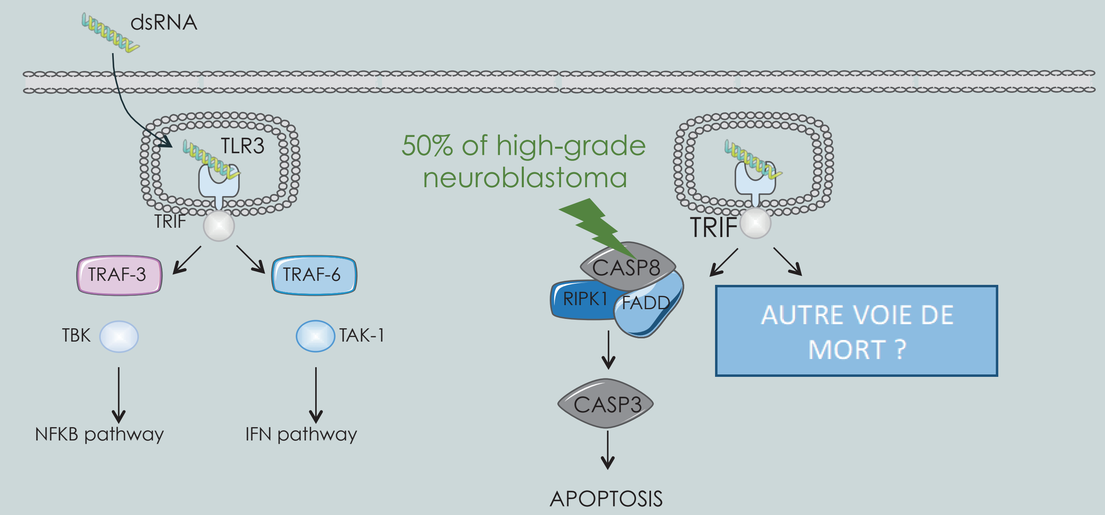

Comme TLR3 est exprimé dans les neuroblastomes, mon projet vise à:

1. Définir si TLR3 peut éliminer les cellules tumorales, y compris celles négatives pour la caspase-8, en activant différentes voies de mort cellulaire.
2. Etablir si cette mort est immunogénique et stimule le système immunitaire.

Résultats

L'expression de TLR3 est un facteur de bon pronostic dans les neuroblastomes

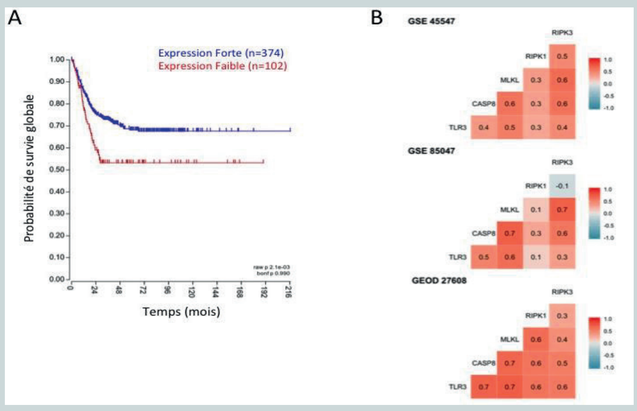

Figure 1 : Analyse transcriptomique du profil d'expression de TLR3 et de ses effecteurs de mort dans les neuroblastomes. **A.** Valeur pronostique de l'expression de TLR3 sur la survie globale. Analyse Kaplan-Meier des données GSE45547 (n=476). **B.** Matrices de corrélation entre TLR3 et ses effecteurs de mort réalisées à partir de 3 jeux de données transcriptomiques (GSE45547, GSE85047 et GEOD27608). Les valeurs indiquées correspondent au coefficient r^2.

L'expression de TLR3 et de ses effecteurs de mort est rétablie par traitement à l'IFN

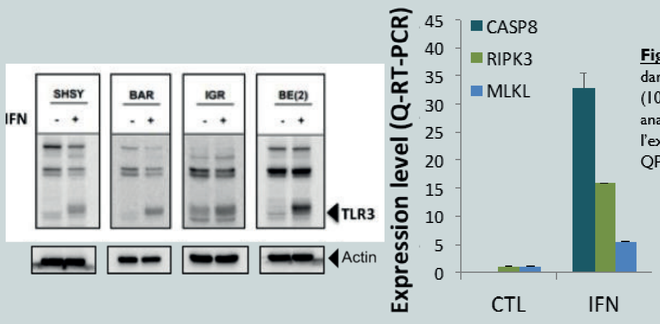

Figure 2 : Panel de gauche: Induction de l'expression de TLR3 dans des lignées de neuroblastome en réponse à l'IFN (1000u/mL). 4 lignées (SHSY-5Y, CLB-BAR, IGR et BE(2) ont été analysées par western-blot. Panel de droite: Induction de l'expression des effecteurs de TLR3 dans la lignée SHSY-5Y. RT-QPCR.

L'activation de TLR3 suffit à induire la mort des cellules de neuroblastome

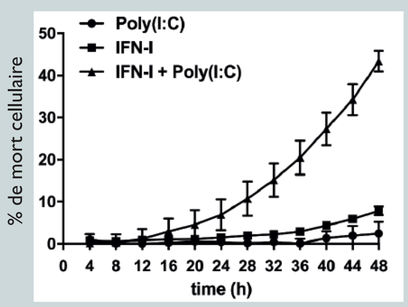

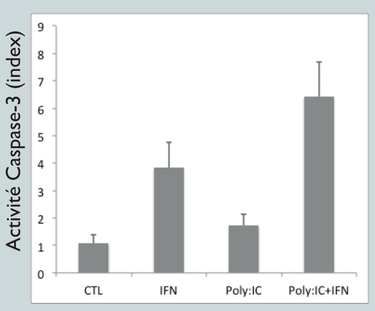

Figure 3 : Panel de gauche: L'activation de TLR3 par des ARNdb synthétiques (Poly:IC) induit la mort des cellules de neuroblastome SHSY-5Y. Panel de droite: Les différentes voies de mort cellulaire activées par TLR3 selon la présence de caspase-8 convergent et induisent l'activation de la caspase-3 effectrice.

Perspectives

Quel est l'impact du **ciblage de TLR3 in vivo**, directement sur l'élimination des cellules tumorales et indirectement sur l'activation du système immunitaire ?

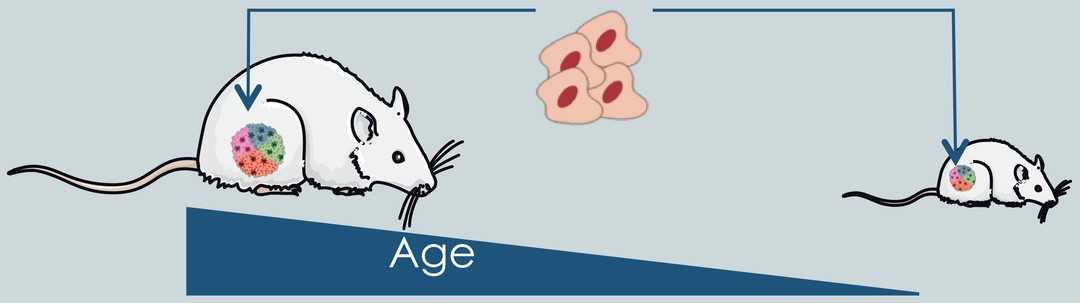

Modèle de greffe syngénique

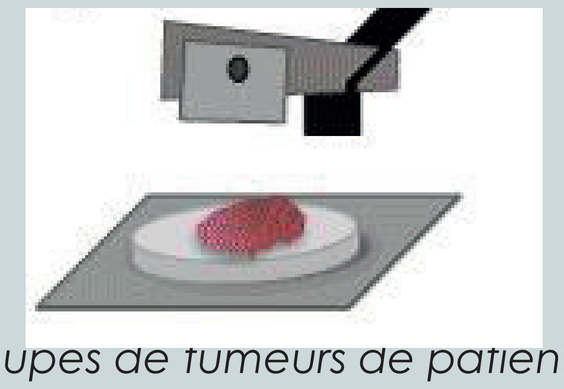

Coupes de tumeurs de patients

Impact du Poly:IC sur la régression tumorale?

Effet direct sur l'induction de la mort des cellules tumorales (Marquage TUNEL, Activité Caspase-3, Clivage de PARP) ?

Effet indirect sur la réactivation du système immunitaire (FACS, Multi-IF) ?

Facteurs de risque professionnels des cancers du poumon aux Antilles

Léïla Cabréra[1], Aviane Auguste[1], Léah Michineau[1], Jacqueline Deloumeaux[2], Clarisse Joachim-Contaret[3], Danièle Luce[1]

1: Inserm UMR_S 1085, Irset (Institut de recherche en santé, environnement et travail), Faculté de Médecine, Campus de Fouillole, 97154 Pointe-à-Pitre, Guadeloupe;
2: Registre des cancers de Guadeloupe, Pointe-à-Pitre, Guadeloupe; 3: Registre des cancers de Martinique, Fort-de-France, Martinique

Contexte et objectif

Le rôle des expositions professionnelles dans la survenue des cancers du poumon n'a jamais été examiné aux Antilles. Il s'agit d'une approche inédite dans ces régions où la population présente une faible prévalence du tabagisme et une proportion importante de cas de cancer du poumon non-fumeurs. L'objectif est d'identifier les professions et secteurs d'activité présentant un risque élevé de cancer du poumon en Guadeloupe et en Martinique.

Méthodes

Nous avons utilisé les données d'une étude cas-témoin en population conduite en Guadeloupe et en Martinique (147 cas et 405 témoins). De nombreuses informations, notamment l'histoire professionnelle détaillée et la consommation de tabac, ont été recueillies par questionnaire.

Les emplois ont été codés à l'aide de la Classification Internationale Type des Professions (CITP) version 1968 pour les professions, et de la Nomenclature d'activités française (NAF) version 2000 pour les secteurs d'activité. Nous avons généré des variables dichotomiques : "avoir travaillé au moins une fois dans sa vie dans une profession/un secteur d'activités donné(e)" versus "ne jamais avoir travaillé dans cette profession/ce secteur d'activité".

Des modèles de régression logistique non conditionnelle ont été utilisés pour estimer les odds-ratios (OR) et leurs intervalles de confiance à 95% (IC 95%). Tous les OR sont ajustés sur l'âge, le sexe, la région et la consommation de tabac.

Résultats

Professions

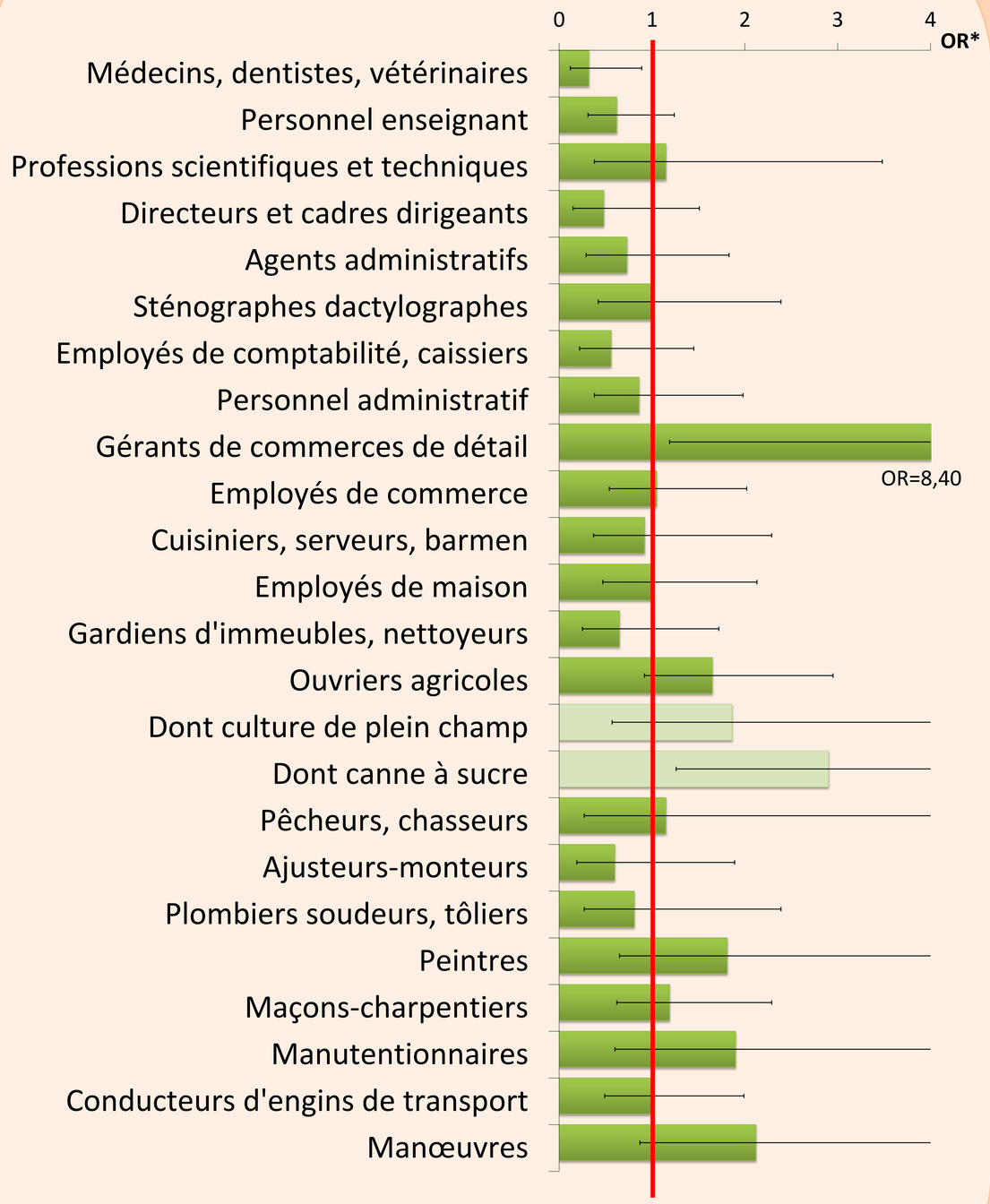

*OR et IC 95% estimés par régression logistique; ajustés sur âge, sexe, région et consommation de tabac

Figure 1. Association entre cancer du poumon et professions

Secteurs d'activité

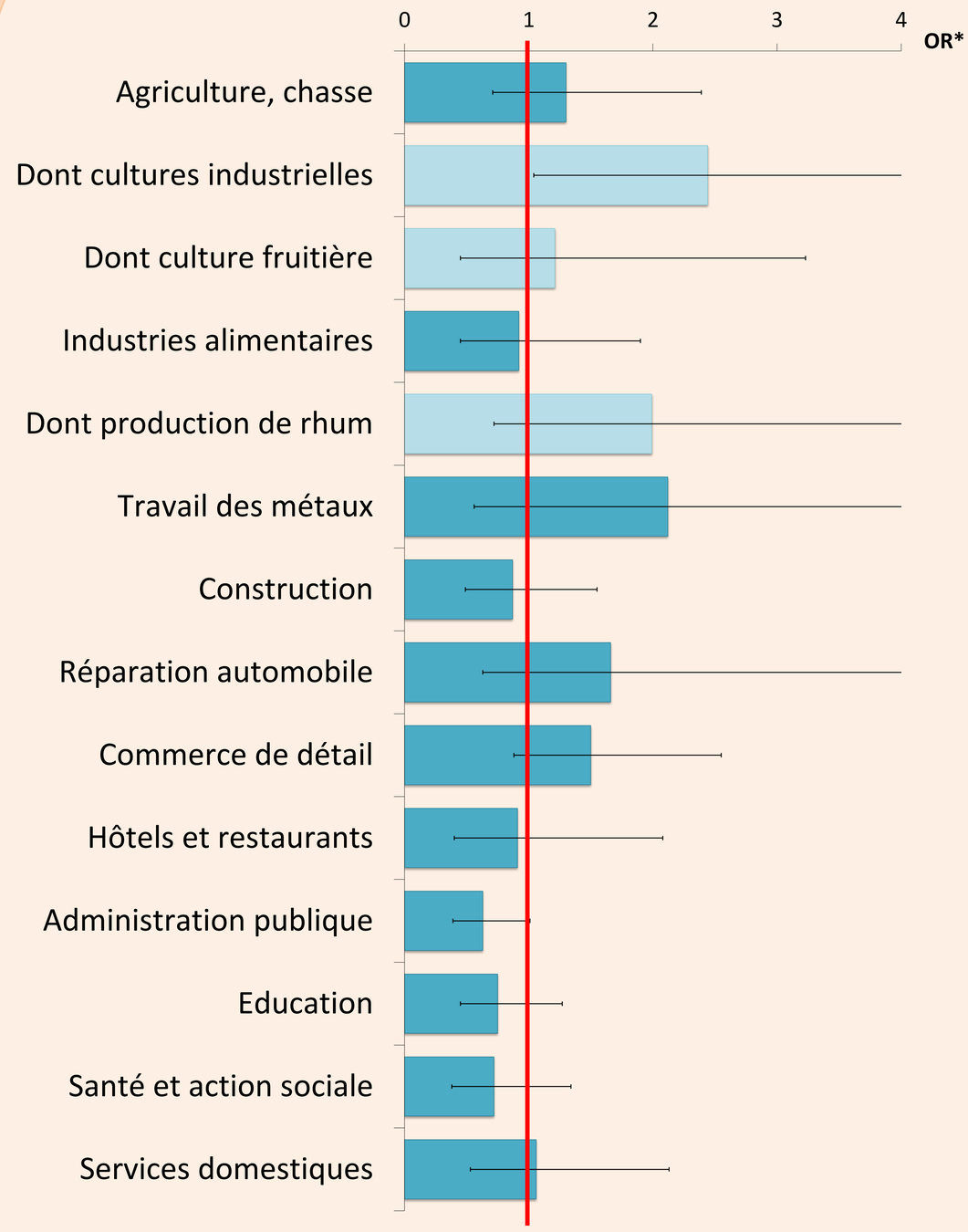

*OR et IC 95% estimés par régression logistique; ajustés sur âge, sexe, région et consommation de tabac

Figure 2. Association entre cancer du poumon et secteurs d'activité

Conclusion

Ces premiers résultats confirment que les facteurs de risque professionnels contribuent à la survenue des cancers du poumon aux Antilles, et mettent en évidence le rôle d'expositions spécifiques liées au travail de la canne à sucre (cultures industrielles et fabrication de rhum). Cette analyse exploratoire en fonction des intitulés d'emplois va être complétée par une analyse en fonction des tâches et des substances.

Financements

Léïla Cabréra a bénéficié d'un financement de la Ligue Nationale Contre le Cancer. L'étude a été financée par l'Institut National du Cancer (INCa) et l'Agence nationale de sécurité sanitaire de l'alimentation, de l'environnement et du travail (Anses).

Contact: leila.cabrera@inserm.fr

Cyclin D1 targets hexokinase 2 for controlling aerobic glycolysis in myeloma cells

Caillot M[1], Bourgeais J[2], Dakik H[3], Costé E[1,3], Mazure NM[4], Lelièvre É[5], Coqueret O[5], Hérault O[2,3], Mazurier F[3] *and* Sola B[1]

[1]Normandie Univ, Unicaen, INSERM, Caen, France
[2]CHRU de Tours, Service d'Hématologie Biologique, Tours, France
[3]CNRS ERL7001 LNOx, Tours, France
[4]Université Côte d'Azur, INSERM, Centre Méditerranéen de Médecine Moléculaire, Nice, France
[5]CRCNA, ICO Paul Papin, INSERM, Université d'Angers, Angers, France

contact : melody.caillot@unicaen.fr

Introduction

Multiple myeloma (MM) is a malignant hemopathy characterized by proliferation and the accumulation of clonal plasma cells in the bone marrow. MM tumor cells are characterized by the overproduction of a monoclonal immunoglobulin (Ig) or a λ/κ light chain, causing hyperproteinemia, renal failure, bone lesions, and immunodeficiency. Despite new treatments, the disease remains incurable. Cyclin D1 is expressed in about half of the MM due to the translocation t (11;14) (q13;q32) or other uncharacterized mechanisms. Due to its role in the regulation of the cell cycle, cells with a high cyclin D1 content have an abnormal proliferation. However, the nuclear and cytoplasmic forms of cyclin D1 have other non-canonical oncogenic functions and in particular the regulation of transcription, the control of chromosome stability and cell migration. We observed a Warburg effect (a shift of the mitochondrial respiration to the oxidative glycolysis, Fig. 1) in MM cells and explored the role of cyclin D1 in this mechanism using clones expressing the nuclear form of cyclin D1 (cyclin D1b).

1. The presence of cyclin D1 causes a shift from mitochondrial respiration to glycolysis

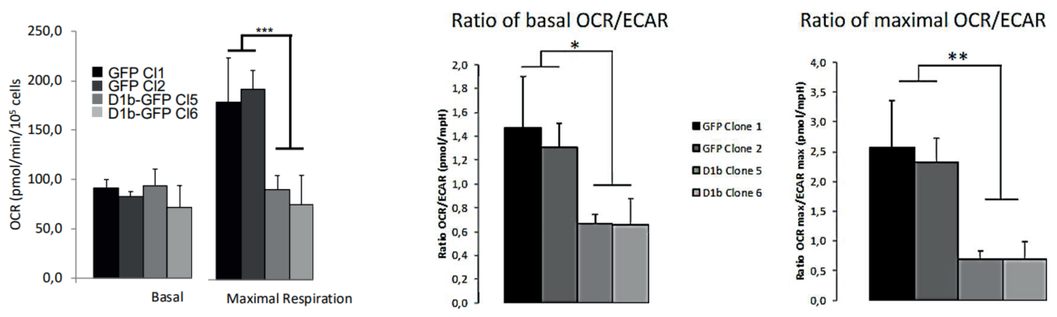

Fig. 1 : Analysis of MM cell clones derived from LP1 expressing either the GFP or a fusion cyclin D1b-GFP protein with a Seahorse XF96 Extracellular Flux Analyzer
The analyzer has two different sensors which detect changes of pH and oxygen concentration reflecting glycolysis and mitochondrial respiration, respectively. The expression of cyclin D1b led to a Warburg effect (also called aerobic glycolysis). MM cells produced energy through a high rate of glycolysis rather than mitochondrial respiration.

2. Cyclin D1 expression is associated with an increased level of HK2 mRNA and protein

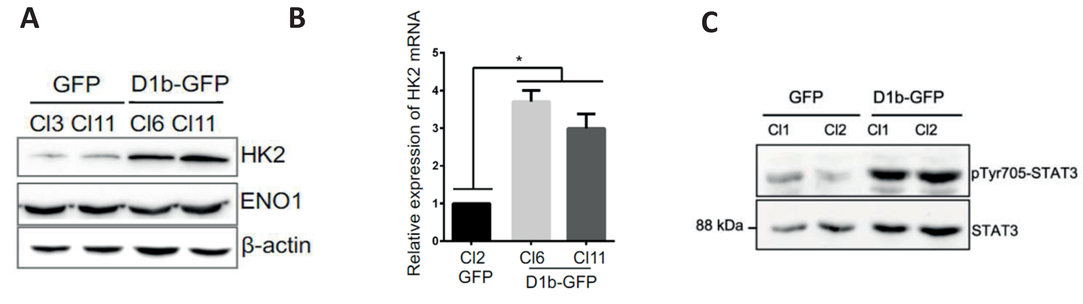

Fig. 2 : HK2 is overexpressed in MM cell lines expressing cyclin D1
(A) Immunoblotting of glycolysis proteins in GFP- or cyclin D1b-expressing cells. Cyclin D1b expression correlated with an increased expression of HK2 protein. (B) Real-time quantitative PCR (RT-qPCR) of LP1 clones. A significant change in the transcription of HK2 was found in the presence of the D1b, (C) Immunoblotting of LP1-GFP and LP1 expressing cyclin D1b (nuclear). The presence of cyclin D1 correlates with an increase in pTyr705-STAT3 level.

HIF1α, a transcriptional regulator of hypoxia and glycolysis

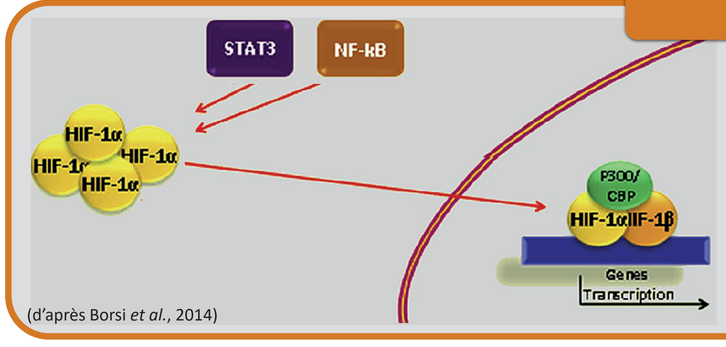

(d'après Borsi *et al.*, 2014)

Our observations are in agreement with a previous report showing that the metabolic reprogramming towards oxidative glycolysis in MM cells is controlled by the STAT3 pathway (Qin et al., 2017).
In tumor cells, including MM cells, activated STAT3 is a positive regulator of the hypoxia-inducible factor (HIF) 1α (Borsi *et al.*, 2014). In addition, HIF1α is the master transcriptional regulator of hypoxia and integrates cell proliferation and glycolysis (Semenza et al., 2013). In the B-cell lineage, hypoxia induces alteration of metabolism and in particular, glycolysis through HIF1α (Schoenhals et al., 2017).

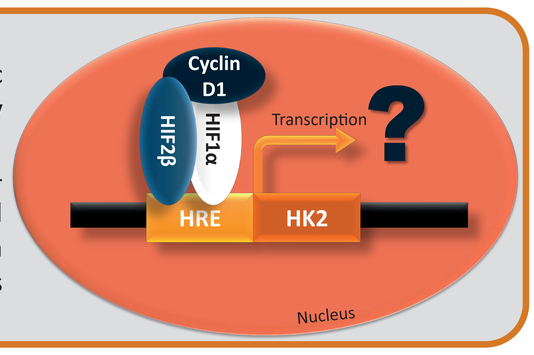

3. The presence of the cyclin D1 allows the nuclear translocation of HIF1α but not its activation

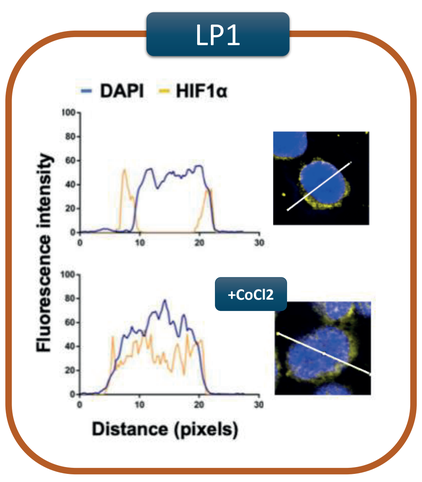

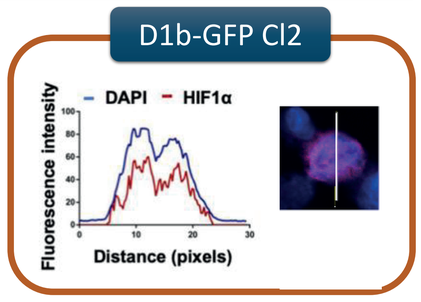

Fig. 3 : Cyclin D1b expression correlated with the nuclear localization of HIF1α. Immunofluorescence of LP1 and LP1-D1b cells. Under normoxic condition, HIF1α is cytoplasmic in parental cells. In cells expressing a cyclin D1b, HIF1α is nuclear.

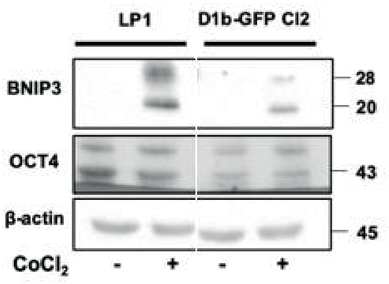

Fig. 4 : The activation of HIF1α and the induction of BNIP3, one target of HIF1α require hypoxic culture conditions. Immunoblotting of LP1 and LP1-D1b cells cultured in hypoxia (with 300 µM of CoCl2) or in normoxia (without CoCl2). BNIP3 is a target of HIF1α and OCT4 of HIF2α. The anti-β-actin antibody served as a control.

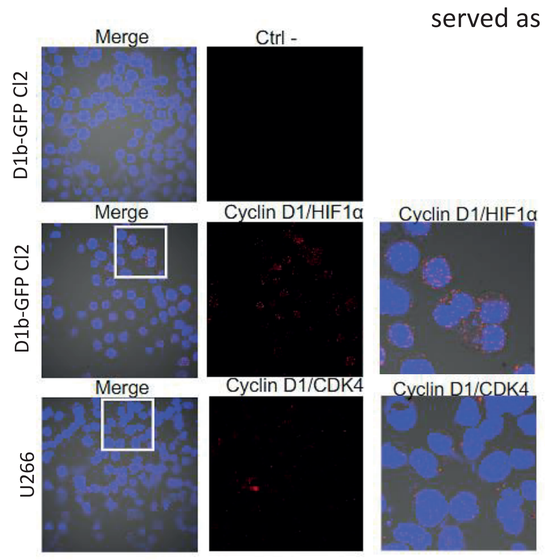

Fig. 5 : HIF1α and cyclin D1 are colocalized under hypoxic culture conditions. Duolink PLA reaction of D1b-GFP Cl2 cells cultured in hypoxia. The colocalization of cyclin D1 and CDK4 in U266 cells served as a control.

4. Cyclin D1 acts as a cofactor of HIF1α to regulate HK2 transcription

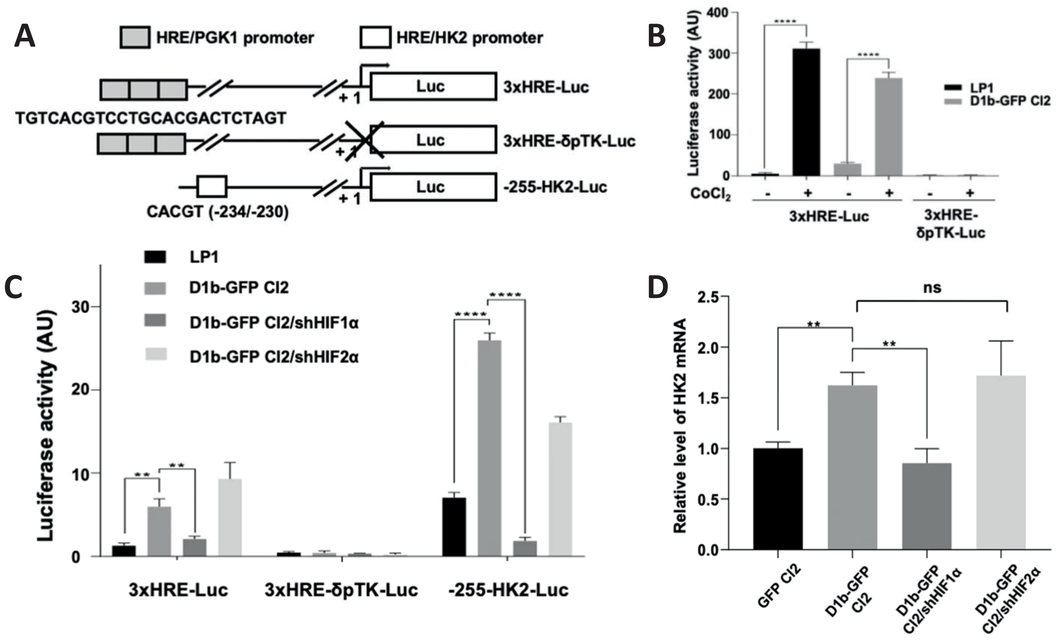

Fig. 6 : Cyclin D1-HIF1α axis regulates *HK2* transcription. (A) Schematic representation of the luciferase reporter plasmids. (B) LP1 and D1b–GFP Cl2 cells were treated for 6 h with 300 µM CoCl2 to mimic hypoxia or left untreated (–), then transfected by electroporation with either the 3× HRE-Luc or 3× HRE-δpTK-Luc plasmids. (C) LP1 and D1b–GFP Cl2 cells transduced with lentiviruses bearing shRNAs against HIF1α or HIF2α were electroporated with 3× HRE-Luc, 3× HRE-δpTK-Luc, or −255-HK2-Luc reporter plasmids. (D) RT-qPCR analyses of HK2 transcripts in GFP Cl2 and D1b–GFP Cl2 cells uninfected or infected with shHIF1α or shHIF2α lentiviruses.

5. HK2 is overexpressed in MM patients

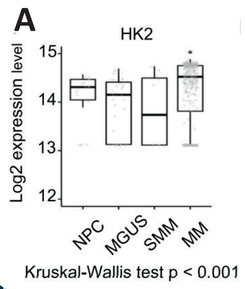

Fig. 7 : HK2 is overexpressed in MM patients and is associated with a poor prognosis. (A) Boxplots of HK2 expression in NPCs (n = 22), MGUS (n = 40), SMM (n = 12), and MM (n = 388) samples. (B) Kaplan–Meier curves showing the correlation of HK2 expression with event-free survival (EFS) and overall survival (OS) in MM cohorts (n=243).

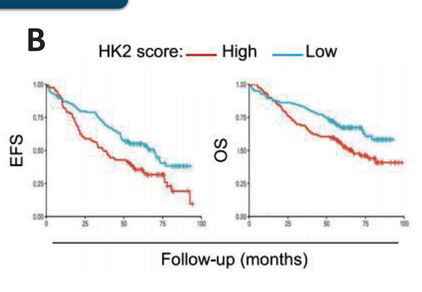

Conclusion

We describe here a new mechanism of glucose metabolism regulation in MM cells. The cyclin D1 oncoprotein sustains a Warburg effect through two concomitant, complementary mechanisms: (a) the mitochondrion-associated form of cyclin D1 decreases mitochondrial respiration[1] and, (b) the nuclear cyclin D1 associates with HIF1α to control HK2 transcription[2]. The resulting increase in HK2 gene transcription leads to an increase in HK2 protein levels and, probably, glycolytic activity. HK2 overexpression is observed in many solid tumors, and is associated with a poor prognosis. Our analysis of a cohort of MM patients further indicated that high HK2 levels were correlated with a shorter EFS and OS. Analyzes are still needed to confirm that HK2 could be a prognostic biomarker and/or a new therapeutic target in MM.

1. Tchakarska et al. Cancer Res 2011, 71, 1690-9
2. Caillot *et al*. Oncogenesis 2020, 12, 2829.

Identification et analyse d'une mutation pathogénique séparation de fonction de RAD50

L'ADN, support de l'information génétique, est une molécule dont la stabilité et l'intégrité doivent être préservées. En effet, l'instabilité génétique est associée à l'oncogénèse. Cependant, l'ADN est sujet à de nombreuses agressions (UV ou radicaux libres par exemple) qui peuvent induire des dommages tels que des cassures double brin. Ces dommages sont pris en charge par des systèmes de réparation adaptés assurant ainsi le maintien de la structure de l'ADN. Le complexe MRN composé des protéines MRE11, RAD50 et NBS1, est un des acteurs de ces systèmes de réparation.

Ce projet est basé sur l'analyse des cellules d'un patient présentant une mutation dans le gène codant la protéine RAD50. Il s'agit du troisième patient décrit au monde jusqu'ici portant des mutations bialléliques de *RAD50*. La protéine exprimée dans les cellules du patient présente une modification dans un de ses domaines dont la fonction reste peu décrite, le domaine en bobine enroulée. Analyser les cellules du patient et les comparer à des cellules sauvages permet donc de mettre en évidence les défauts induits par la mutation, de préciser le rôle de la protéine RAD50 et plus particulièrement de son domaine muté.

Marie Chansel Da Cruz, Marcel Hohl, Ilaria Ceppi, Laëtitia Kermasson, Laurence Maggiorella, Mauro Modesti, Jean-Pierre de Villartay, Talia Ileri, Petr Cejka, John H. J. Petrini et Patrick Revy
marie.da-cruz@institutimagine.org

Un patient avec des symptômes évoquant un défaut de réparation de l'ADN et/ou de maintenance des télomères

Un patient avec des mutations bialléliques dans le gène *RAD50*

Un patient exprimant une protéine RAD50 mutée dans son domaine en bobine enroulée

Insuffisance médullaire
Déficit immunitaire
Microcéphalie
Retard de croissance
Dysmorphie

⇩

Recherche d'un gène candidat impliqué

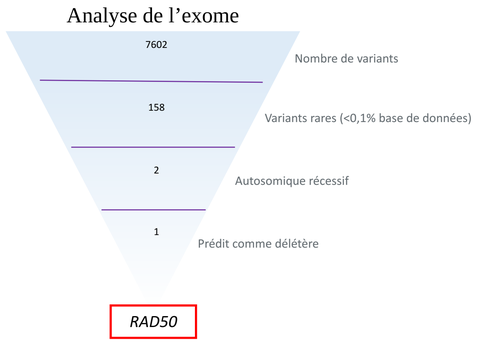

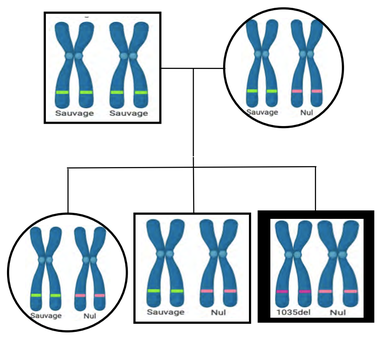

⇒ **Mère**
Allèle *RAD50* sauvage codant une protéine RAD50 sauvage
Allèle *RAD50* avec délétion d'un nucléotide
Apparition d'un codon STOP prématuré
Allèle NUL ne codant pas de protéine RAD50

⇒ **Patient**
Mutations bialléliques dans le gène *RAD50*
Allèle NUL hérité de la mère
Allèle avec délétion *de novo* de 3 nucléotides
Mutation en phase
Allèle muté 1035del codant une protéine mutée

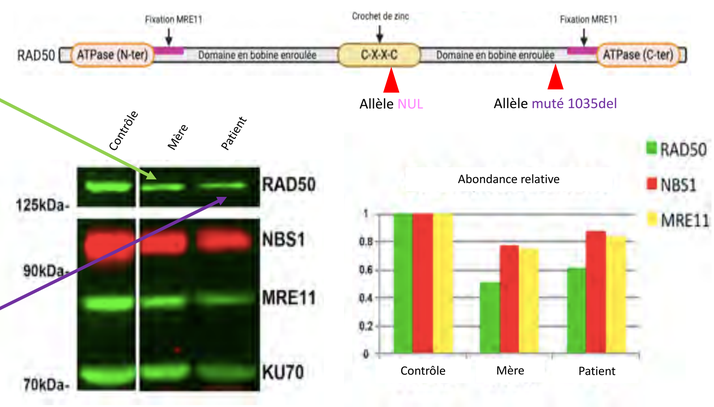

Analyse du phénotype des cellules du patient : précision du rôle du domaine en bobine enroulée de RAD50

RAD50 membre du complexe MRN (MRE11-RAD50-NBS1)

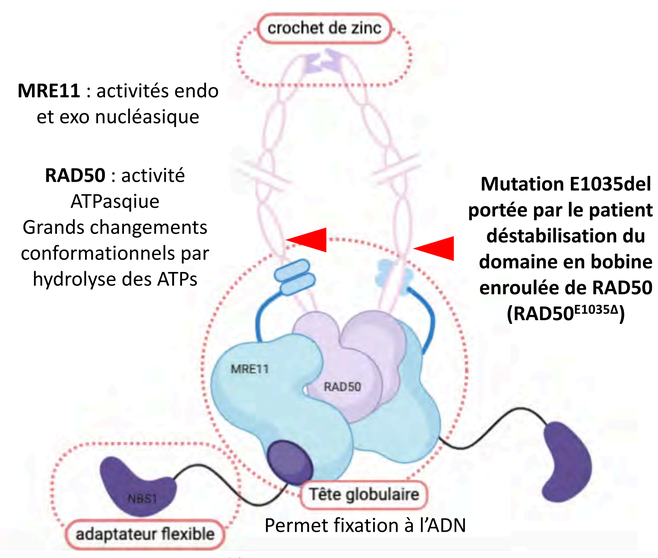

MRE11 : activités endo et exo nucléasique

RAD50 : activité ATPasique
Grands changements conformationnels par hydrolyse des ATPs

Mutation E1035del portée par le patient : déstabilisation du domaine en bobine enroulée de RAD50 ($RAD50^{E1035\Delta}$)

Permet fixation à l'ADN

Permet interactions clés

Les fonctions du complexes MRN sont **en partie** altérées dans les cellules du patient : mutation séparation de fonction

Recrutement du complexe au site de cassure comparable à celui d'une cellule contrôle.

DETECTION ✔

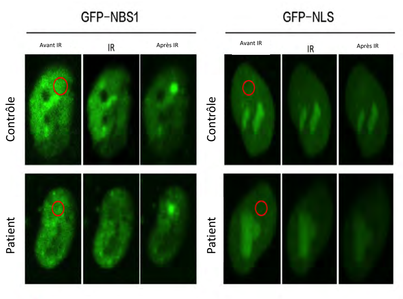

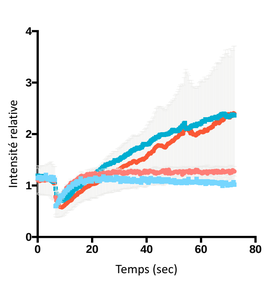

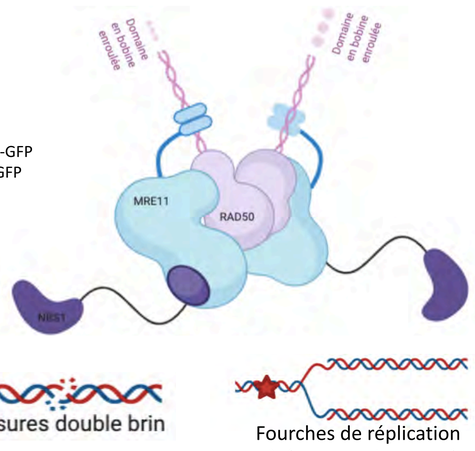

Cassures double brin

Fourches de réplication arrêtées ou endommagées

Les cellules du patient présentent un ralentissement de la progression des fourches de réplication

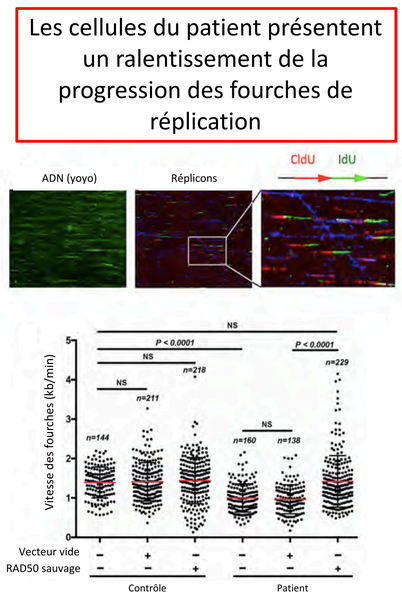

1 - Le complexe MRN permet la détection des cassures double brin

2' – La réparation de la cassure double brin est réalisée principalement par jonction d'extrémités non homologues ou par recombinaison homologue (RH)

2 - le complexe MRN active la voie de signalisation dépendante d'ATM

3 – Le complexe MRN permet le redémarrage des fourches de réplication endommagées ou arrêtées

REPLICATION ✘

MRN et Recombinaison Homologue (RH)

La réparation des cassures double brin peut s'effectuer par RH, mécanisme basé sur la résection d'un brin d'ADN de part et d'autre de la cassure créant des segments d'ADN simple brin recouverts par RPA et RAD51.

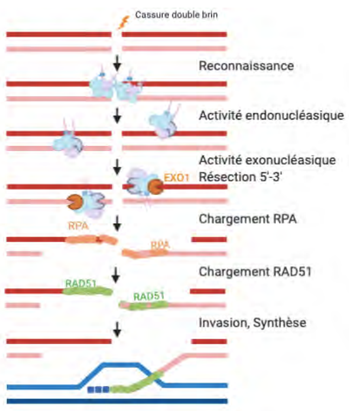

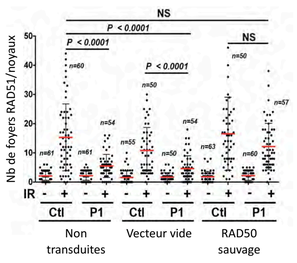

Quasi absence de foyers RAD51 dans les cellules du patient après irradiation. RH défectueuse.

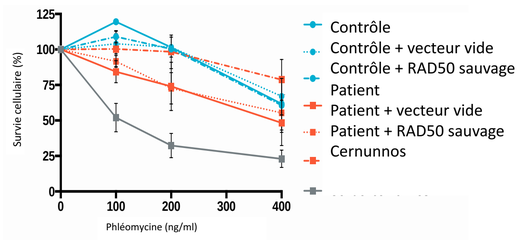

Sensibilité des cellules du patient à différents agents induisant des cassures double brin.
Phénotype sauvage restauré par expression ectopique de la forme sauvage de RAD50.

REPARATION ✘

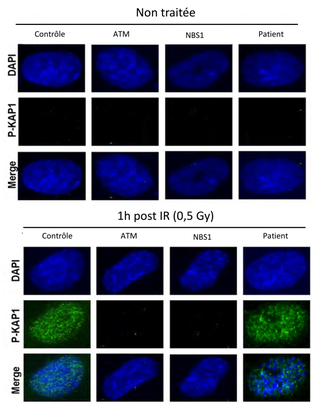

KAP1 phosphorylée par ATM recrutée

Activation du facteur clé ATM comparable à une cellule contrôle

SIGNALISATION ✔

Après un stress replicatif, les fourches de réplication sont stoppées puis résectées. Pas de résection dans les cellules du patient.

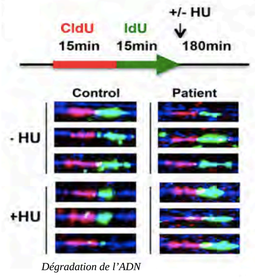

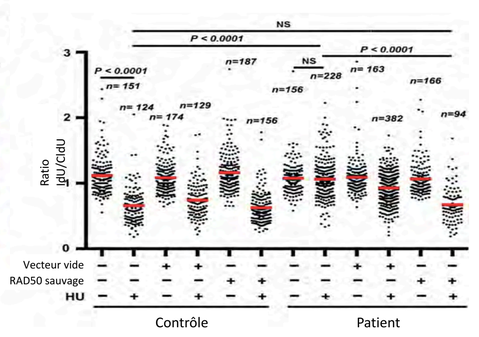

REDEMARRAGE ✘

La réparation par RH et le redémarrage des fourches de réplication endommagées ou arrêtées : deux phénomènes dépendants de l'activité exonucléasique de MRE11

Protéines recombinantes

Complexe MRE11-$RAD50^{1035\Delta}$:
Diminution des capacités d'accrochage à l'ADN
Maintien de l'activité endonucléasique
Hydrolyse de l'ATP possible
Diminution de l'activité exonucléasique

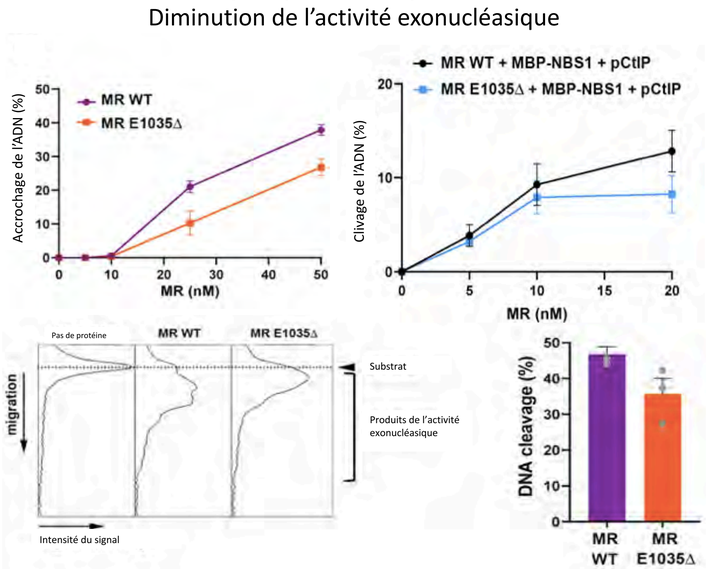

MRN : deux conformations majoritaires

En forme d'anneau relâché pour la détection
En forme de tige rigide pour l'activité exonucléasique
Passage entre les conformations dépendante de l'hydrolyse de l'ATP via un intermédiaire conformationnel ayant hydrolysé l'ATP mais fixant toujours un ADP+Pi
Intermédiaire permet activité endonucléasique

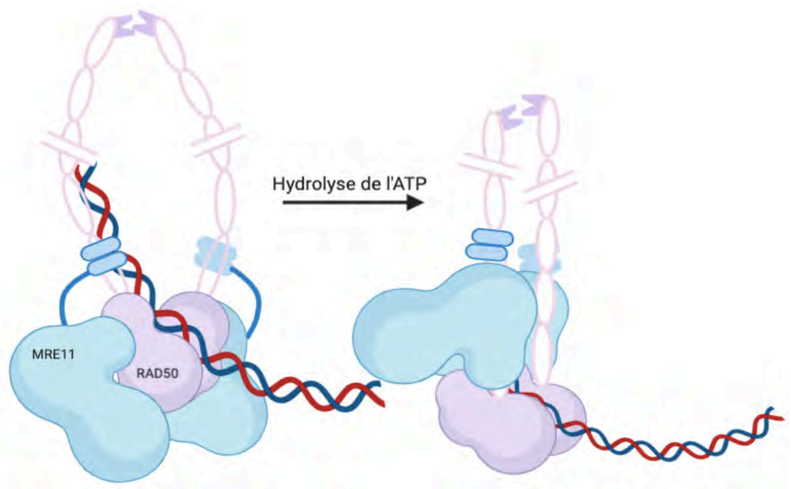

Modélisation de l'impact de la mutation portée par le patient

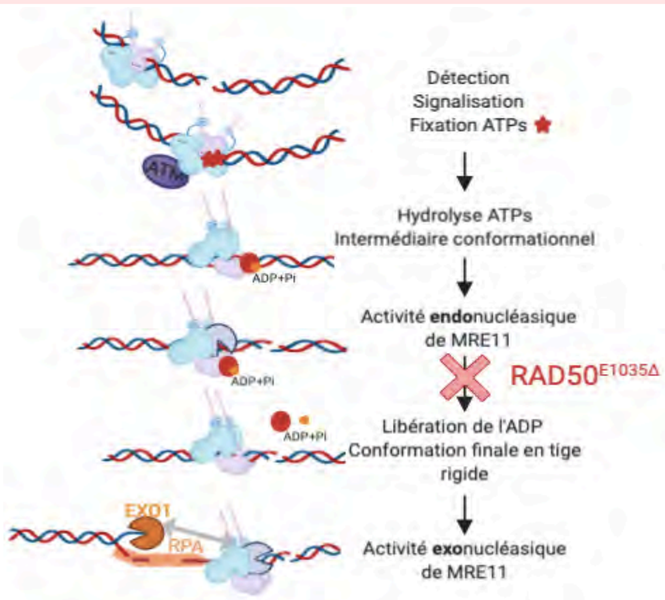

Cette étude met en lumière le rôle essentiel du domaine en bobine enroulée de RAD50 dans la régulation des fonctions du complexe MRN permettant la réparation de l'ADN.

La Mambaquarétine, une toxine de venin de mamba vert, nouvel antagoniste du récepteur V2 pour le diagnostic et le traitement potentiel du cancer rénal

Amélia Chorfa[1], Maithé Corbani[1], Nicolas Gilles[2], Bernard Mouillac[1] et Christiane Mendre[1]

[1]Institut de Génomique Fonctionnelle, Université Montpellier, CNRS, INSERM, Montpellier, France
[2]Service d'Ingénierie Moléculaire des Protéines, Institut des Sciences du Vivant Frédéric Joliot, Commissariat à l'Energie Atomique, Université Paris-Saclay, Gif sur Yvette, France

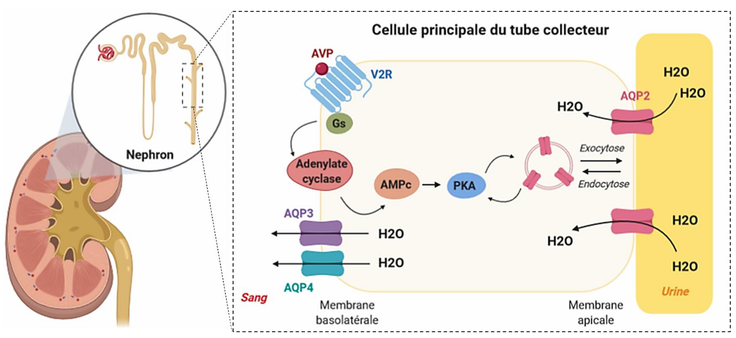

Effet antidiurétique du V2R dans le rein

Le cancer du rein représente environ 3% de l'ensemble des cancers. Malgré les traitements actuels, le taux de survie après 5 ans chez les patients atteints d'un cancer rénal à un stade avancé est de seulement 8%. Le développement de nouvelles approches est donc nécessaire pour identifier de nouvelles cibles impliquées.
Le récepteur V2 de la vasopressine (V2R) est exprimé au niveau du rein et son activation par la vasopressine (AVP) induit l'effet antidiurétique par la production d'AMPc. Etant surexprimé dans les tumeurs rénales, le V2R pourrait être une cible thérapeutique intéressante. De plus, ses antagonistes spécifiques sont capables d'inhiber la prolifération cellulaire *in vitro* et la formation de tumeurs *in vivo* chez la souris. **(1),(2)** Malheureusement, les antagonistes V2R sur le marché actuel sont hépatotoxiques, c'est le cas du Tolvaptan. Il est donc nécessaire de développer d'autres outils thérapeutiques pour cette cible.
La Mambaquarétine (MQ) est une toxine peptidique issue du venin de mamba vert caractérisée dans notre laboratoire en tant qu'antagoniste sélectif du V2R. Cette molécule est capable d'inhiber la formation de kystes rénaux dans un modèle *in vivo* de polykystose rénale chez la souris. **(3)**

Mamba vert

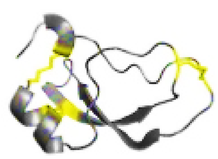

Structure de la MQ

Objectif : Tester la MQ sur des lignées cancéreuses rénales humaines (ACHN, Caki-2 et A498) afin de caractériser son utilisation potentielle dans le cancer du rein

Outil diagnostic

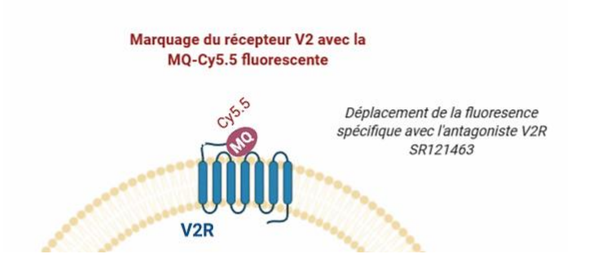

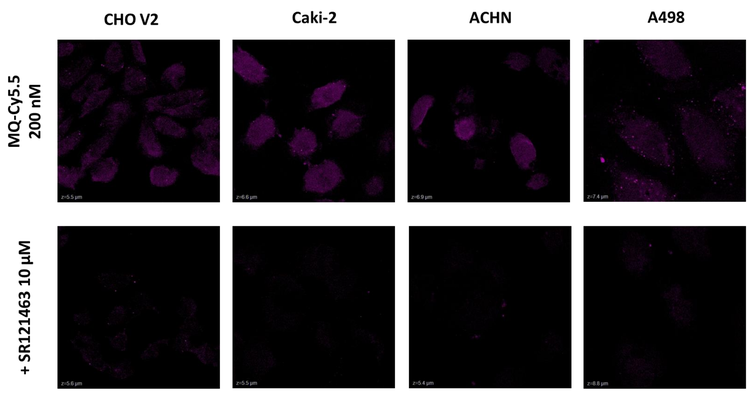

Mise en évidence de la présence du V2R sur les lignées cancéreuses rénales : Caki-2, ACHN et A498

Etude publiée : Droctové et al., Theranostics, 2020

Outil pharmacologique

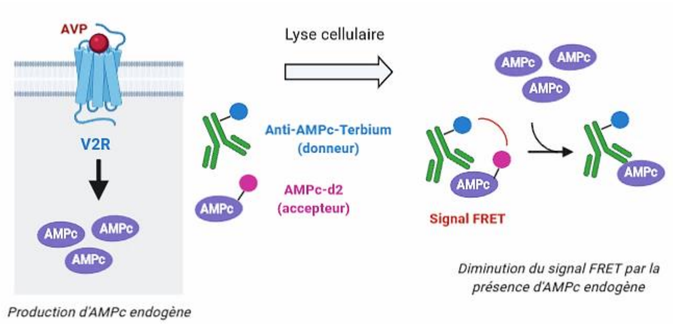

Test HTRF du dosage de l'AMPc

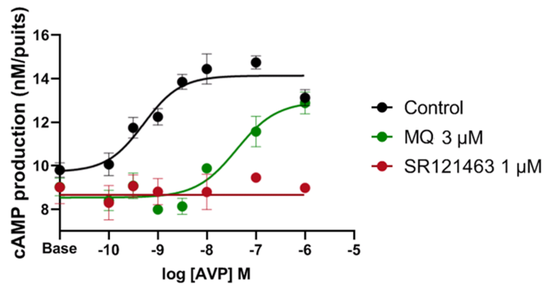

Inhibition de la production d'AMPc induite par l'AVP avec la MQ sur les cellules Caki-2

Outil thérapeutique

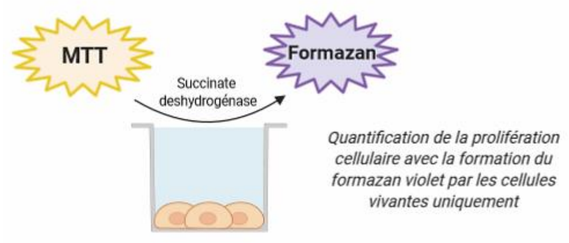

Test de prolifération MTT

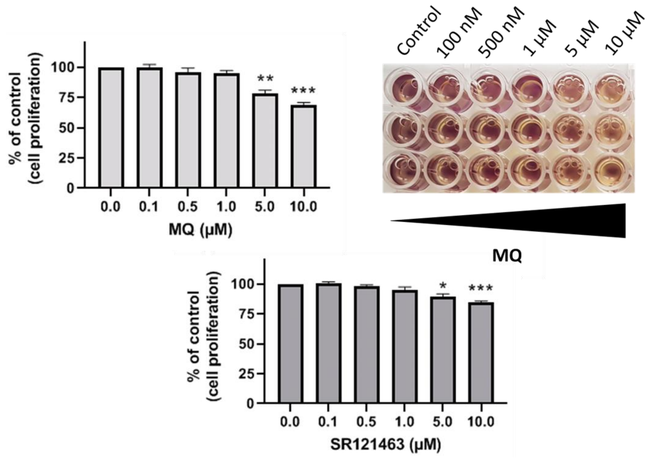

Effet inhibiteur significatif de la MQ sur la prolifération cellulaire de la lignée ACHN

Le récepteur V2 constitue une cible pertinente pour laquelle la MQ est un excellent outil de marquage spécifique et une molécule thérapeutique potentielle pour le cancer du rein. Cependant, des expériences de marquage sur tissus tumoraux et sur l'animal entier ainsi que des essais thérapeutiques *in vivo* sur des modèles de xénogreffes, nous permettraient de valider que la MQ serait un candidat intéressant pour le traitement du cancer rénal.

Références : ***(1)*** *Bolignano et al, Urologic. Oncology, 2009, 642-7 ;* ***(2)*** *Sinha et al, Oncogene, 2019, 1059-60 ;* ***(3)*** *Ciolek et al, PNAS, 2017, 7154-9*

Contact : amelia.chorfa@hotmail.fr

Autophagy, a new potential therapeutic target in JAK2V617F Myeloproliferative Neoplasms

Charly Courdy, Isabelle De Araujo, Stéphane Manenti, Véronique De Mas and Carine Joffre
Centre de Recherches en Cancérologie de Toulouse (CRCT) Université Paul Sabatier (UPS) Toulouse III, Inserm, UMR1037, CNRS ERL 5294
Equipe Labellisée Ligue contre le Cancer

Contact : charly.courdy@inserm.fr

Introduction

Myeloproliferative Neoplasms (MPN) are a group of chronic haematological malignancies described as an excessive clonal expansion of myeloid lineage cells. In a majority of MPN, the identification of the JAK2V617F mutation as a major cause of the occurrence of the disease led to the development of a targeted therapy, Ruxolitinib, a JAK1/JAK2 inhibitor. Because of its limited efficiency in patients, identification of new therapeutic targets is required.

In this context, we are interested in autophagy, a dynamic process of degradation and recycling of cellular components. However, the precise role of autophagy remains controversial, as it has been associated in other haematological malignancies with resistance or, conversely, with induction of cell death upon treatment. In JAK2V617F-positive MPN, the function of autophagy remains poorly documented. Thus, the objective of my PhD thesis is to study the role and the regulation of autophagy in JAK2V617F-positive MPN, and to determine whether it could be a potential therapeutic target for this pathology.

Autophagy process

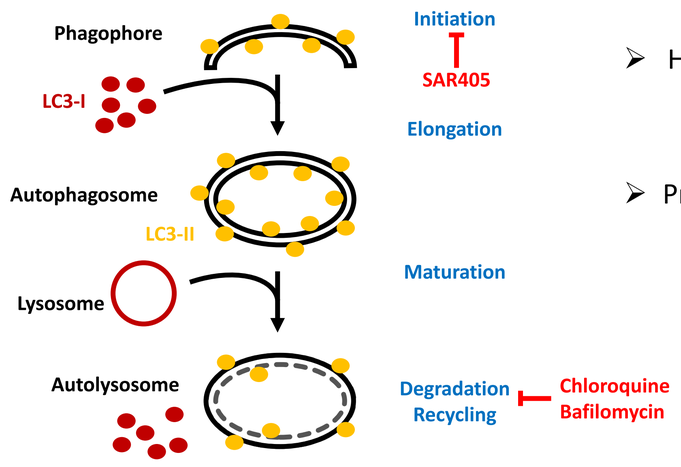

Models

- Human cell lines expressing JAK2V617F
  - HEL (homozygous)
  - SET-2 (heterozygous)
- Primary samples
  - MPN patients (JAK2V617F)
  - Healthy donors (JAK2WT)

Results

1- Ruxolitinib, a JAK1/2 inhibitor, induces an increase of autophagy

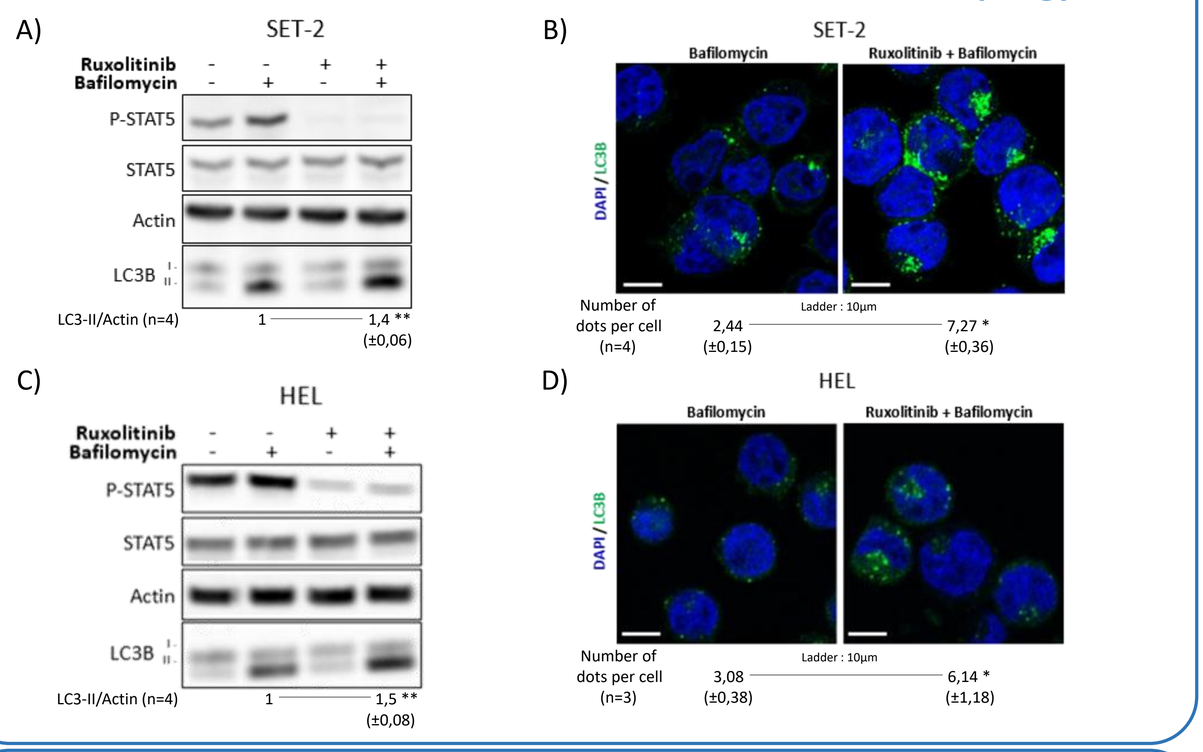

2- Involvement of mTORC1 kinase inhibition and Protein Phosphatase 2A (PP2A) reactivation in Ruxolitinib-induced autophagy

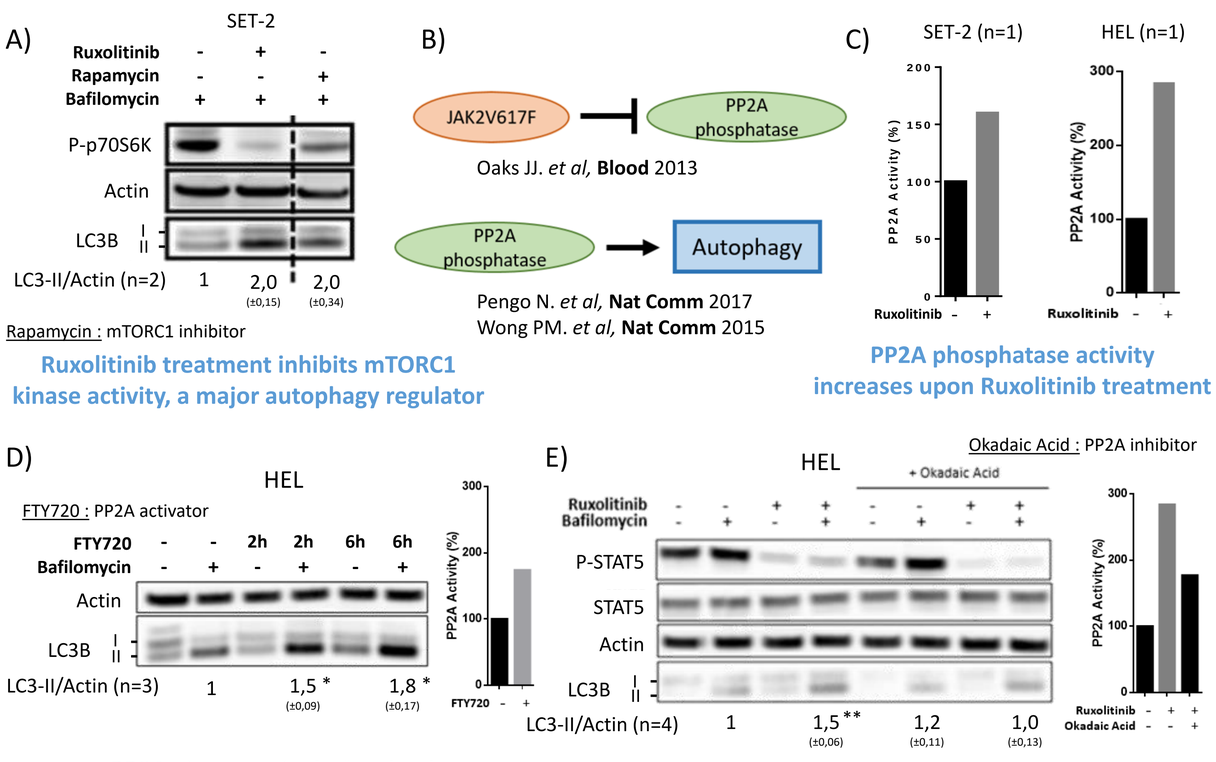

Ruxolitinib treatment inhibits mTORC1 kinase activity, a major autophagy regulator

PP2A phosphatase activity increases upon Ruxolitinib treatment

PP2A pharmacological activation induces an increase of autophagy

PP2A inhibition blocks Ruxolitinib-induced autophagy

3- Autophagy inhibition potentiates cytotoxic effects of Ruxolitinib *in vitro* in JAK2V617F-positive human cell lines

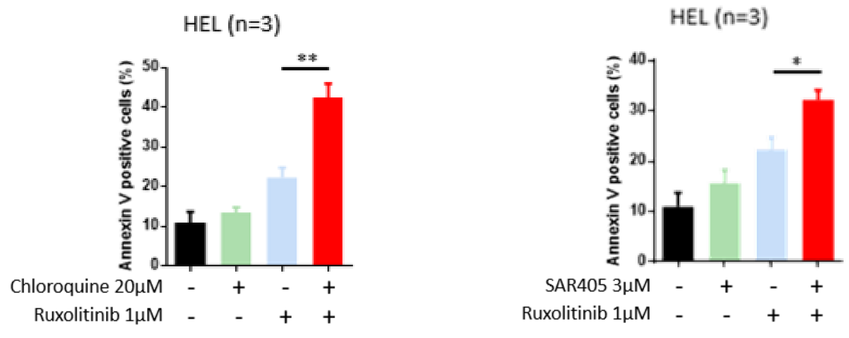

4- Autophagy inhibition potentiates the effects of Ruxolitinib *in vitro* in JAK2V617F-positive MPN patient samples

A) Primary cells isolation

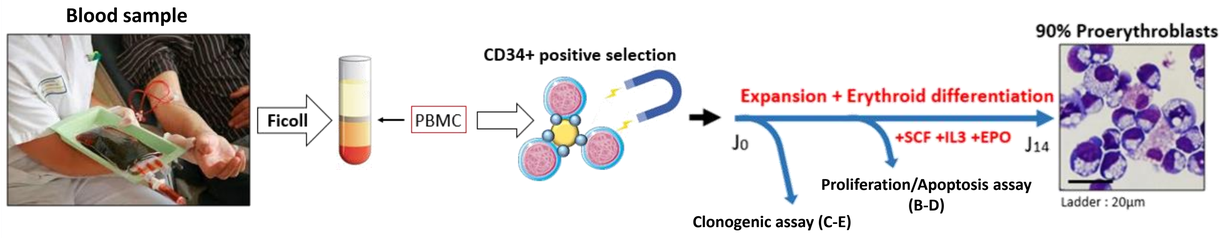

MPN primary samples

B) Proliferation/Apoptosis assay

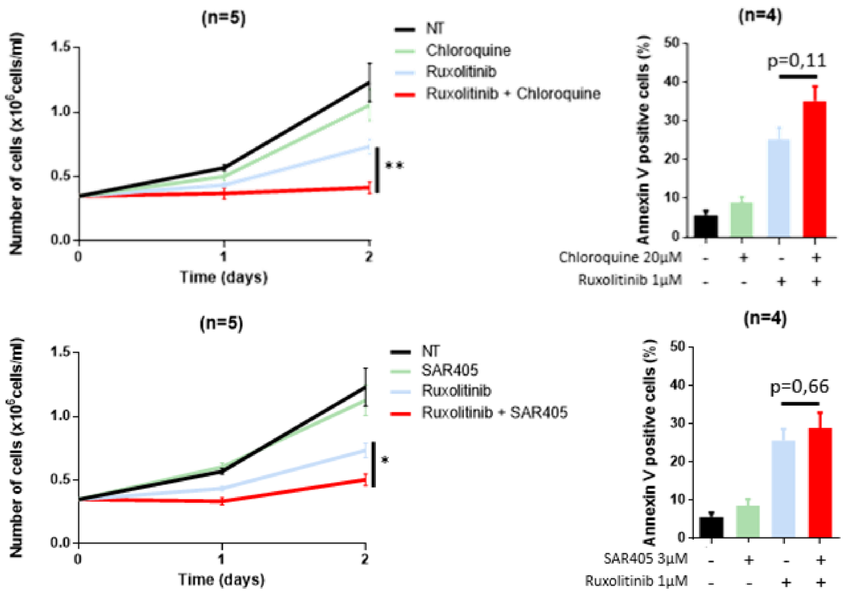

Autophagy inhibition in combination with Ruxolitinib reduces the proliferative potential of JAK2V617F-positive MPN patient cells

C) Clonogenic assay

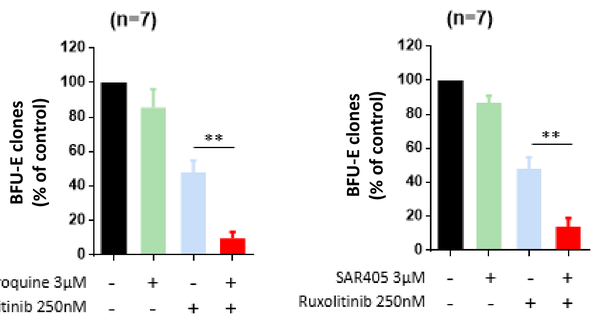

Inhibition of autophagy combined with Ruxolitinib significantly reduces the clonogenic properties of JAK2V617F-positive MPN patient cells in semi-solid culture

Healthy Donors

D) Proliferation assay

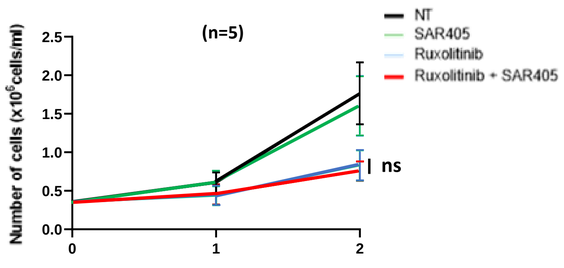

E) Clonogenic assay

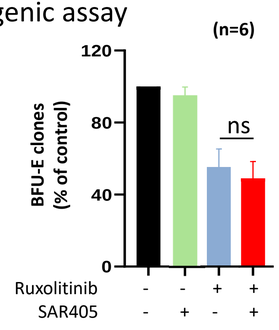

Inhibition of autophagy with SAR405 does not impact the effects of Ruxolitinib *in vitro* in healthy donor cells

Autophagy is not implicated in Ruxolitinib resistance mechanisms in healthy haematopoietic cells

Conclusion

- Ruxolitinib treatment induces a cytoprotective autophagy
- Ruxolitinib-induced autophagy relies on PP2A activation upon treatment

Autophagy inhibition represents an interesting therapeutic approach to enhance Ruxolitinib efficiency in MPN patients

Perspectives

- Validation *in vivo* :
  - JAK2V617F Knock In mouse model (Marty C. *et al*, **Leukaemia** 2013) treated with Ruxolitinib +/- Autophagy inhibitor (collaboration I. Plo - Inserm U1287)
- Identification of molecular actors involved in Ruxolitinib-induced autophagy :
  - Implication of JAK2V617F using a JAK2 siRNA
  - Identification of PP2A substrates :
    - Candidate approach (ULK1, ATG4b, ATG13, …)
    - Global approach (mass spectrometry)

Genetic Predisposition in Uveal Melanoma

Anne-Céline Derrien

Derrien A.C.[1], *Mobuchon L.*[1], *Houy A.*[1], *Rodrigues M.* [1,2], *Eeckhoutte A.*[1], *Dayot S.* [1], *Stern M.H.*[1,3]

[1]INSERM U830, DNA Repair and Uveal Melanoma (D.R.U.M.), Equipe labellisée Par la Ligue Nationale Contre le Cancer, Institut Curie, Paris, France.
[2]Department of Medical Oncology, Institut Curie, PSL Research University, Paris, France. [3]Department of Genetics, Institut Curie, Paris, France.

Introduction

Uveal Melanoma (UM)

- UM is a **cancer of the eye** in adults**.** It arises from the transformation of melanocytes from the **uveal tract**
- It is a **rare** cancer (5.6 cases per million per year)
- There are 50% chances of metastasis (**liver** in >90% cases)
- **UM has a very poor prognosis:** the mean survival is 8 months for metastatic cases, which are **treatment-refractory**

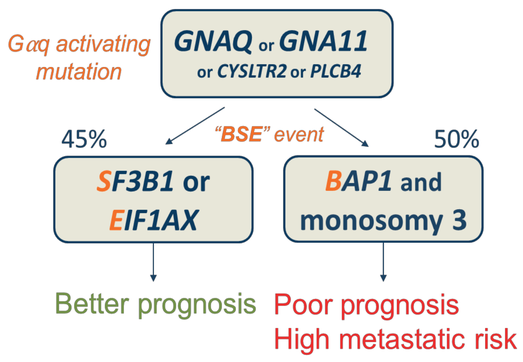

Fig 1. Oncogenic pathway in UM: a 2-step progression model

Genetics and epidemiology

- UM tumors are genetically simple: 2 oncogenic driver events (Fig.1)
- No UV mutation signature in UM, and very low mutational burden
- UM is associated with **European ancestry, blue eyes and fair skin**
- The incidence of UM has remained stable in Europe, North America and Australia over time.

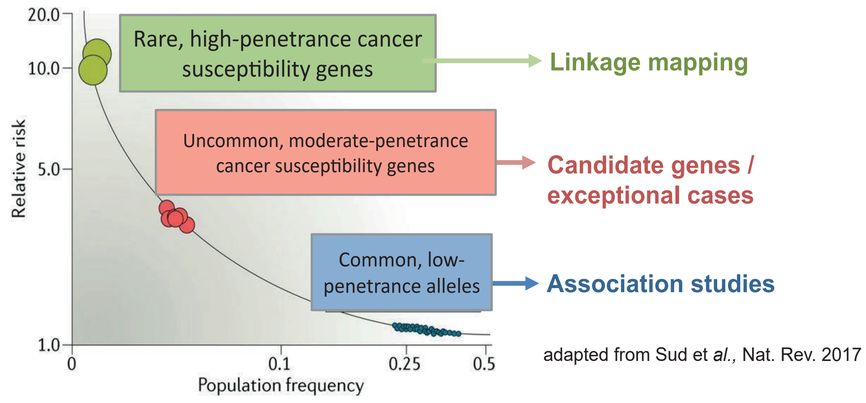

adapted from Sud et *al.*, Nat. Rev. 2017

Fig 2. Identifying the genetic basis of a disease

Aims and hypothesis

HYPOTHESIS

There are some genetic risk factors predisposing to UM, characterized by a prevalence of risk alleles in populations of European ancestry.

OBJECTIVES

To identify main genetic risk factors for UM and to refine UM tumorigenesis:

- **I - Association study in UM:** Identifying causal SNPs and gene(s) among candidate variants identified by a Genome-Wide Association Study (GWAS) in UM;
- **II – Other cancer susceptibility genes:** role of the *MBD4* gene in UM predisposition

I – Association study

Background & methods

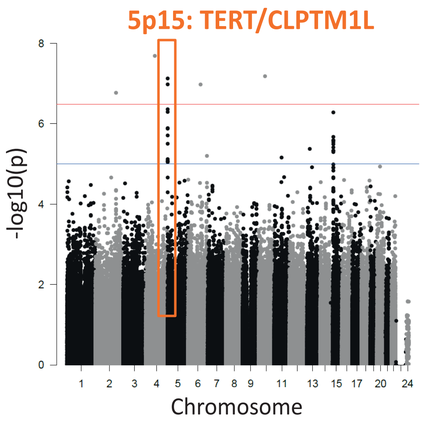

Fig 3. Association Study in UM.
This GWAS of 259 UMs and 401 controls identified risk polymorphisms in the *CLPTM1L* locus. Black dots represent SNPs. Red line shows statistical significance.

Post-GWAS functional study

- Which SNP(s)?
- Effects on genetic environment (TF, chromatin)?
- Which gene?

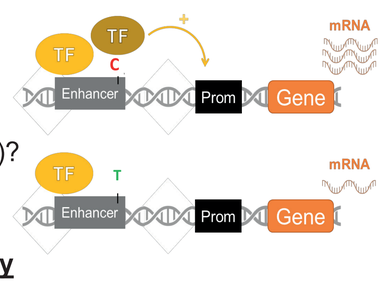

1 - Luciferase Reporter Assay

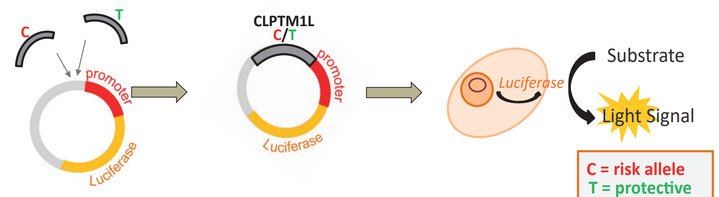

2 - Electrophoretic Mobility Shift Assay (EMSA)

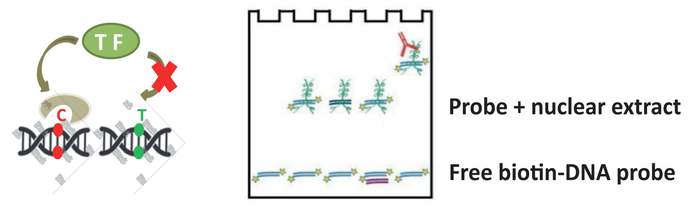

Results

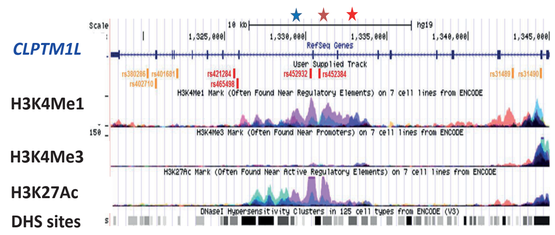

Fig 4. Regulation of the 5p15.33 region (ENCODE database) indicates an open chromatin region of active transcription and enhancer activity.

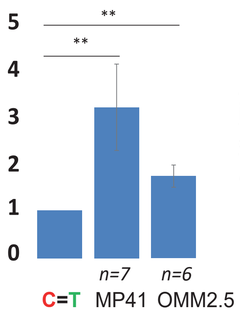

Fig 5. Risk alleles in *CLPTM1L* intron drive higher gene expression in UM cell lines.
Luciferase expression fold-change with risk vs. protective allele.
Risk / Protective expression ratio

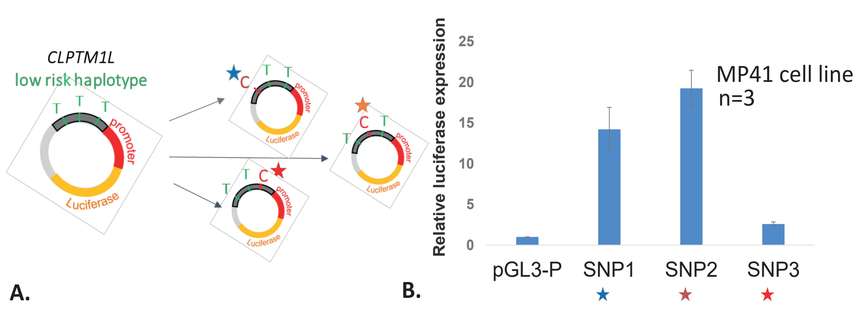

Fig 6. Validation of causal SNP(s) with directed mutagenesis (A) and effects of the risk allele of each SNP on gene expression (B). Gene expression in quantified by relative luciferase signal compared to empty vector signal. As seen, SNPs 1 or 2 may induce gene expression.

rs452384 (SNP2)				rs452932 (SNP1)			
T	C	T	C	T	C	T	C
-	-	+	+	-	-	+	+

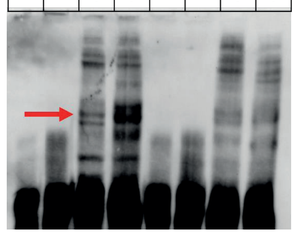

Fig 7. EMSA for SNPs 1 and 2 consensus binding sites. Arrow shows differential nuclear factor binding for SNP2–C or –T allele.

Conclusions and perspectives

- We identified a risk region for uveal melanoma on chromosome **5p15,** in the ***TERT/ CLPTM1L* locus** (Fig.3).
- This risk region is located in an **open chromatin** environment with **enhancer** activity (Fig.4).
- UM **risk alleles** lead to **higher gene expression** than protective alleles (Fig.5) and rs452384 is associated with differential transcription factor binding (Fig.7).
- Future work involves the identification of nuclear factors binding to rs452384 by **mass spectrometry** and the identification of **genes** regulated by these risk factors.

II – *MBD4* mutations in UM

Background & Methods

- An exceptional metastatic UM patient showed extremely high **sensitivity to anti-PD1** treatment.
- The tumor was associated with a high **CpG>TpG** mutation burden, and a **hypermutator phenotype** (Fig8)
- She had a **germline** deleterious mutation in the ***MBD4* gene**, and **somatic inactivation** in the tumor.

Are *MBD4* mutations frequent in UM?

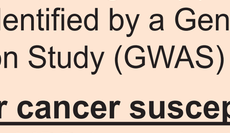

***MBD4* mutation frequency**

Are *MBD4* germline mutations a UM risk factor (is *MBD4* a UM predisposition gene)?

→ Genetic screen for *MBD4* mutations in germline DNA of 1,093 UM patients and 210 tumors

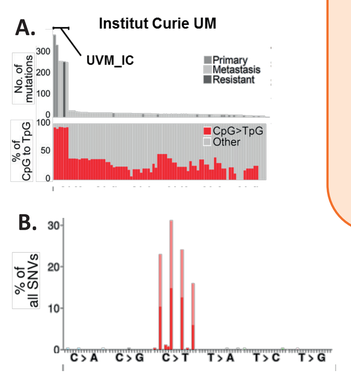

Fig 8. Mutational signature in a UM tumor with *MBD4* deficiency.
A. Number of mutations in tumor (Curie UM cohort). **B.** Mutational pattern in the patient's tumors: relative proportion of each substitution.

Results

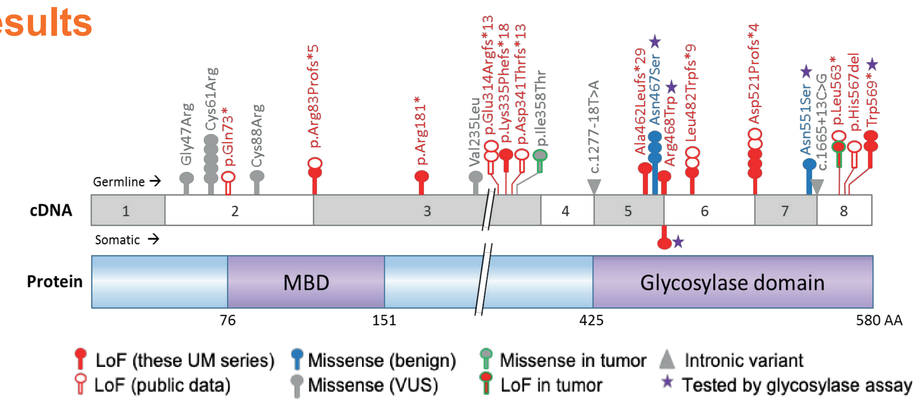

Fig 9. Identification of deleterious *MBD4* variants in UM patients (n= 1,093 germline DNA and n=210 tumoral DNA): 8 loss-of-function (LoF) mutations in the consecutive series of germline DNA of UM patients, and 5 additional LoF mutations in tumor monosomy 3 samples.

Conclusions and perspectives

- Identification of 8 ***MBD4* deleterious germline variants** (Fig.8) out of 1,093 consecutive UM patients: ***MBD4* is a UM predisposition gene.**
- MBD4 inactivation is associated with a high **CpG>TpG** mutational signature, and **hypermutated tumors** (Fig.10).
- Tumors arising in such a context have clinical relevance and should be recognized as they may respond to immunotherapy.
- **Perspectives:** Mutational targets and transcriptomic analysis of *MBD4*-inactivated UM

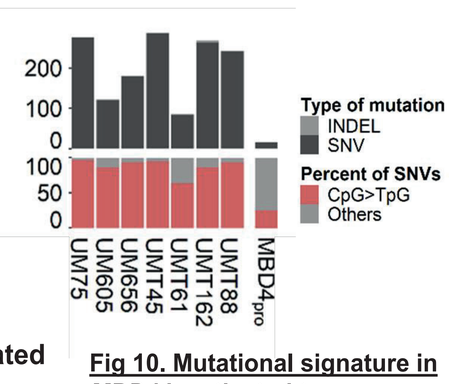

Fig 10. Mutational signature in *MBD4*-inactivated tumors.

References

1. Mobuchon, L et al. A GWAS in uveal melanoma identifies risk polymorphisms in the *CLPTM1L* locus. *NPJ Genomic Medicine*, **2** (2017)
2. Derrien AC et al. Germline MBD4 mutations and Predisposition to Uveal Melanoma. *JNCI* (2020)

Development of innovative nanocomposite hydrogels for the locoregional treatment of Glioblastoma

Amel DJOUDI – 1st year PhD student -ED BS

Thesis supervisor: Pr. Frank BOURY

Amel Djoudi[1] , Rodolfo Molina-Peña[1] , Nela Buchtová[1] , Clément Toullec[1,2] , Sylvie Avril[1], Nicolas Hauville[1] , Carmen Alvarez-Lorenzo[3] , Christine Jérôme[2] , Emmanuel Garcion[1] , Frank Boury[1]

1-CRCINA, INSERM, Université de Nantes, Université d'Angers, Angers, France

2-Center for Education and Research on Macromolecules (CERM), Université de Liège, Liège, Belgium

3-Departamento de Farmacia y Tecnología Farmacéutica at the University of Santiago de Compostela, Spain

I-Pathology context:

- Incidence: 0.6-3.7 for 100 000
- Surgery: tumor resection (stereotaxy/MRI/Gliolan®)
- Standard therapy: Temozolomide (TMZ) + Radiotherapy (RT)
- Loco-regional therapy: Gliadel®: Carmustin wafer not selective
- Recurrence: involves Cancer Stem Cells (CSC) close (1 to 2 cm) to the resection cavity (RC)[1,4]

Needs to better target CSC to reduce their resistance against RT

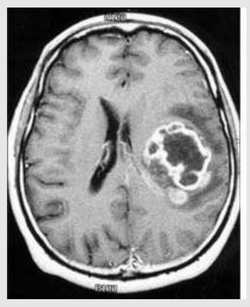

Cerebral MRI after injection of contrast product (Gadolinium) in human

TMZ,RT & Gliadel®: OS 1 to 2 years

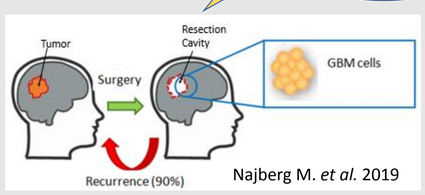

Najberg M. *et al.* 2019

II-Project specifications:

Objective 1:

- Nanoencapsulation of radiosensitizing cytokine within biodegradable nanoparticles via phase separation[3] to achieve sustained release

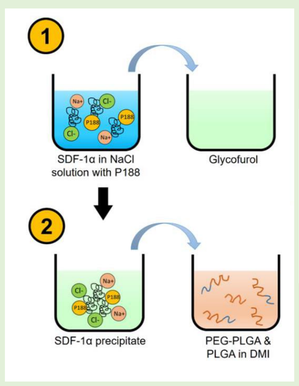

Haji Mansor *et al.* 2018

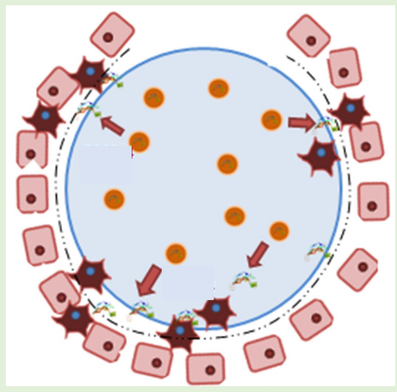

Objective 2:

- Implantable/injectable hydrogel incorporating cytokine-loaded nanoparticles

Objective 3:

- Validation of the safety and efficacy of the device

III-Therapeutic strategy:

Differentiating/radiosensitizing compound

Bone Morphogenic Protein (BMP-4)
TGF-β family's cytokine

- Allow locoregional CSC to leave the CSC compartment and give them increased radiosensitivity
- Involved in <u>early differentiation</u> of the embryo establishment of the dorso-ventral axis and <u>differentiation</u> processes (cartilage, bone , sympathetic neurons)[2,4]

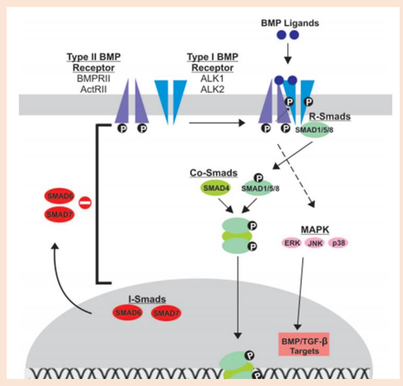

Beederman *et al* 2013

Hydrogel development

Hyaluronic Acid (HA)

- Main brain ECM component
- Involved in morphogenesis, oncogenesis, inflammation or cicatrization
- Mechanical properties close to the brain ones (Young modulus:0,1-1kPa)
- Biocompatible, biodegradable, Approved Pharmaceutical Ingredient (GRAS)[4]

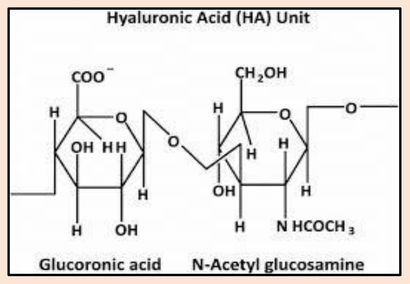

Nasr. 2008

IV-*In vitro/ in vivo* characterization and evaluation:

2D Adherent model
(+ 10% FBS)

3D Organoid model
(+B27, heparin, bFGF, and EGF)

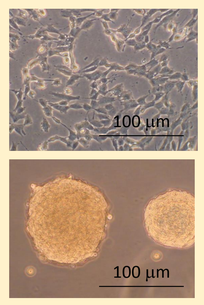

Optical microscopy images of F98 GB cells after 4 days of culture at 37 °C and 5% CO_2 (DMEM high glucose and 1% antibiotics)

Fischer rat intracavitary surgery

3 evaluation levels:

1. <u>2D evaluation</u> in transwell: BMP-4 activity from the scaffolds (signaling and survival studies +/- RX)
2. <u>3D bioassays</u> in matrigel: BMP-4 scaffolds +/- RX (differentiation, migration, growth, sensitizing effects)
3. <u>*In vivo* intracavitary models</u> (xenogeneic human U87MG in nude rats & syngeneic F98 Fischer rat model)

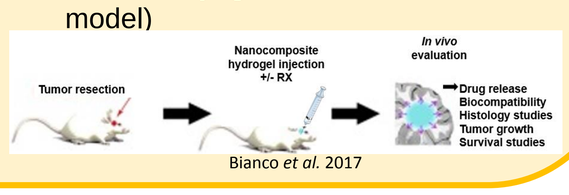

Bianco *et al.* 2017

V-Conclusion:

- **The current project is based on the development of an injectable nanocomposite hydrogel. This new therapy relies on a differentiation strategy by BMP-4 for the Cancer Stem Cells (CSC) to acquire a RT-sensitive phenotype.**
- **Nanoprecipitation of BMP-4: hydrogel formulation and physico-chemical characterizations include protein stability studies, rheology assays, NPs DLS studies, in course.**
- **Nanoencapsulation of the BMP-4: encapsulation efficiency and release studies through ELISA dosages.**
- ***In vitro/in vivo* studies to obtain a preclinical package (cytocompatibility, biocompatibility, bioperformances)**

References:

1. Stupp, R., M. Brada, M. J. van den Bent, J.- C. Tonn, et G. Pentheroudakis. « High-grade glioma: ESMO Clinical Practice Guidelines for diagnosis, treatment and follow-up ». *Annals of Oncology* 25, nº suppl 3 (29 avril 2014): iii93-101.
2. Piccirillo, S. G. M., B. A. Reynolds, N. Zanetti, G. Lamorte, E. Binda, G. Broggi, H. Brem, A. Olivi, F. Dimeco, et A. L. Vescovi. « Bone Morphogenetic Proteins Inhibit the Tumorigenic Potential of Human Brain Tumour-Initiating Cells ». *Nature* 444, nº 7120 (décembre 2006): 761-65
3. Haji Mansor, Muhammad, Mathie Najberg, Aurélien Contini, Carmen Alvarez-Lorenzo, Emmanuel Garcion, Christine Jérôme, et Frank Boury. « Development of a Non-Toxic and Non-Denaturing Formulation Process for Encapsulation of SDF-1α into PLGA/PEG-PLGA Nanoparticles to Achieve Sustained Release ». *European Journal of Pharmaceutics and Biopharmaceutics* 125 (avril 2018): 38-50.
4. Bastiancich, C., P. Danhier, V. Préat, et F. Danhier. « Anticancer Drug-Loaded Hydrogels as Drug Delivery Systems for the Local Treatment of Glioblastoma ». *Journal of Controlled Release* 243 (décembre 2016): 29-42.

Contact:

amel.djoudi@univ-angers.fr

https://www.linkedin.com/in/amel-djoudi-bba241173/

Up-regulation of the Hexosamine Pathway is a distinctive feature of Lung Adenocarcinoma that Sustains EGFR Signalling

Helena Dragic, Sofiane Belfeki, Virginie Barbet, Audrey Barthelaix, Cédric Duret, Christelle Machon[1], Jerome Guitton[1], Paul Hofman[2], Justine Rudewicz[3], Konstantinos Voutetakis[4], Toufic Renno and Serge N Manié[5]

Centre de Recherche en Cancérologie de Lyon, Centre Léon Bérard, INSERM U1052, CNRS UMR5286, Université Lyon 1, F-69000 Lyon, France.
1- Hospices Civils of Lyon, Biochemistry laboratory of Lyon Sud, F-69495 Lyon, France. 2- CHU Nice, CNRS 7284, Université de Nice Sophia Antipolis. 3-Bordeaux Bioinformatic Center, Bordeaux, France. 4-National Hellenic Research Foundation, Athens, Greece. 5- Centre Eugène Marquis, INSERM U1242 COSS, 35042 Rennes.

INTRODUCTION

Tumours reprogram pathways of nutrient acquisition and metabolism to meet the exacerbated demand of malignant cells. However, this increased demand often depletes the local nutrient supply, such that many tumour cells reside in nutrient-poor environment to which they have to adapt in order to survive. The hexosamine biosynthetic pathway (HBP) plays a central role in sensing the nutritional status of the cell since it integrates molecules coming from carbohydrates, fatty acids, amino acids and nucleotides metabolism. It converts fructose-6-phosphate, a glucose derivative, into UDP-N-acetylglucosamine (UDP-GlcNAc) that serves as a precursor for N-glycosylation and O-GlcNAcylation of proteins. The HBP is becoming of high importance in cancer biology, yet its role in human lung cancer remains unclear.

1. Human Lung Adenocarcinoma (LUAD) display distinctive HBP up-regulation

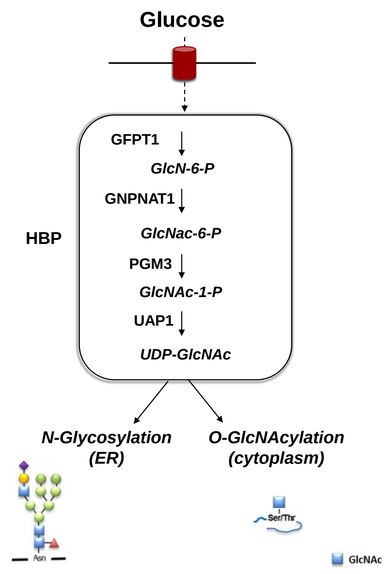

Figure 1: Schematic representation of the Hexosamine biosynthetic pathway.

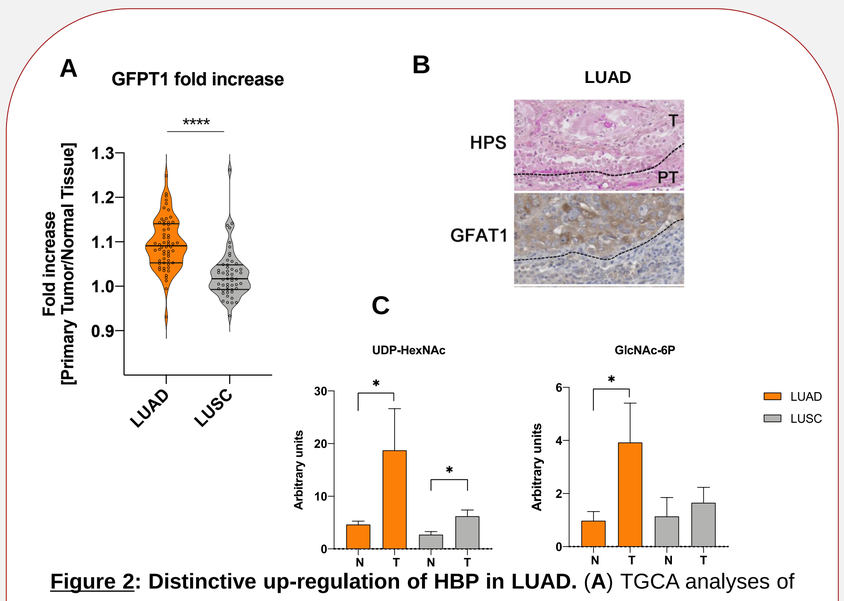

Figure 2: Distinctive up-regulation of HBP in LUAD. (**A**) TGCA analyses of GFPT1 mRNA expression lung adenocarcinoma (LUAD) and squamous cell carcinoma (LUSC) presented as fold increase. (**B**) Representative immunohistochemistry analyses on LUAD tissue. (**C**) LC-MSMS analyses of HBP metabolites in LUAD and LUSC.

2. Human LUAD display distinctive XBP1s up-regulation

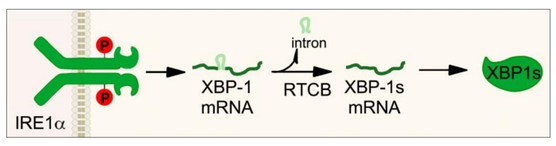

Figure 3: XBP1s up-regulation in LUAD. (**A**) Schematic representation of XBP1s cleavage. XBP1s production is part of the ER stress response. (**B**) Differential transcript usage (DTU) analysis of XBP1 transcript isoforms

3. Transformed HBEC-RL53 cells appropriate model for studies in vitro

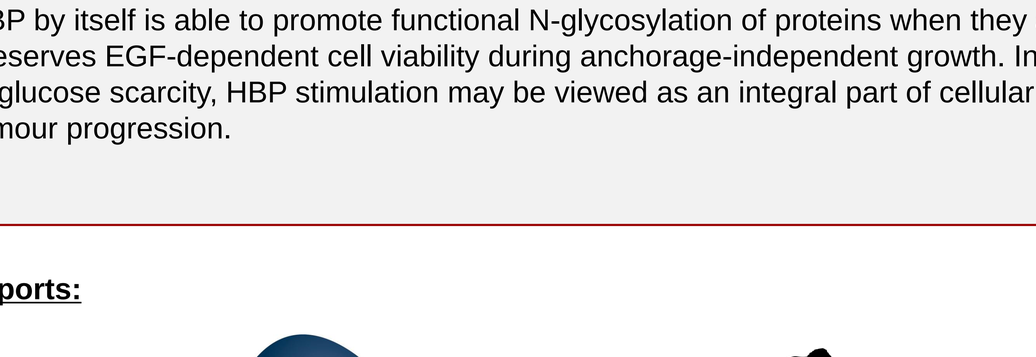

Figure 4: Glucose shortage in HBEC-RL53 cells recapitulates HBP and XBP1s up-regulation. (**A**) XBP1s mRNA level expression upon different glucose concentrations. (**B**) mRNA level of HBP enzymes upon different glucose concentrations.

4. Reduced levels of UDP-GlcNAc upon glucose scarcity preferentially sustains protein *N*-glycosylation rather than *O*-GlcNAcylation

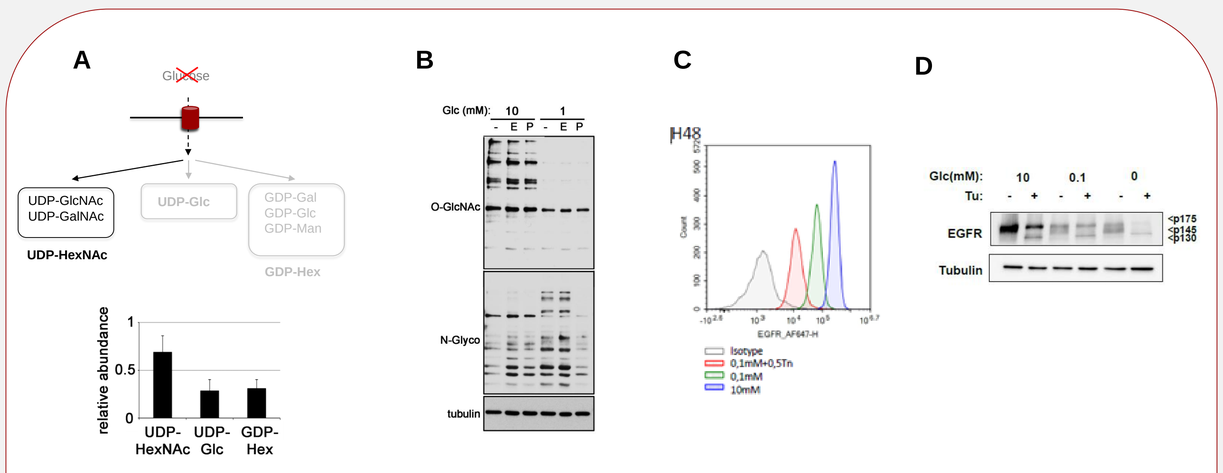

Figure 5: Upon low glucose levels HBP flux is rechanneled towards N-glycosylation of proteins in the ER (**A**) Schematic representation of nucleotide sugars level upon glucose deprivation accompanied by the graph of MS analysis. (**B**) WB analysis of O-GlcNAcylation and N-Glycosylation modifications. (**C**) FACS analysis of EGFR surface expression upon Tunicamycin treatment. (**D**) WB analysis of EGFR surface expression upon Tunicamycin treatment.

5. HBP up-regulation upon low glucose rescues EGFR signalling dependent cellular viability during anchorage-dependent growth

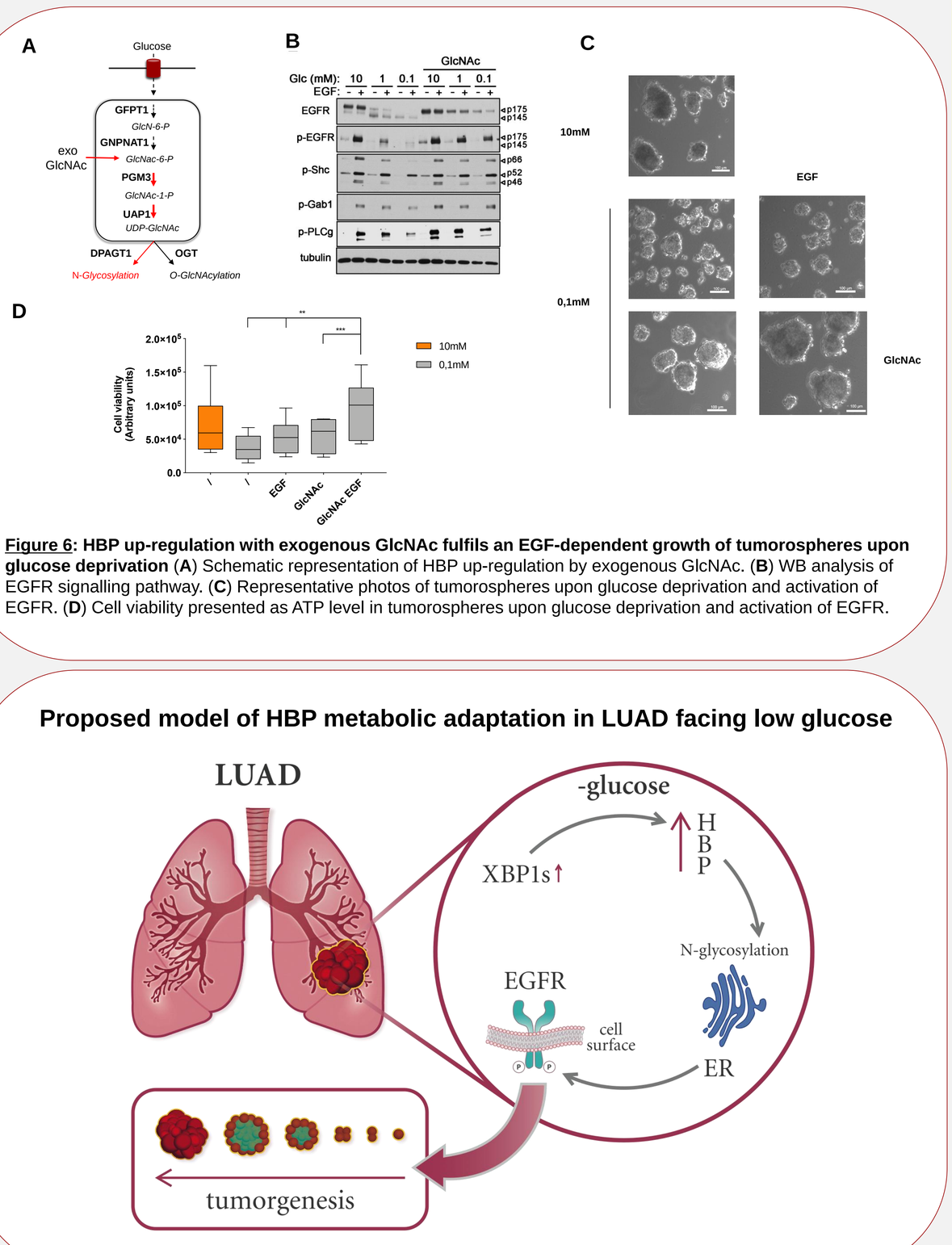

Figure 6: HBP up-regulation with exogenous GlcNAc fulfils an EGF-dependent growth of tumorospheres upon glucose deprivation (**A**) Schematic representation of HBP up-regulation by exogenous GlcNAc. (**B**) WB analysis of EGFR signalling pathway. (**C**) Representative photos of tumorospheres upon glucose deprivation and activation of EGFR. (**D**) Cell viability presented as ATP level in tumorospheres upon glucose deprivation and activation of EGFR.

Proposed model of HBP metabolic adaptation in LUAD facing low glucose

CONCLUSION

HBP by itself is able to promote functional N-glycosylation of proteins when they are facing glucose shortage. This capability permits the maintenance of EGFR on the cellular surface and preserves EGF-dependent cell viability during anchorage-independent growth. In a context where human lung adenocarcinoma displays an increased HBP flux and experience conditions of glucose scarcity, HBP stimulation may be viewed as an integral part of cellular adaptation to low glucose, helping malignant cells to combat excess of ER stress and advance towards tumour progression.

Contact: ***helena.dragic@lyon.unicancer.fr , serge.manie@lyon.unicancer.fr***

Supports:

Exacerbation of senescence induced by pX deficiency restrains telomerase non-canonical functions in kidneys of adult mice.

Lou Duret, Yannick Gache, Catherine Pons, Eric Gilson, Dmitry Bulavin and Marina Shkreli
Institute for Research on Cancer and Aging, Nice (IRCAN), CNRS UMR7284 – INSERM U1081 – UNS – UCA Nice, France
Contact : Lou.DURET@univ-cotedazur.fr

Telomerase is a ribonucleoprotein composed of 2 main subunits: the protein component TERT, and the RNA subunit TERC.
Telomerase carries two independent roles: **(1)** elongation of telomeres, and **(2)** activation of cell proliferation *in vivo*. The latter activity is called the non-canonical activity of telomerase. The adult mammalian kidney is particularly sensitive to telomerase non-canonical activity.
In this project, we aim to determine if and how pX protein regulates telomerase non-canonical activity.

1. TERT overexpression *in vivo* induces reprogramming of kidney podocytes

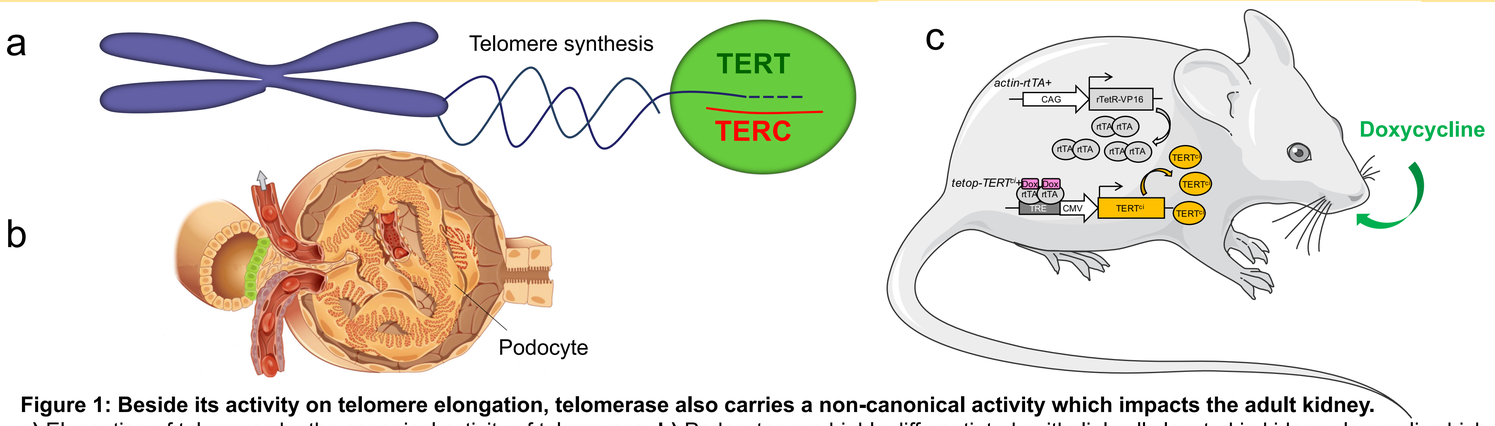

Figure 1: Beside its activity on telomere elongation, telomerase also carries a non-canonical activity which impacts the adult kidney.
a) Elongation of telomeres by the canonical activity of telomerase. **b)** Podocytes are highly differentiated epithelial cells located in kidney glomeruli, which support filtration function. **c)** Double transgenic inducible-TERT^{ci} mice (i-TERT^{ci}) allowing conditional overexpression of TERT^{ci} (catalytically inactive TERT) in adult mice. **d)** TERT^{ci} overexpression induces loss of differentiation markers of podocytes, WT1 and Synaptopodin, and subsequent proliferation of these cells that leads in turn to a collapsing Focal Segmental GlomeruloSclerosis (FSGS).

2. pX deficiency impairs this activity of TERT

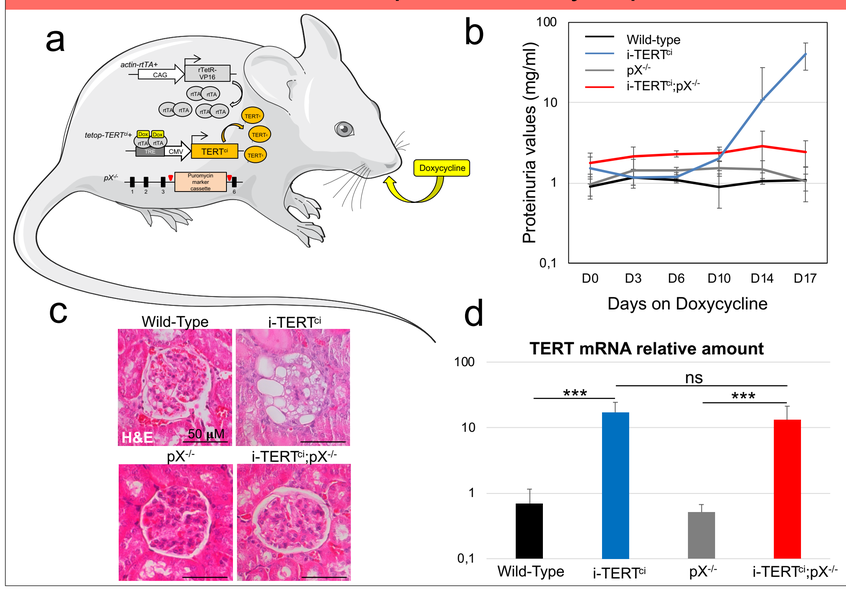

Figure 2 : pX invalidation inhibits TERT non-canonical functions on kidney epithelium. (A) Schematic of the i-TERT^{ci};pX$^{-/-}$ transgenic system. **(B)** Kinetic Analysis by Bradford assay of proteinuria from wild-type (*n=4*), i-TERT^{ci} (*n=4*), pX$^{-/-}$ (*n=4*), and i-TERT^{ci};pX$^{-/-}$ (*n=4*) mice treated with Doxycycline for 17 days and showing absence of kidney filtration dysfunction in i-TERT^{ci};pX$^{-/-}$ mice (red line) when compared to i-TERT^{ci} mice (blue line). **(C)** Glomerular histology by Hematoxylin and Eosin staining from wild-type, i-TERT^{ci}, pX$^{-/-}$, and i-TERT^{ci};pX$^{-/-}$ mice all on Doxycycline treatment for 17 days and showing no kidney damages in i-TERT^{ci};pX$^{-/-}$ mice when compared to i-TERT^{ci} mice. **(D)** TERT mRNA levels by qRT-PCR in whole kidneys from wild-type (*n=4*), i-TERT^{ci} (*n=4*), pX$^{-/-}$ (*n=4*), and i-TERT^{ci};pX$^{-/-}$ (*n=4*) mice treated with Doxycycline for 17 days showing effective induction of TERT^{ci} transgene in i-TERT^{ci};pX$^{-/-}$ mice. Data are represented as mean ± SEM.

3. pX deficiency prevents TERT^{ci}-induced glomerular cell proliferation

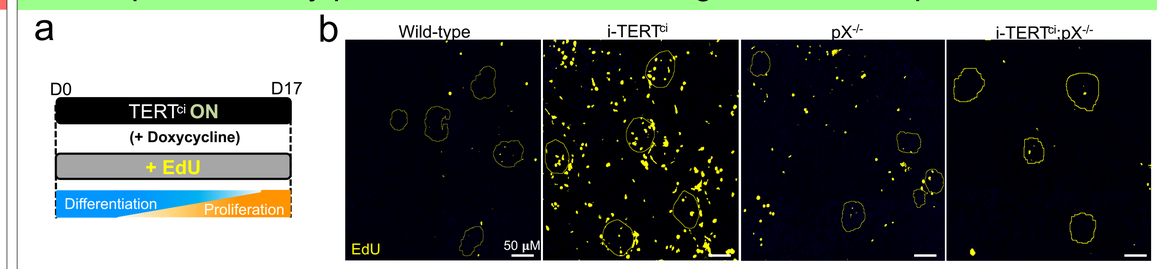

Figure 3 : pX knock-out blocks cell proliferation induced by TERT^{ci} overexpression whithin the kidney. (A) Schematic representation of EdU experiment protocol upon TERT induction in mice. Wild-type (*n=4*), i-TERT^{ci} (*n=4*), pX$^{-/-}$ (*n=4*) and i-TERT^{ci};pX$^{-/-}$ (*n=4*) mice were simultaneously treated with Doxycycline and EdU in the drinking water for 17 days. **(B)** Immunostaining for EdU (yellow), a thymidine analog, showing significant inhibition of TERT^{ci}-induced cell proliferation upon pX deficency in TERT^{ci}–overexpressing mice. Glomeruli are pointed out by yellow dashed circles. **(C)** Quantitative analysis of data in (B) showing the percentage of glomeruli with EdU-positive cells in each group of mice. Data are represented as mean ± SEM.

4. Defects in TERT^{ci} non-canonical functions when pX is knocked-out is not due to Wnt signaling pathway inhibition

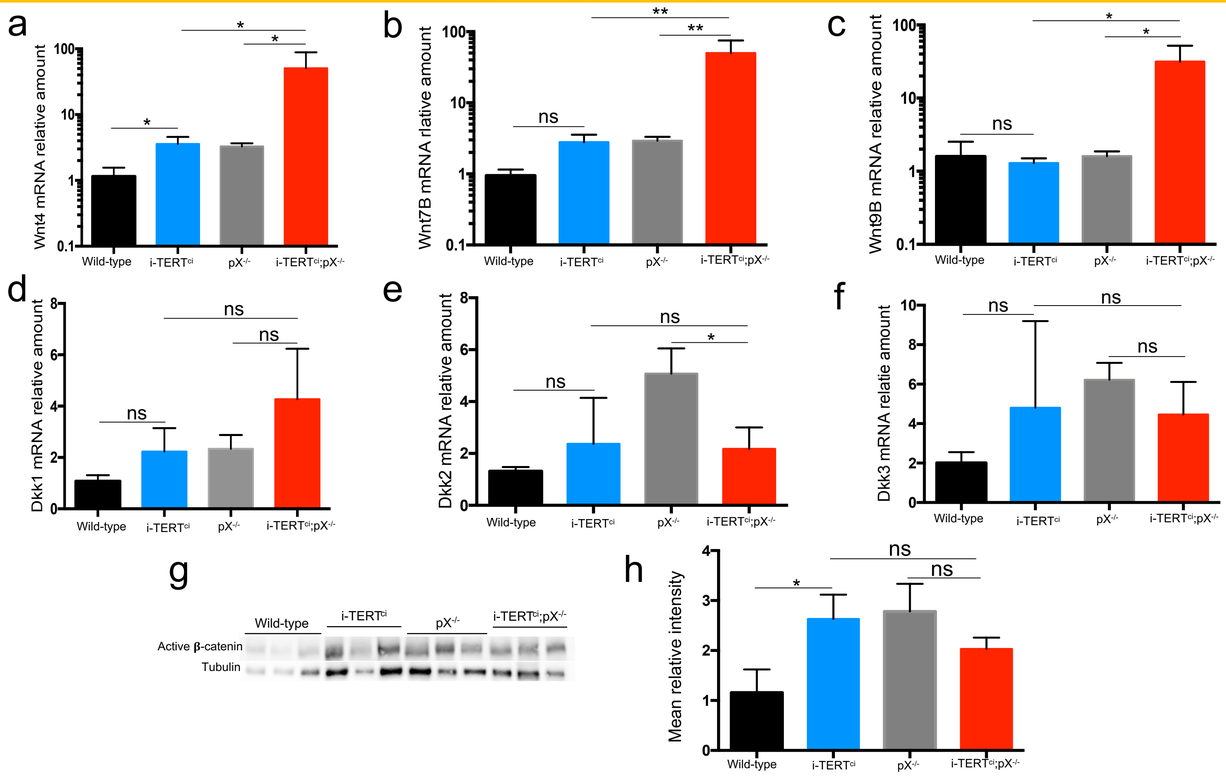

Figure 4 : Defect in TERT ability to promote glomerular cell proliferation is not due to Wnt signaling pathway inhibition. (A-C) Wnt agonists, Wnt4, Wnt7B and Wnt9B, mRNA levels by qRT-PCR in whole kidneys from wild-type (*n=4*), i-TERT^{ci} (*n=4*), pX$^{-/-}$ (*n=4*), and i-TERT^{ci};pX$^{-/-}$ (*n=4*) mice treated with Doxycycline for 17 days, showing that pX deletion is associated with significant up-regulation of Wnt agonists in the kidneys of mice upon TERT^{ci} overexpression. Data are represented as mean ± SEM. **(D-F)** qRT-PCR analysis for Wnt antagonist Dkk1, Dkk2 and Dkk3 in kidneys from wild-type (*n=4*), i-TERT^{ci} (*n=4*), pX$^{-/-}$ (*n=4*), and i-TERT^{ci};pX$^{-/-}$ (*n=4*) mice treated with Doxycycline and EdU during 17 days, showing a trend for Dkk1 up-regulation in kidneys of i-TERT^{ci};pX$^{-/-}$ mice. Data are represented as mean ± SEM. **(G)** Western-blot for active **β**-catenin (ABC), the central player of Wnt signaling, in kidneys from mice treated with Doxycycline for 17 days, showing an up-regulation of active **β**-catenin in i-TERT^{ci};pX$^{-/-}$ compared to wild-type mice. **(H)** Quantification of data in (G). Data are represented as mean ± SEM.

5. pX deficiency activates the DNA damage response pathway upon TERT^{ci} overexpression

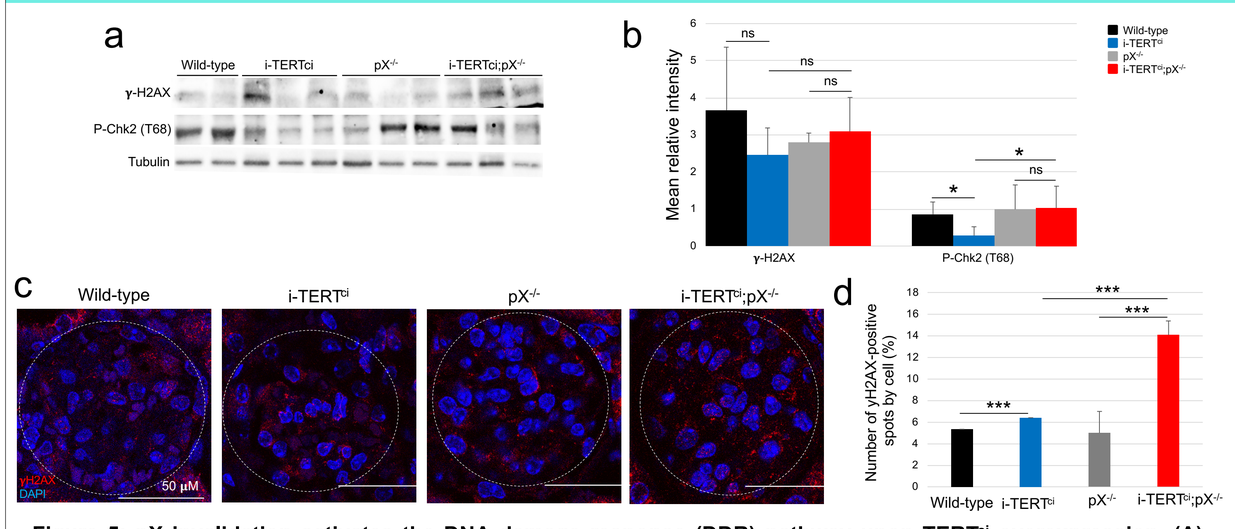

Figure 5: pX invalidation activates the DNA damage response (DDR) pathway upon TERT^{ci} overexpression. (A) Western blotting for DDR components on kidney from mice treated with Doxycycline for 17 days. **(B)** Quantification of data in (A). Data are represented as mean ± SEM. **(C)** Immunohistochemistry for **γ**-H2AX (red) in glomeruli (white dashed circles) from wild-type, i-TERT^{ci}, pX$^{-/-}$ and i-TERT^{ci};pX$^{-/-}$ mice treated with Doxycycline for 17 days. **(D)** Quantification of data in (C). Data are represented as mean ± SEM.

6. pX deficiency promotes the senescence process upon TERT^{ci} overexpression

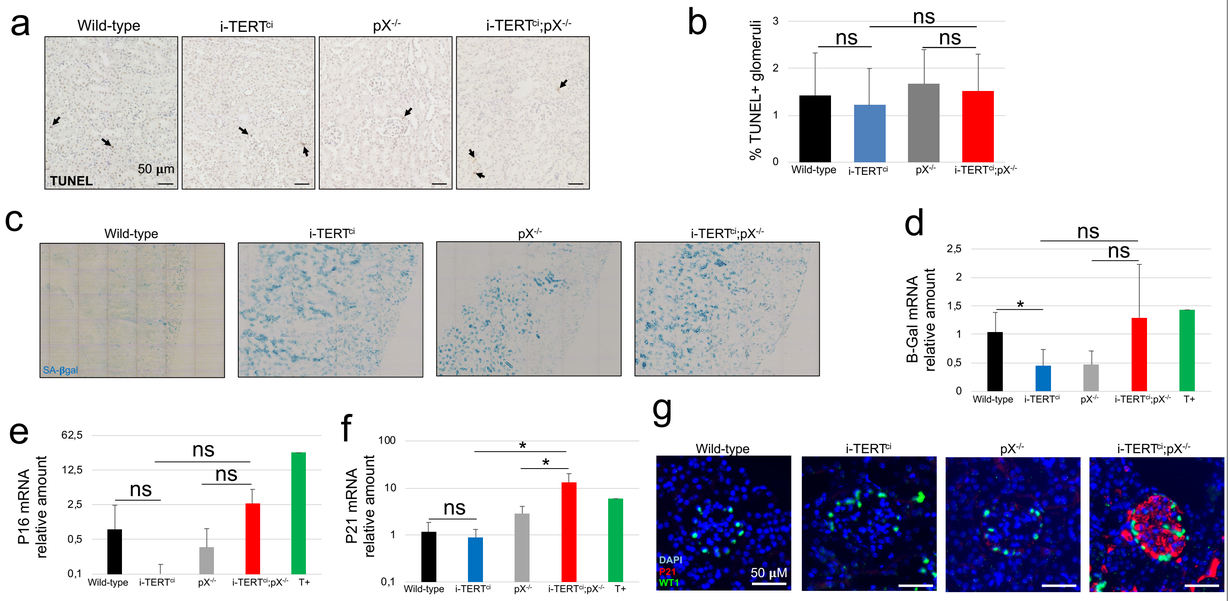

Figure 6: Exacerbation of the DDR upon TERT^{ci} overexpression when pX is deleted doesn't lead to apoptosis but rather promotes senescence through p21 activation. (A) TUNEL assay of kidneys sections from wild-type, i-TERT^{ci}, pX$^{-/-}$ and i-TERT^{ci};pX$^{-/-}$ mice treated with doxycycline for 17 days. **(B)** Quantification of data in (A). Data are represented as mean ± SD. **(C)** SA-**β**galactosidase staining in whole kidney from wild-type, i-TERT^{ci}, pX$^{-/-}$ and i-TERT^{ci};pX$^{-/-}$ mice treated with doxycycline for 17 days. **(D)** **β**galactosidase mRNA levels by qRT-PCR in whole kidneys from wild-type (*n=4*), i-TERT^{ci} (*n=4*), pX$^{-/-}$ (*n=4*) and i-TERT^{ci};pX$^{-/-}$ (*n=4*) mice treated with doxycycline for 17 days. Data are represented as mean ± SEM. T+ is a 2-years old mouse. **(E)** p16 mRNA levels by qRT-PCR in whole kidneys from wild-type (*n=4*), i-TERT^{ci} (*n=4*), pX$^{-/-}$ (*n=4*) and i-TERT^{ci};pX$^{-/-}$ (*n=4*) mice treated with doxycycline for 17 days. Data are represented as mean ± SEM. **(F)** p21 mRNA levels by qRT-PCR in whole kidneys from wild-type (*n=4*), i-TERT^{ci} (*n=4*), pX$^{-/-}$ (*n=4*) and i-TERT^{ci};pX$^{-/-}$ (*n=4*) mice treated with doxycycline for 17 days. Data are represented as mean ± SEM. **(G)** Immunohistochemistry for p21 (red) and WT1 (green), a marker of glomerular podocytes in wild-type, i-TERT^{ci}, pX$^{-/-}$ and i-TERT^{ci};pX$^{-/-}$ mice treated with doxycycline for 17 days.

Conclusion

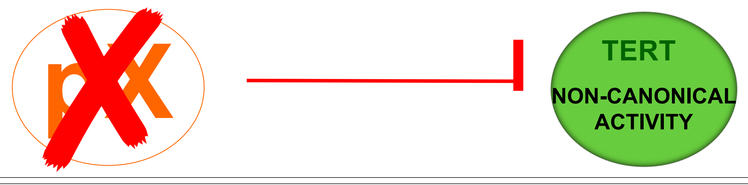

Perspectives

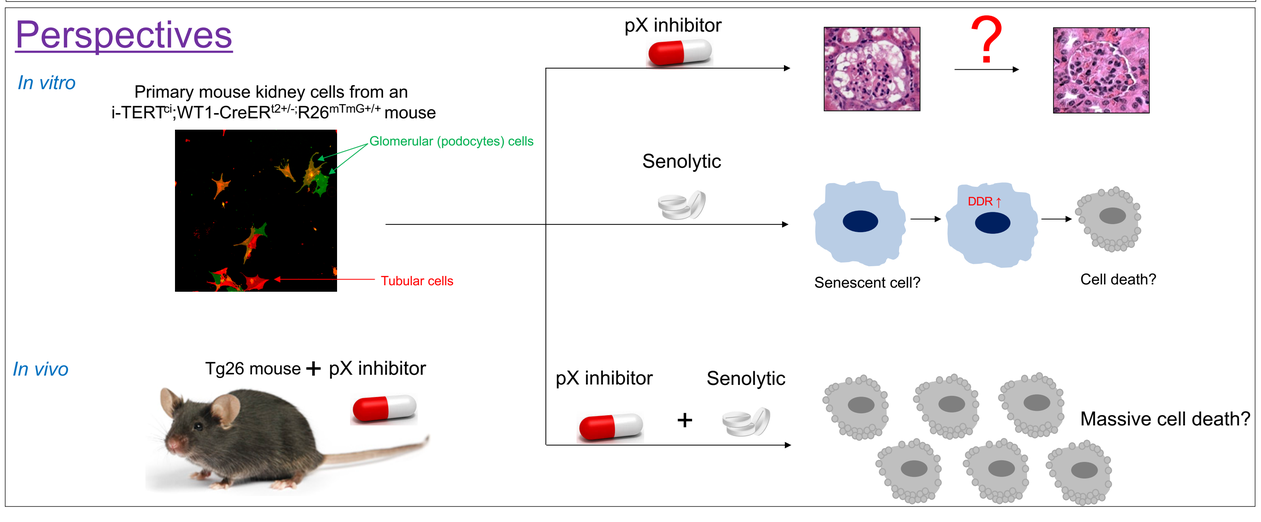

shallowHRD: detection of Homologous Recombination Deficiency from shallow Whole Genome Sequencing

Alexandre Eeckhoutte[1], Alexandre Houy[1], Elodie Manié[1], Manon Reverdy[1], Ivan Bièche[2], Elisabetta Marangoni[2], Oumou Goundiam[2], Anne Vincent-Salomon[3], Dominique Stoppa-Lyonnet[3], François-Clément Bidard[1,3], Marc-Henri Stern[1], Tatiana Popova[1]

[1] Research Department ; [2] Department of Translational Research ; [3] Hospital ; Institut Curie

Introduction & Method

GOAL: Detect if a tumor is deficient in Homologous Recombination with a cheap DNA sequencing method called shallow Whole Genome Sequencing

Inactivation of **Homologous Recombination** (**HR**) **genes** repairing DNA Double Strand Break

=

BRCA1, ***BRCA2***, ***RAD51C*** & *PALB2*

↓ **Genomic instability**

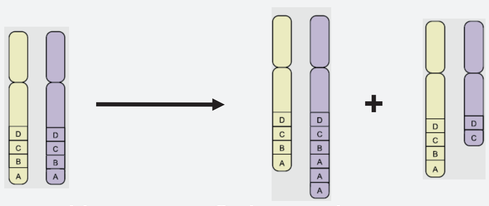

Numerous Gains and Losses in Copy Number

↓ **Tumorigenesis**

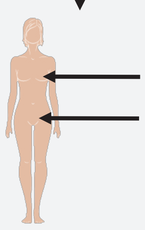

Breast cancer

Ovarian cancer

↓ **Existing treatments for HR Deficiency**

PARP inhibitors, platinum therapy....

Large-scale **signature** of **H**omologous **R**ecombination **D**eficiency (**HRD**) based on its **characteristic** genomic profile

Signature of **HRD** developed first on **SNParray**

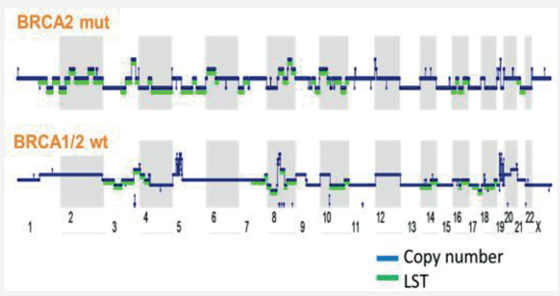

LST = Chromosomal break of adjacent region of at least 10 Mb in the same chromosomal arm

↓

HRD can be distinguished by an higher level of large chromosomal break (**LST**s)

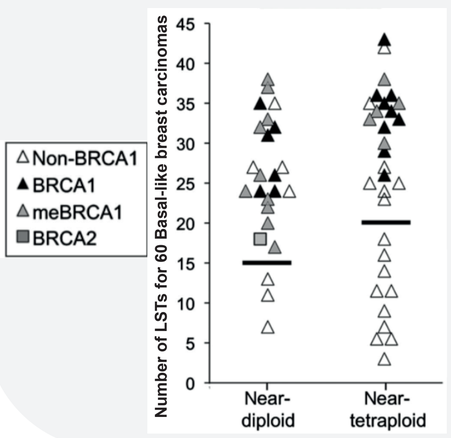

Homologous **R**ecombination **D**eficiency

No **HRD**

Popova et al., 2014

Shallow Whole Genome Sequencing (**sWGS**) to establish and optimize a genomic profile and call **L**arge-scale **G**enomic **A**berrations (**LGA**s)

sWGS = **Cheap DNA sequencing method** where the **entire genome** is covered in average by less than one small DNA copy - called **reads** - for each of its nucleotides

Method:

1. Counts reads in fixed windows of 20kb along the genome (**black dot**)

↓ 1

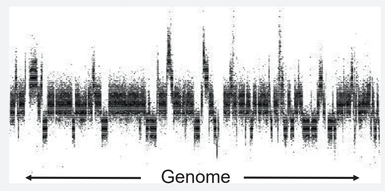

2 →

2. Correct read count biases (GCcontent & mappability) for each window and **normalize** it

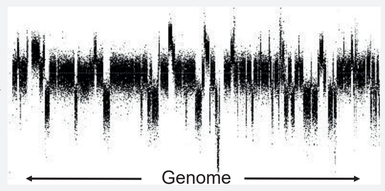

3 ↓

3. Separate in equivalent **segments** (in **red**) the genomic profile

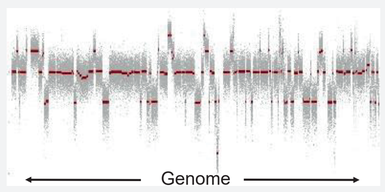

← 4

4. Determination of a **relative Copy Number difference cut-off** used to **optimize the profile**

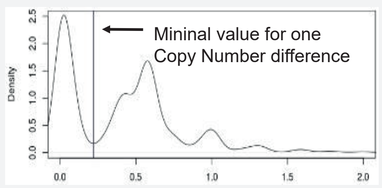

↓ 5

5. Call **LGA**s (in **green**) on the optimized genomic profile

LGA is the equivalent of LST but based on **sWGS** and relying on a **relative Copy Number difference cut-off**

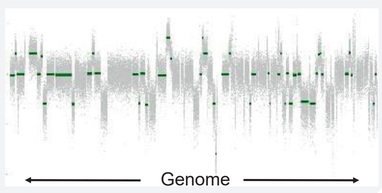

Results

Comparison of LGA in sWGS to the "gold standard" LSTs in SNParray

A **excellent correlation** can be found between the number of **LGA**s and **LST**s for 79 downsampled WGS of The Cancer Genome Atlas-breast cases

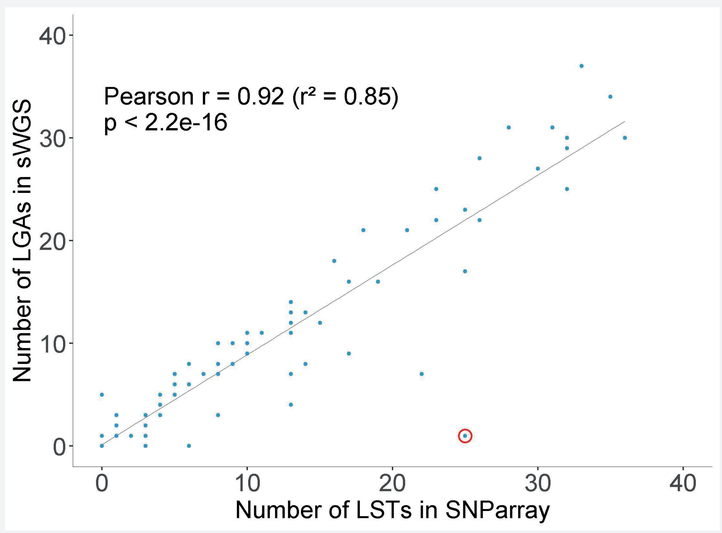

Outlier case circled = Tumor proficient for Homologous Recombination with a high number of copy-neutral LOH not counted in sWGS

Performance of shallowHRD and comparison to other methods

- shallowHRD has a sensitivity of 87.5% and a specificity of 90.5% which is **comparable with other state-of-the-art approaches** (see Figure and Table below)
- **Borderline** classification bring attention to low confidence calls, because the **ploidy** used in SNParray to diagnose HR is **problematic to infer in sWGS**

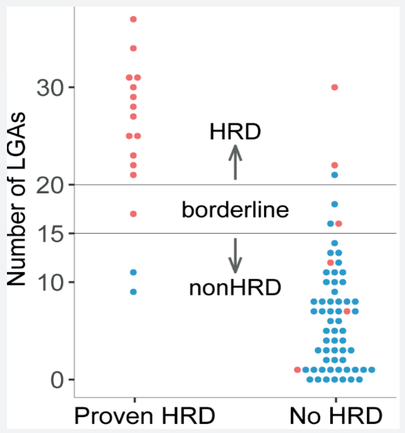

Blue points: TCGA cases classified as proficient for HR with SNParray
Red points: TCGA cases classified as deficient for HR with SNParray

Technique	Method	Sensitivity	Specificity
WGS	HRDectect	99	99
WGS/WES	Signature 3	84	90
WES/gene panel	SigMA	74	90
WES	scarHRD	87.5	61.4*
SNParray	LST	99	54*
sWGS	shallowHRD	87.5	90.5

* : Specificity as indicated in the related publications
Low value largely due to lack of HRD annotation
SNParray: Close to shallowHRD (**blue** and **red** points)
scarHRD: No *RAD51C* promoter methylation assessment

Conclusion & perspectives

shallowHRD implements an efficient procedure while having several **advantages**:

1. **Cheap** ~150 €
2. Suited also for **F**ormalin-**F**ixed **P**araffin-**E**mbedded (**FFPE**) samples
3. **Don't require germline** sequencing
4. Storable **light data**
5. **Sequencing diagnosis implemented**

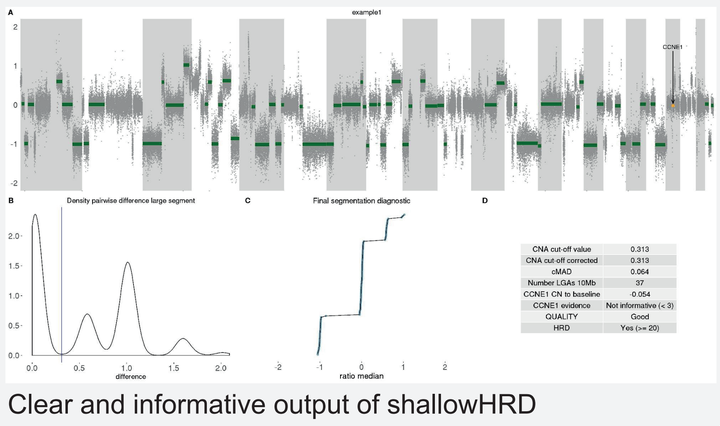

Clear and informative output of shallowHRD

shallowHRD **applied routinely in clinics** for ovarian tumors in **Institut Curie**

Same sequencing library (Lower cost)

sWGS & shallowHRD + Targeted gene panel sequencing

↓

Both genes **and** genomic profile information on HRD

This work was supported by the Ligue Nationale contre le Cancer that is financing Alexandre Eeckhoutte PhD thesis

References

shallowHRD : Eeckhoutte et al, 2020 ; LST-SNParray : Popova et al, 2014 ; HRDetect : Davies et al., 2017 ; Signature3 : Gulhan et al., 2019 ; SigMA : Polak et al., 2017 ; scarHRD : Sztupinszki et al., 2018

Synchrotron Microbeam Radiation Therapy increases the therapeutic ratio for brain tumor treatment.

L. Eling[1], A. Bouchet[1], A Ocadiz[1], J.F. Adam[1], Sarvenaz Kershmiri[1], H. Elleaume[1], M. Krisch[2], C. Verry[3], J.A. Laissue[4], J. Balosso[5], R. Serduc[1]
[1]Synchrotron Radiation for Biomedicine, INSERM UA7, Grenoble, France [2]ESRF, Grenoble, France [3]Grenoble University Hospital, Grenoble, France
[4]University of Bern, Switzerland [5]CRLCC Francois Baclesse, Caen, France

Introduction

Intracerebral tumors

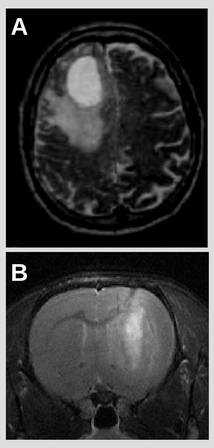

T_2w MRI of a glioblastoma.
A – Human brain tumor.
B – Rat 9L glioblastoma model.

Radiotherapy (RT) represents the most effective treatment for **glioblastoma** but it often leads to severe side effects due to damage of normal tissues. New irradiation protocols are therefore in need [1].

Microbeam Radiation Therapy (MRT) allows the generation of e.g. 50 µm wide, parallel X-ray beams, deposing a **peak dose** of up to 1000 Gy into the microbeam paths. The **valley dose**, diffusing in-between the beams, consists of only ~5 % of the peak dose.

ESRF in Grenoble, France

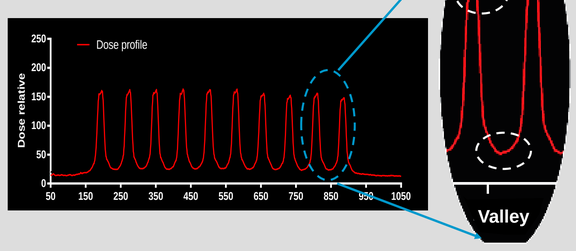

Dose profile of peak and valley doses.

Synchrotron RT

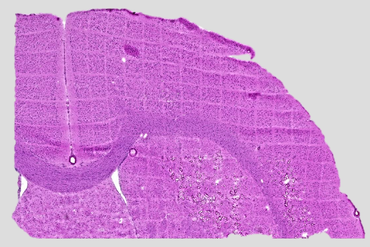

Cell loss in microbeam paths, 12 months post MRT. [Eling 2020, unpublished]

A remarkable **tolerance of normal tissue** has been shown [2] while MRT has a preferential effect on tumor vessels leading to **tumor asphyxia and necrosis** [3].

Material and Method

How to optimize MRT protocols?

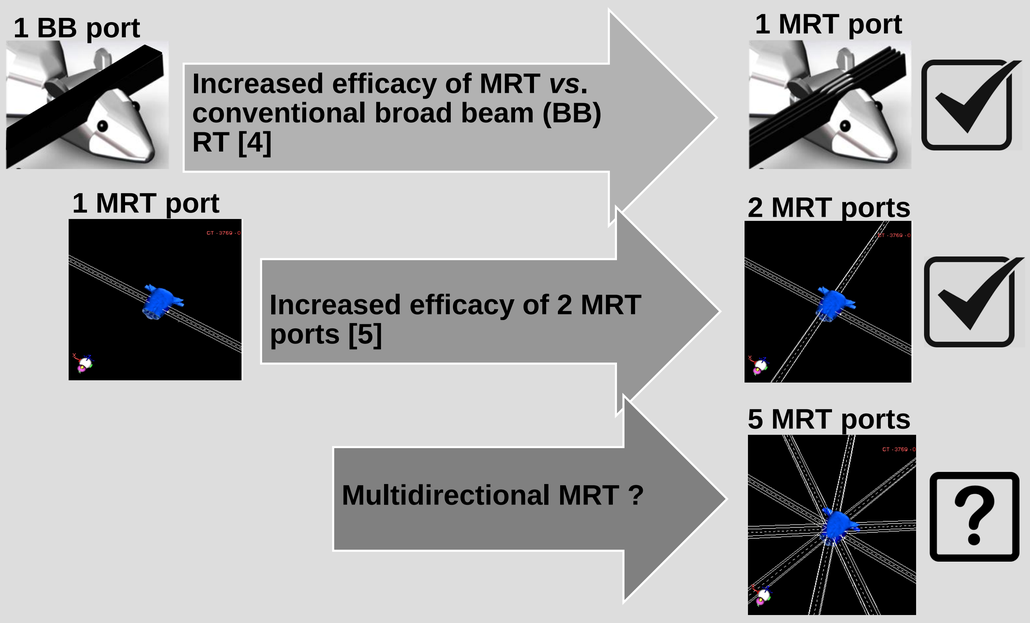

<u>Normal tissue toxicity</u>: Normal Fischer rats (n=34) were irradiated with 2 and 5 MRT ports (MRT2/5, 10 Gy cumulated valley dose), crossed BB (BB2, 10 Gy) or left untreated. We tested for **behavioral** deficits during one year, combined with **MRI** and **histologic analysis**.

<u>Tumor study</u>: Male Fischer rats (n=160) bearing **9L gliosarcoma** were irradiated ten days after implantation (T0) with MRT1-5 (10 Gy valley dose), BB2 (10 Gy) or left untreated. We analyzed **tumor volume**, **survival** and **histologic sections**.

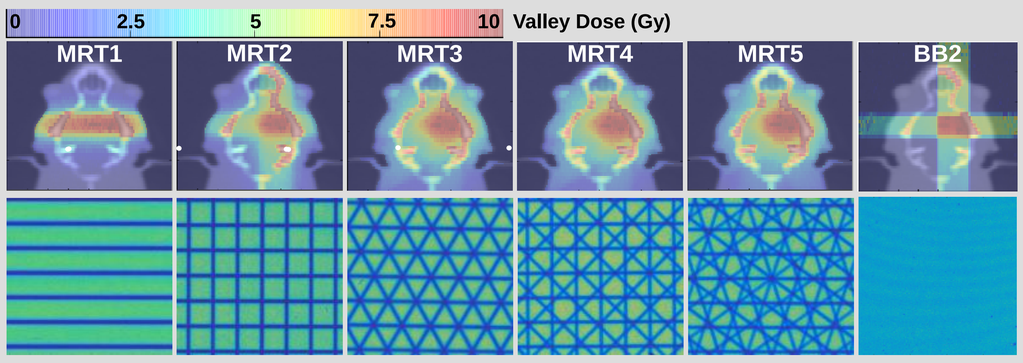

TPS dose maps (top) and radiochromic film (bottom) of the irradiation configurations in MRT mode (1 to 5 incidences) and crossed BB.

Results

Multi-port MRT modifies normal rat locomotion …

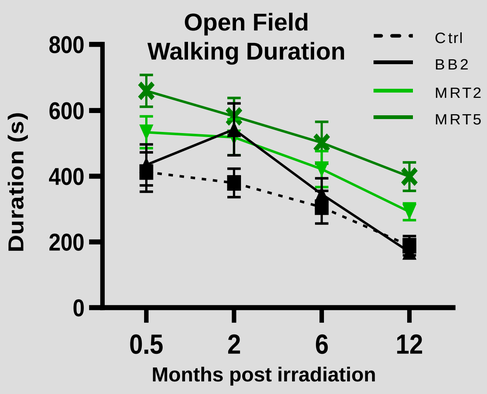

Behavioral testing of normal irradiated rats. **Increased locomotor activity** in MRT treated animals.

… BUT extends survival of tumor-bearing rats …

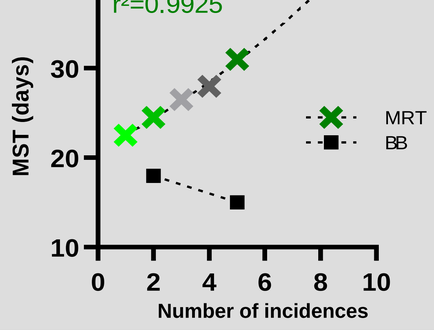

Median Survival Time (MST) of tumor-bearing rats increased exponentionally after multidirectional MRT **(35 days)** compared with BB2 **(18 days).**

… AND increases tumor control.

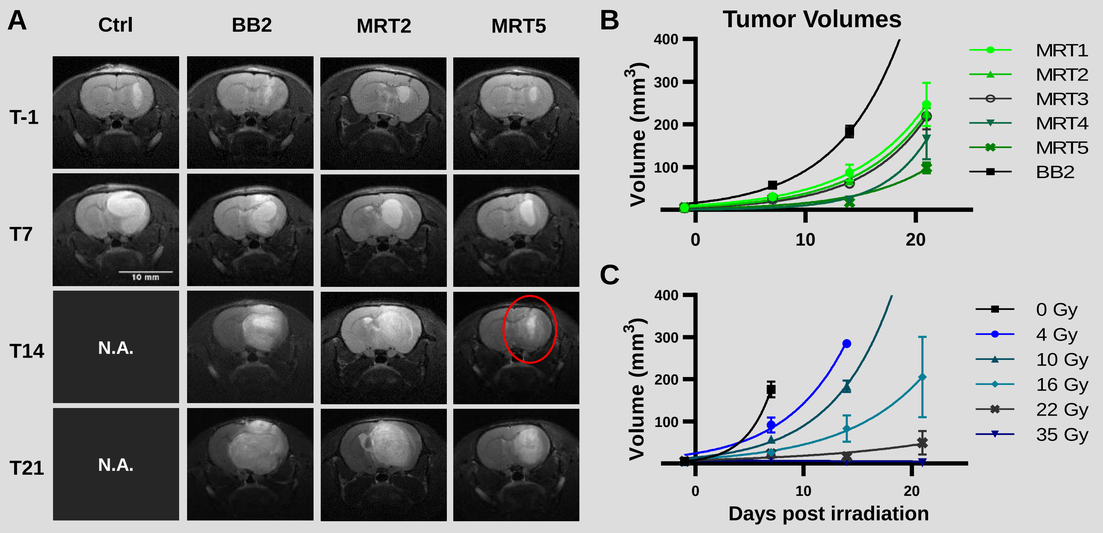

A – MR images of brain tumor-bearing rats: controls, irradiated with crossed BB or MRT2/5.
B – Tumor volumes after multiport MRT. At T14, tumors were **10.6 times smaller after MRT5** than after BB2.
C – Reference tumor-dose response after conventional crossed BB therapy.

Determination of equivalent doses

Survival Log-Rank tests comparisons (*p* values)								
	MST	**EquiED (Gy)**	**MRT1**	**MRT2**	**MRT3**	**MRT4**	**MRT5**	**BB2**
Ctrl	10.5	**0**	**0,003**	**0,003**	**0,049**	**0,001**	**0,001**	**0,001**
MRT1	22.5	**14.5**		0,27	0,24	**0,025**	0,06	0,10
MRT2	24.5	**16.9**			0,56	0,11	0,14	**0,049**
MRT3	26.5	**19.3**				0,22	0,13	*0,09*
MRT4	28	**20.9**					0,84	**0,001**
MRT5	31	**23.8**						**0,005**
BB5	16	**6.5**						0,18

Survival summary (MST), biological equi-effective doses (EquiED) and Log-Rank tests comparisons between groups. A 10 Gy valley dose with 5 MRT ports was equivalent to ~24 Gy crossed BB therapy.

Conclusions

✓MRT modifies anxiety-like behavior and leads to moderate **hyperactivity**
✓Multidirectional MRT (↑ cumulated volume of peak doses) → **greater tumor control and exponentially increasing animal survival**
✓**EquiED was increased by x2.4 using 5 MRT ports** compared with BB2
✓Dose reduction per incidence → **preservation of normal brain tissues**
✓**Prescription of MRT valley doses and number of ports** with equivalence to standard BB doses → **advancement towards clinical trials**

✓**Biological mechanisms?** V**ascular and immunological responses ?**

References

[1] Kazda T et al. 2018, Radiol. Oncol. 52(2):121-8.
[2] Serduc R et al. 2006, Int. J. Radiat. Oncol. Biol. Phys. 64:1519-27.
[3] Bouchet A et al. 2013, Radiother. Oncol. 108:143-8.
[4] Bouchet A et al. 2016, Int. J. Radiat. Oncol. Biol. Phys. 95(5):1485-94.
[5] Laissue J et al. 1998, Int. J. Cancer 78:654-60.

Acknowledgements

- Team STROBE INSERM UA7 – S. Bayat, E. Bräuer-Krisch…
- La Ligue Contre le Cancer
- INCA / LABEX PRIMES / ARC
- Université Grenoble-Alpes / EDISCE

Contribution of resident and circulating precursors to tumor-infiltrating CD8+ T cell populations in non-small cell lung cancer patients

Paul Gueguen[1,2], Christina Metoikidou[1,2], Thomas Dupic[7], Myriam Lawand[1,2], Christel Goudot[1,2], Sylvain Baulande[1], Sonia Lameiras[1], Olivier Lantz[1,2], Nicolas Girard[5], Agathe Seguin-Guivelet[5], Marine Lefevre[5], Aleksandra Walczak[6], Thierry Mora[6] Josh Waterfall[1,3,4], Sebastian Amigorena[1,2]

1-Institut Curie, PSL Research University, F-75005 Paris, France.
2-INSERM U932, F-75005, Paris, France.
3-Institut Curie, Translational Research Department, F-75005 Paris, France.
4-France INSERM U830, F-75005 Paris, France.
5-Institut du Thorax Curie - Montsouris, F-75014 Paris, France.
6-Laboratoire de physique de l'École normale supérieure, F-75005 Paris, France
7 - .Department of Organismic and Evolutionary Biology, Harvard University, Cambridge, MA, USA

Contact : paul.gueguen@curie.fr

Introduction

T cells inside tumors express high levels of inhibitory receptors and become hyporesponsive (called **dysfunctional** or exhausted), losing their cytotoxic activity.

In order to improve patient stratification and to identify novel candidate therapeutic targets it is necessary to improve our fundamental understanding of **T cell differentiation** in human cancer patients. Recent technological advances have provided important insights into the heterogeneity and programming of hyporesponsive T cell populations in chronic infection and cancer. It has become clear that **distinct T cell subsets with distinct transcriptional and epigenetic programs** and functional states harbor distinct requirements for therapeutic reprogramming.

Here we characterize at the single cell level the landscape of Tumor Infiltrating Lymphocytes (TILs) in **11 early-stage NSCLC patients in 3 tissues (tumor, juxta-tumor and blood)**, identify sub-populations based on their transcriptional profiles and better characterize their functional phenotypes (exhaustion, stemness, cycling...) as well as analyzing their **clonal expansion** using single cell TCR-Sequencing.

CD8⁺ T cell dysfunction

In **cancer** and **chronic infection**, the T cell differentiation program is compromised, and antigen-specific CD8 T cells differentiate to a hyporesponsive state generally referred to as T cell exhaustion.

Exhausted T cells are thought to be reinvigorated with checkpoint blockade.

Early / stem-like (TCF1+) exhausted T cells appear to be **more responsive** to checkpoint inhibitor therapy, which is thought to release dysfunctional cells, returning them to the cytotoxic effector state (Sade-Feldman et al. 2018).

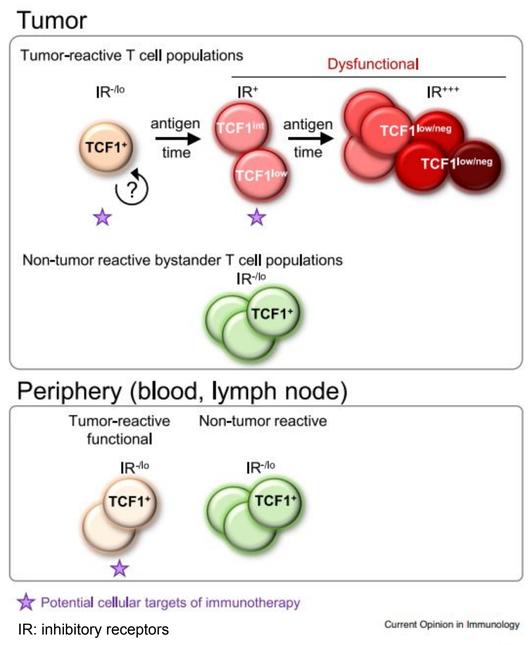

From Philip et al. 2019

Methodology

Single cell isolation workflow

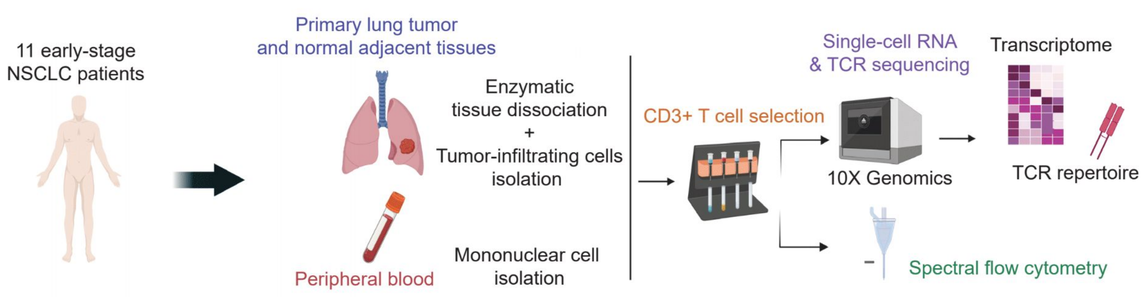

Bioinformatics workflow

- Distinguish droplets that encapsulated a cell from the empty ones using **Emptydrops** (A.Lun 2018)
- Analysis using **Seurat** (Stuart et al. 2019)
  - **~50000** single cells selected after quality control (filters on number of genes and percentage of mitochondrial genes)
  - Selection of Highly Variable Genes
  - Samples were merged using **Seurat v3 anchoring** approach to enable comparison (Stuart et al. 2019)
  - Graph-based **clustering** using Louvain Algorithm
  - Dimension reduction using PCA + **UMAP** (McInnes et al. 2018)
  - TCR analysis using custom scripts

Results

Transcriptional states of CD3+ tumor-infiltrating lymphocytes in NSCLC

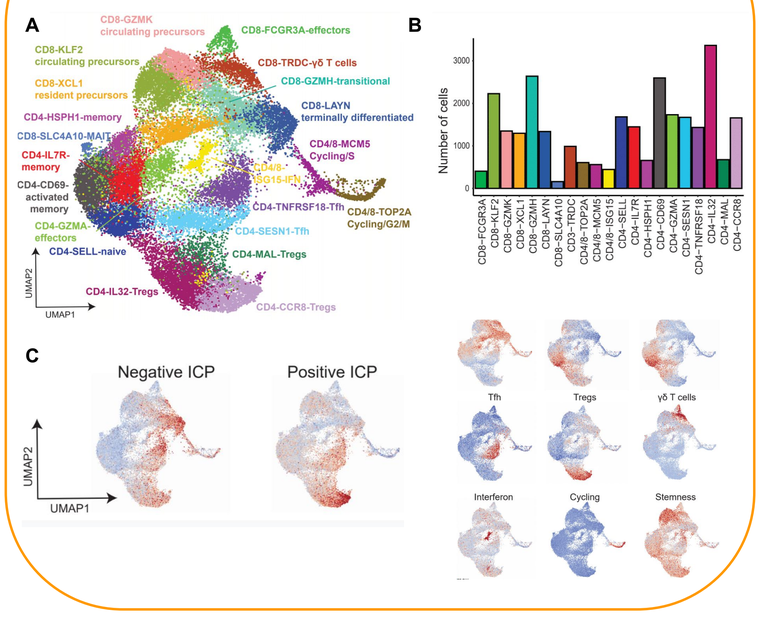

Memory-like precursors and terminally differentiated CD8+ TILs

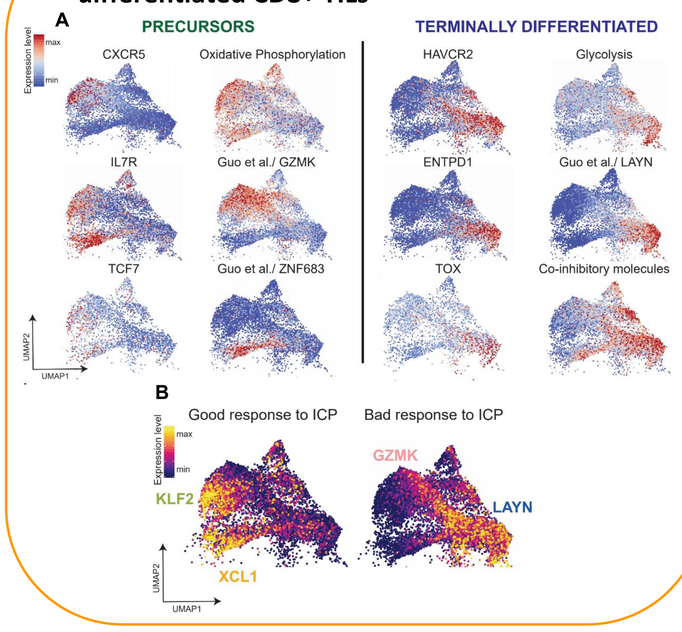

Tissue-residency features

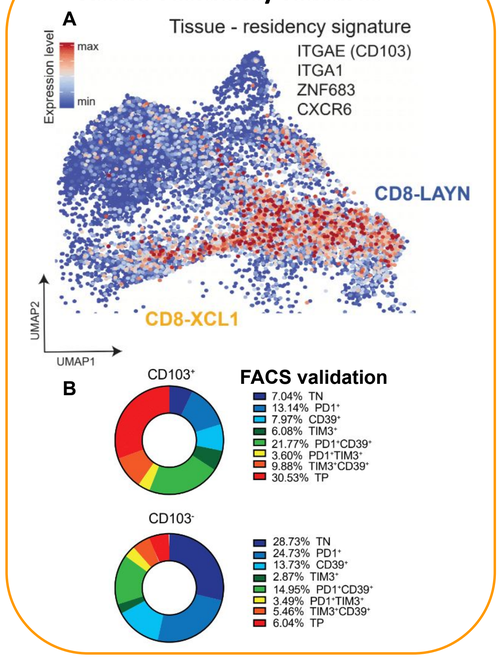

CD8-GZMH cluster is transitional state

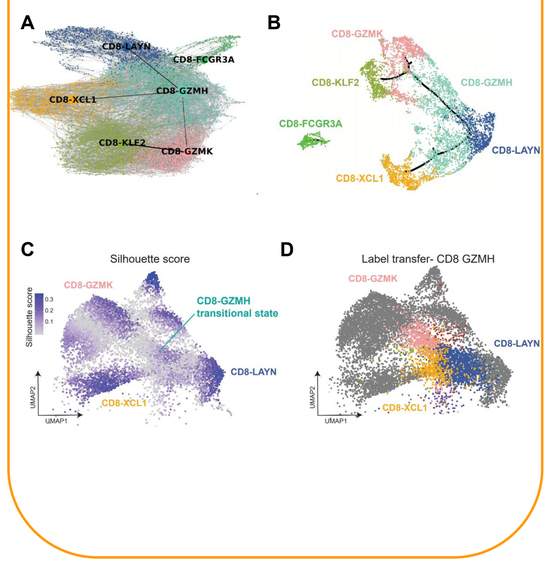

Clonal sharing between clusters informs differentiation

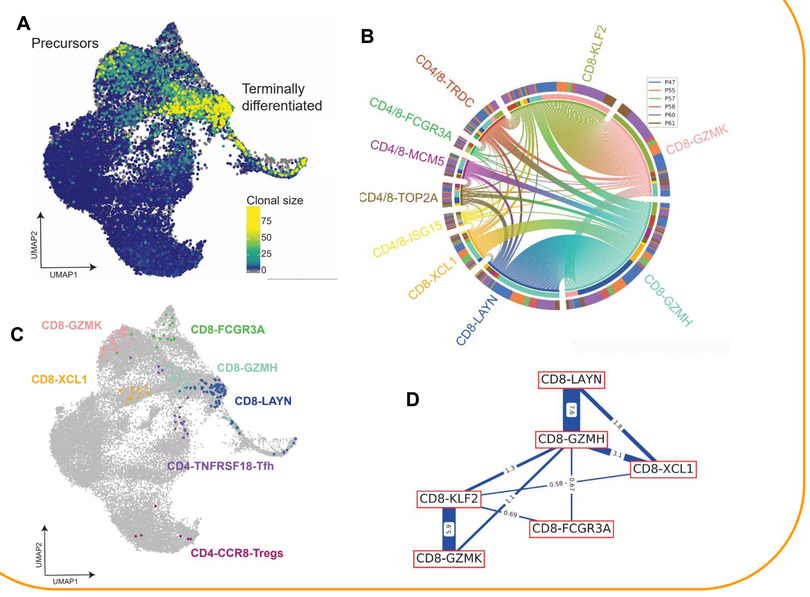

Terminally differentiated, not memory-like, CD8⁺ T cells are in cell cycle

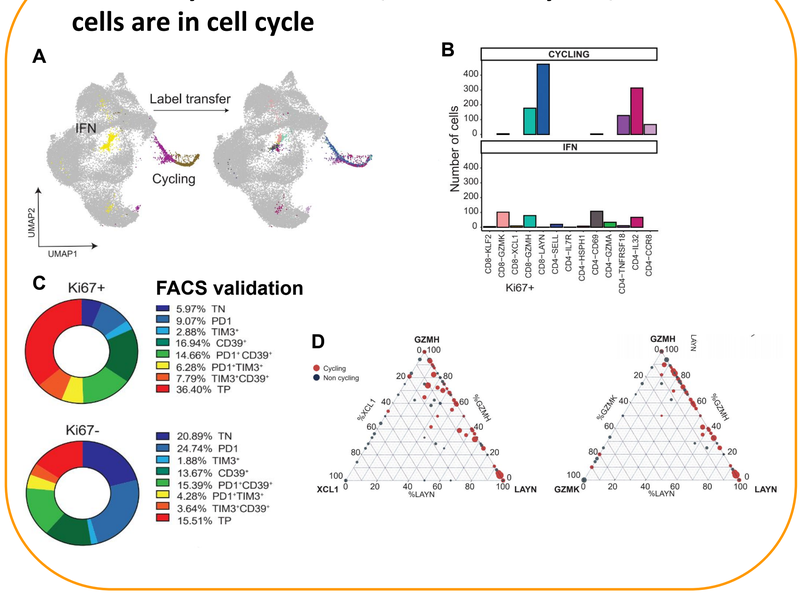

Resident versus circulating origin and tissue distribution of TILs

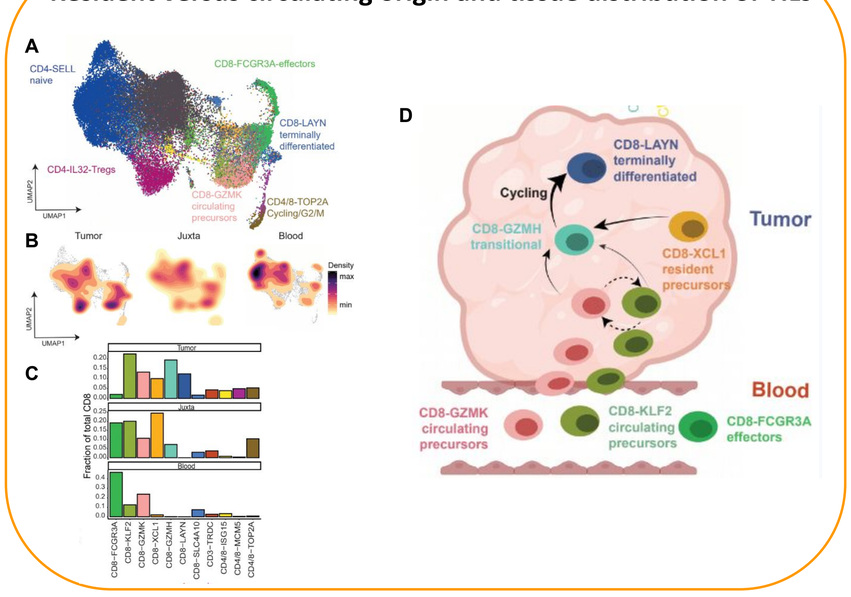

Highlights

- Analysis of more than **50K TILs** at the single cell resolution
- Building of a **patient tumor census** thanks to careful patient merging
- Definition of 2 subsets of TILs precusors, resident and circulating precusors
- CD8 LAYN correlates with a **tissue residency signature**, consistent with the clones not recirculating and accumulating in the tumor
- Clonal expansion is highly cluster specific, mainly happening in CD8 LAYN / CD8 GZMH
- Clonal sharing is able to give insights about how clusters are related
- Differentiation is associated with TCR expansion, and transition from precursor to late differentiated states correlates with intratumor **T cell cycling**
- **Coherent working model** for TIL origin, filiation and functional organization in primary NSCLC.

Rôle de PARP3 dans le cancer de la prostate

Daisy Harwood *(daisy.harwood@etu.unistra.fr)*, Françoise Dantzer

Poly(ADP-ribosyl)ation et intégrité du génome, UMR 7242, CNRS,

Institut de Recherche de l'Ecole de Biotechnologie de Strasbourg, 67412 Illkirch, France

Poly(ADP-ribose) polymérase 3 : les implications identifiées à ce jour

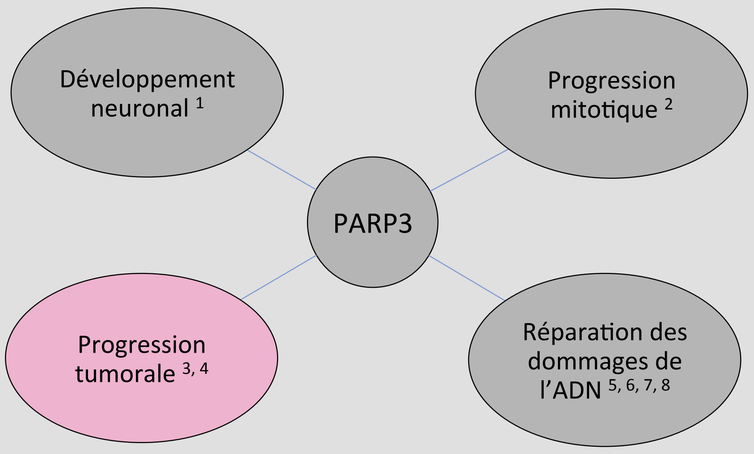

Le cancer de la prostate en France[9]

- 1er pays en Europe (incidence, 2018)
- 26% de l'ensemble des cancers masculins
- 3ème rang de décès par cancer chez l'homme

Génération de lignées de cancer de la prostate déficientes en PARP3

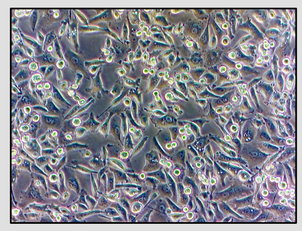

Lignée PC-3:
- Site métastatique de l'os
- Modèle « androgène-indépendant »

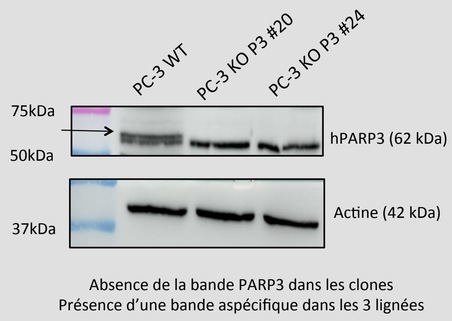

Absence de la bande PARP3 dans les clones
Présence d'une bande aspécifique dans les 3 lignées

Technologie CRISPR/Cas 9
Exon 2 – Exon 5

L'absence de PARP3 dans les PC-3 n'a pas d'impact sur la prolifération ou la mortalité cellulaire, mais induit un changement dans leur morphologie

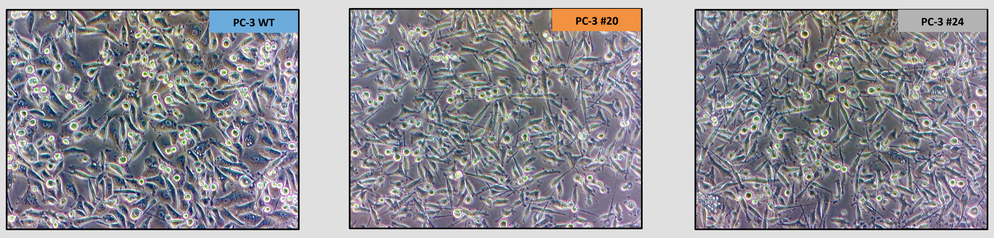

- Morphologie de type épithéliale pour les PC-3 WT
- Morphologie plus fine, allongée, avec prolongations de type neurites pour les 2 clones PC-3 KO PARP3

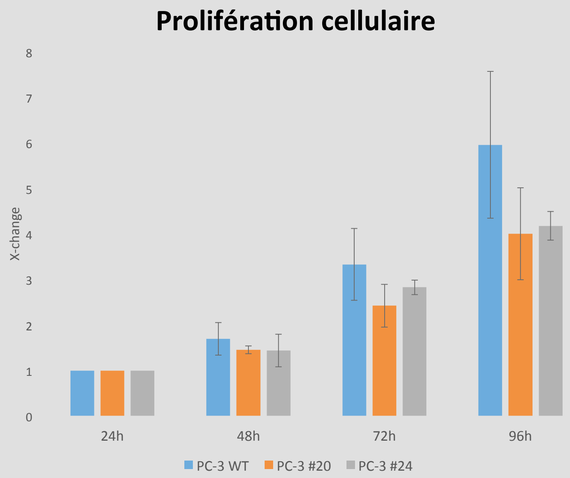

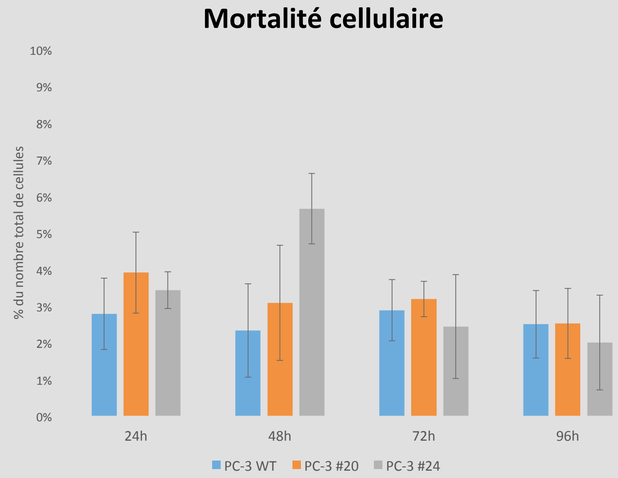

L'absence de PARP3 dans les PC-3 augmente la capacité migratoire et induit une répression de gènes codant des protéines de l'adhésion

- **Test d'évasion à partir de sphéroïdes (*hanging drop*)**

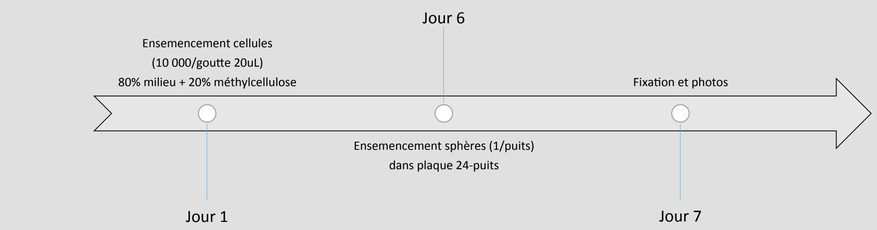

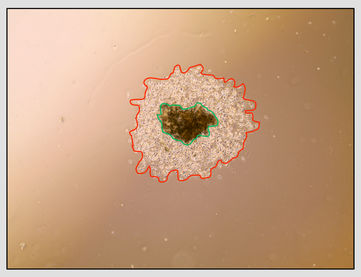

Surface totale – surface de la sphère = surface occupée par cellules ayant migré

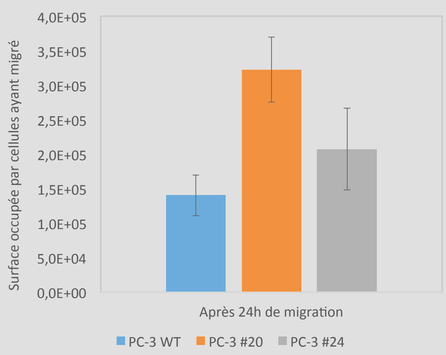

- **Perte de l'expression du marqueur épithélial E-Cadhérine**

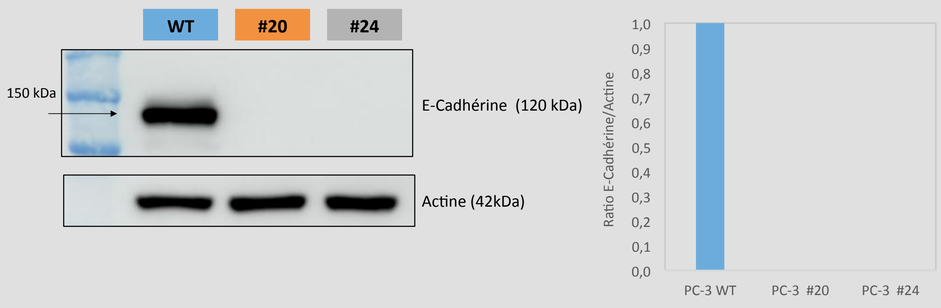

- **L'analyse transcriptomique révèle une répression de gènes codant pour des protéines de l'adhésion avec confirmation par RT-qPCR**

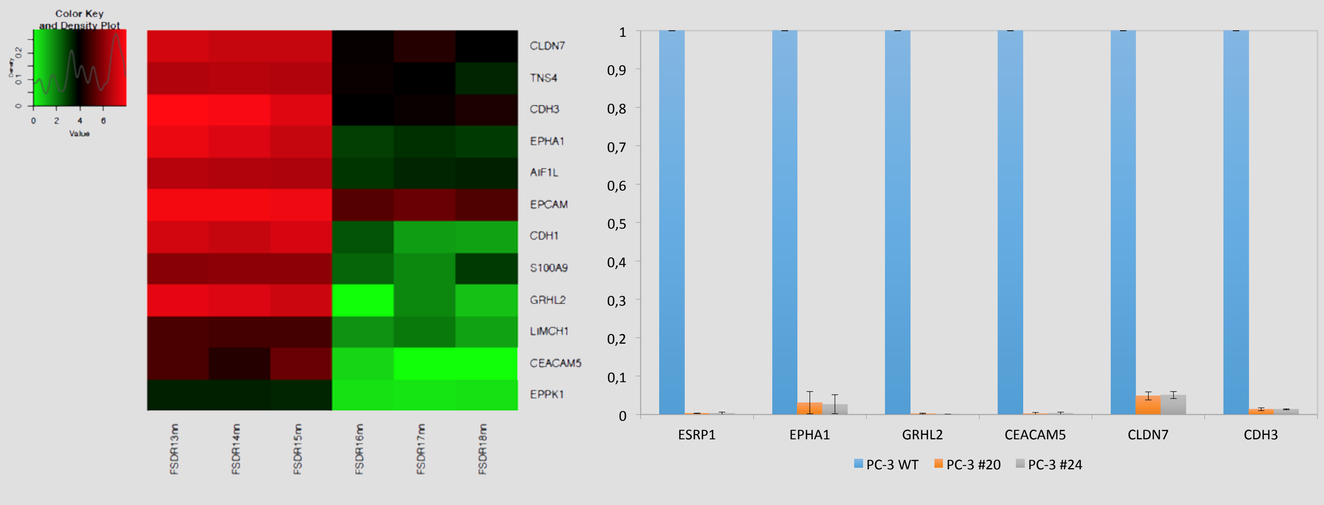

Perspectives

PARP3 freine-t-elle la progression tumorale dans la lignée PC-3 du cancer de la prostate?

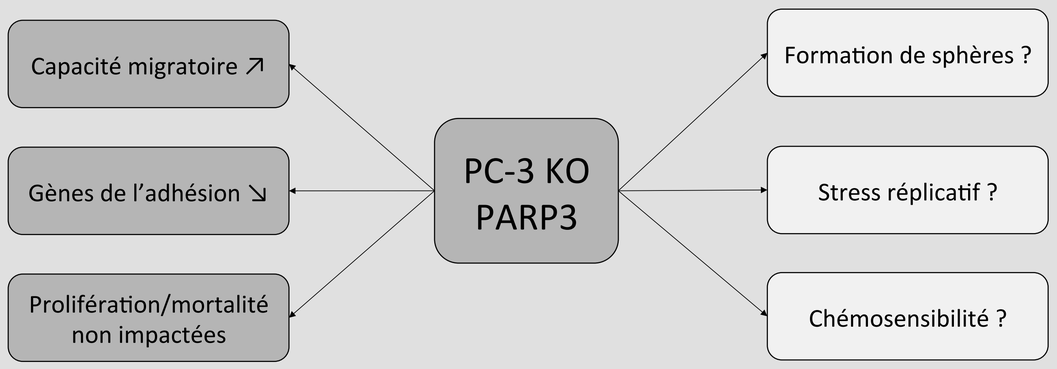

Et dans d'autres lignées de cancer de la prostate?

[1] Rouleau *et al*. **2011** PLoS One [2] Boehler *et al*. **2011** Proc Natl Acad Sci USA [3] Karicheva *et al*. **2016** Oncotarget [4] Beck *et al*. **2019** Cell Death Diff
[5] Boehler *et al*. 2011 PNAS [6] Rulten *et al*. **2011** Mol Cell [7] Day *et al*. **2017** Nat Commun [8] Beck *et al*. **2014** NAR [9] GLOBOCAN 2018 (International Agency for Research on Cancer)

Journée Jeunes & Chercheurs de La Ligue Contre le Cancer - 20/10/2020

Les antioxydants protègent les cellules souches hématopoïétiques contre la perte de leur potentiel fonctionnel lié au stress oxydant

Henry E, Picou F, Sobrino S, Barroca V, Six E, Hérault O, Pflumio F and Arcangeli ML

Laboratoire des cellules souches hématopoïétiques et leucémiques, LSHL, INSERM U1274-CEA-iRCM

Introduction

Arbre hématopoïétique humain

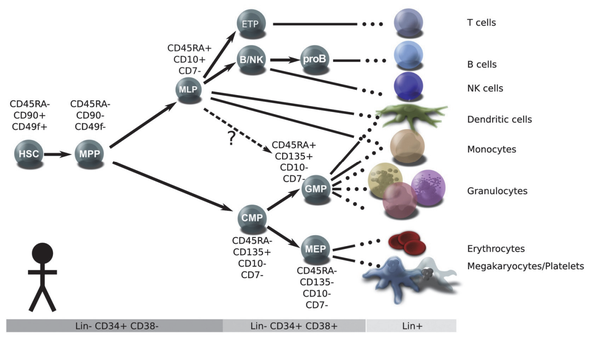

Doulatov S. et al (Cell Stem Cell, 2012)

Protocoles de thérapie génique et cellulaire

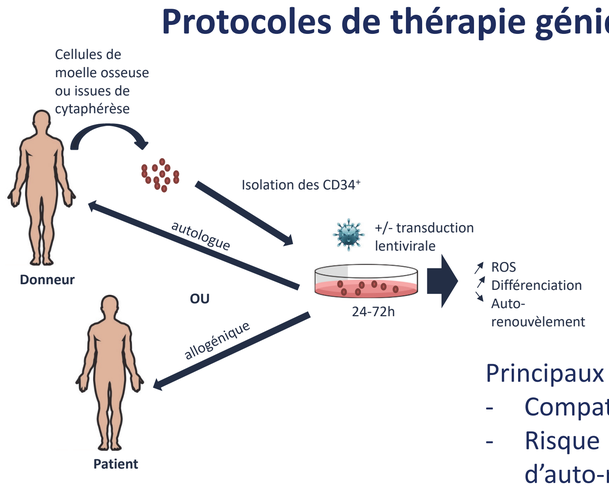

Traitement de pathologies hématologiques et immunologiques
- Leukemia
- SCID
- β-thalassemia…

Principaux défauts :
- Compatibilité donneur-patient
- Risque d'échec de la greffe à long-terme (défaut d'auto-renouvèlement des CSH)

ROS et CSH

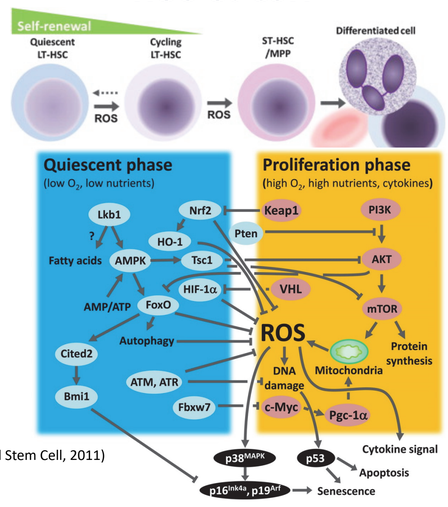

Suda T, et al (Cell Stem Cell, 2011)

Hypothèse : La réduction pharmacologique des ROS par des antioxydants pourrait permettre une meilleure prise de greffe des CSH après culture

→ Pré-traitement des cellules avant l'étape de culture

Analyse transcriptomique

Comparaison entre cellules cultivées (Jour 2) et fraîches Jour 0)

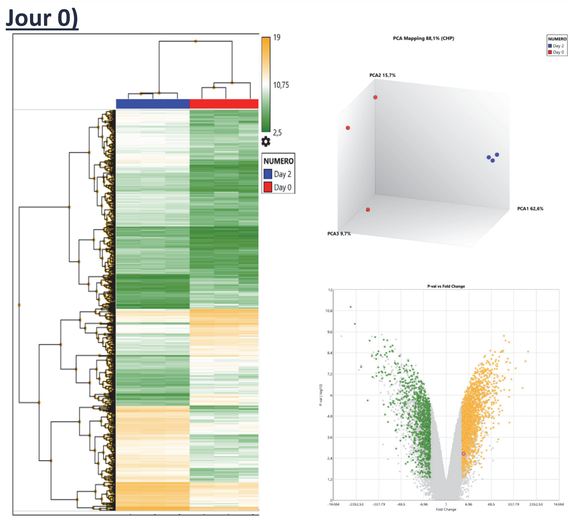

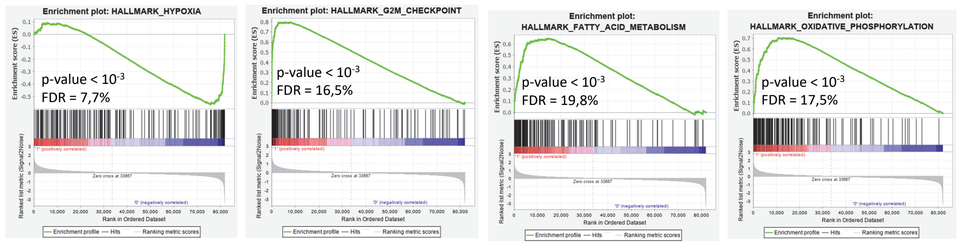

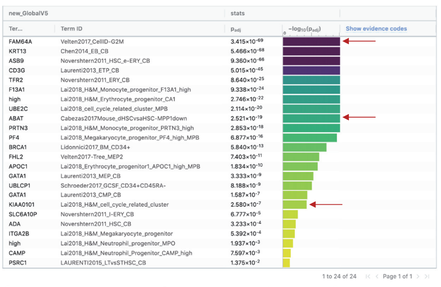

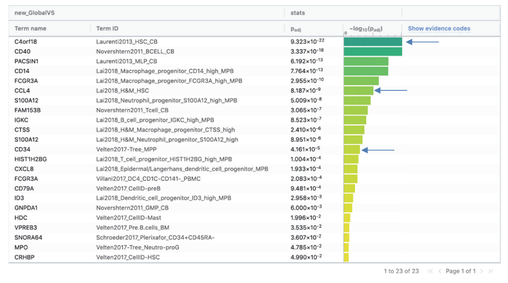

La culture induit des différences majeures dans le transcriptome des CSH, liées à la differentiation et au stress oxydant.

Amélioration de la reconstitution hématopoïétique *in vivo*

CSPH de sang de cordon
$CD34^+$ +/- NAC ou Tempol,
2h de pré-traitement

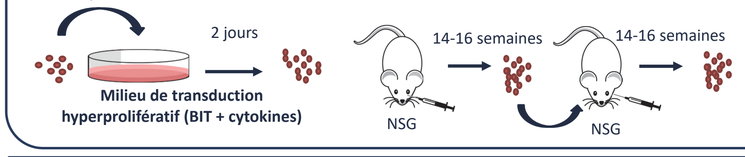

Faibles doses de $CD34^+$ (10 000 - 25 000 cellules)

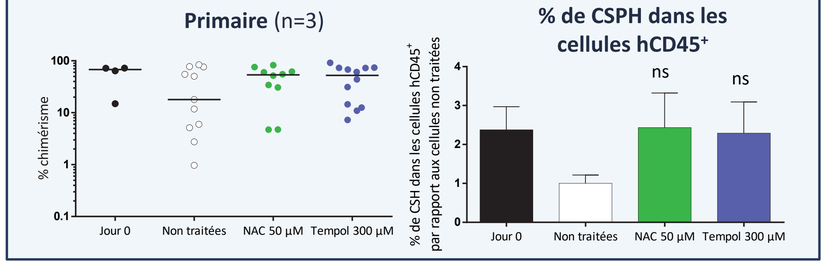

Dose saturante de $CD34^+$ (>100 000 cells)

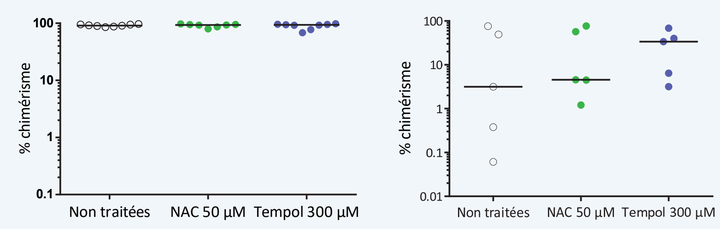

Les antioxydants améliorent les capacités de reconstitution hématopoïétique en série

Amélioration de la fonctionnalité des CSPH *in vitro*

Contrôle
NAC 50 µM
Tempol 300 µM

CSPH de sang de cordon
$CD34^+$ ($CD38^{low}$ $CD45RA^-CD90^+$)
+/- NAC ou Tempol, 2h de pré-traitement

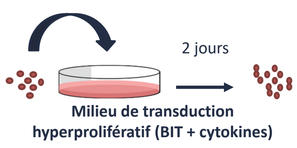

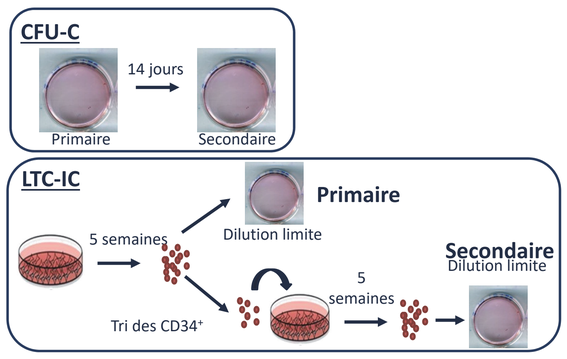

Analyse du phénotype

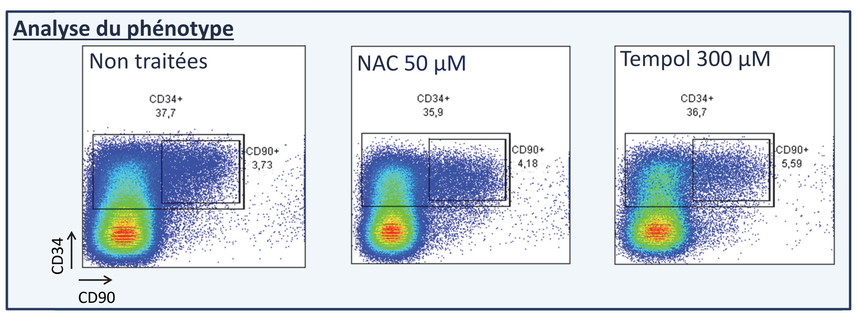

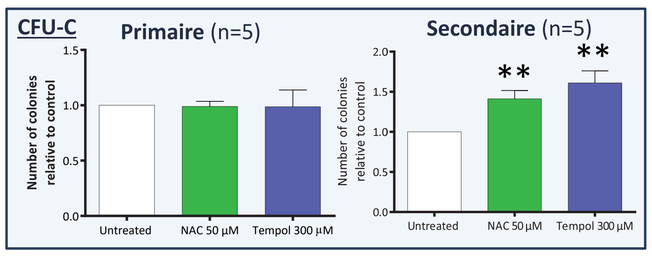

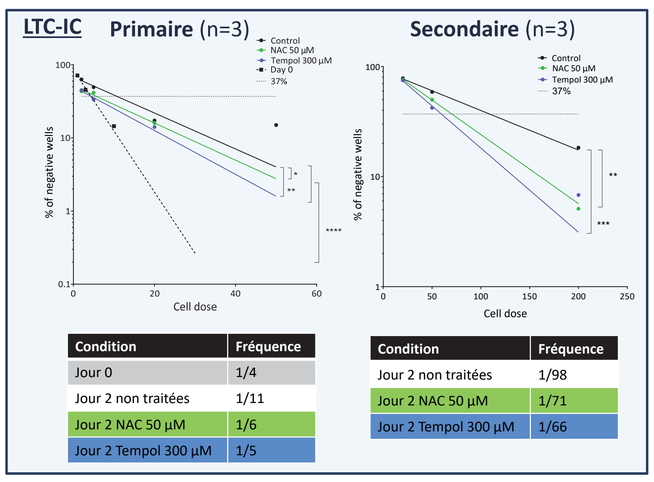

Condition	Fréquence
Jour 0	1/4
Jour 2 non traitées	1/11
Jour 2 NAC 50 µM	1/6
Jour 2 Tempol 300 µM	1/5

Condition	Fréquence
Jour 2 non traitées	1/98
Jour 2 NAC 50 µM	1/71
Jour 2 Tempol 300 µM	1/66

Les antioxydants améliorent la fonctionnalité des CSPH et préservent l'expression des marqueurs de surface

Conclusions

- ✓ NAC et Tempol améliorent les capacités fonctionnelles à long-terme des CSH *in vivo* et *in vitro*.
- ✓ Tempol permet un meilleur maintien du phenotype des CSH *in vitro* et permet de diminuer leur activité métabolique,
- ✓ La diminution des ROS corrèle avec une diminution d'activation de la voie de signalisation p38MAPK.

Les antioxydants semble maintenir voire augmenter les propriétés "souche" des CSPH en culture via la voie p38MAPK.

Mesure des ROS

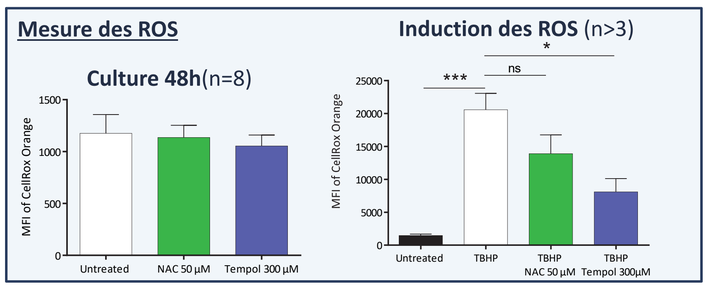

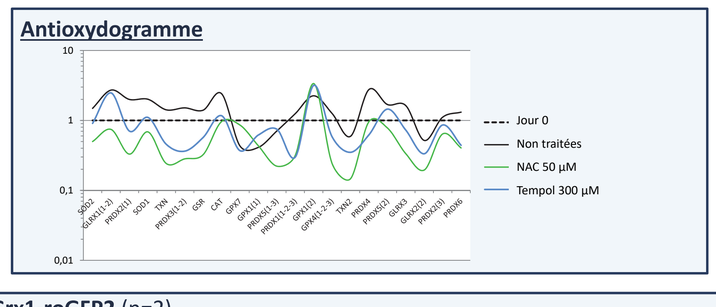

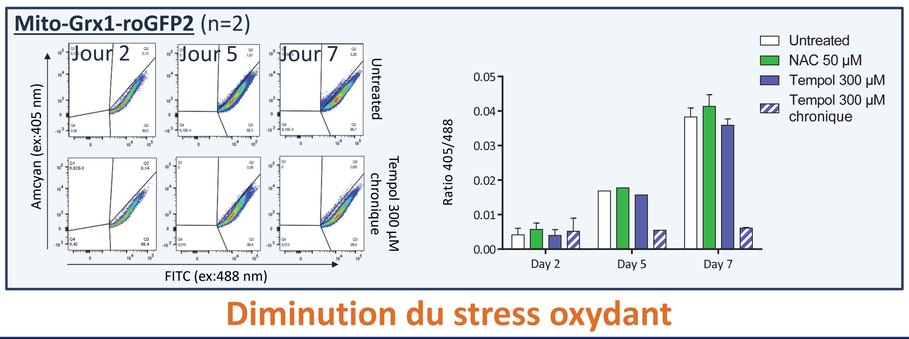

Diminution du stress oxydant

Mécanismes

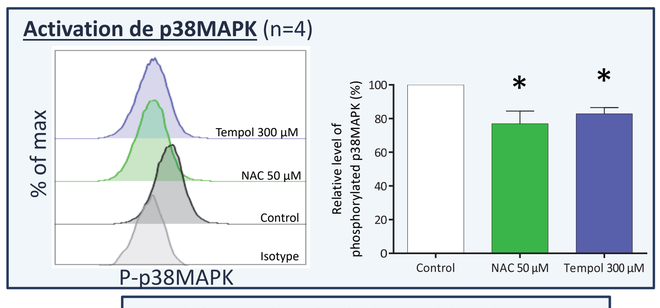

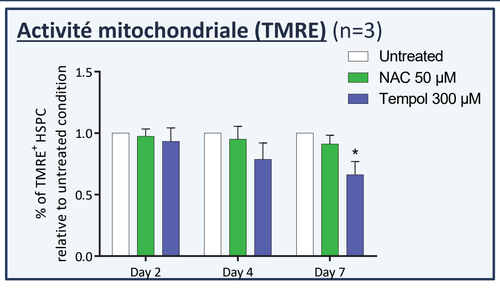

Implication de p38MAPK et du métabolisme

Perspectives

- Implication d'autres voies de signalisation?
- Rôle du VEGFα ?

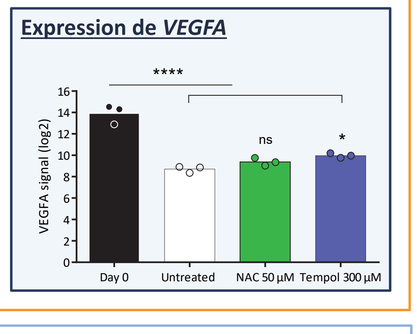

iRCM et LSHL

LSHL

Marie-Laure Arcangeli
Françoise Pflumio

Irina Naguibneva
Rima Haddad
Vilma Barroca
Laurent Renou
Guillaume Piton
Julien Calvo
Veronica Alonso-Perez
Charly Le Maout
Caroline Devanand

Plateformes de l'iRCM

Irradiation
Cytométrie en flux
Imagerie
Animalerie
Transcriptomique

Financements

Investissements d'Avenir
cea
La Ligue contre le cancer
Instituts thématiques Inserm
Institut national de la santé et de la recherche médicale
Cancéropôle Île-de-France
Cordons de vie Association Monegasque

Activation of purinergic receptor P2RX7 inhibits lung tumor growth

Serena Janho dit Hreich[1,2,4], Laetitia Douguet[1,2], Alina Ghinet[5], Paul Hofman[1,2,3,4] and Valérie Vouret-Craviari[1,2,4]

1. Université Côte d'Azur, CNRS, INSERM, IRCAN, Nice **2.** Centre Antoine Lacassagne, Nice **3.** Laboratoire de Pathologie Clinique et Expérimentale, Hôpital Pasteur, Nice **4.**FHU OncoAge, Nice **5.**Hautes Etudes d'Ingenieur (HEI), Yncréa Hauts de France, UCLille, INSERM U995

serena.janho-dit-hreich@etu.univ-cotedazur.fr

Background : HEI3090 inhibits lung tumor growth by targeting immune cells

P2RX7 is an ionotropic receptor activated by high extracellular ATP (eATP) levels found in the tumor microenvironnment. Its activation increases calcium influx and macropore opening that ultimately leads to cell death. Its activation also induces NLRP3 inflamasomme assembly and the release of pro-inflammatory cytokines IL-1β and IL-18.

We have shown that P2RX7's expression restrains tumor growth (Hofman *et al*, 2015) and hypothesized that enhancing its activation would inhibit tumor growth. We therefore synthesized a novel positive modulator of P2RX7, named HEI3090, that enhances P2RX7's activities only in the presence of eATP. We show that HEI3090 inhibits lung tumor growth of Lewis Lung Carcinoma cells (LLC) in a syngenic mouse model. It targets immune cells, and not tumor cells, to trigger anti-tumor immunity.

The goal of this study is to determine the cellular and molecular targets of HEI3090.

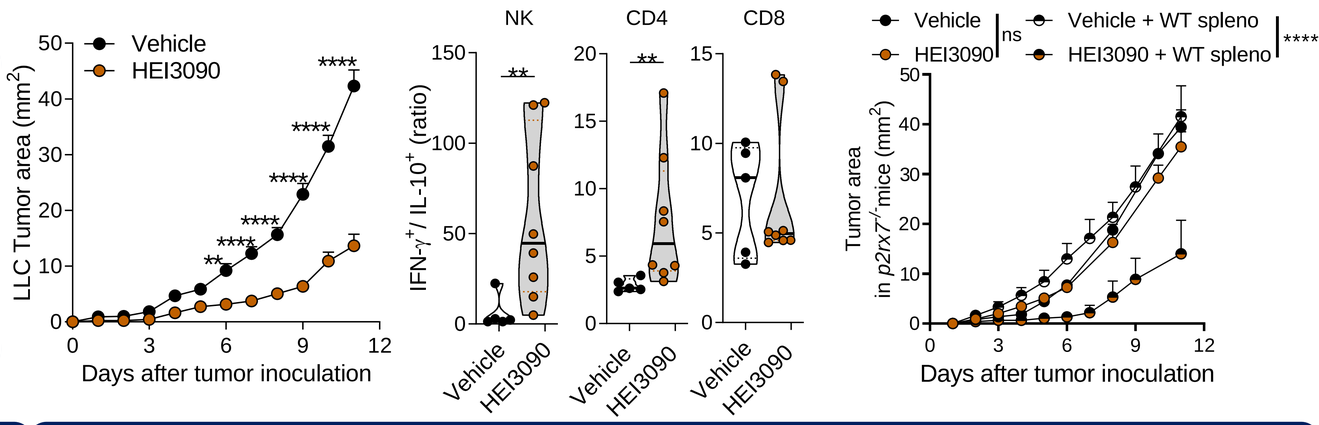

1- HEI3090 is a positive modulator of P2RX7

- Calcium influx (Fluo-4-AM probe) and macropore opening (TO-PRO-3 dye uptake) were assessed in HEK293 cells expressing the mouse P2RX7 (mP2RX7) or the control (pcDNA6) as well as in WT or *p2rx7*$^{-/-}$ splenocytes

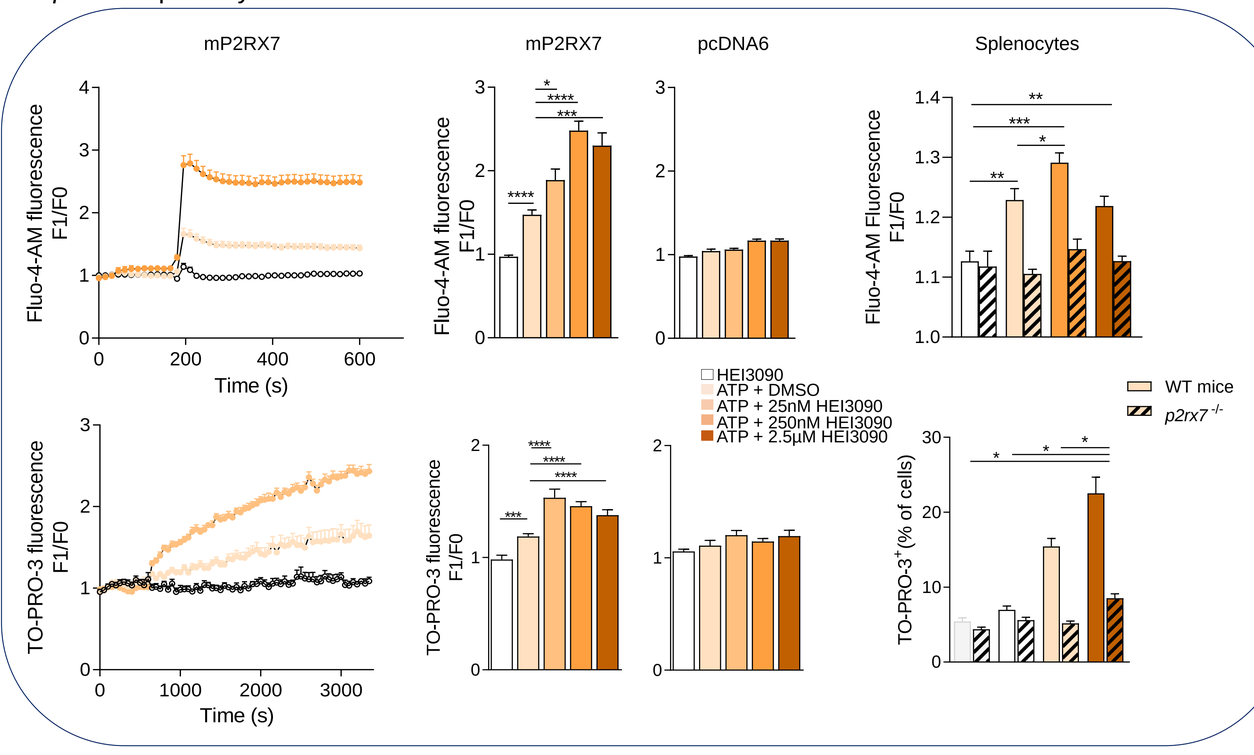

2- HEI3090 targets dendritic cells to inhibit tumor growth

- Phagocytic cells, such as macrophages and dendritic cells (DC), were depleted in WT mice by repeated injections of clodronate liposomes.
- WT DCs were adoptively transferred to *p2rx7*$^{-/-}$ mice that were treated with HEI3090.

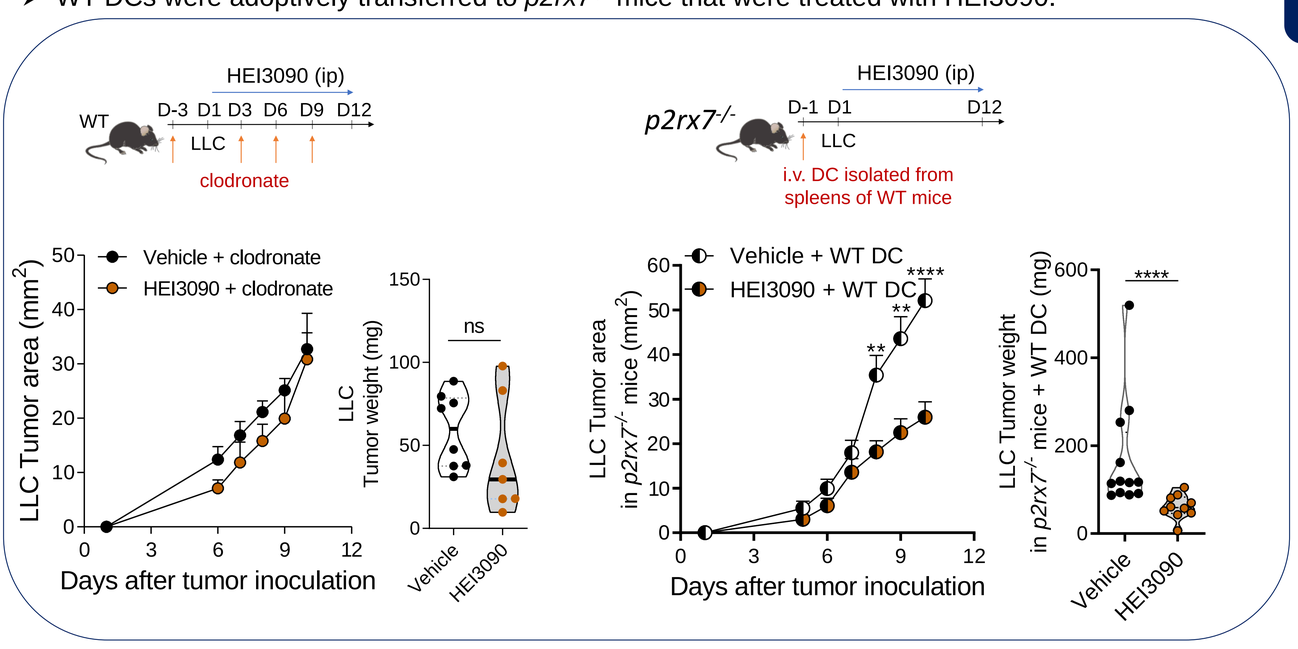

3- HEI3090 anti-tumor effect relies on IL-18

- IL-1β and IL-18 levels were determined by ELISA in sera of WT mice.
- IL-1β and IL-18 were neutralized by repeated injections of neutralizing antibodies in WT mice.
- IL-18's role in HEI3090's antitumor activity was further confirmed in *il18*$^{-/-}$ mice.

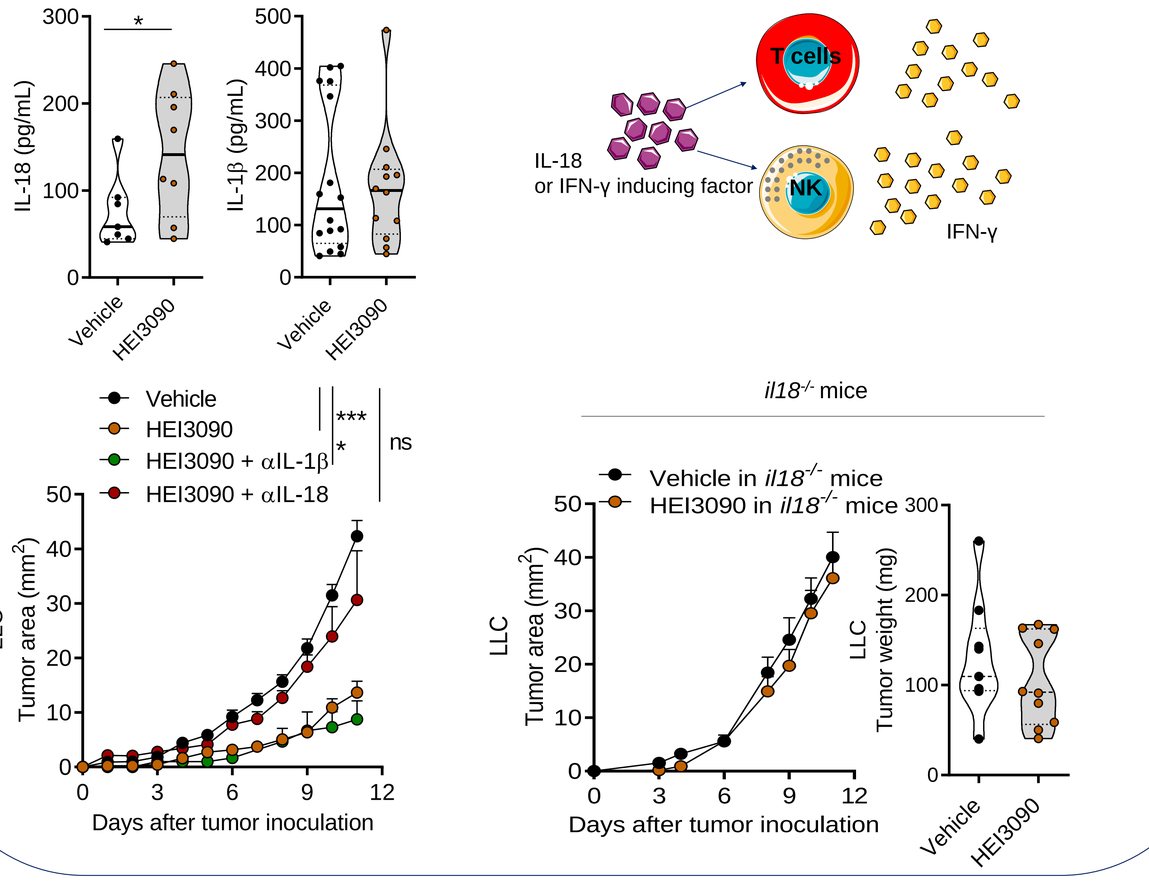

4- IL-18 release by HEI3090 is NLRP3-dependent

- NLRP3's role in HEI3090's release was studied in peritoneal macrophages. IL-1β and IL-18 levels were quantified by ELISA.
- Caspase-1 cleavage was analyzed by western blot as well as NLRP3 and ASC expression.

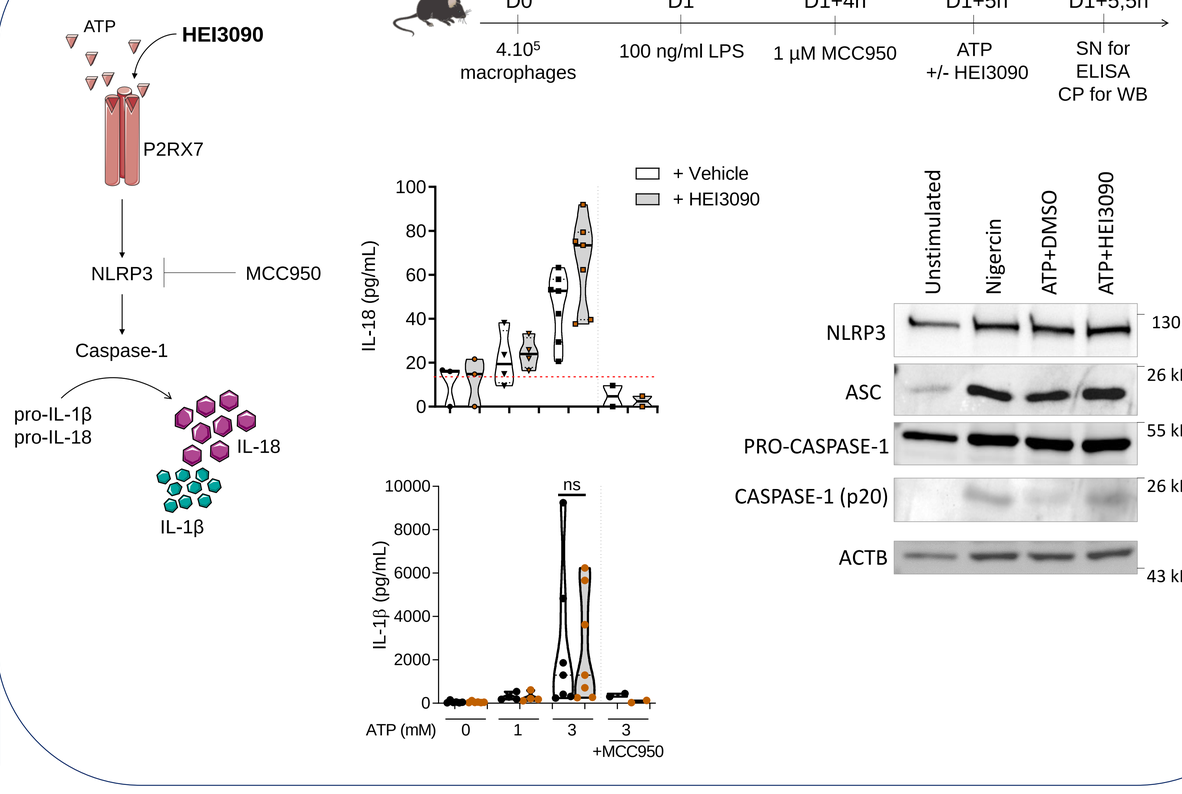

Conclusion

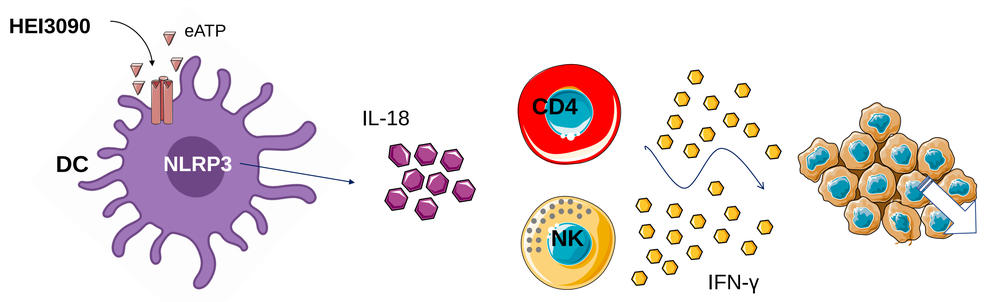

HEI3090 enhances P2RX7's activation by eATP in dendritic cells to release IL-18 in a NLRP3-dependent manner to orchestrate the anti-tumor immune response and to inhibit tumor growth.

Surprisingly, HEI3090 does not affect IL-1β release even though it is released by the same eATP/P2RX7/NLRP3/caspase-1 axis as IL-18.

Perspectives

We hypothesize that IL-1β's processing and/or release is regulated downstream of NLRP3.

IL-1β is pro-inflammatory cytokine involved in many inflammatory diseases and its release and stability are tightly regulated by several mechanisms that could be linked to P2RX7's activation that we're currently investigating.

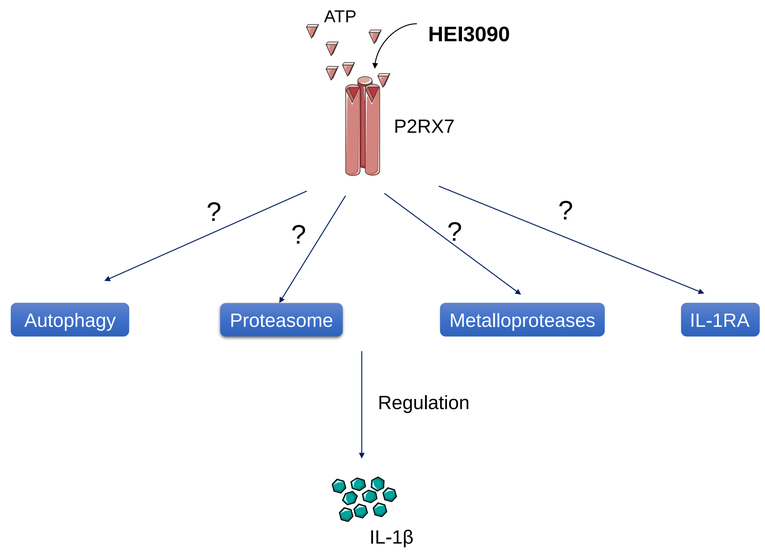

Connaissances et pratiques des professionnels de santé en oncologie auprès des jeunes aidants

Une étude visant à améliorer les pratiques

Pauline JUSTIN, Géraldine DORARD, Aurélie UNTAS
Laboratoire de Psychopathologie et Processus de Santé, Université de Paris, France
pauline.justin@u-paris.fr

Introduction

Jeunes aidants (JA) :
Enfants ou adolescents apportant une aide significative et régulière à un proche ayant une maladie ou un handicap (American Association of Caregiving Youth, 2012)

- Peu connus dans le cancer même si on sait que les jeunes ont parfois des responsabilités importantes (Faulkner & Davey, 2002)
- Situation qui entraîne des conséquences négatives sur la santé et le quotidien des jeunes (Sahoo & Suar, 2009)
- Professionnels qui rencontreraient fréquemment des JA, mais sans les identifier comme tels (Leu et al., 2018)
- JA qui rapportent avoir besoin de l'aide des soignants sans savoir comment l'obtenir (Bjorgvinsdottir & Halldorsdottir, 2014)

Objectifs

1. Explorer les connaissances et les pratiques que les professionnels en oncologie ont auprès des JA
2. Déterminer s'ils parviennent à les identifier, ce qu'ils font face à cette situation et explorer leurs besoins

Méthode

Participants : 31 professionnels de santé (*cadre de santé, médecin, IDE, aide-soignant.e, psychologue, assistant.e des services sociaux*), travaillant en service d'oncologie adulte, pédiatrique et en Hospitalisation à Domicile

Procédure : entretien qualitatif semi-directif pour recueillir des informations socio-démographiques et professionnelles, les représentations et expériences en lien avec les JA

Méthode d'analyse : analyse thématique inductive

Résultats

88% **Ont déjà rencontré un JA mais sans réellement connaître le terme**

Découverte de la situation :
- ☑ Par le proche aide
- ☑ Par des collègues
- ☑ En observant une ou plusieurs situations

Facteurs favorisant le fait d'être JA :
- ☒ Famille monoparentale
- ☒ Familles isolées, absence de soutien social

Bonne représentation de l'aide apportée :
- ❖ Type d'aide
- ❖ Personnes aidées
- ❖ Conséquences positives et négatives

ACTIONS
- → Faire appel au psychologue, à l'assistant social
- → Se rendre disponible si besoin
- → Mettre en place des aides concrètes, au domicile
- → Orienter le jeune

FREINS
- ❖ Conditions de travail hospitalières
- ❖ Sensibilisation insuffisante aux JA
- ❖ Refus de l'aide de la famille ou du JA
- ❖ Manque d'accès au JA

BESOINS
- → Aide à l'identification des JA
- → Aide à l'accompagnement des JA
- → Aide à l'orientation des JA

Perspectives

→ Mener une étude quantitative sous la forme d'enquête nationale pour mieux généraliser les représentations et les pratiques des professionnels de santé en oncologie en France

→ Construire des interventions de sensibilisation et de formation adaptées aux spécificités des professionnels et des services pour les aider à ajuster leurs pratiques pour mieux accompagner les JA

Doxorubicin (DOX) Gd (III)-biopolymer–Au (III)-complex: A new way to tune hybrid bimetallic nanorods as theranostic agent against cancer.

Memona Khan, Sarah Boumati, Celia Arib, Amadou Diallo, Nadia Djaker, Bich-Thuy Doan*, Jolanda Spadavecchia*

Introduction and aim of the study

In this study, in the context of developing novel therapy with nanotheranostics, we have designed and formulated for the first time, a novel synthesis of doxorubicin (DOX) loaded bimetallic gold nanorods in which gold salt ($HAuCl_4$) is chelated with anthracycline (DOX), diacid polyethylene-glycol (PEG-COOH) and gadolinium salt ($GdCl_3$ * 6 H_20) to form DOX IN-Gd-AuNRs compared with DOX ON-Gd-AuNRs in which the drug was grafted onto the bimetallic pegylated nanoparticle surface by electrostatic adsorption. The physical and chemical evaluation was performed by spectroscopic analytical techniques (Raman spectroscopy, UV-Visible and transmission electron microscopy (TEM). Magnetic features with high relaxivity values at 7T were also measured. Cytotoxicities studies on MIA PaCa-2, human pancreatic carcinoma and TIB-75 hepatocytes cell lines were carried out to evaluate their biocompatibility and showed a 320 fold higher efficiency for DOX after encapsulation. Furthermore, these nanomaterials are notably devoted to the destruction of cancer cells in photothermal therapy due to their light induced heating properties. These results will consolidate the role of gadolinium as complex to gold and DOX in order to give a hybrid theranostic agent in the field of nanomedicine. The therapeutic vector will be used against pancreatic cancer models.

Synthesis of gold nanorods

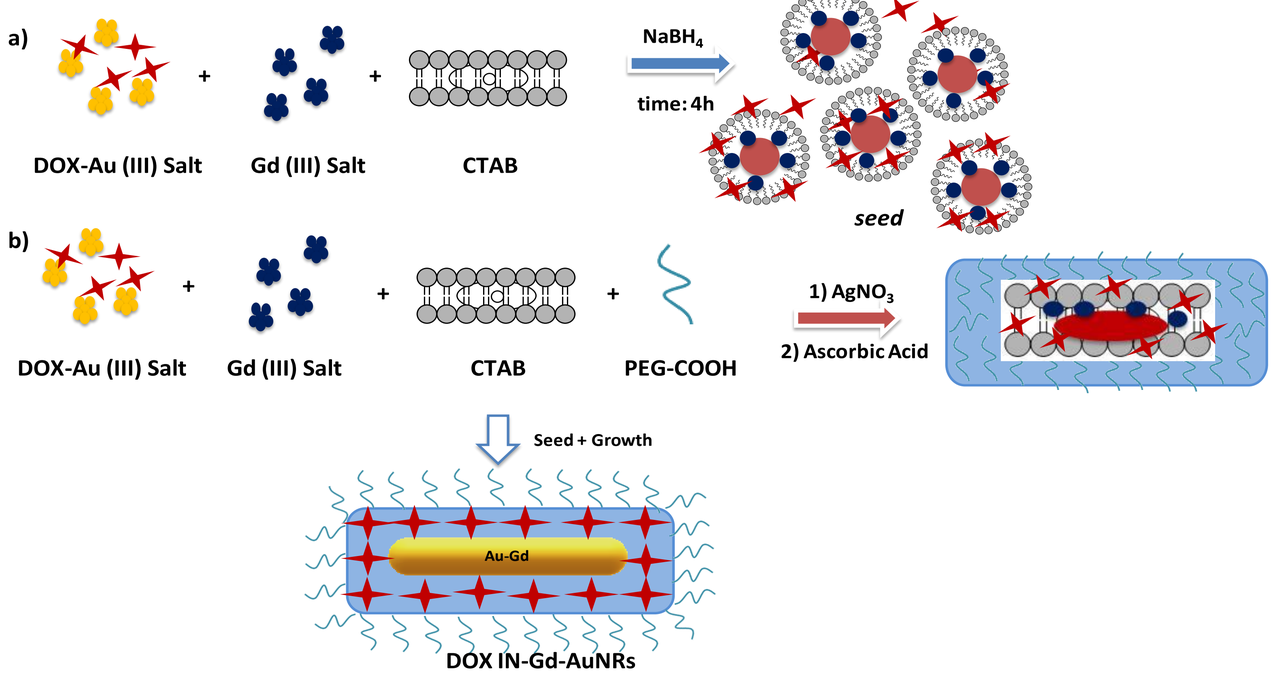

Scheme 1. Schematic representation of seed mediated synthesis of DOX-IN-Gd-AuNRs

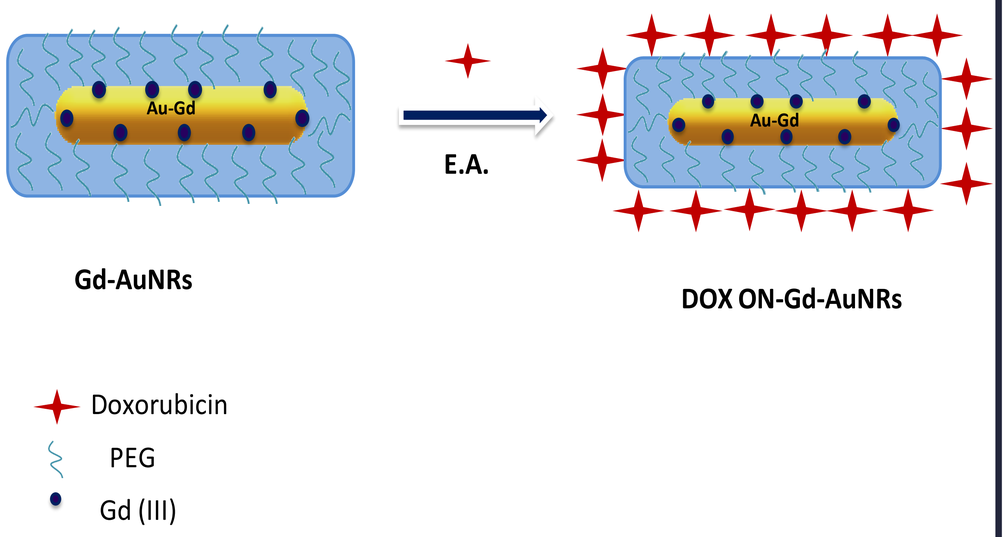

Scheme 2. Schematic representation of Electrostatic Adsorption of DOX onto the NP, names DOX-ON-Gd-AuNRs.

Characterization of gold nanorods

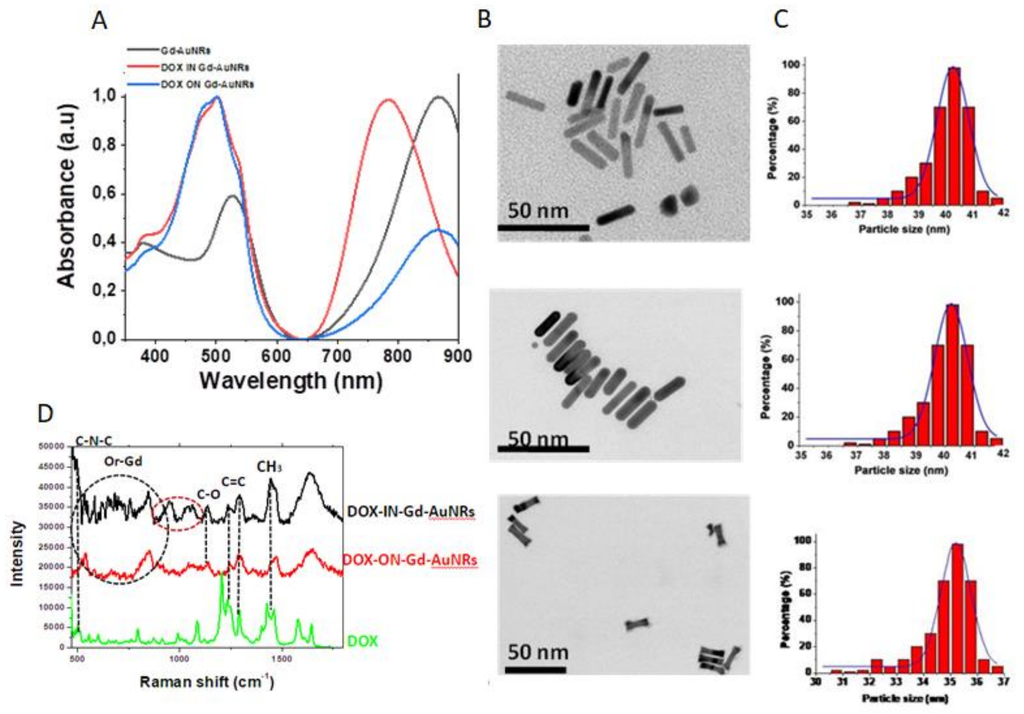

Figure 1. A) Normalized UV-Vis absorption of GdAuNRs (blackline) , DOX IN-Gd-AuNRs (red line) and DOX ON-Gd-AuNRs (blue line); (**B**) TEM images of Gd-AuNrs DOX IN-Gd-AuNRs (panel **2**) and; DOX ON-Gd-AuNRs (panel **3**) and (**C**) their corresponding histogram size distribution; **(D)** Raman spectra of DOX IN-Gd-AuNRs products (black line), DOX ON-Gd-AuNRs (red line) and DOX alone (green). Experimental conditions: λexc=785 nm; laser power 20 mW; total 180 s.

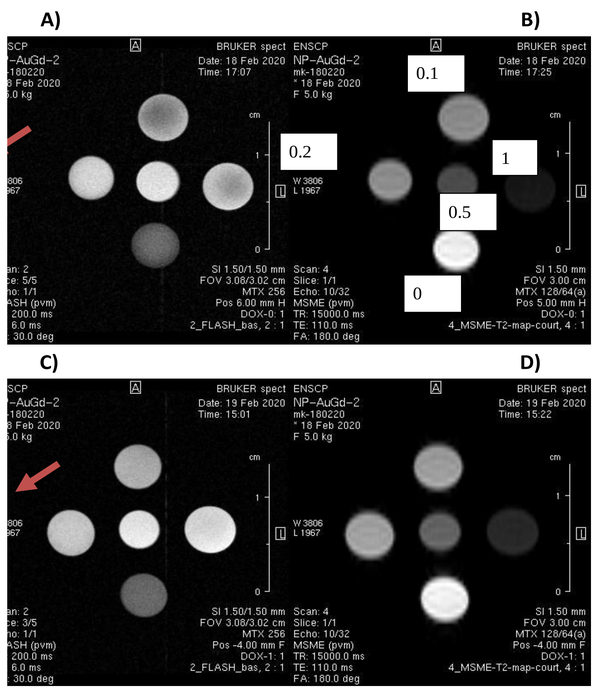

Figure 2. Examples of T1 and T2 weighted MR images of Gd-AuNRs: alone (A and B, respectively, DOX IN-Gd-AuNRs (C and D).

Contrast agents	r1	r2	r2/r1
DOTAREM	4.0	3.9	1.1
Gd3+	9.5	5	1.9
DOX IN-Gd-AuNRs	9.9	14.7	1.5
DOX ON-Gd-AuNRs	10.3	12.7	1.2

Table 1. Table of r1 and r2 relaxivities values measured at 7T, 273K, corrected with ICP AES elementary analysis

⇒ Stable and well structured nanorods of 35 to 40 nm hydrodynamic diameter, water soluble
⇒ Efficient MRI contrast agents at 7T

Cytotoxicity tests

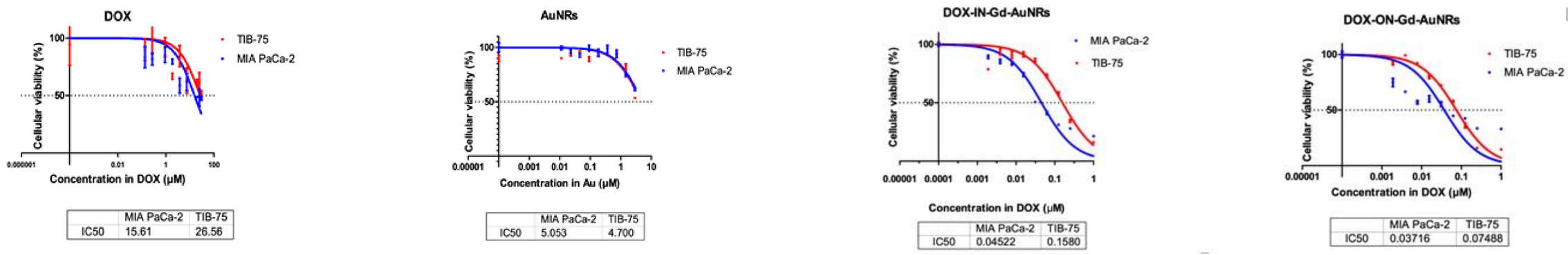

	MIA PaCa-2	TIB-75
IC50	15.61	26.56

	MIA PaCa-2	TIB-75
IC50	5.053	4.700

	MIA PaCa-2	TIB-75
IC50	0.04522	0.1580

	MIA PaCa-2	TIB-75
IC50	0.03716	0.07488

Figure 3. Cytotoxicity MTT tests with cell lines (MIA PaCa-2, TIB-75); IC50 values in concentrations of Au, Gd and DOX.A) DOX alone; B) AuNRs; C) DOX IN –Gd-AuNRs; D) DOX ON-Gd-AuNRs

=> Weakly toxic AuGd NP, enhancement of toxicity with DOX (IC50 <0,1uM) by a factor of 320

Conclusion

In this work, we have developed a novel theranostic nanoparticle composed of gadolinium complexes to gold ions, with a PEG biopolymer matrix conjugated with antitumoral doxorubicin, providing multifunctional therapeutic features. Exhaustive physicochemical characterization studies were conducted showing a mid size of 20 to 40 nm diameters obtained with low polydispersity, efficient synthesis using seed mediated synthesis with chelation reaction with high scale-up, long duration stability, specific doxorubicin release with acidic pH, strong photothermal abilities at 808 nm in the NIR transparency window, strong magnetic $r_1$relaxivities for positive MRI, well adapted for image guided therapy and therapeutical purpose in biological tissues.

Acknowledgements

This work has been partly performed on the CNanoMat platform of the University Sorbonne Paris Nord. The MRI experiments were performed at the LIOPA/MRI imaging facility of the consortium Plateformes d'Imageries du Vivant of Paris Descartes, PIV and UTCBS/SEISAD/ENSCP team. The IDEX SPC Sorbonne Paris Cité IDV Imageries du Vivant is also acknowledged. We also thank *la Ligue contre le Cancer* for financing MK's thesis.

contact

Memona KHAN 1 rue de chablis, 93000 Bobigny
memonakhan94@gmail.com

Adolescents et jeunes adultes – AJA – atteints de cancer : représentations et quête de sens chez le patient et ses parents

Voskan Kirakosyan, Dolorès Albarracin, Nicolas Dauman, Alain Ducousso-Lacaze

EA 4050 CAPS, Département de Psychologie, Université de Poitiers

contact : voskan.kirakosyan@univ-poitiers.fr

Introduction

La notion de représentation est au cœur des travaux en psychologie qui s'intéressent au vécu des malades, et à leur discours.

Pédinielli (1999) considère les représentations individuelles originales des patients comme des « théories profanes », par opposition aux théories savantes de la médecine.

Elles fournissent aux patients :

- une explication personnelle de la maladie et de sa survenue
- une nécessité d'un travail psychique d'élaboration, une véritable quête de sens contre les effets traumatiques

Objectifs

Déterminer s'il existe une spécificité de représentations chez les AJA ? Sont-elles différentes de celles de leurs parents ?

Méthodologie

Etude multicentrique menée à :

- Institut Bergonié (Unicancer Bordeaux)
- MARADJA (Maison Aquitaine Ressources pour Adolescents et Jeunes Adultes, CHU de Bordeaux)
- Association « On est là ».

Etude qualitative :

- Menée auprès des AJA (n=15) et leurs parents (n=30)
- Entretiens de recherche semi-directifs, intégralement retranscrits
- Méthode d'analyse proposée par Braun et Clarke (2006)

L'objectif de l'analyse thématique : organiser les représentations autour de thèmes développés (étapes) et les regrouper en différentes catégories (Negura, 2006)

Résultats

Les représentations des adolescents et des jeunes adulte – AJA –		
Thème 1 **« S'approprier le cancer»**	Thème 2 **« Maintenir l'idée d'une guérison »**	Thème 3 **« Mise à l'épreuve subjective »**
Sous-thèmes • « Quête de sens et origine du cancer » • « Le cancer comme un évènement inéluctable »	Sous-thèmes • « Se fier aux convictions personnelles » • « Agir à l'aide de la médecine et de l'acte médical »	Sous-thèmes • « Répression des affects » • « Lâcher-prise émotionnel » • « Avoir le sentiment de mise à l'écart »
Les représentations des parents		
Thème 4 **« Recherche d'explication et quête de sens à la survenue du cancer »**	Thème 5 **« Vouloir vaincre la maladie»**	Thème 6 **« Stratégies pour s'adapter au cancer»**
Sous-thèmes • « Maintenir l'idée d'une transmission » • « Penser une cause psychique et stressante» • « Trouver des explications à travers la nourriture »	Sous-thèmes • « Compter sur la médecine» • « Se focaliser sur les convictions personnelles » • « S'appuyer sur des croyances et des rites »	Sous-thèmes • « Positiver l'Hôpital et les traitements» • « Contrôler les émotions»

Discussion

Nos résultats indiquent :

- une forte similarité des représentations centrées sur l'idée d'une guérison (thème2 et thème5), exprimées de plusieurs façon.
- une forte divergence des représentations :
  - Chez les AJA : travail d'appropriation de la maladie et d'une mort possible (thème1), qui témoigne de la mise à l'épreuve subjective (thème3)
  - Chez les parents : recherche d'une quête de sens à la survenue du cancer de leur enfant (thèmes4) et pour ce faire ils ont recours à diverses stratégies (thème6).

Ces représentations permettent d'analyser ce qui met à mal la subjectivité des AJA malades et celle des parents et offrent la possibilité de mieux comprendre les interactions parents-enfant et leurs comportements d'adaptation face au cancer.

Remerciements à la Ligue Nationale contre le cancer et ainsi qu'à ses comités départementaux du Maine-et-Loire et de le Vienne pour leur soutien

Bibliographie:
Braun, V., & Clarke, V. (2006). Using thematic analysis in psychology. Qualitative research in psychology, 3(2), 77-101.
Negura, L. (2006). L'analyse de contenu dans l'étude des représentations sociales. SociologieS.
Pedinielli, J. L. (1999). Les théories personnelles des patients. Pratiques psychologiques (Le Bouscat), (4), 53-62.

Metabolism's implication in osteosarcoma resistance towards bromodomains proteins inhibitors

Mélanie LAVAUD[1], Robel TESFAYE[1], Steven Georges[1], Alexandre PELLETIER[1], Louise MARCHANDET[1], Camille JACQUES[1], Céline CHARRIER[1], Marc BAUD'HUIN[1], François LAMOUREUX[1], Benjamin ORY[1]

[1] UMR UN INSERM U1238 Bone sarcomas and remodeling of calcified tissues, 1 rue Gaston Veil 44035 Nantes, FRANCE

melanie.lavaud@univ-nantes.fr

BACKGROUND

Osteosarcoma identity :

- Is the most malignant bone tumour
- Affects children and young adults
- Has a mesenchymal/osteoblastic origin
- Is generally localized :
  - in the knee region (distal femur or proximal tibia)
  - in the shoulder region (proximal humerus)
- Has 3 subtypes : high, intermediate, low grade

Osteosarcoma treatments :

Surgeries - Chemotherapies - (Radiations)

➢ 5 years survival rates :
- Localized forms : 60 %
- Metastasis, chemoresistance : **20%**

Chemotherapies used unchanged since the 1970's : Need to develop new molecules…

Dana-Farber Cancer Institute

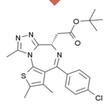

JQ1

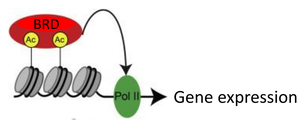

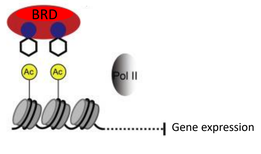

BRD : Bromodomains proteins
Ac : Histones acetylation
POL II : RNA Polymerase II

Selective inhibition of BET bromodomain epigenetic signalling interferes with the bone-associated tumour vicious cycle

François Lamoureux[1,2,*], Marc Baud'huin[1,2,3,*], Lidia Rodriguez Calleja[1,2], Camille Jacques[1,2], Martine Berreur[1,2], Françoise Rédini[1,2], Fernando Lecanda[4], James E. Bradner[5,6], Dominique Heymann[1,2,3] & Benjamin Ory[1,2]

Efficacy of JQ1 proved as a potential new molecule to fight against osteosarcoma
(Lamoureux et al., 2014 - Nature communications)

Chemoresistance phenomena : Need to anticipate osteosarcoma JQ1 resistance apparition…

Development of a JQ1 resistant osteosarcoma cell line by continuous and progressive JQ1 treatment

HOS MNNG

HOS MNNG JQ1 resistant (HOS MNNG JQ1R)

HYPOTHESIS

Simple observation :

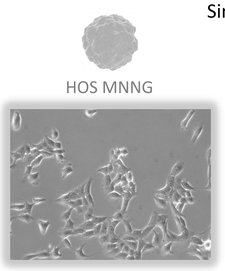

High throughput analysis to characterise JQ1 sensitive and resistant osteosarcoma cell lines

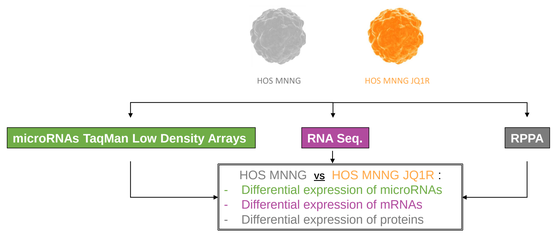

Energetic metabolism seems to be different between JQ1 sensitive and JQ1 resistant osteosarcoma cell lines
May explain slower development of HOS MNNG JQ1R
Focus on **Lactate Deshydrogenase A** (**LDHA**) enzyme

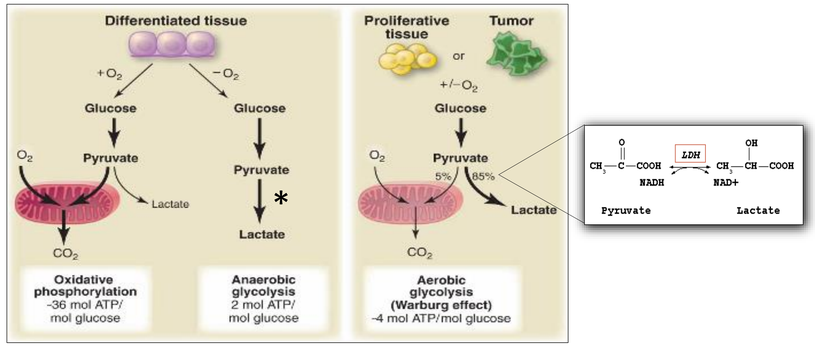

* LDHA is also involved in anaerobic glycolysis

Overcoming cetuximab resistance in Ewing's sarcoma by inhibiting lactate dehydrogenase-A
Fu et al., 2016

Inhibition of lactate dehydrogenase A by microRNA-34a resensitizes colon cancer cells to 5-fluorouracil
Li et al., 2014

RESULTS

Development of JQ1 resistant osteosarcoma cell line

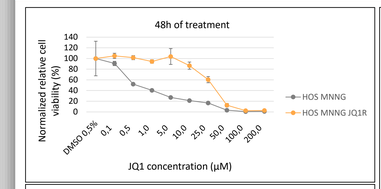

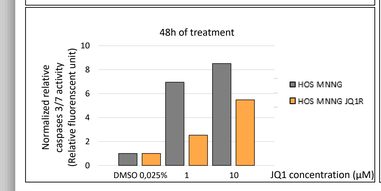

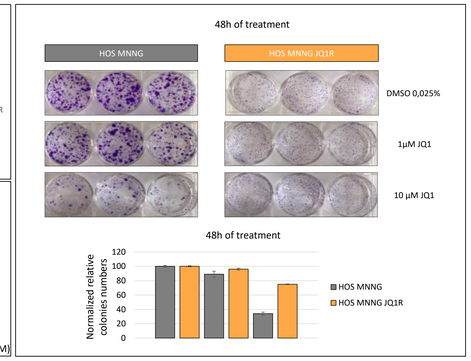

HOS MNNG JQ1R are less sensitive to JQ1 treatment than HOS MNNG
1. Viability assay. HOS MNNG JQ1R's viability is less impacted by different JQ1 concentration treatment (48h of treatment) compared to HOS MNNG
2. Clonogenic capacity assay. Clonogenic capacity of JQ1 resistant osteosarcoma cell line after 48h of JQ1 treatment (2 concentrations) is less affected compared to HOS MNNG
3. Caspases 3/7 activities assay. Apoptosis is less activated in HOS MNNG JQ1R than HOS MNNG after 48h of treatment with 2 different doses of JQ1

JQ1 resistant osteosarcoma cell line present an over expression and an over activity of LDHA

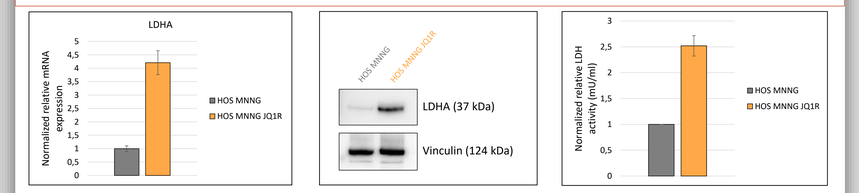

HOS MNNG JQ1R present a marked aerobic glycolytic metabolism compared to JQ1 sensitive osteosarcoma cell line
1. RT-qPCR. HOS MNNG JQ1R overexpress *LDHA* transcript compared to HOS MNNG
2. Western blot. JQ1 resistant osteosarcoma cell line overexpress LDHA enzyme compared to HOS MNNG
3. LDH activity assay. LDH enzymes are more active in HOS MNNG JQ1R than HOS MNNG

JQ1 sensitive osteosarcoma cell line become more resistant to JQ1 treatment under increased activity of LDHA

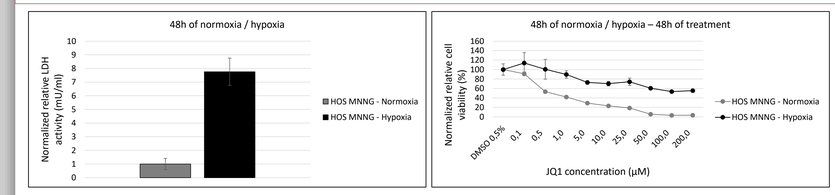

Increased LDHA activity by hypoxia desensitises HOS MNNG to JQ1 treatment
1. LDH activity assay. After 48h of proliferation under hypoxic condition (1% O^2) HOS MNNG present a higher LDH activity compared to HOS MNNG cultured 48h under normoxic condition
2. Viability assay. After 48h of culture under hypoxic condition, HOS MNNG are less sensitive to JQ1 treatment (progressive JQ1 doses, 48h of treatment under hypoxia) than HOS MNNG cultived for 48h under normoxic condition and treat with JQ1 (different concentrations for 48h under normoxia)

PERSPECTIVES

JQ1 resistance of osteosarcoma tumor cells may occur by a modification of their metabolism compared to sensitive osteosarcomatic cells. LDHA enzyme, which is involved in pyruvate transformation into lactate in aerobic glycolysis, may play a crucial role in JQ1 resistance development in osteosarcoma. JQ1 being a new promising molecule to treat patients suffering from osteosarcoma, this study, which has just begun, need to be followed to anticipate JQ1 resistance emergence in patients treated with this molecule.

Spontaneous physical activity in obese conditions modulates tissue hormonal signals leading to reduced tumor growth

Delphine Le Guennec[1], Victor Hatte[1], Stéphanie Rougé[1], Marie-Chantal Farges[1], Florence Caldefie-Chézet[1], Marie- Paule Vasson[1,2], Adrien Rossary[1]

([1]) University of Clermont Auvergne, INRA, Human Nutrition Unit, ECREIN team, BP 10448, F-63000 Clermont-Ferrand, France ;
([2]) Clermont-Ferrand University Hospital, Centre Jean Perrin, Nutrition Unit, CLARA, F-63000 Clermont-Ferrand, France.

1. Introduction

In obese situation, fat tissue deregulation induces the secretion of estrogens and pro-inflammatory adipokines (leptin) at the expense of anti-inflammatory adipokines (adiponectin). An increase in oxidative stress associated with a decrease in antioxidant capacities maintains chronic inflammation promoting a pro-carcinogenic microenvironment (E. Ramos-Nino M, ISRN Oncology, 2013). Physical activity (PA), a preventing factor of obesity and cancer, promotes the antioxidant response and the secretion of anti-inflammatory adipokines (Schnyder et al, Bone, 2015) but the mechanisms in breast cancer remain poorly understood, particularly in obese conditions.

The aim of this study is to characterize the impact of spontaneous physical activity on tumor growth in a murine breast carcinogenesis model associated with obesity.

2. Materials and methods

Mice
C57BL/6
33 weeks

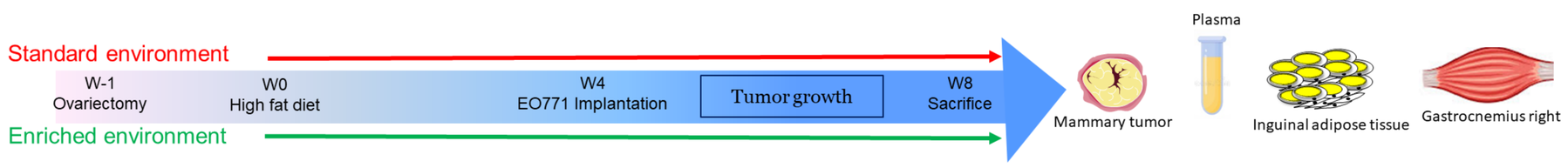

Metabolic pathways	Analytes	Tumor	Inguinal adipose tissue	Gastrocemius	Plasma	Mammary gland
Inflammation	IL-6, isoprostanes, COX-1, COX-2	X				
Metabolism	Adiponectin, leptin, resistin	X	X	X	X	X
Angiogenesis	EGF, HGF, VEGF-A, PECAM soluble	X	X	X	X	X
Tissue remodeling	proMMP9, MMP3, MMP2, MMP12	X	X	X		X
Antioxidant response	HO-1, thiols, glutathione reduced and total, GST, GR, thioredoxine reductase	X				
Signalisations pathways	JNK, p38, STAT5, AKT/NFκB	X	X	X		X

Actimetry, body data, time required to reach the tumor growth limit point, tumor growth rate

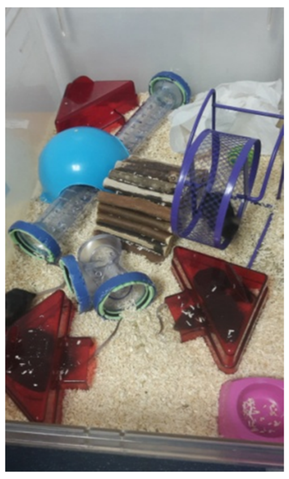

Statistical analyses

- **Multi-Factoriel Analyses (MFA)** : R (version 3.2.2) and FactomineR package. Centered and reduced data.
- *9 groups of quantitative variables : muscle masses, fat tissue masses, physical tumor parameters, tumor antioxidant status, tumor biology, inguinal fat tissue biology, gastrocnemius biology, plasma biology and left mammary gland biology.*
- *1 qualitative variable : environment*
- Correlation test
- ANOVA 2 ways and Mann Witney t-test

3. Results

1. Anthropometric, physical activity and tumor data

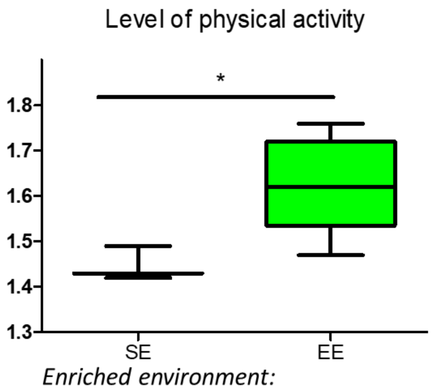

Enriched environment:
Increased physical activity level

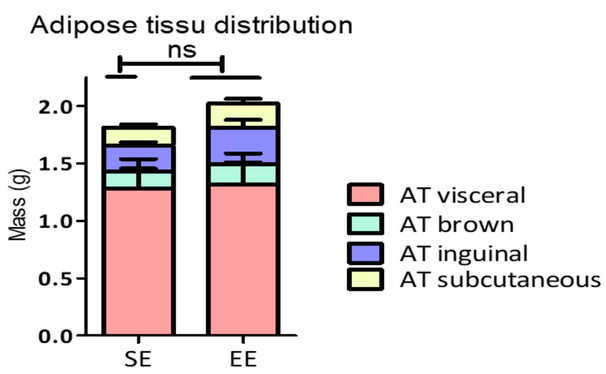

Enriched environment:
No difference in fat mass distribution or quantity

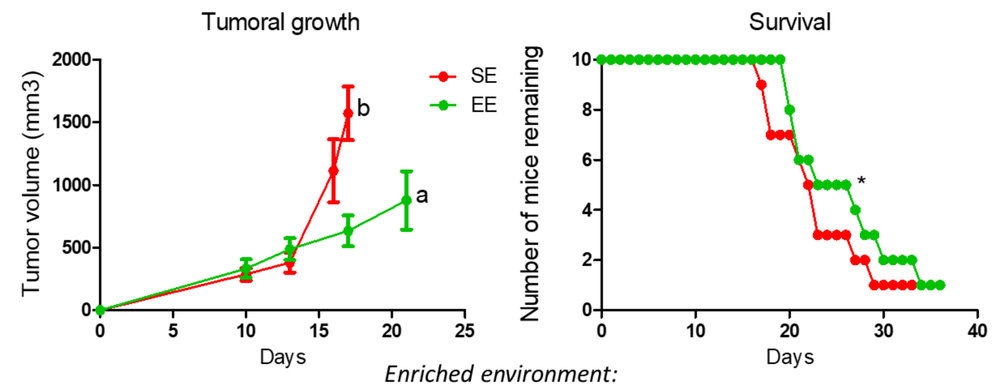

Enriched environment:
Slower tumor growth, Increased survival

2. Multi-Factoriel Analyses : global analysis of the environment impact

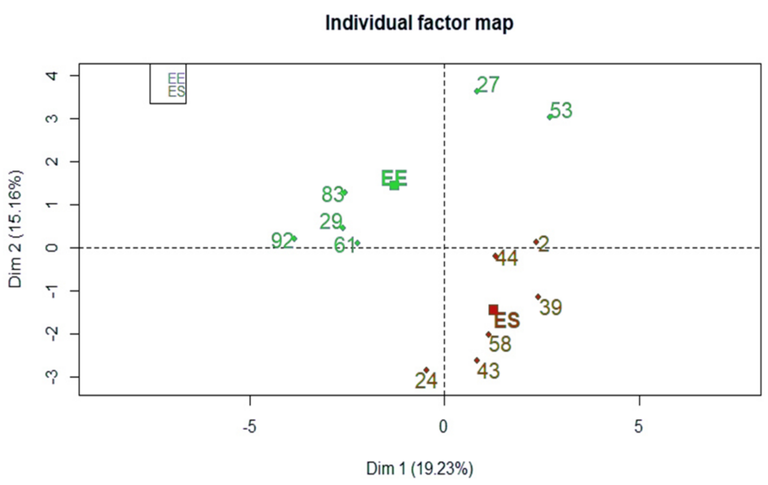

First two dimensions = 34% of the variance
Individual separation according to the two environmental groups.

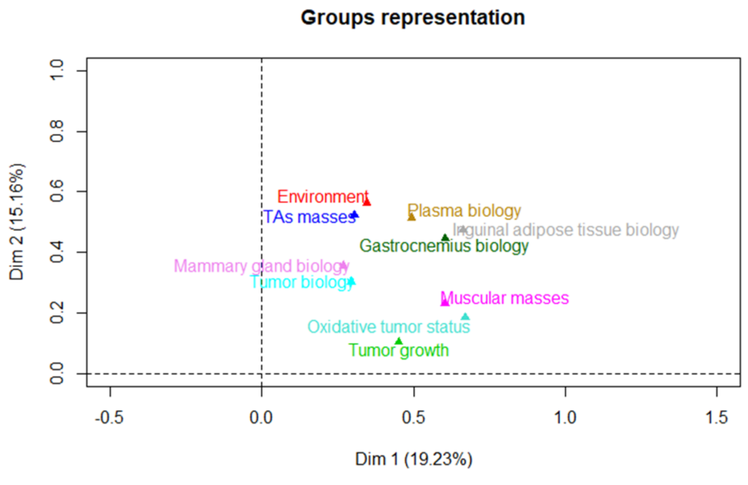

High impact of plasma, gastrocnemius and inguinal adipose tissue biology.
Dim1 mainly represented by the muscular mass and the tumor growth.
Dim2 more affected by the adipose tissue masses and the environment.

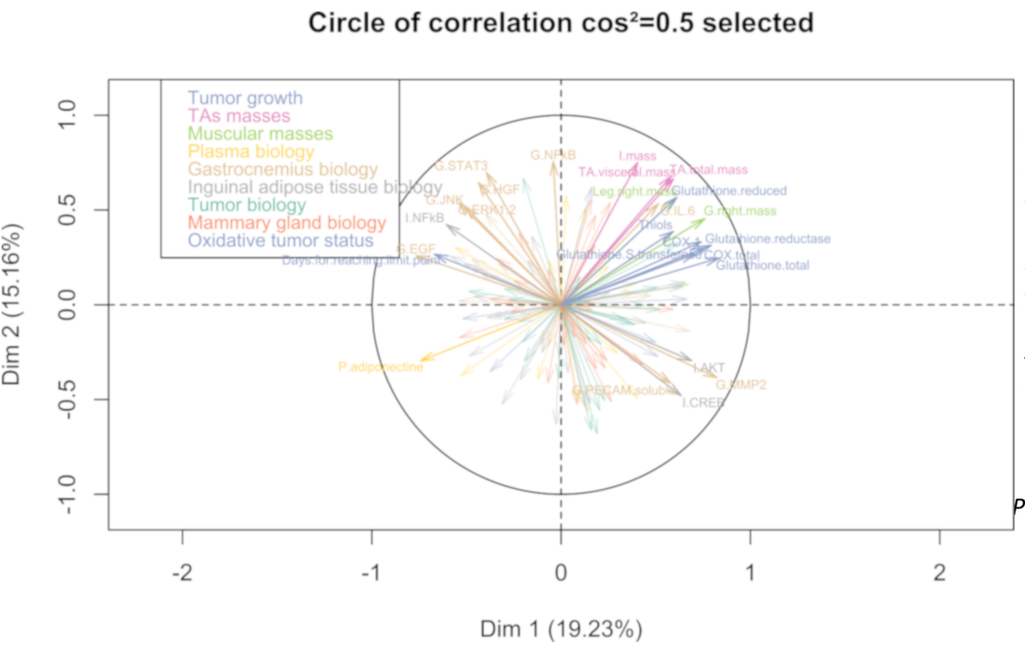

Variables associated with EE: growth factors (EGF,HGF) and gastrocnemius signaling pathways (STAT3,JNK,ERK1/2,NFKB), inflammation of inguinal adipose tissue (NFKB), also related to slowing tumor growth.

Variables associated with SE: activation of inguinal adipose tissue signaling pathways (AKT,CREB).

A balance between adiponectin and oxidative stress is observed in a border area between the 2 environments.

P=plasma ; T=tumor ; G=gastrocnemius ; M=mammary gland

3. Correlations

P=plasma ; T=tumor ; G=gastrocnemius ; M=mammary gland

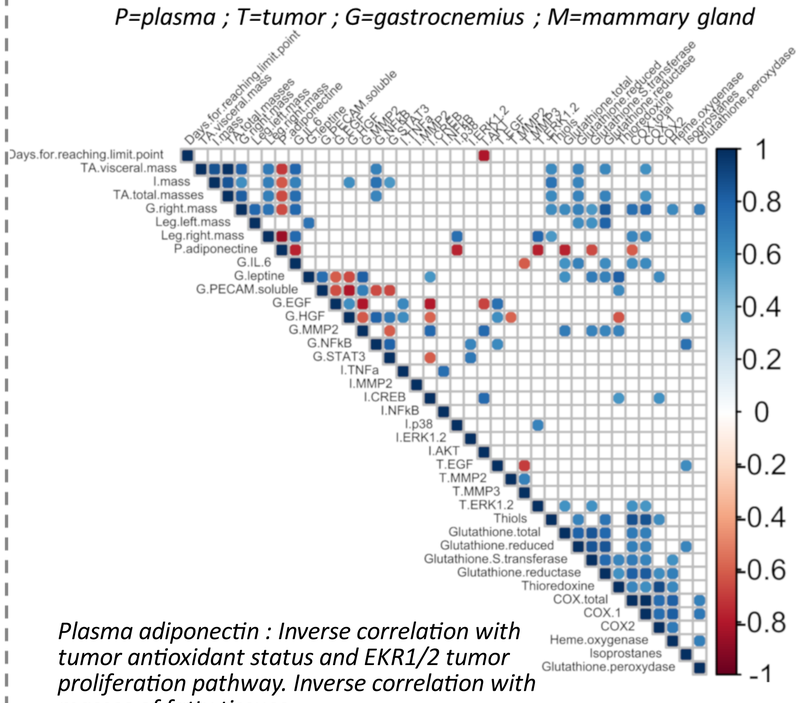

Plasma adiponectin : Inverse correlation with tumor antioxidant status and EKR1/2 tumor proliferation pathway. Inverse correlation with masses of fatty tissues.

- *The weight of the right gastrocnemius: positive correlation with all markers of antioxidant status and oxidative stress.*

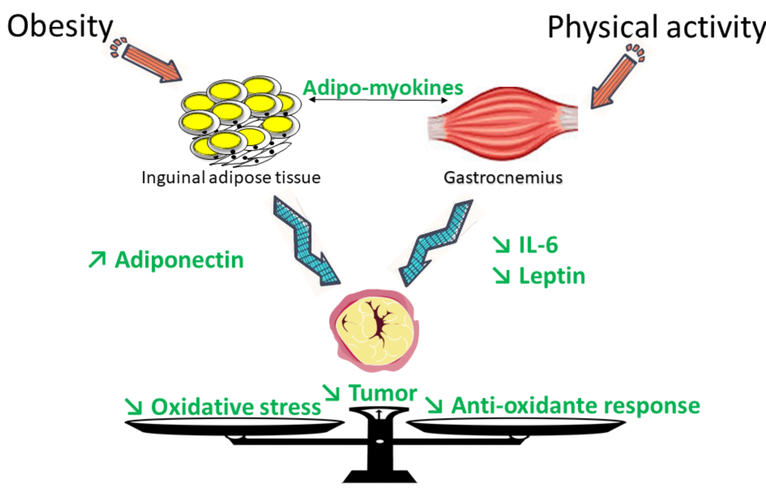

4.Discussion & conclusion

Spontaneous moderate physical activity, guaranteed by the enriched environment, shows a significant effect on the muscle, which is reflected at the central level by a strengthening of circulating anti-inflammatory adiponectin and at the tumor level by an antioxidant response and a reduced oxidative stress leading to a slowing of tumor growth. Is this regulation depend on the physical activity intensity ?

Investigating the role of Ten eleven translocation 1 (TET1) protein in modulating chromatin architecture

Audrey Lejart, Catherine Chapuis, Agnès Burel, Aurélien Dupont, Xavier Pinson, Stéphanie Dutertre, Sébastien Huet, Gilles Salbert.
Institut de Génétique et Dévelopement de Rennes (IGDR), UMR6290 CNRS, Université de Rennes, France
et MRic, Microscopy Rennes imaging center, BIOSIT UMS 3480, université de Rennes, France
audrey.lejart@univ-rennes1.fr

Background

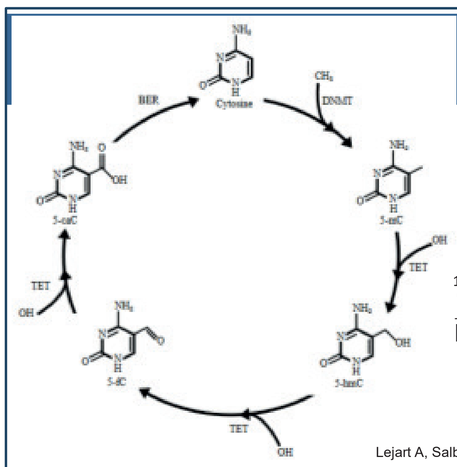

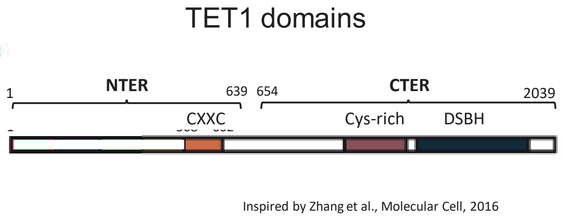

Lejart A, Salbert G, Huet S. (2018) *AIMS Biophysics*, 5(3):182-193.

The chromatin is a complex multi-scale structure composed of DNA wrapped around nucleosomes. The chromatin compaction state is finely regulated by epigenetic marks targeting not only the nucleosomes but also the DNA itself. Among epigenetic tags, the most studied DNA modification is 5-methylcytosine (5-mC). Methylation of the cytosines at CpG localized in promoters is associated with a closed chromatin state and repression of transcription. On the contrary, enrichment of 5-hydroxymethylcytosine (5-hmC), one of the oxidation products of 5-mC by TET (ten-eleven translocation) enzymes, on promoters and enhancers promotes transcription activation and is associated with an open chromatin state. Building on these findings, our team aims to decipher the influence of TET activity on the chromatin state. Here we show that overexpression of the N-terminal domain of TET1 (NTER) is sufficient to induce a global chromatin reorganization. We plan to analyze the characteristics of this modified chromatin state at the nucleus, fibre and nucleosome scales.

NTER-TET1 overexpression leads to chromatin reorganization

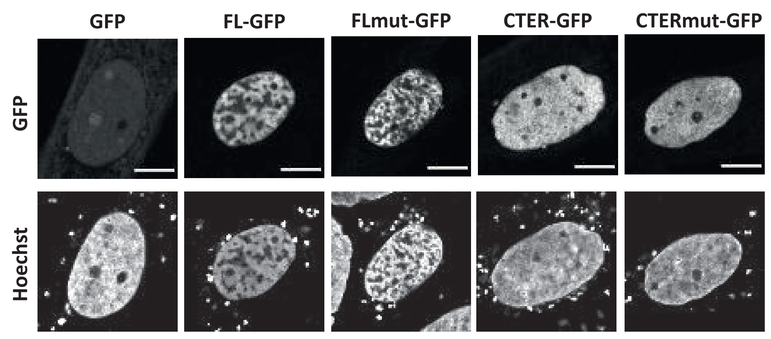

The chromatin structure is remodeled upon TET1 overexpression and this process does not require TET1 catalytic activity

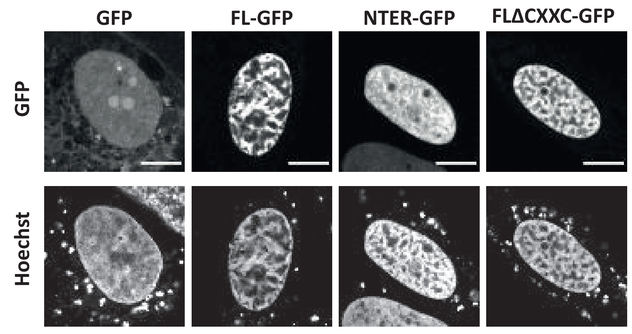

Scale bar=10µm

The NTER domain of TET1 is sufficient to induce chromatin rearrangement

Can TET1-dependent chromatin redmodeling be due to interaction between the NTER domain of TET1 with an unknown factor?

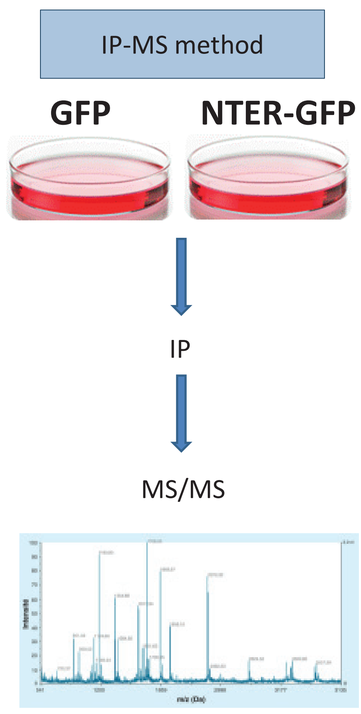

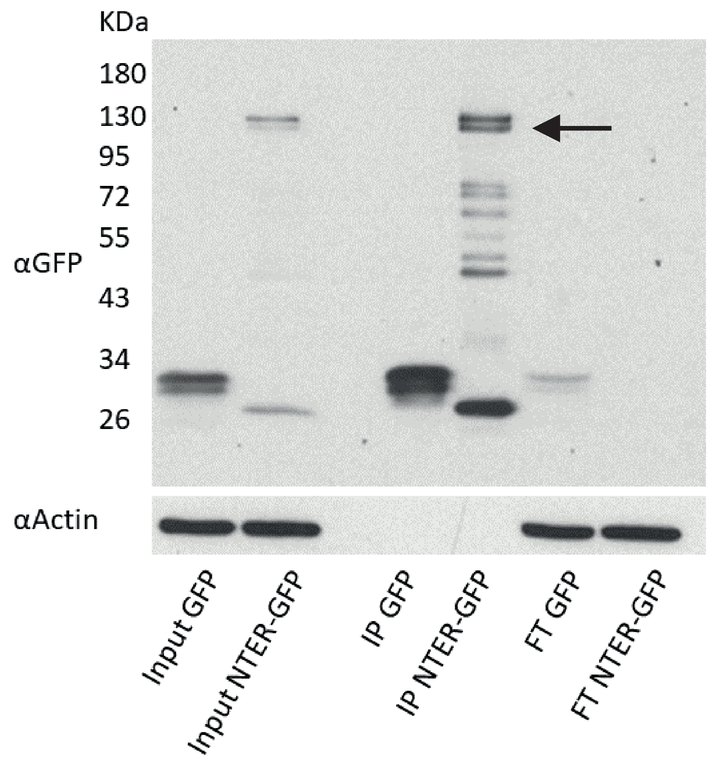

The NTER domain can be immunoprecipitated with GFP-trap beads

Characterization at the ultrastructural and molecular scales of the chromatin structure reorganized by TET1 overexpression

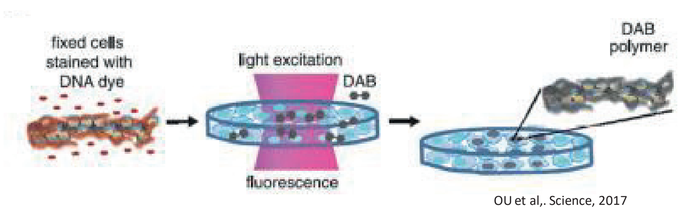

OU et al,. Science, 2017

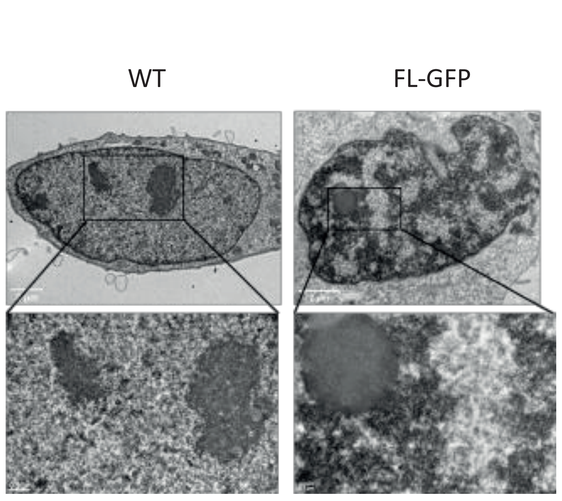

The FL of TET1 induced chromatin nucleoplasm segregation

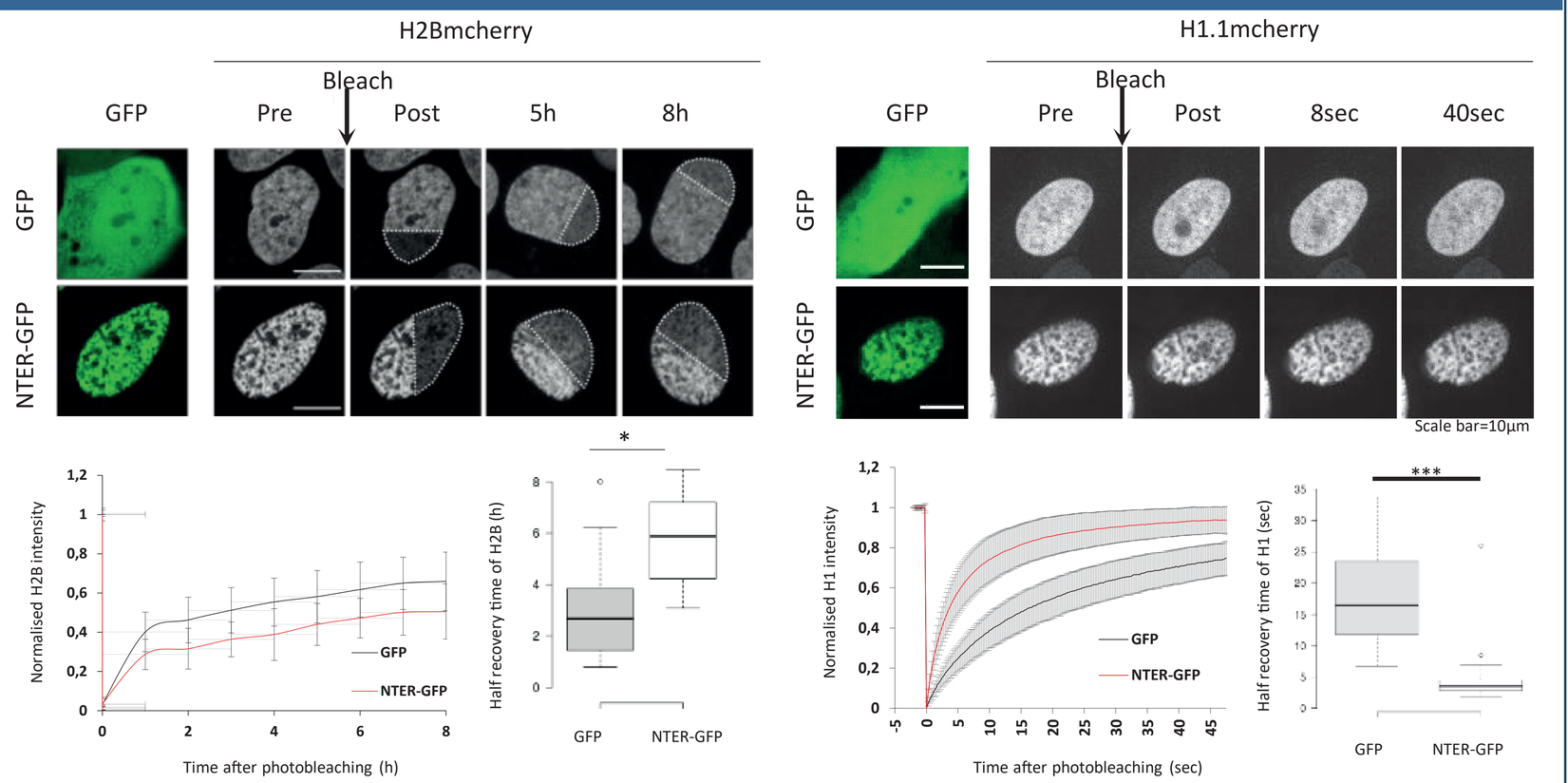

Histone turnover is modified in the presence of the N-terminal domain of TET1

T.test P<0.05*, P<0,005**, P<0,0005***

Conclusion and perspectives

Ours images obtained by confocal and electron microscopy reveal that overexpression of the N-terminal domain of TET1 induces a global chromatin reorganization in U2OS cells. Moreover, we showed that dynamic of chromatin components such as histones is modified in this condition. Therefore the N-terminal domain of TET1 overexpression inducing chromatin restructuration impacts not only the high order chromatin organization but also affect its molecular behavior. Because the catalytic activity of TET enzymes is not required for chromatin reorganization, we aim to analyze potential partners of the NTER domain which could be involved in this phenomenon througth the IP followed by MS analysis.

Synchronizing retrograde transport: New assays, new questions, new applications

Yen-Ling Lian, Séverine Divoux, Franck Perez and Gaelle Boncompain

Institut Curie, CNRS UMR144 Research Center, Paris, France

(Contact: yen-ling.lian@curie.fr)

Abstract

Mammalian cells are characterized by the co-existence of multiple pathways, including anterograde and retrograde transport of proteins. The Golgi apparatus has a central role in processing and sorting cargos in the bi-directional trafficking. The Retention Using Selective Hooks (RUSH) system allows the synchronization of the transport of cargos from the ER to downstream compartments and to systematically analyze the secretory routes (Boncompain et al., 2012). Owing to the interaction of streptavidin (CS) fused to an ER-resident protein and streptavidin-binding peptide (SBP) fused to the reporter protein, the reporter can be retained in the ER and then released with the addition of biotin. However, biotin has a high affinity to streptavidin, impairing reversibility of RUSH assay. With the newly identified ligands, named Artificial Ligands of Streptavidin (ALiS), Golgi-to-ER retrograde transport can be monitored using RUSH assay upon the washout of ALiS (Terai et al. 2015; Tachibana et al. 2017).

To set-up a sensor to detect the binding of the hook and reporter in real-time and to easily quantify the amount of ER-retrieved proteins, we employed Split Fluorescence-Activating and absorption Shifting Tag (SplitFAST) (Tebo and Gautier, 2019) in the RUSH system. Our results revealed that SplitFAST tags may disrupt the interaction between streptavidin and ALiS-1, and thus prevent the disassembly of the tags and fluorogenic chromophore.

Evaluating the transport of Golgi enzymes in the context of their overexpression might disturb their trafficking mechanisms, we intend to analyze their transport at endogenous level, using CRISPR-Cas9 knock-in of the SBP and a fluorescent protein. We have generated knock-in clones in the SUM159 cell line, edited to express β-1, 4-galactosyltransferase 1 (GalT)-SBP-EGFP. Although the subcellular distribution of GalT-SBP-EGFP was detected in the Golgi apparatus, up to now we are unable to detect its retrieval in the ER by overexpressing the hook CS-KDEL and CS-myc-KDEL. Utilizing a human invariant g chain protein (Ii) fused to streptavidin could be an interesting strategy to investigate different retrograde (Golgi-to-ER) trafficking routes. Also, genome-wide screening (eg. RNAi or CRISPRi) would be integrated to identify the key players in the retrograde transport.

Introduction

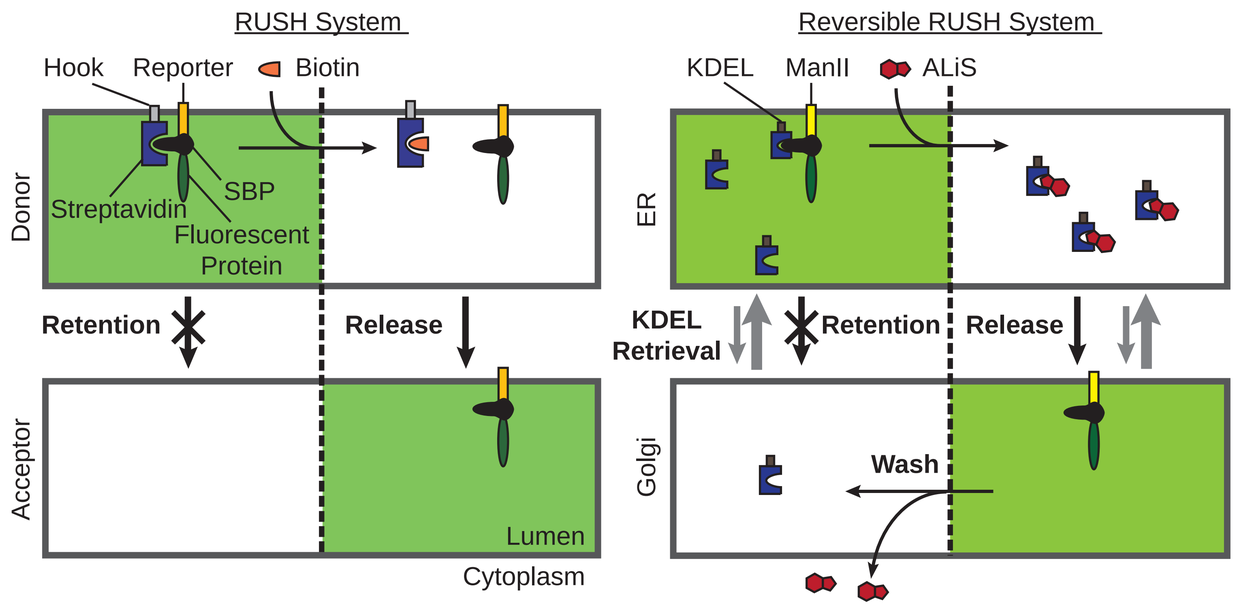

Results

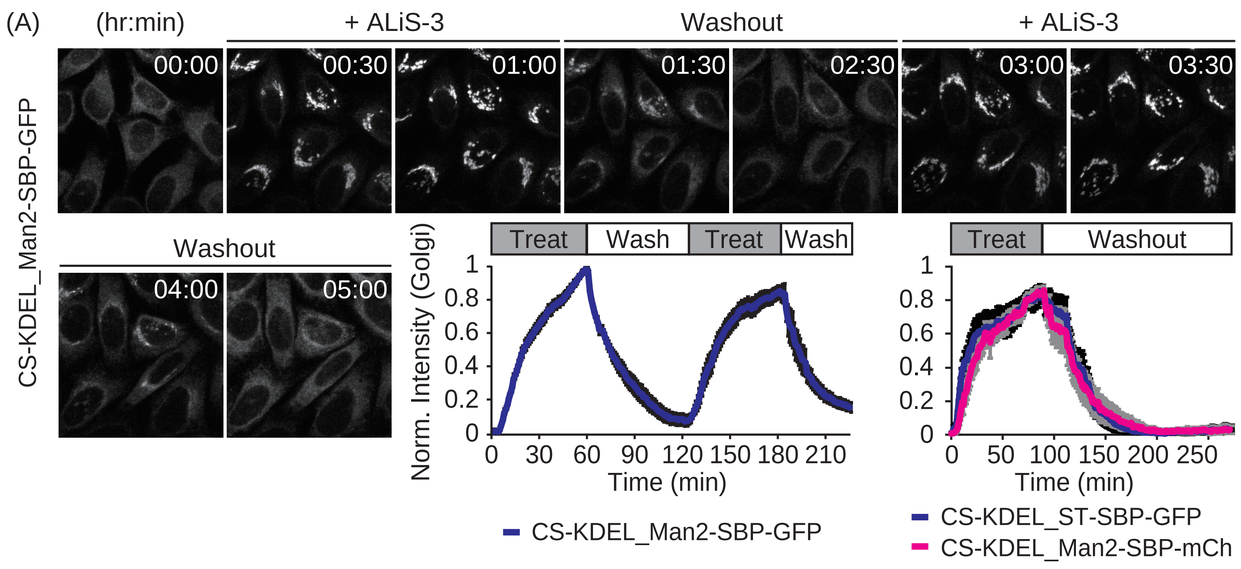

Project 1: Develop a tool to detect the association of the hook and reporter and quantify Golgi-to-ER transport

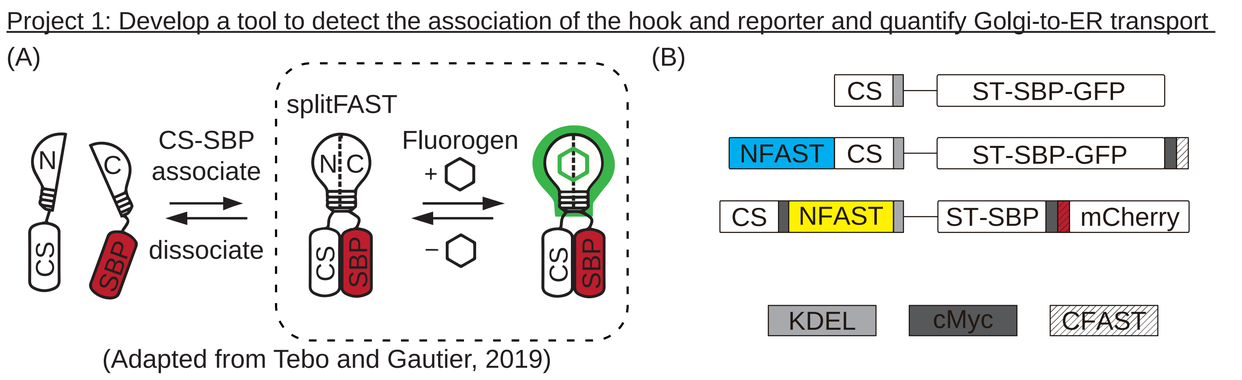

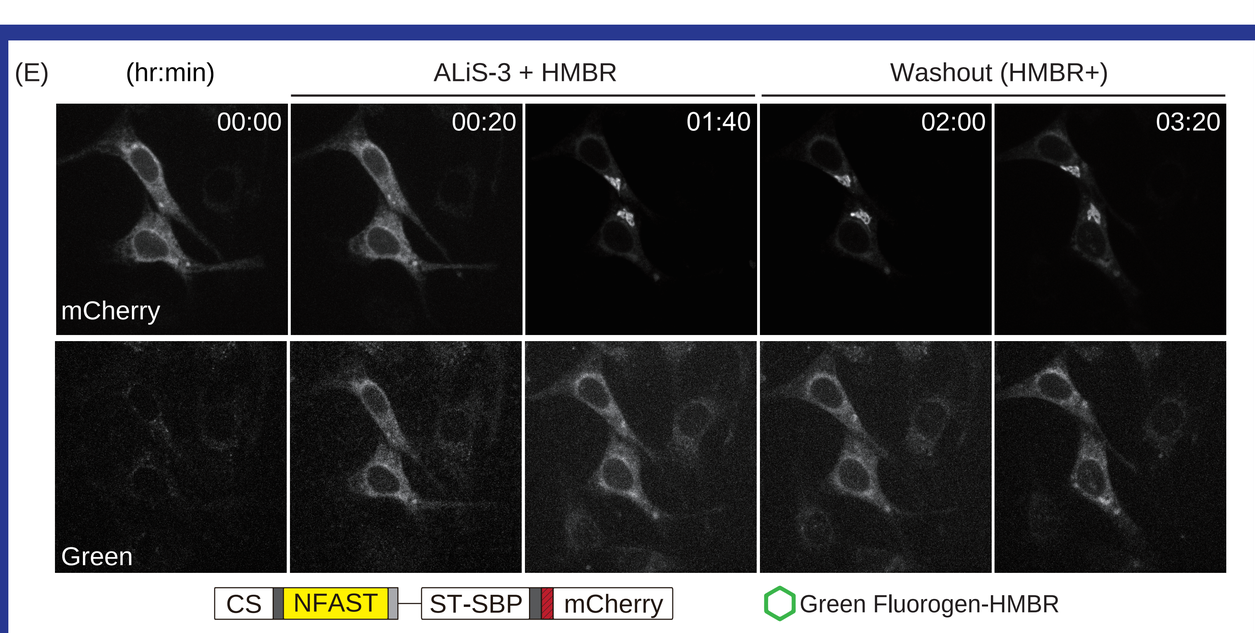

Project 2: Set-up “RUSH-synchronizable” endogenous Golgi enzymes using CRISPR-Cas9

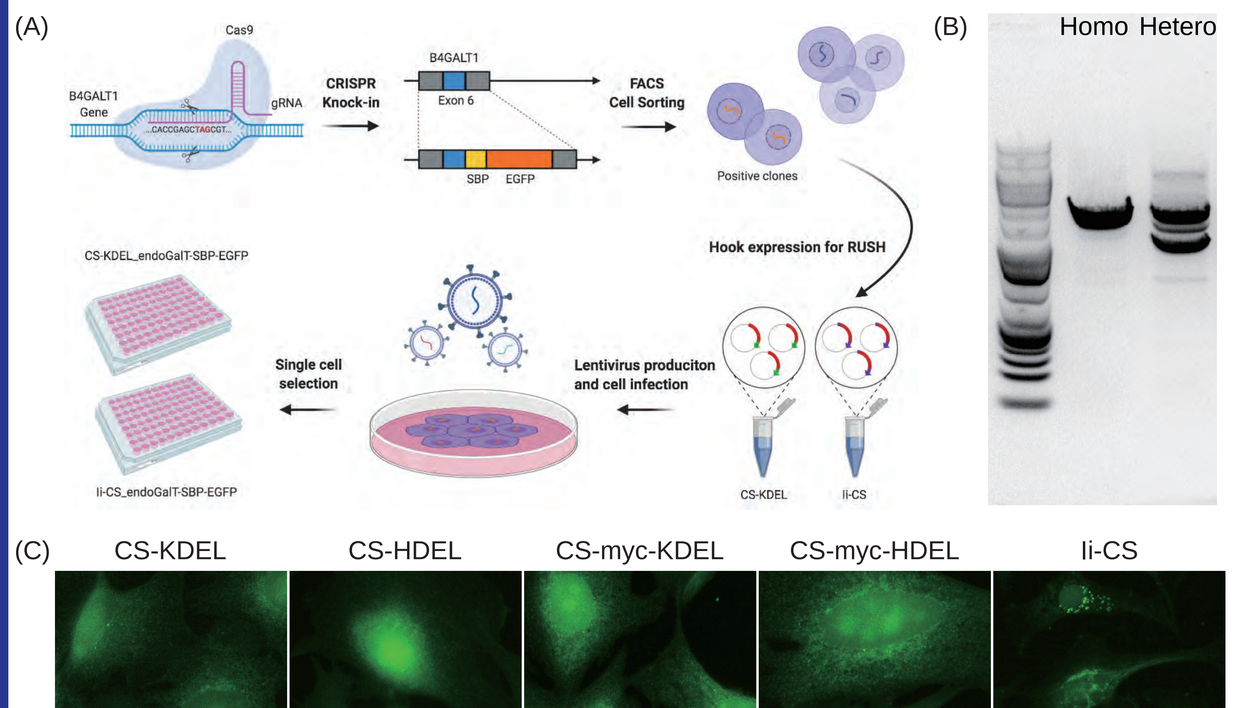

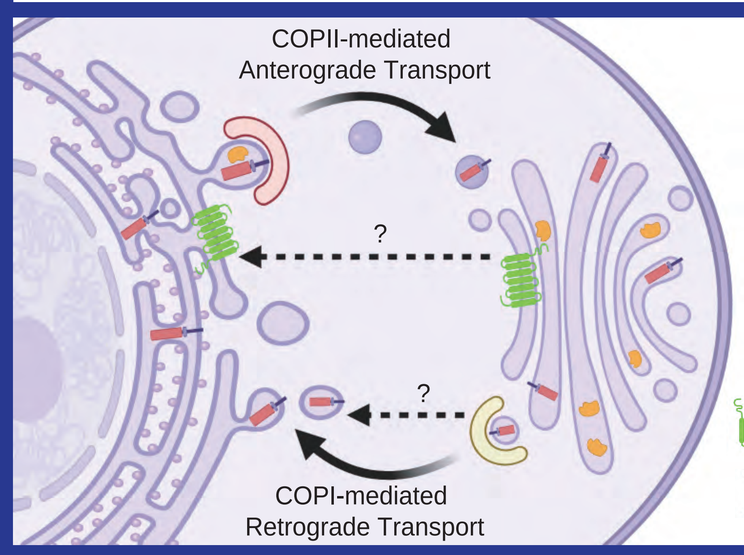

Perspective

Aim 1. Examine the regulatory factors in retrograde transport (eg. KDELR-dependent pathway)

Aim 2: Identify the golgi enzymes recycling in retrograde transport through genome-wide screening (eg. RNAi or CRISPRi)

KDELR
Cargo
Golgi enzyme
COPI
COPII

Genomic functions of the OvoL/Shavenbaby transcription factor, a conserved regulator of Epithelium Mesenchyme plasticity

A. Mancheno-Ferris[1 3], P. Lhoumaud[2 3], S. Plaza[1 3], O. Cuvier[2 3], C. Polesello[1 3], F. Payre[1 3]

1. Centre de Biologie du Développement ; 2. Laboratoire de Biologie Moléculaire Eucaryote ; 3. Centre de Biologie Intégrative (CBI) de Toulouse.

Contact: alexandra.mancheno-ferris@univ-tlse3.fr

Introduction

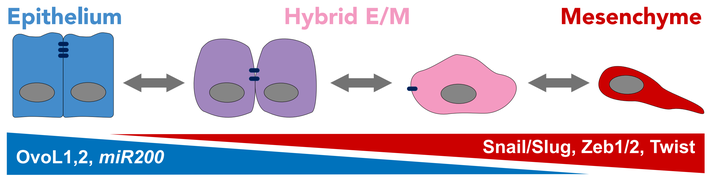

Epithelium-mesenchyme plasticity plays key roles in the aggressiveness of epithelial tumors, such as breast, lung, prostate and colorectal cancers. There are bi-directional transitions between epithelial (E) and mesenchymal (M) phenotypes, progressing through a series of **hybrid E/M** states. The hybrid E/M state is a hallmark of adult stem cells, as well as cancer stem cells that favor metastasis and resistance to treatment. A core of transcription factors (Snail, Zeb1/2, Twist, ...) is renowned to induce epithelium to mesenchyme transition 5EMT). OvoL1/3 have recently been identified as key epithelial factors, counteracting EMT and stabilizing the hybrid E/M phenotype in normal and cancer stem cells. Understanding the molecular activity of OvoL factors is therefore an important challenge, but it has been hampered by the existence of three paralog genes, each encoding different protein isoforms.

We address this issue using as a model system *Drosophila* that encodes a single *OvoL* gene, called **Ovo/Shavenbaby (Svb)**. Svb governs epithelial remodeling during epidermis development, and our recent studies demonstrate the importance of Svb in adult stem cells. Svb is translated as a long repressor, **SvbREP**, which is processed into a shorter transcriptional activator, **SvbACT**, in response to **Polished rice (Pri)** peptides that trigger limited degradation by the proteasome.

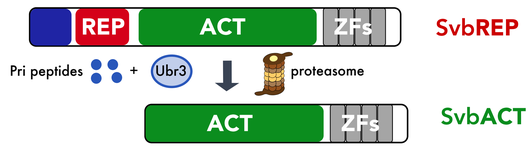

To investigate how Svb regulates genome expression, we engineered S2 cell lines producing each of the two Svb isoforms and performed RNA-seq and ChIP-seq experiments and bioinformatic analyses.

Genomic Binding Sites

ChIP-seq
- SvbACT
- SvbREP

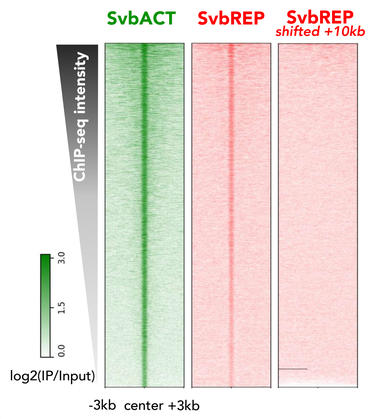

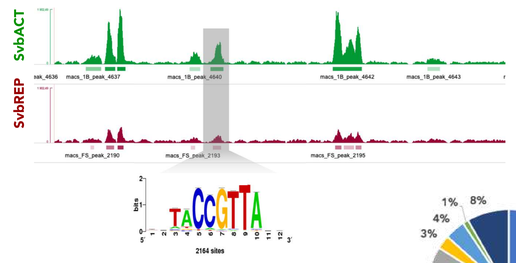

SvbACT and SvbREP bind to same genomic sites. Peaks are enriched in consensus Svb binding motifs; they are mostly located in promoter/ enhancer regions.

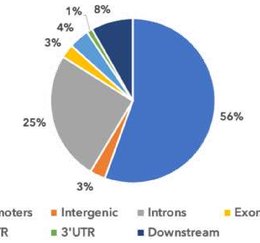

Target Genes

RNA-seq
- Ctrl
- SvbACT
- SvbREP

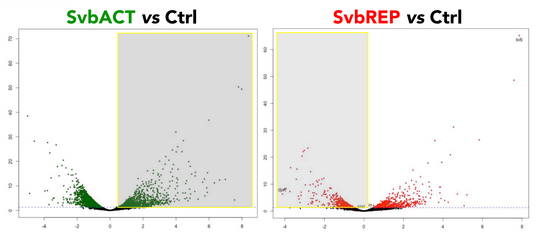

logFC SvbACT >0 [AND] logFC SvbREP < 0
[AND] pValueBenjamini SvbACT/SvbREP < 0.05

288 candidates

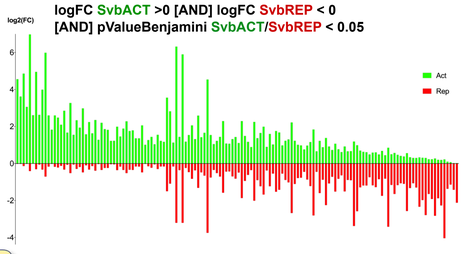

Data integration
- RNA-seq
- ChIP-seq

Svb Target Genes [AND] Svb Binding

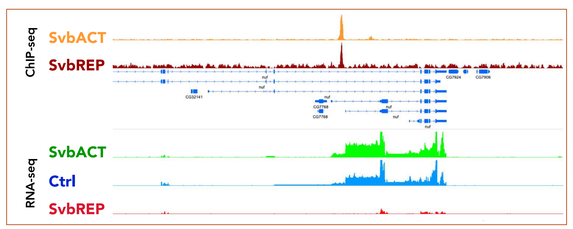

247 Svb Direct Target Genes

Comparison between Cell Types

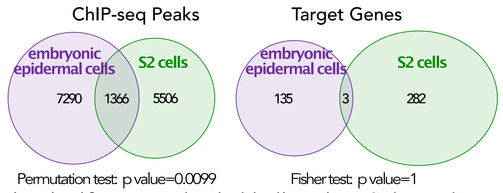

Despite significant overlap in binding sites, Svb regulates different sets of target genes between embryonic and S2 cells.

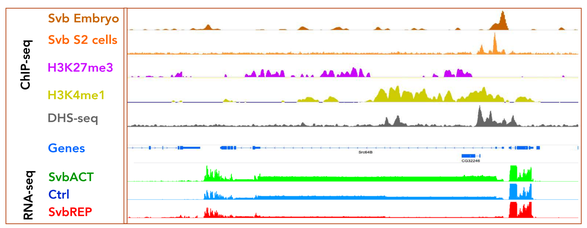

Binding sites associated with Svb target genes in S2 cells can be bound by the Svb factor in embryonic epidermal cells.

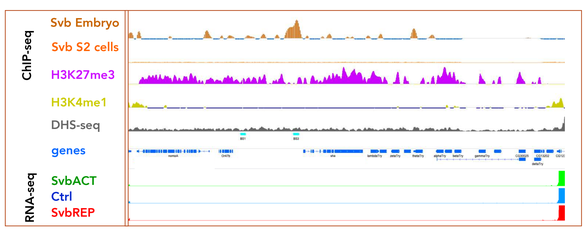

In S2 cells, Svb does not bind to embryonic target enhancers, which often display hallmarks of inactive chromatin.

Chromatin Landscape

Data mining
- ChIP-seq

Available ChIP-seq raw data for histone PMTs

Standardized Bioinformatic pipelines

Predictive model of Svb/ chromatin interactions

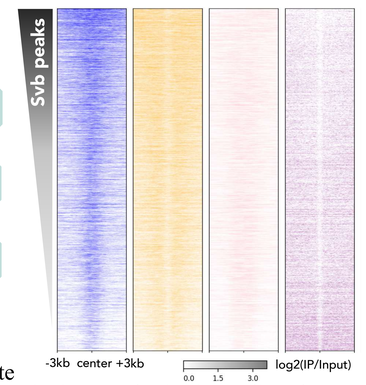

Data mining shows that Svb binding sites correlate with regions enriched for H3K27ac and H3K4-me1/3 and anticorrelate with H3K27me3 .

ChIP-seq
- histone PMTs in the 3 cell lines

We tested our model by performing ChIP-seq experiments for histone PMTs in control S2, or SvbACT or REP cells.

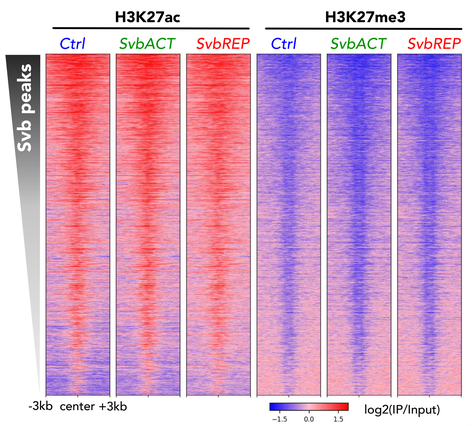

Conclusions

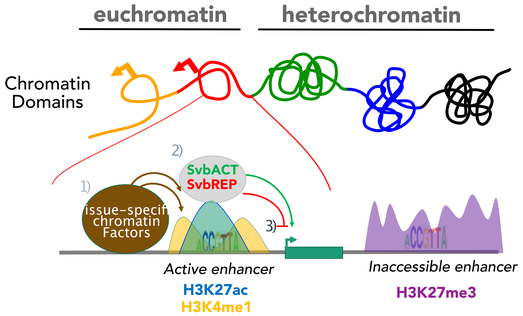

SvbACT and SvbREP regulate positively or negatively gene expression through binding to a same array of genomic regions, the accessibility of which is gated by specific histones PMTs that define the set of Svb target genes between cell types.

Acknowledgments

We are very grateful to la Ligue contre le cancer for supporting AMF, members of the FP and OC teams and M. AGUIRREBENGOA for discussion and help, as well as M. THOMAS-CHOLLIER (IBENS, Paris) and S. AERTS (VIB-KU, Leuven).

References

Al Hayek *et al.*, in revision
Mancheno *et al.*, **Medecine/Sciences** 2020
Ray *et al.*, **Elife** 2019
Bohere *et al.*, **Nature Communications** 2018
Zanet*, Benrabah* *et al.*, **Science** 2015
Chanut *et al.*, **Nature Cell Biology** 2014
Menoret*, Santolini* *et al.*, **Genome Biology** 2013
Kondo*, Plaza* *et al.*, **Science** 2010

ICELLNET: a transcriptome-based framework to dissect intercellular communication

Floriane Noël[1,2,3*], Lucile Massenet-Regad[1,2,3*], Irit Carmi-Levy[1,2], Antonio Cappuccio[1,2], Maximilien Grandclaudon[1,2], Coline Trichot[1,2], Fanny Coffin[1,4,5], Yann Kieffer[1,6], Philippe Hupé[1,4,5,7], Fatima Mechta-Gregoriou[1,6], and Vassili Soumelis[1,2,3]

[1]Institut Curie, [2] Inserm U932, [3]Inserm U976, [4]Inserm U900, [5]Mines ParisTech, [6]Inserm U830, [7]CNRS, UMR144

CONTACT: lucile.massenet@inserm.fr

INTRODUCTION

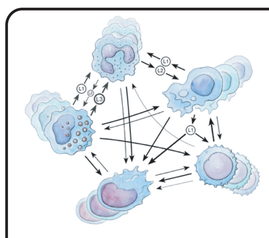

- Study intercellular communication
- Development of a computational framework to quantify and visualize intercellular communication
- Application of different public transcriptomic profiles from tumoral microenvironnement (RNAseq) and lupus nephritis (scRNAseq)

Existing tools
- Based only on scRNA-seq data
- Big ligand/receptor (L/R) databases
- Communication based on co-expression or correlation

ICELLNET framework
- Application to transcriptomic profiles of cell populations (R-NA-seq, microarray, scRNAseq)
- Small but expert-curated L/R database
- Versatility of the tool (cell granularity, L/R classification, di-versity of visualisation outputs)

RESULTS

1. Development of ICELLNET, a computational pipeline to dissect intercellular communication

First step: selection of cells of interest

Central Cell

Transcriptomic profile
Cell of interest

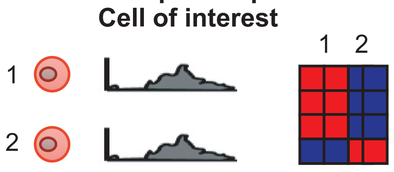

Partner Cell

Transcriptomic profile of other cells of interest
or
Human Primary Cell Atlas (public dataset)

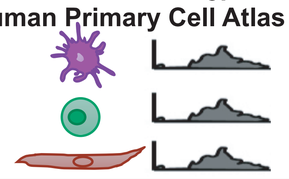

32 cell-types

734 samples

Cell granularity selection

Second step: selection of L/R expression

Expert-curated database of ligands/receptors

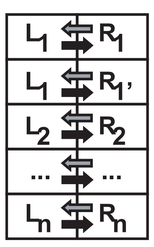

6 families

7 sub-families of cytokines

380 couples

Communication molecules granularity selection in database

Selection of ligand/receptor expression in partner cells and central cells

Expression data scaling by gene

Third step: communication score computation

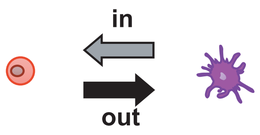

$$S_{j \to k} = \sum_i L_i^j \times R_i^k$$

L: Ligand mean expression
R: Receptor mean expression

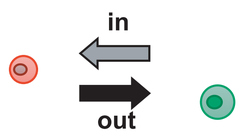

Communication score visualisation

Intercellular communication network representation

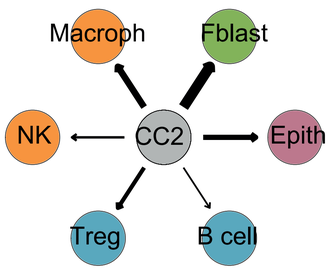

Communication molecules distribution

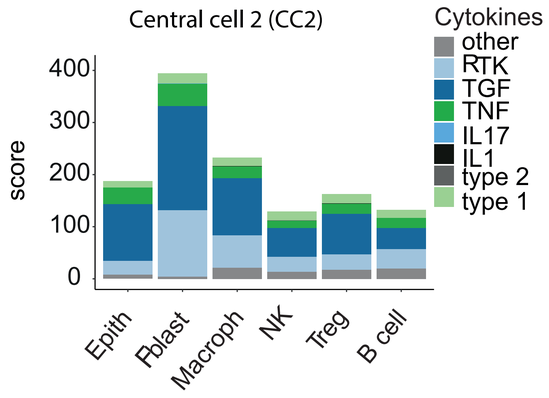

Communication score matrix

	CC1	CC2
Epith	255	188
Fblast	408	394
Macroph	289	232
NK	167	129
Treg	212	163
Bcell	171	132

Statistical score comparison

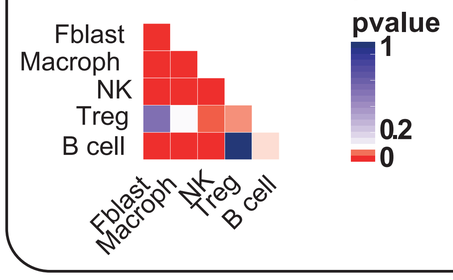

Individual communication scores distribution

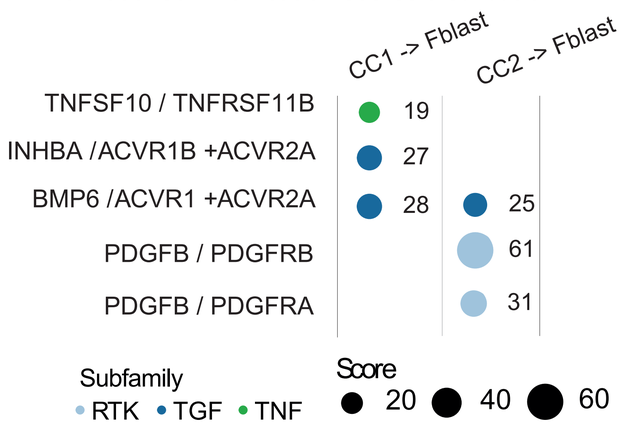

2. Application of ICELLNET to study human breast cancer-associated fibroblasts: CAF-S4 uses specific communication channels to interact with the TME components

A Workflow for study of Triple Negative Breast Cancer CAF subsets

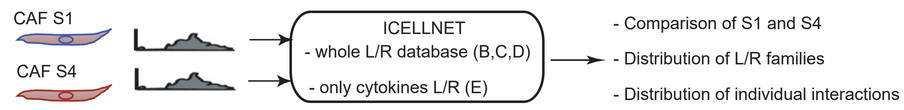

B Outward communication from CAF-S1 (n=6) and CAF-S4 (n=3) subsets to partner cells (Human Primary Cell Atlas)

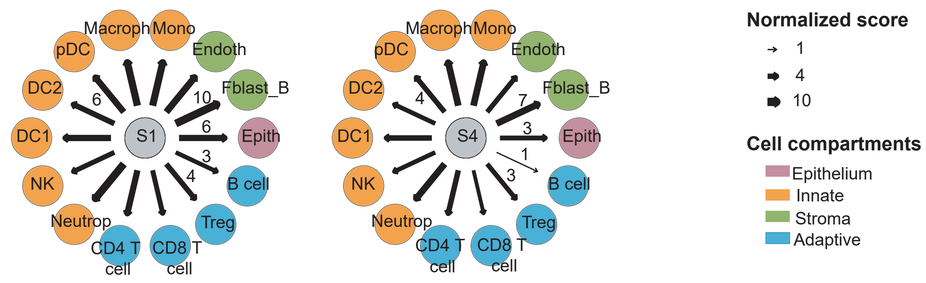

C Contribution of molecules families to above communications scores for selected partner cells

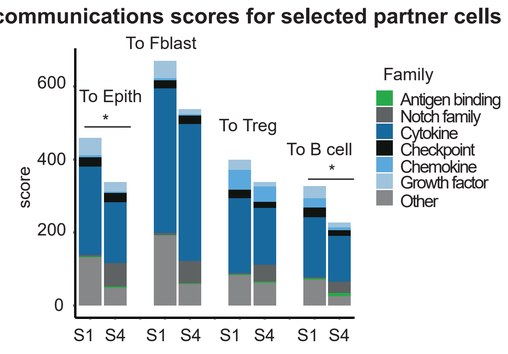

D Individual interaction scores between CAF subsets and Tregs

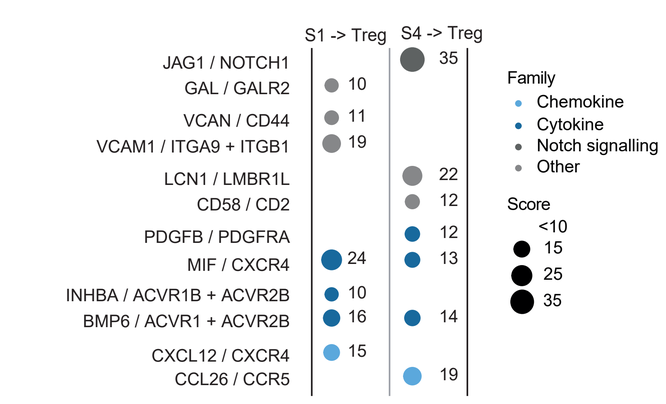

E Cytokine mediated intercellular comunication - Contribution of each subfamilies of cytokines

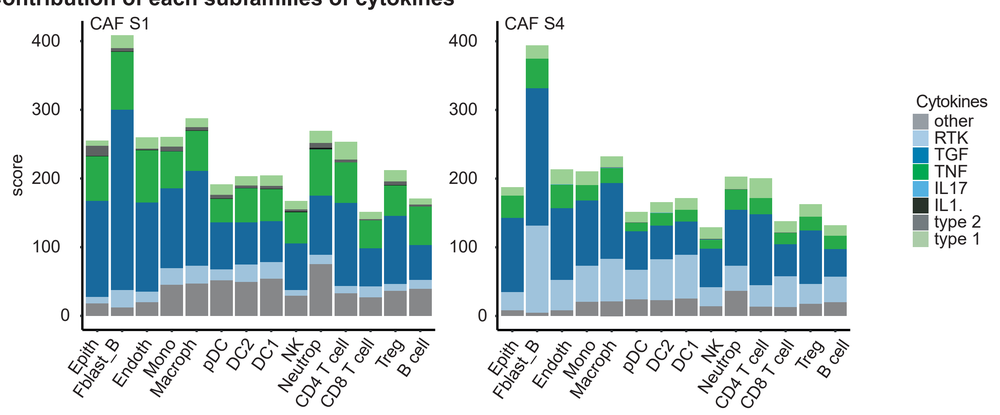

3. Lupus nephritis cell-cell communication network infered from single cell RNAseq datasets using ICELLNET

A Cellular content of the public dataset of lupus nephritis

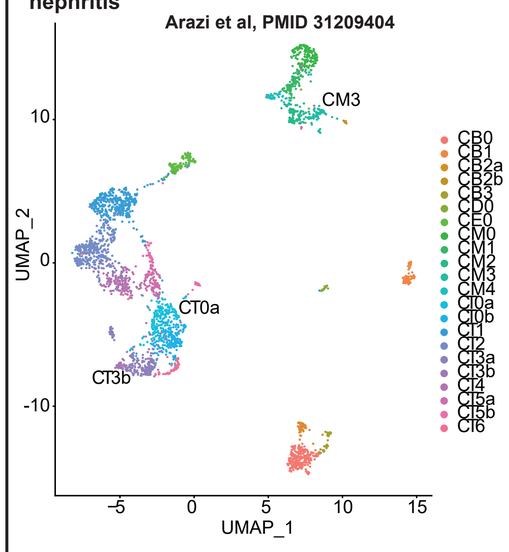

B Focus on DC-T communication: ICELLNET pipeline by taking average expression of DC (CM3) and T (CT3b / CT0a) clusters.

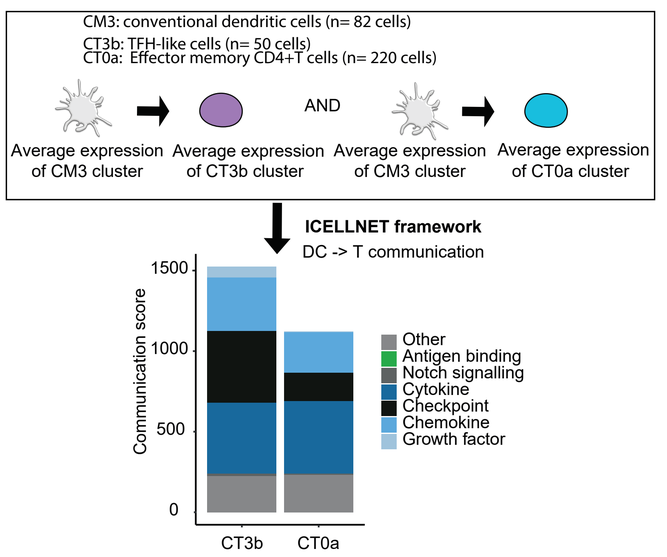

C Specific individual interaction scores that most differ

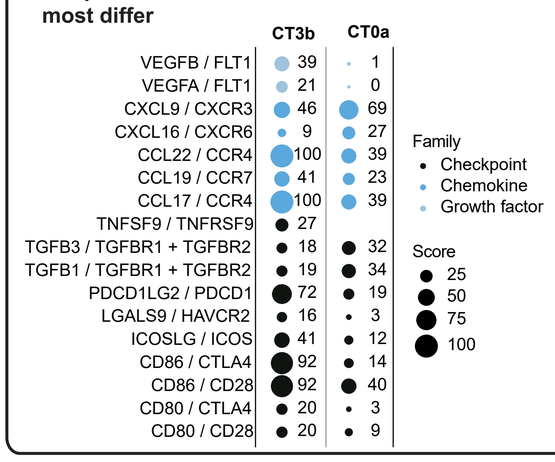

D Comparison of communication scores using ICELLNET resource (Human Primary Cell Atlas) for DC instead of CM3 cluster: Number of L/R interactions contributing to communication scores

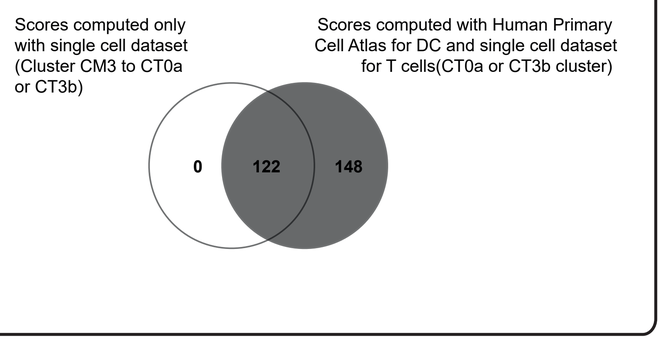

CONCLUSION

- Development of ICELLNET, a new framework to study intercellular communication
- Useful resource for the scientific community with a expert-curated database of ligands and receptors
- Easy to apply on transcriptomic profiles of various cell populations (scRNAseq, RNAseq, microarray)
- Diversity of output visualisation to generate hypothesis on cell-cell communication channel
- Tool partially experimentally validated in a DC-T in vitro model (not shown here, see preprint)

PROSPECTS

- Increase L/R database in collaboration with experts
- Improve the granularity of the cell types and conditions, and the families/subfamilies of molecules
- Apply to immune cell populations to study communication in different cancers (breast, head and neck..) or disease context

LINK TO PREPRINT: https://www.biorxiv.org/content/10.1101/2020.03.05.976878v1
GITHUB: https://github.com/soumelis-lab/ICELLNET/

ACKNOWLEDGMENTS

CYTOMETRY PLATFORM, INSTITUT CURIE
NGS PLATFORM, INSTITUT CURIE

Trajectoires d'adhésion à l'hormonothérapie adjuvante après un diagnostic de cancer du sein : étude populationnelle à partir de la Cohorte Cancer

V.Memoli [a], *G.Lailler* [b], *C.Le-Bihan* [b], *MK.Bendiane* [a], *S.Lauzier* [c], *J.Mancini* [a], *PJ.Bousquet* [b], *AD.Bouhnik* [b]

Contact : victoria.memoli@inserm.fr

a. Aix Marseille Univ, INSERM, IRD, SESSTIM, Sciences Economiques & Sociales de la Santé & Traitement de l'Information Médicale, Marseille, France.
b. Health data and assessment department, Survey, data-science and assessment division, Institut National du Cancer (INCa), Boulogne Billancourt, France
c. CHU de Québec-Université Laval Research Center, Canada

Introduction

- L'**H**ormonothérapie **A**djuvante (**HA**) est prescrite pour les femmes qui ont un **c**ancer du **s**ein (**CS**) hormono-sensible (60 à 80% des CS). Elle doit être prise quotidiennement pendant une durée d'au moins 5 ans pour réduire les risques de récidive et de mortalité
- Une proportion importante de femmes seraient non-persistantes et/ou non-adhérentes ce qui augmenterait le risque de récidive et de mortalité

Objectifs

- ✓ Identifier les profils d'adhésion à l'HA sur une période de 5 ans après une chirurgie pour un CS en 2011
- ✓ Etudier les facteurs associés à chacun des profils d'adhésion

Méthode

Base de données : Cohorte Cancer de l'INCa

Population : Femmes avec une chirurgie pour un primo-CS non métastasé en 2011 et avec au moins un remboursement d'HA 12 mois maximum après la chirurgie

Mesure de l'adhérence : calcul de la **P**roportion de **J**ours **C**ouverts (PJC) à partir des données de remboursement d'HA de la Cohorte Cancer

Analyses :

- **G**roup-**B**ased **T**rajectory **M**odeling (GBTM) : identifier des groupes de femmes qui ont des profils d'adhérence similaire en fonction du temps
- Régression logistique : étudier les facteurs associés à chaque trajectoire

Résultats

A. Caractéristiques des patientes

- Population totale = 33 260
- > 60 ans : **54%**
- Mastectomie : **20%** (tumorectomie **80%**)
- Chimiothérapie adjuvante : **35%**
- Radiothérapie adjuvante : **73%**
- 1ere prescription d'HA : **71%** IA (vs **29%** tamoxifène)
- Changement d'HA : **33%**
- Décès : **5,44%**
- Récidive : **13,2%**

B. Trajectoires d'adhésion à l'HA

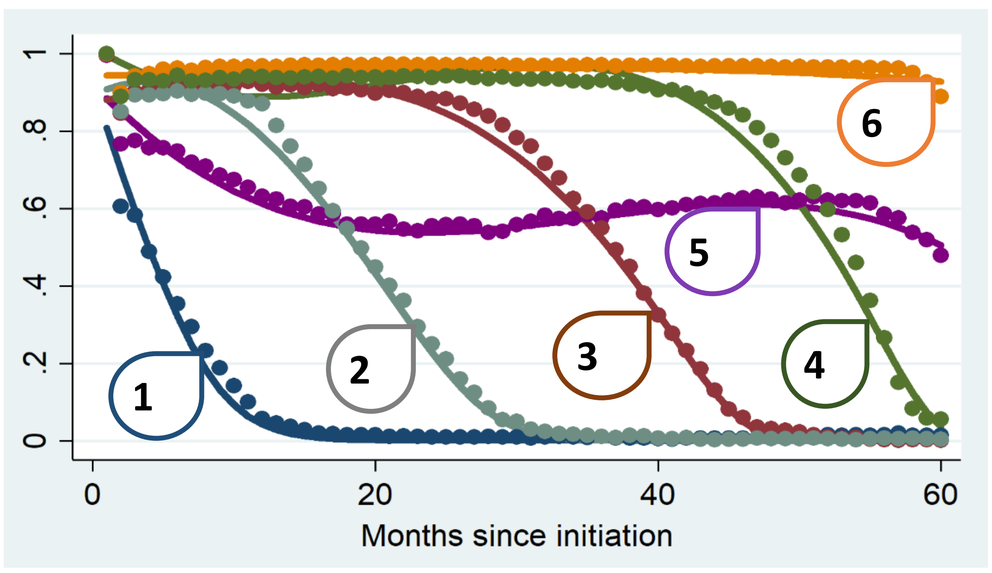

Description des groupes de trajectoires :

1) **Arrêt dès la 1ere année : 6,6%**
2) **Arrêt précoce : 5,7%**
3) **Bonne adhérence puis arrêt : 6,3%**
4) **Arrêt tardif : 8,3%**
5) **Adhérence sous optimale durant les 5 années : 4,3%**
6) **Adhérence optimale : 68,8%**

C. Facteurs associés à chaque trajectoires

Groupe de référence : Trajectoire 6 adhérence optimale

Facteurs associés	Associés + ou -	Trajectoire
>70 ans ***vs*** 60-70 ans	+	1 2 3 4 5
50-60 ans ***vs*** 60-70 ans	+	5
	-	3
< 50 ans ***vs*** 60-70 ans	+	2 5
Mastectomie ***vs*** Tumorectomie	+	2 3
Chimiothérapie néo-adjuvante	+	3 5
	-	4
Chimiothérapie adjuvante	-	1 2 4
Radiothérapie adjuvante	-	1 4 5
Changement d'HA	+	1 2 3 4 5
Zone défavorisée Haute ***vs*** Basse	+	1 5

Discussion/Conclusion

1. 6 groupes de trajectoires d'adhérence ont été identifié :
   - 4 groupes de femmes non-persistantes
   - 1 groupe de femme non-adhérentes
   - 1 groupe de femmes adhérentes sur la totalité de la période
2. À 5 ans du diagnostic, 70% des femmes ont une adhérence optimale
3. Les principaux facteurs associés à la non-adhérence sont l'âge et les changements d' HA

Transmembrane coordination of preprotein recognition and motor coupling by the mitochondrial presequence receptor Tim50

Cyril Moulin (cyril.moulin1@univ-tlse3.fr), Raffaele Ieva, Anne Caumont-Sarcos

Caumont-Sarcos A.*, Moulin C.*, Poinot L., Guiard B., van der Laan M. and Ieva R.
Cell Reports, March 2020, 3;30(9):3092-3104 *equal contribution

Introduction

Import of protein via the presequence pathway

Mitochondria are essential organelles involved in nutrient catabolism, energy conversion and signaling pathways. Maintenance of mitochondrial functionality is thus a key cellular priority and relies on the organelle proteome. This PhD project aims to decipher the regulatory mechanisms that promote correct protein biogenesis and support the maintenance of mitochondrial function. Roughly 70 % of mitochondria imported proteins carry a presequence and are calle preproteins. Preproteins are first transported accross the mitochondrial outer membrane and then recognised by TIM23, the presequence translocase.
TIM23 transports proteins into the matrix or the inner membrane (IM). To import preproteins into the matrix TIM23 recruits the presequence translocase associated motor (PAM) that actively pull preproteins segments using energy provided by ATP hydrolisis (A). If the preprotein possess a hydrophobic stop transfer signal after the presequence, matrix import is stopped. The hydrophobic protein segment is then released in the inner membrane via the opening of a lateral gate in TIM23 (B).

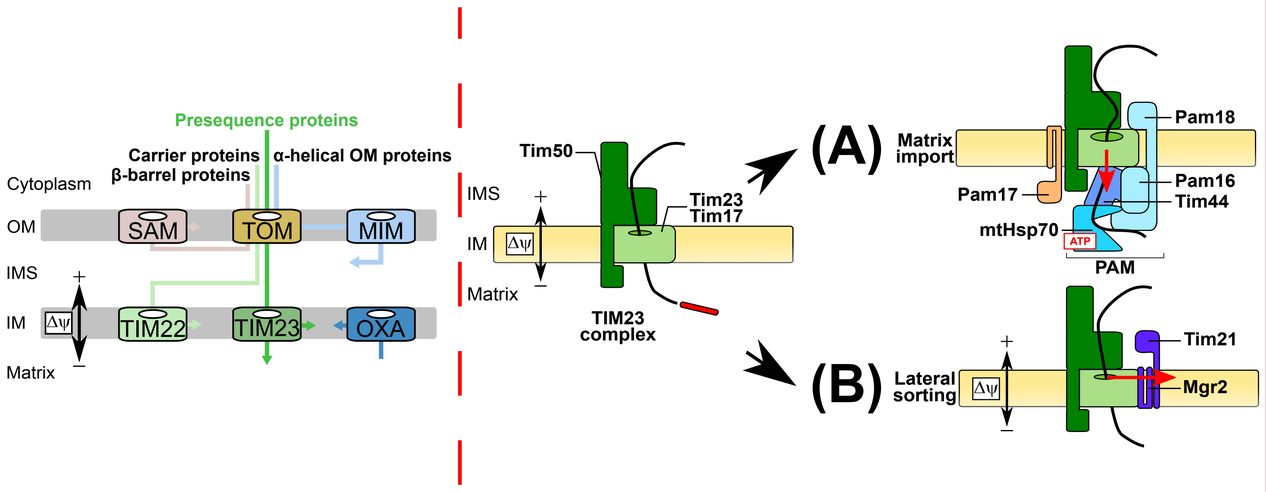

How is preprotein targeting signals transduced across the IM into matrix or IM transport task ?

Tim50 : presequence receptor

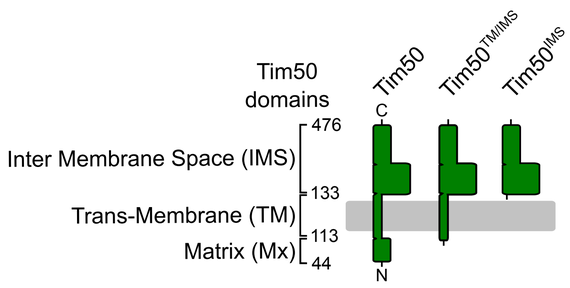

Tim50^{IMS} is sufficient for presequence receptor function

What are the role of the matrix and transmembrane domains of Tim50 ?

1 Tim50^{IMS}: presequence recognition and channel gating

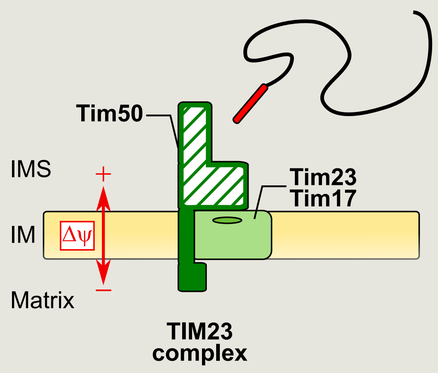

2 Tim50^{Mx}: Pam17 recruitment

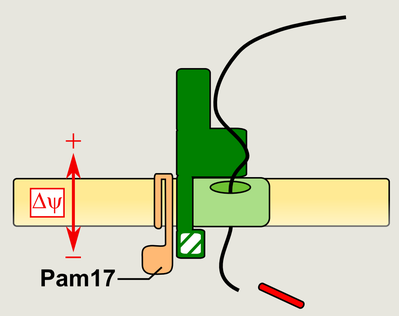

Tim50^{Mx} promotes for Pam17 recruitment

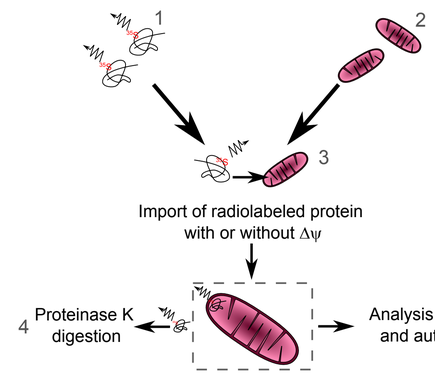

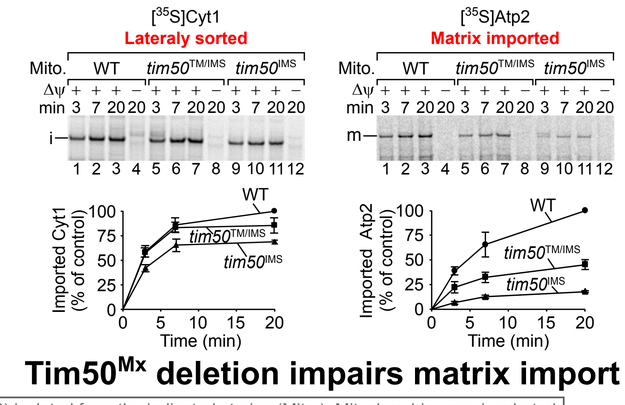

Tim50^{Mx} deletion impairs matrix import

Methods : import of radiolabeled preprotein (1) in mitochondria (2) isolated from the indicated strains (Mito.). Mitochondria were incubated in the presence of the radiolabeled preprotein for the indicated amount of time in the presence or absence of the Δψ (3), critical for the import. Preprotein that were not imported were digested by proetinase K treatment (4). Amounts of imported protein were quantified and compared between wild type and mutant strains (5).

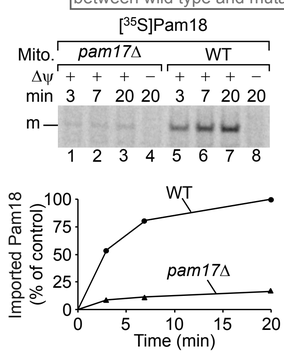

Pam18 import is dependent on TIM23 and requires the presence of Pam17.

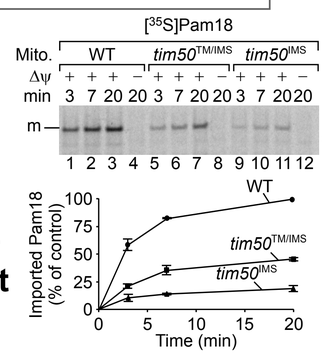

Tim50^{Mx} deletion impairs Pam17-dependent import

Tim50^{Mx} deletion impairs Pam17 recruitment

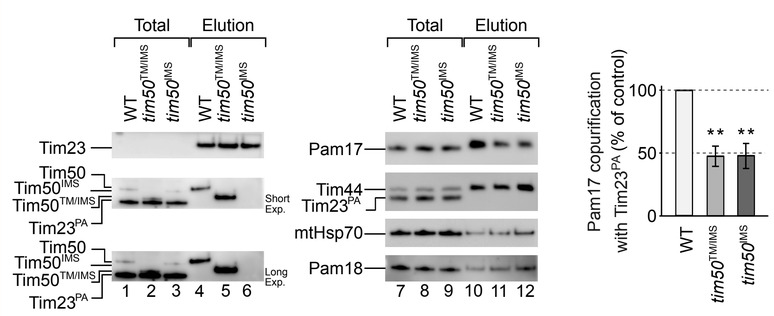

Methods : protein co-purification using the ProteinA-Tim23 fusion protein. This experiment allows quantification of TIM23 subunits recruitment in different mutants. Analysis of protein co-purified with TIM23 by SDS-PAGE followed by immuno-blotting.

Tim50^{IMS} is involved in motor assembly

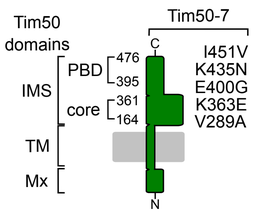

A collection of Tim50 heat-sensitive mutants strains was screened for defective import. Out of this screen, the mutant Tim50-7 was selected as it contains mutation that do not affect presequence recognition and that are only present in the IMS domain.

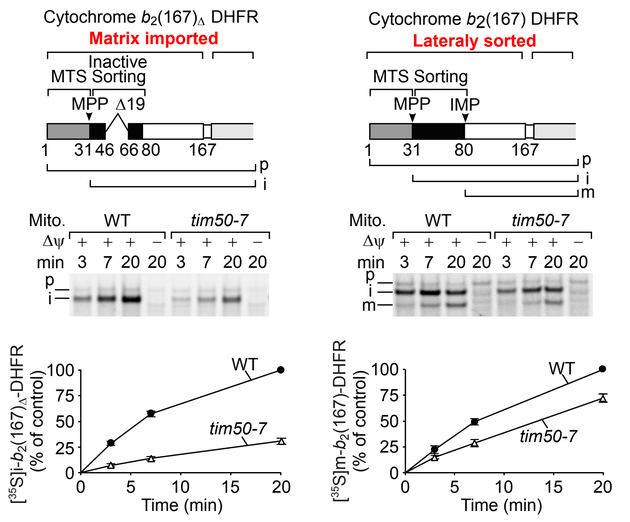

Mutations in Tim50^{IMS} affect matrix import

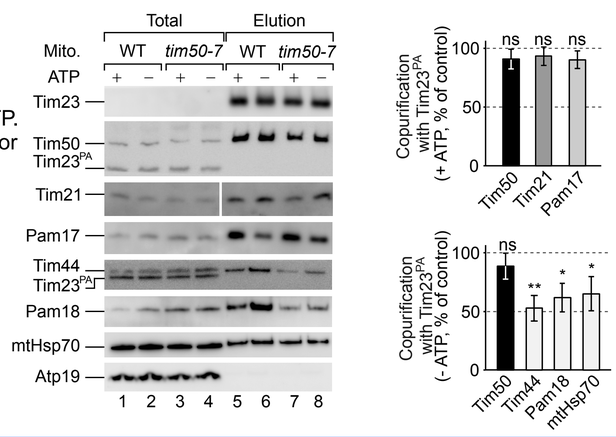

Protein co-purification using the ProteinA-Tim23 fusion protein. Analysis of TIM23 composition in the presence or absence of ATP. ATP depletion interrupts motor cycling and stabilizes TIM23-motor interactions.

Mutations in Tim50^{IMS} impair recruitment of motor subunits

3 Tim50^{IMS}: import motor assembly

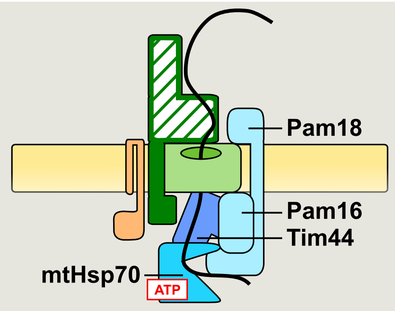

4 Tim50^{TM}: import motor activity

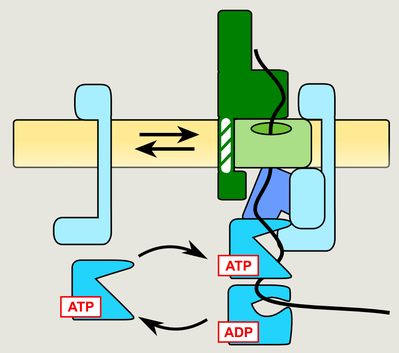

Tim50^{TM} promotes motor cycling

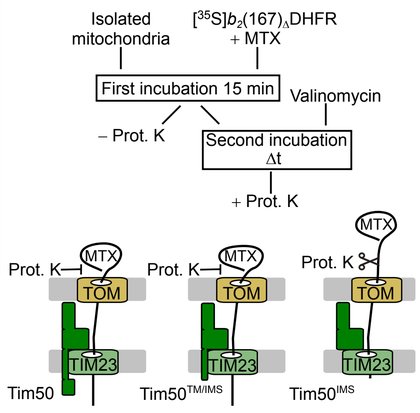

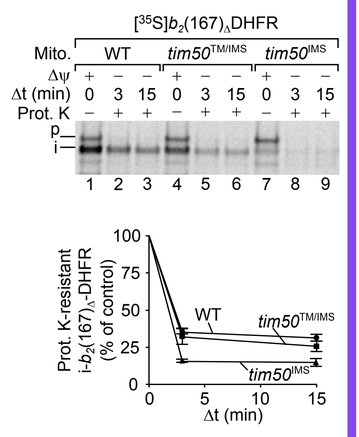

Tim50^{TM} deletion impairs motor activity

Methods : Fusion of cytochrome b2 $(167)_{\Delta}$ with the DHFR protein can be used to assess motor activity. In the presence of metotrexate (MTX), the DHFRmoiety folds. Folded DHFR is too large to pass via the TOM complex, blocking this fusion preprotein in a two membrane-spanning conformation. Active motor pulling on the substrate reuces accessibility to proteinase K (PK) digestion while defect in motor pulling allows back sliding of the substrate and PK accessibility. In this assay, comparison of amount of PK protected substrate with the amount of total imported substrate (-PK lanes) allows to estimate PAM activity.

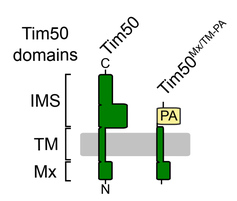

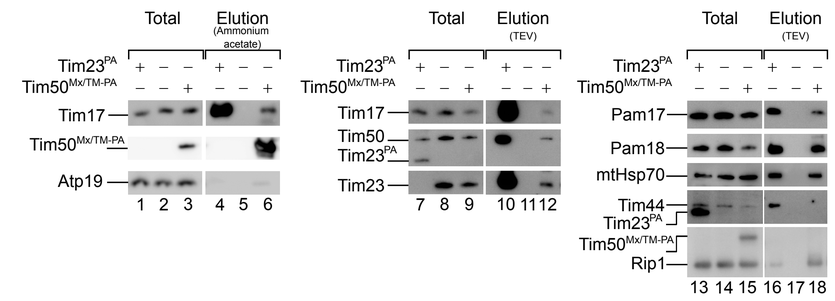

Tim50$^{Mx/TM-PA}$ pull-down allows to investigate the interacting partners of Tim50^{Mx} and Tim50^{TM}. We found that in addition to Pam17, also Hsp70 and Pam18 interact with the N-terminal moiety of Tim50. This result suggest the intriguing hypothesis that Tim50$^{Mx/TM}$ may stimulate the cycling of Hsp70 and Pam18 at the translocase.

Tim50^{TM} is implicated in motor cycling

Conclusion

Tim50 is involved in three distinct and consecutive steps of matrix import suggesting a trans-membrane coordination of signal reconition in the IMS with motor activation in the matrix

Open questions

Molecular mechanism implicated in the different functions caracterised for Tim50 are still unknown

How does Tim50 stimulate PAM activity?

How does Pam17 promote PAM assembly ?

Distinct immunopathological mechanisms of EBV-positive and EBV-negative post-transplant lymphoproliferative disorders

Cecilia Nakid-Cordero[1], Sylvain Choquet[2], Nicolas Gauthier[1], Noureddine Balegroune[2], Nadine Tarantino[1,3],, Véronique Morel[2], Nadia Arzouk[4], Sonia Burrel[5], Géraldine Rousseau[6], Fréderic Charlotte[7], Martin Larsen[1,3], Vincent Vieillard[1,3], Brigitte Autran[1], Véronique Leblond[2] and Amélie Guihot[1, 8] for the K-virogref study group.

1 Sorbonne Université (Univ. Paris 06), INSERM U1135, Centre d'Immunologie et des Maladies Infectieuses (CIMI-Paris), Hôpital Pitié-Salpêtrière, Paris, France; 2 Service d'Hématologie, Hôpital Pitié-Salpêtrière, Paris, France; 3 CNRS ERL8255, Centre d'Immunologie et des Maladies Infectieuses (CIMI-Paris), Paris, France; 4 Service de Néphrologie, Urologie et Transplantation Rénale, Hôpital Pitié-Salpêtrière, Paris, France; 5 Service de Virologie, Hôpital Pitié-Salpêtrière, Paris, France; 6 Service de Chirurgie Digestive, Hépato-Bilio-pancréatique et Transplantation Hépatique, Hôpital Pitié-Salpêtrière, Paris, France; 7 Service d'Anatomopathologie, Hôpital Pitié-Salpêtrière, Paris, France; 8 Département d'Immunologie, Assistance Publique-Hôpitaux de Paris (AP-HP), Groupe Hospitalier Pitié-Salpêtrière, Paris, France.

1. Background

Post-transplant lymphoprolipherative disorders (PTLDs) are the second most frequent neoplasia in transplant recipients, often associated with the oncogenic virus of Epstein-Barr (EBV). **EBV-induced PTLDs** (EBV+PTLDs) **arise in different immune/viral contexts than EBV-negative PTLDs** (EBV-PTLD).

2. Hypothesis and study rationale

We have formulated the hypothesis that EBV+PTLDs might have a different immunopathology than EBV-PTLDs.

To examine this hypothesis, we conducted a **multicentric prospective study** with **60 EBV-positive and 39 EBV-negative PTLD patients of the K-VIROGREF cohort,** recruited at PTLD diagnosis and before treatment (2013-2019), and compared them to PTLD-free Transplant Controls (TC, n=21).

3. Methods

Multiparameter flow cytometry

-Absolute lymphocyte counts (n=111).

-NK- and T-cell detailed phenotypes (n=49 and 97)

-Detection of total EBV-specific T cells by intracellular-cytokine staining after stimulation with EBV latent and lytic peptides (n=45).

ELISpot IFNγ

-Study of the distribution of effector and effector-memory T cell responses against EBV EBNA-3A and BZLF-1 proteins.

EBV peptides

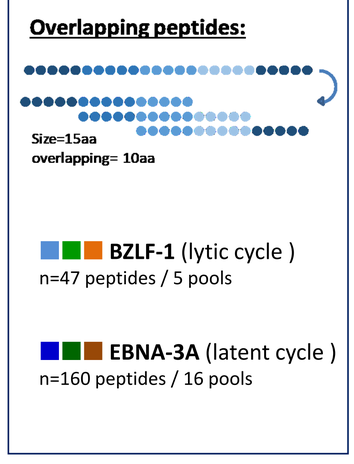

4. Results

Peripheral NK cell lymphopenia at EBV+PTLD and EBV-PTLD diagnosis is related with AICD

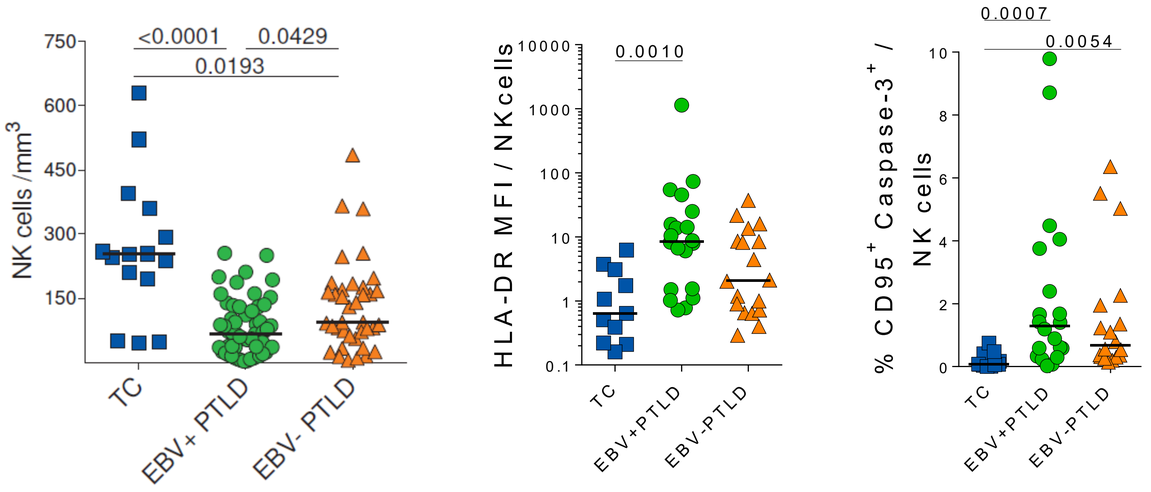

CD4+T cell lymphopenia is associated with poor outcome in EBV-PTLD patients

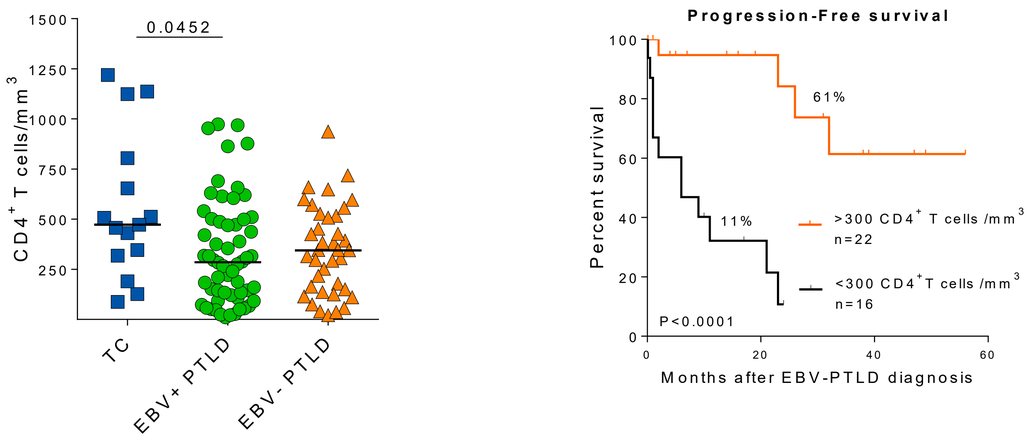

Distinct profiles of immune-checkpoint expression on NK cells of EBV+PTLDs and EBV-PTLDs

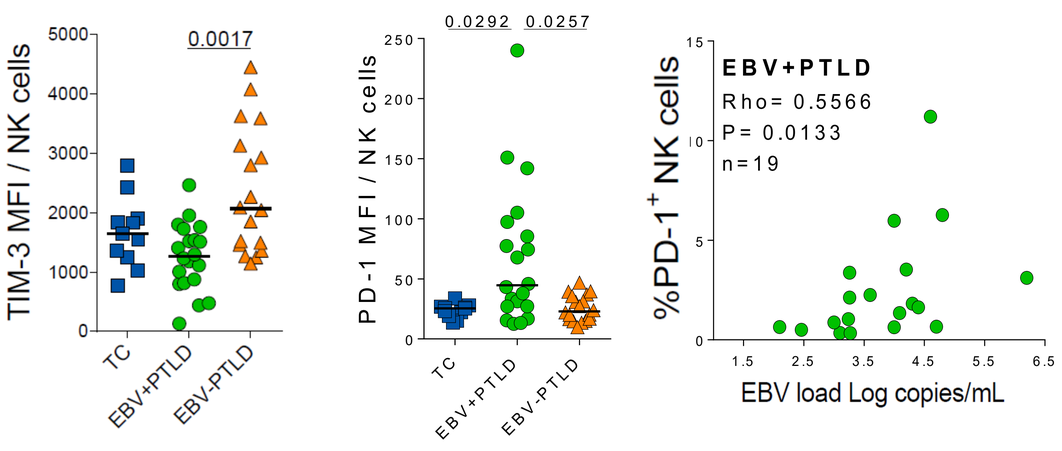

NK cells detected by flow cytometry as live lymphocytes CD3- CD56+

Alterations of the EBV-specific T cell responses at EBV+PTLD diagnosis

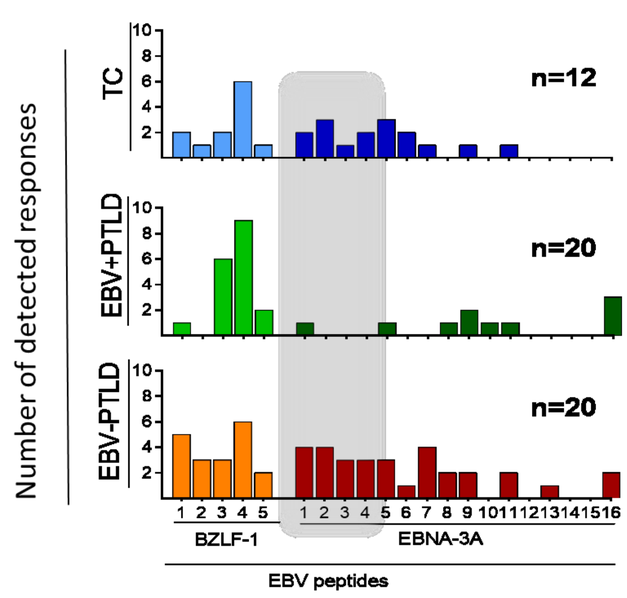

EBV-specific T cells responses detected by ELISpot IFNγ

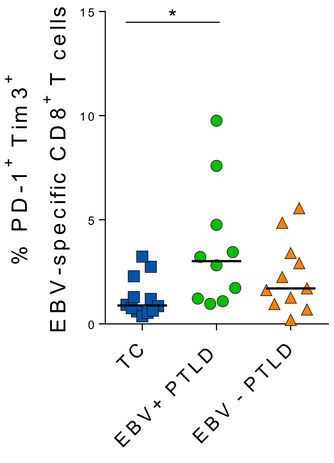

EBV-specific T cell (IFNγ+ IL-2+ and/or TNFα+) phenotype studied by flow cytometry

5. Conclusions:

Here we show both quantitative and qualitative alterations in the main cytotoxic lymphocytes (NK- and T CD8+) involved in EBV control at EBV+PTLD diagnosis, while EBV-PTLDs outcome is associated with the depth of immunosuppression.

These results provide new insights in the immunopathology of PTLDs, showing distinct patterns of immune exhaustion that might favor the development of EBV+ and EBV- PTLDs and suggesting predictive biomarkers for prevention and prognosis of EBV- PTLD, whilst encouraging innovating immunotherapies for PTLDs.

6. Aknowledgements:

This study was supported by INCA-DGOS-Inserm_12560 : SiRIC CURAMUS and by a PhD grant (C.N.-C; TAQK18773) from **La Ligue contre le cancer (www.ligue-cancer.net).** The authors would like to thank the K-GREF study group for sharing data, Christophe Parizot, the T4/T8 department, Alice Rousseau, Catherine Blanc and the staff of the Flow Cytometry Core CyPS (Sorbonne University, Pitié-Salpêtrière Hospital, Paris, France) for technical help, as well as Guislaine Carcelain for providing latent EBV peptides and Dormeur Investment Service Ltd. That provided funding to purchase equipment.

Boosting Self-Esteem in Oncology : the Lexical Association Technique

NIVEAU Noémie[1,2], NEW Boris[1], BEAUDOIN Marine[2]

[1] Univ. Savoie Mont Blanc, Univ. Grenoble Alpes, CNRS, LPNC, 73000 Chambéry, France
[2] Univ. Savoie Mont Blanc, Univ. Grenoble Alpes, LIP/PC2S, 73000 Chambéry, France
Contact : Noémie NIVEAU, noemieniveau@gmail.com

INTRODUCTION

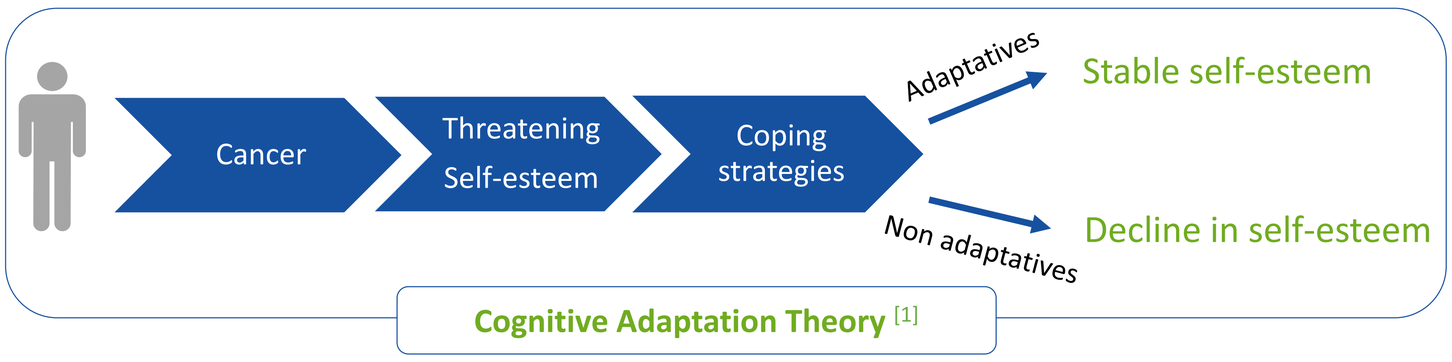

Cognitive Adaptation Theory [1]

- Self-esteem is related to **happiness**, **quality of life** and **coping skills** [2].
- Self-esteem is a strong predictor of **depression** and **anxiety symptoms** [3].
- Self-esteem is a moderator of the impact of **stressful life events** on the development of **depression** [4].

- Preventive and therapeutic tools for self-esteem disorders have many limitations (duration, cost, introspective efforts), which limit their **applicability with cancer patients**[5].

➡ **Need for a new technique**

LEXICAL ASSOCIATION TECHNIQUE

- Based on social and cognitive psychology models:
  - The self-knowledge is stored in an **associative memory network** [6]
  - The principles of **co-occurrence** and **repetition** help to strengthen associative links[6, 7, 8].

Purpose: Boost Self-Esteem by **strengthening associative links** between the Self and positive trait attributes in memory through a **reading and mental imagery** task.

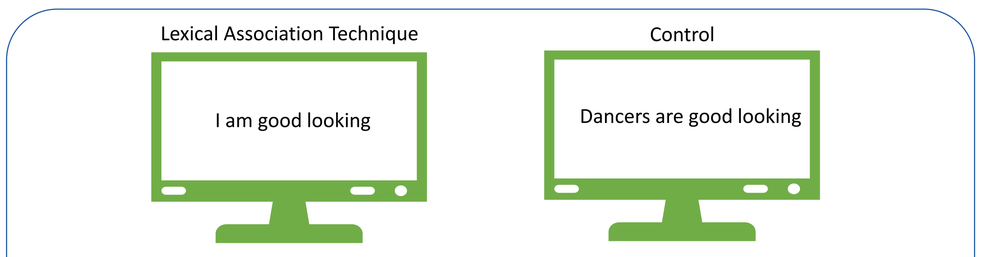

Examples of sentences

METHODS

Controlled Randomized Trial with Pre/Post intervention design and Double-Blind Procedure

Assessement:
- French version of **the Rosenberg Self Esteem Scale** (RSES) [9]
- French version of **the Positive and Negative Affect Schedule** (PANAS) [10]

Intervention phase: 6 x 5 min of reading and mental imagery
- **Lexical Association Technique (LAT)**: 19 sentences associating the self-concept with positive or valued attributes in competence, social and physical dimensions.
- **Control**: 19 sentences associating some social groups with positive or valued attributes in competence, social and physical dimensions.

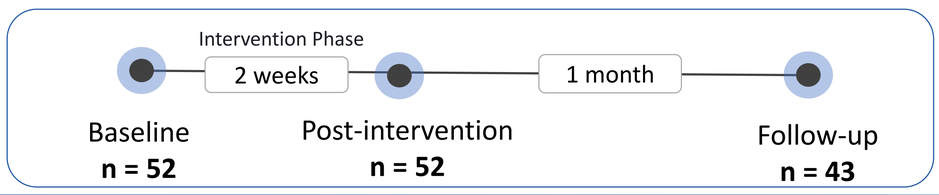

Sample

Breast Cancer Women
Age ≤ 70

Radiotherapy Department of the Metropole Savoie Hospital

French First Language

Access to a **computer** with an internet connection at home

Exclusion criteria

- Statistical outliers
- History of cancer in the last 5 years
- Historical or current diagnosis of a psychiatric disorder (excluding depression/anxiety)
- Other type of cancer
- Failure to complete more than 2 sessions during the intervention phase

PRELIMINARY RESULTS

Statistical analyses : Mixed ANOVAs 2 (group) x 2 (time) and simple effects (t-test).

Confirmatory analyses (RSES)

Immediate efficacy : baseline / post-intervention
- Increase in RSES scores in the LAT group
  F*(1) = 5.77, *p* = .024
- Stability in RSES scores in the control group
  F(1) = 0.00, *p* = .948, NS
- Interaction (group x time) marginally significant
  ***F*(1, 47) = 2.89, *p* = .096†, η_p^2 = .058**

One-month efficacy: baseline / follow-up
- Increase in RSES scores in the LAT group
  F*(1) = 7.31, *p* = .014
- Stability in RSES scores in the control group
  F(1) = 0.47, *p* = .502, NS
- Interaction (group x time) not significant
  F(1, 38) = 0.95, *p* = .337, η_p^2 = .024, NS

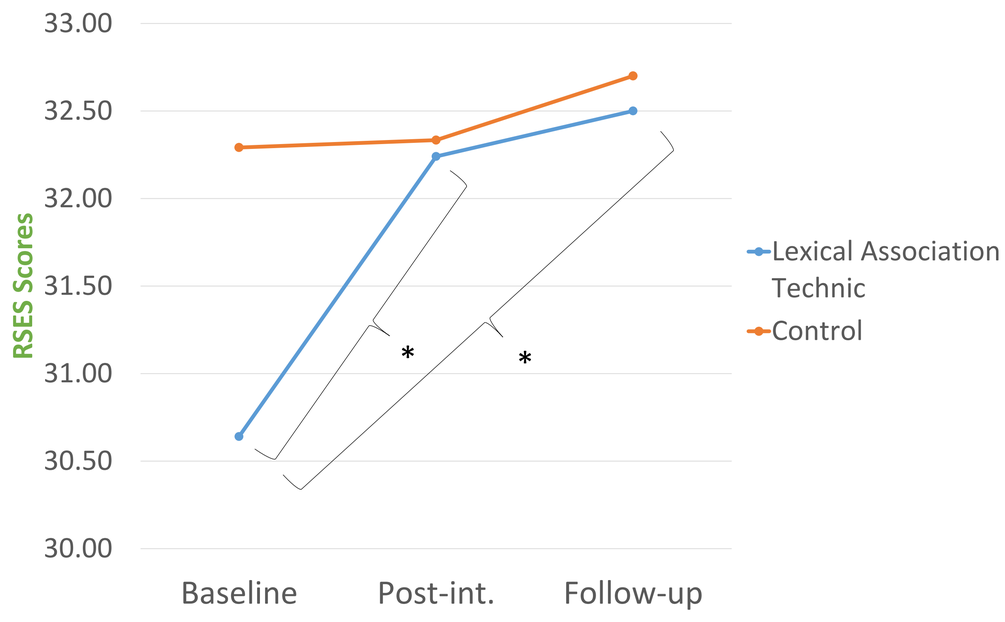

Exploratory analyses on immediate efficacy (PANAS)

Negative affectivity (NA):
- Decrease in NA scores in the LAT group
  F*(1) = 9.57, *p* = .005*
- Stability in NA scores in the control group
  F(1) = 0.40, *p* = .532, NS
- Interaction (group x time) not significant
  F(1, 50) = 2.22, *p* = .142, η_p^2 = .043, NS

Positive affectivity (PA):
- Stability in PA scores in the LAT group
  F(1) = 2.21, *p* = .149, NS
- Increase in PA scores in the control group
  F*(1) = 7.89, *p* = .010*
- Interaction (group x time) not significant
  F(1, 49) = 0.78, *p* = .381, η_p^2 = .016, NS

DISCUSSION

- **Efficacy** of the lexical association technique on **increasing self-esteem** with breast cancer patients.
- Need to **include more patients** in the trial to demonstrate significant **interaction effects** (N = 88).
- Need to deepen the understanding of the **mechanisms** underlying the effectiveness of the task:
  - **episodic memory involvement** in lexical associations
  - **affective** influences
  - **depth of stimulus processing.**
- Encouraging results despite the need for **further investigations**:
  - prolongation of **medium- and long-term effects**
  - **Other clinical applications** (e.g. patients with other cancer locations).

CONCLUSION

Preventive and therapeutic technique with many **advantages**:

Speed (6 sessions x 5 min)

Easy execution (computer implementation)

Low cognitive investment required (simple tasks)

Possibility of application to various **conceptual fields**

References:

[1] Taylor, S. E. (1983). Adjustment to threatening events: A theory of cognitive adaptation. *American Psychologist, 38*(11), 1161–1173.
[2] Baumeister, R. F., Campbell, J. D., Krueger, J. I., & Vohs, K. D. (2003). Does high self-esteem cause better performance, interpersonal success, happiness, or healthier lifestyles? *Psychological science in the public interest, 4*(1), 1-44.
[3] Sowislo, J. F., & Orth, U. (2013). Does low self-esteem predict depression and anxiety? A meta-analysis of longitudinal studies. *Psychological Bulletin, 139*(1), 213–240.
[4] Dentale, F., Vecchione, M., Alessandri, G., & Barbaranelli, C. (2018). Investigating the protective role of global self-esteem on the relationship between stressful life events and depression: A longitudinal moderated regression model. *Current Psychology*. 1-12.
[5] Hall, P. L., & Tarrier, N. (2003). The cognitive-behavioural treatment of low self-esteem in psychotic patients: a pilot study. *Behaviour research and therapy, 41*(3), 317-332.
[6] Greenwald, A. G., Banaji, M. R., Rudman, L. A., Farnham, S. D., Nosek, B. A., & Mellott, D. S. (2002). A unified theory of implicit attitudes, stereotypes, self-esteem, and self-concept. *Psychological review, 109*(1), 3-25.
[7] Bower, G. H., & Gilligan, S. G. (1979). Remembering information related to one's self. *Journal of Research in Personality, 13*(4), 420-432.
[8] Anderson, J. R. (1983). A spreading activation theory of memory. *Journal of verbal learning and verbal behavior, 22*(3), 261-295.
[9] Vallieres, E. F., & Vallerand, R. J. (1990). Traduction et validation canadienne-française de l'échelle de l'estime de soi de Rosenberg. *International journal of psychology, 25*(2), 305-316.
[10] Gaudreau, P., Sanchez, X., & Blondin, J. P. (2006). Positive and negative affective states in a performance-related setting testing the factorial structure of the PANAS across two samples of French-Canadian participants. *European Journal of Psychological Assessment, 22*(4), 240–249.

CONDITIONAL GENERATION OF FREE RADICALS BY PEPTIDE-BIOCONJUGATED ALKOXYAMINES: TOWARDS MORE EFFECTIVE AND LESS TOXIC TARGETING OF BRAIN TUMOURS.

P. Piris[1], D. Buric[1], T. Yamasaki[2], MP. Montero[1], M. Rossi[1], N. André[1], S. Combes[1], P. Brémond[1] and M. Carré[1]

[1]Centre de Recherche en Cancérologie de Marseille (CRCM), Inserm UMR1068, CNRS UMR7258, Aix-Marseille Université UM105, Institut Paoli Calmettes – Faculté de Pharmacie, Marseille, France
[2]Institut de Chimie Radicalaire, CNRS UMR7273, Aix-Marseille Université – Faculté des Sciences, Marseille, France

Contact : patricia.piris@etu.univ-amu.fr

Biological and chemical context

Glioblastoma multiform (GBM) is the most common intracranial tumor observed in adults. Despite a significant progress in clinical management over the last decade, these tumors have one of the poorest prognoses for survival due to a poor response to therapeutic strategies. GBMs are thus aggressive tumors that present unique challenges for identification of new drugs.

Our previous results showed theranostic properties for **alkoxyamines** R^1–ONR^2R^3 (Moncelet D *et al*, Mol Pharmacol 2014; Yamasaki T *et al*. Bioorg Med Chem 2019). These molecules can undergo homolisys to generate: 1) a highly toxic alkyl radical (R^1•), which trigger the cell death process in GBM cells; 2) a non-toxic nitroxide (R^2R^3NO•), which can be used to enhance the MRI signal.

In the present project, we propose to improve the efficacy of the alkoxyamines while triggering their homolysis through peptide homolysis by matrix metalloproteases (MMP). Therefore, we have synthesized a range of 85 novel alkoxyamines as putative prodrugs for GBM. End-point and real-time cytotoxicity assays in 2D cultures as well as in 3D spheroids of GBM human cells led to a selection of the most efficient molecule, *i.e.* K1.

The latter has shown better efficacy in intracranial cancer cells (including GBM stem cells) than in cells from other cancer types. K1 was then bioconjugated to a peptide selectively recognized by MMP (Kline T *et al*, Mol Pharm 2004). This bioconjugate successfully inhibited survival, proliferation, migration and invasion of the GBM cells.

To further characterize its activity, we developed an innovative organotypic model based on the graft of stably-fluorescent GBM spheroids in *ex vivo* mice normal brain slices. Response to treatment was daily monitored by live cell microscopy and high-resolution fluorescence well scanning, and showed that K1-bioconjugate was promising in inhibiting GBM progression in this co-culture system. No severe side-effects to the healthy tissue was observed at experiment completion.

Lastly, results from a Physiollogically-Based Pharmacokinetics analysis (PBPK) supported that K1 was a good candidate for further preclinical tests in brain tumors. Moreover, the results obtained are being transposed on **medulloblastoma**, the most common malignant brain tumor in children.

I. Screening and selection of alkoxyamines for bioconjugation

Cytotoxicity of a panel of alkoxyamines

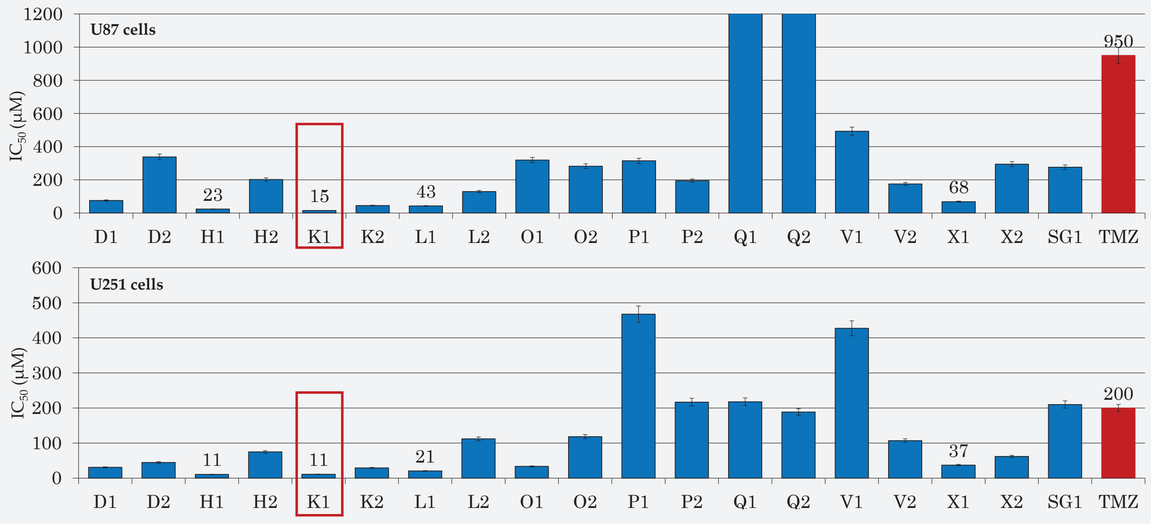

19 alkoxyamines, with half-life of less than 72 hours, were selected to be tested for cytotoxicity (MTT assay) in U87 and U251 glioblastoma cell 2D cultures. IC_{50} values were determined and compared to the current standard of care Temozolomide (TMZ). **The alkoxyamine K1 showed the highest efficacy in the two GBM** cell lines and was selected for further investigation.

K1 efficacy in other cancer cell types

K1 was also highly active in murine GBM cells, in **GBM stem-like** cells, as well as in **medulloblastoma** cells (ONS76, UW228 and HDMB03) of cerebellar origin.

As compared, cells from **lung** (A549) and **breast** (MCF7) adenocarcinomas or from **neuroblastoma** (SHEP) were 2 to 3 times less responsive to K1.

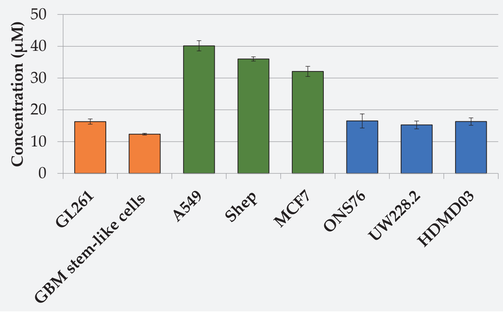

Spheroid growth

U251-MG cells

Treatment of 3D spheroids with K1 confirmed its efficacy in GBM models. The alkoxyamines L1 and X1, whose IC_{50} values were close to those of K1 in 2D cultures, had no activity on spheroids at similar doses (data not shown).

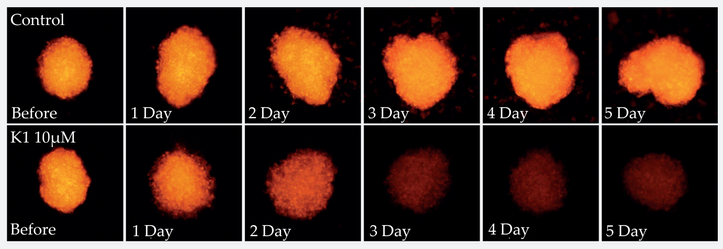

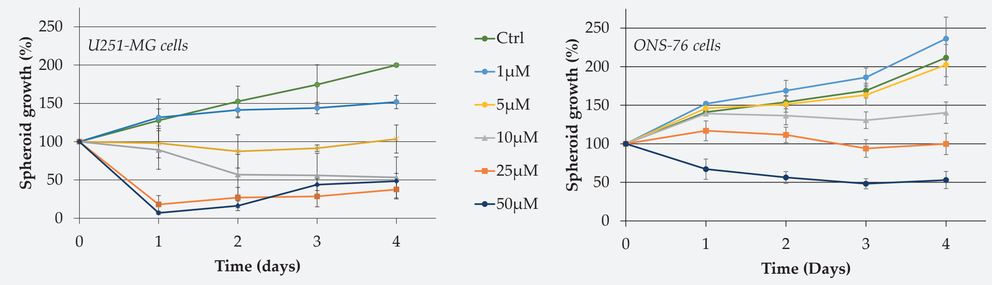

Similar results were obtained in U87-MG glioblastoma cells and in ONS-76 medulloblastoma cells

K1 significantly impair cell motility

Cell motility test (Transwell®) revealed that the alkoxyamine K1 significantly impaired GBM cell migration at low concentrations, while the H1 molecule was efficient at higher concentrations (data not shown).

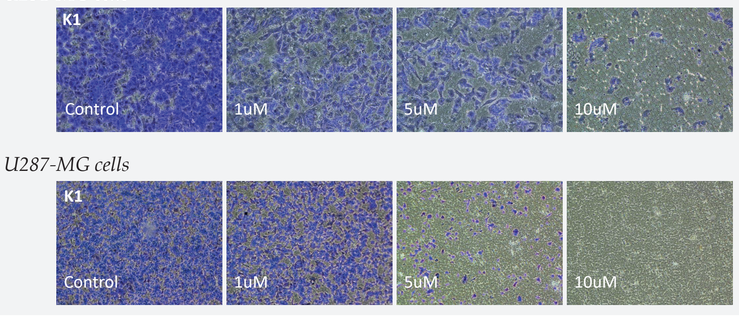

II. Mechanism of action

Intracellular incorporation of alcoxyamines

GBM cells were exposed to a highly stable **alkoxyamine coupled with the fluorochrome FITC**, which showed **a cytoplasmic accumulation** after only 2h.

Same results have been obtained with K1-FITC.

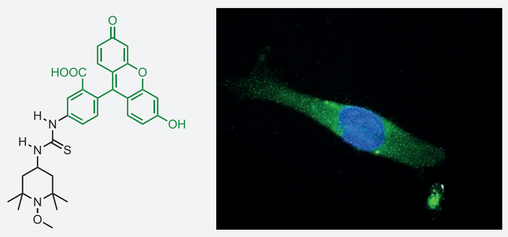

K1 acts through production of Reactive Oxygen Species (ROS)

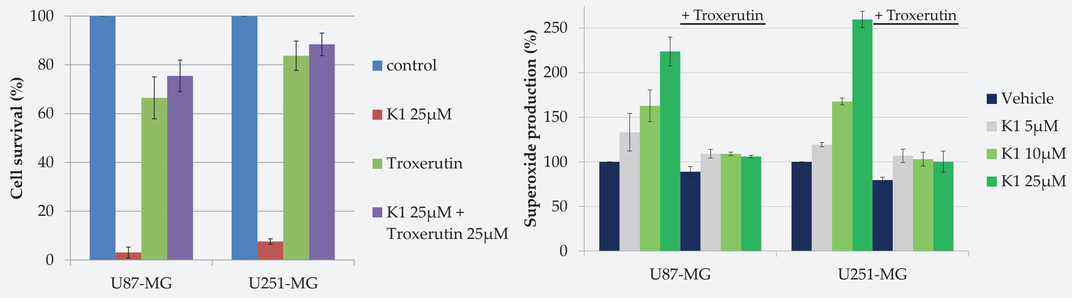

The alkyl radical scavenger Troxerutin has a rescue effect on the cytotoxic activity of K1. The release of alkyl radicals leads to a dose-dependant increase in endogenous superoxide production (at 6h) by GBM cells, which is required for the cytotoxic activity of alkoxyamines.

Mitochondrial fragmentation induced by K1

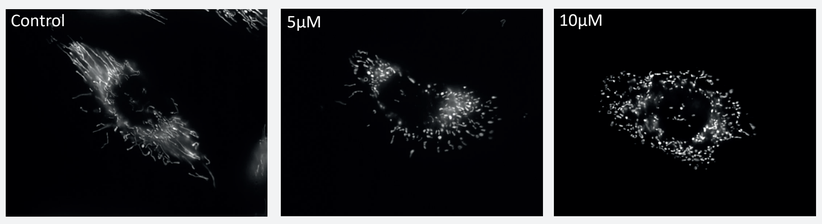

Fluorescence microscopy, U251-MG cells, 6h of treatment

Treatment with K1 results in an **early fragmentation of the mitochondrial network**, suggesting a disruption of mitochondrial functions that triggers generation of ROS, key step in the alkoxyamine-induced apoptotic cell death. Similar results were obtained in U87-MG GBM cells and both in ONS-76 and UW-228 medulloblastoma cells.

III. Bioconjugation of K1 with peptides

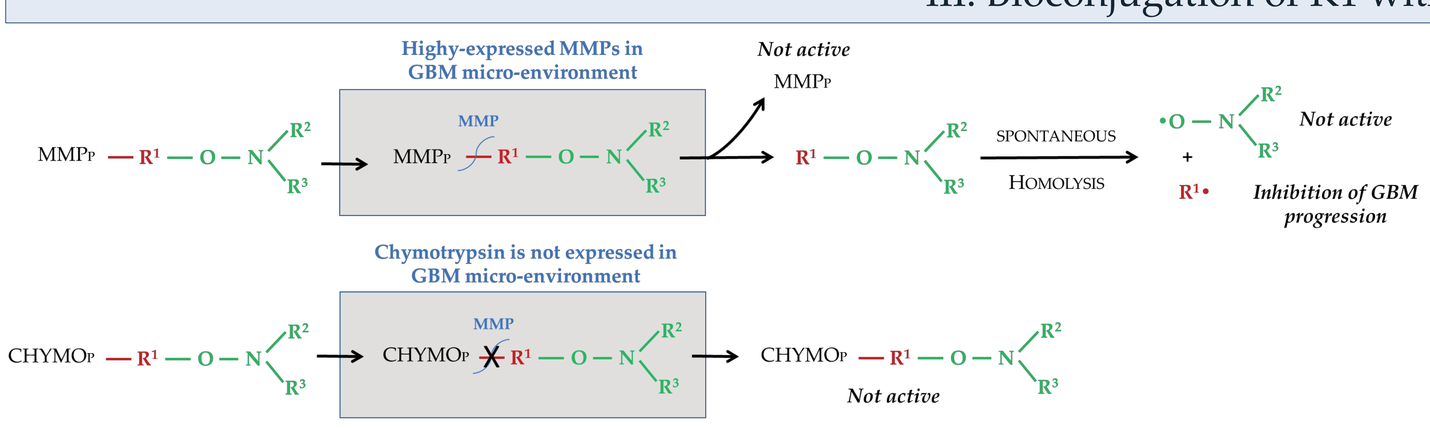

K1-MMPp inhibits invasion and growth of GBM cells in brain organotypic models

We developed an organotypic model based on the **grafting of stably-fluorescent GBM spheroids in *ex vivo* mice normal brain slices**.

Response to treatment was daily monitored by live microscopy and high-resolution well scanning, showing that K1-MMPp was highly effective in inhibiting GBM progression. No severe side-effects to the healthy tissue was observed at experiment completion (data not shown).

Similar results were obtained in U87-MG glioblastoma cells

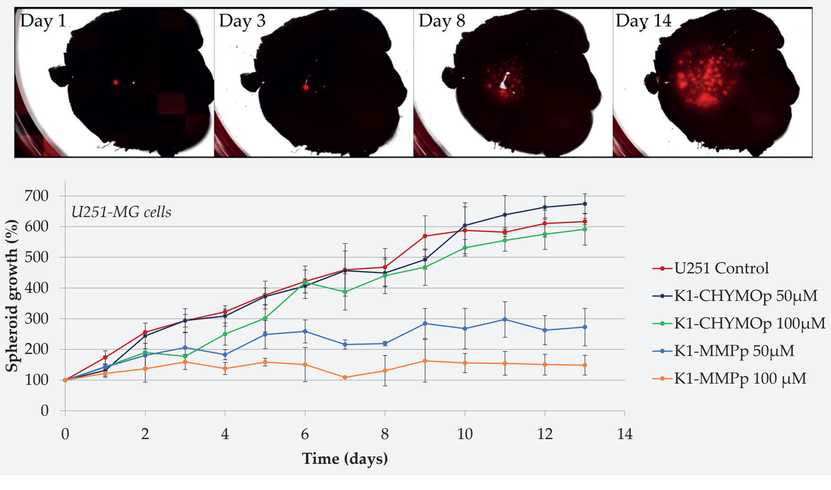

K1-bioconjugate with MMPp selectively impairs GBM spheroid growth

The alkoxyamine **K1, conjugated to a target peptide of MMPs** (MMPp), shows significantly stronger efficacy than when conjugated to a control peptide (CHYMOp, recognized by chymotrypsin).

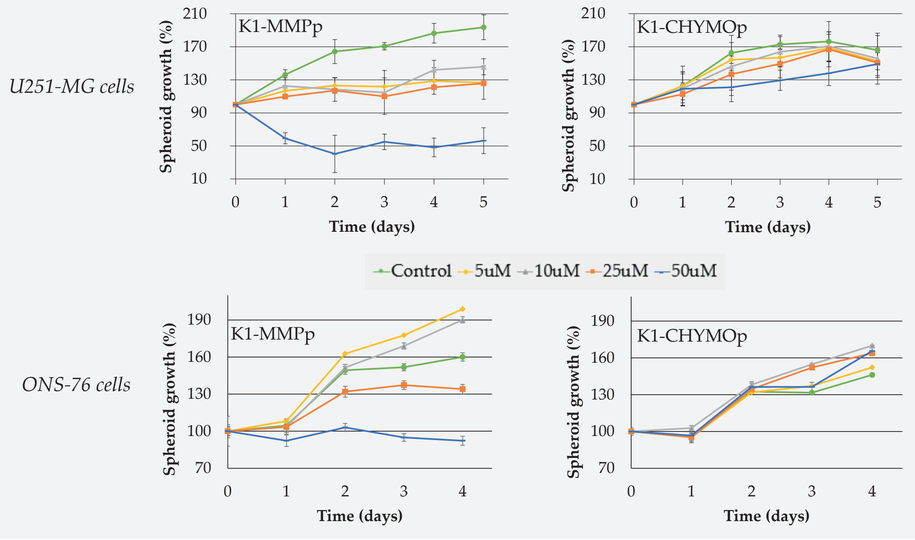

Conclusion and perspectives

This work led to the selection of the alkoxyamine K1 for its cytotoxic and anti-invasive properties, and to its bioconjugaison to a peptide specifically recognized by MMPs to be activated in the tumor microenvironment.

The project is now focused :

(i) On the synthesis of halogen derivatives of K1 to increase the selectivity of alkoxyamines for MMP9 (Tranchant I *et al*., 2014), and

(ii) On the generation of conditional fluorescence alkoxyamines (redox-sensitive) to monitor, in real-time, the homolysis process.

Comment évaluer la parole après traitement de cancer de la Cavité buccale et de l'oropharynx ?

Marie Rebourg[1], M. Lalain[1], A. Ghio[1], C. Fredouille[2] V. Woisard[3]
(1) Aix-Marseille Université, CNRS, Laboratoire Parole et Langage, UMR 7309, Aix-en-Provence, France,
(2) Laboratoire d'Informatique d'Avignon, Avignon, France, (3) Service ORL, CHU Larrey, Toulouse, France
marie.rebourg@lpl-aix.fr

Cancers de la cavité buccale et de l'oropharynx

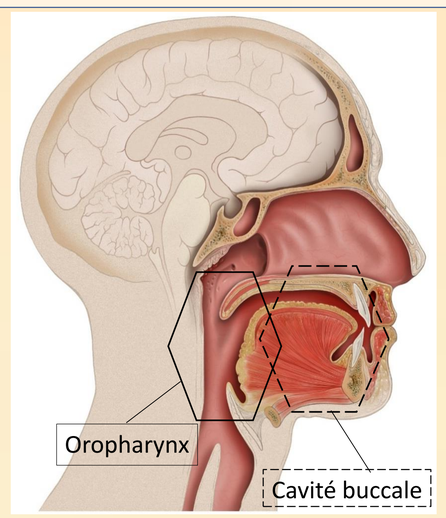

Traitements

Chirurgie
Chimiothérapie
Radiothérapie

Effets secondaires

Mutilant
Rigidifiant

Enjeux médicaux

1. Survie
2. Respiration
3. Alimentation
4. **Communication**

Quelle communication parlée ?

Clinique
- Evaluation
- Rééducation

Qualité de Vie
- Autonomie
- Achat pain
- Prise de rdv

Evaluer l'intelligibilité

Contexte : les troubles de la production de parole (TPP) (ex: Cancers des VADS) - Élément du bilan orthophonique, prise en charge clinique des TPP
Méthode d'évaluation : La production du patient est évaluée **perceptivement** : le degré de compréhension de l'auditeur représente le degré d'intelligibilité du patient.

Problèmes

Listes courtes et fermées de **mots**

- Scores ≠ Réalité
- Items lexicaux reconstruits par les mécanismes de perception : Restauration lexicale (Un auditeur restaure les phonèmes distordus lors de la perception de parole (Warren et al., 1970))
- Forte prédictibilité des items
- Familiarisation à la tâche et au test : La familiarité de l'auditeur avec le matériel linguistique perturbe la perception => tendance à sur-évaluer (Beukelman et Yorkson, 1992)

Solutions ?

Solutions proposées par le projet C2Si : un grand répertoire de pseudo-mots pour réaliser la tâche de DAP
Objectif : Valider la pertinence de la tâche de DAP par une analyse des transcriptions. Une tâche de jugement perceptif *designée* pour tester l'effet de répétition de la tâche

=> Evaluation de la Compréhensibilité

Décodage Acoustico-Phonétique avec des Pseudo-mots

Décodage Acoustico-Phonétique (DAP) : Un auditeur **écoute** les productions de patients et de témoins, et **transcrit** orthographiquement les unités qu'il perçoit

Ex : Zinvo, limblant, donou, prasta, glouvi

Des pseudo-mots :
· Règles phonotactiques de la langue
· Fréquences d'occurrences des phonèmes
· En fonction de leur position
· Structure syllabique CV ou CCV
· ~~Sens~~

Produits par 20 locuteurs : 10 patients et 10 sujets contrôles

En très grand nombre : · ~~Effet d'apprentissage~~ · ~~Effet de répétition~~ (Ghio et al. 2017)

Pourquoi ? Pallier les problèmes inhérents aux tâches habituellement proposées et au matériel linguistique utilisé : liste courtes et fermées de mots

=> Evaluation de l'Intelligibilité

Traitement des données

Transcriptions orthographiques → phonétisées (LIAPhon) (Béchet, 2001)

Comparaison : transcriptions phonétisées VS cibles phonétiques
Accord inter-auditeur : chaque stimulus est transcrit par 3 auditeurs différents ⇒ 1 score moyen / stimulus

Score de Déviation Phonologique Perçue (DPP) : nombre de traits moyen altéré par phonème (Ghio et al. 2018)

Mots vs Pseudo-mots

• Effet du matériel linguistique

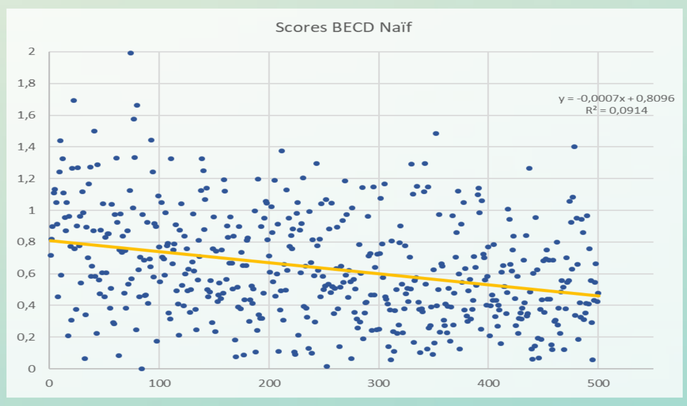

Effet d'apprentissage BECD (p < 0,001)

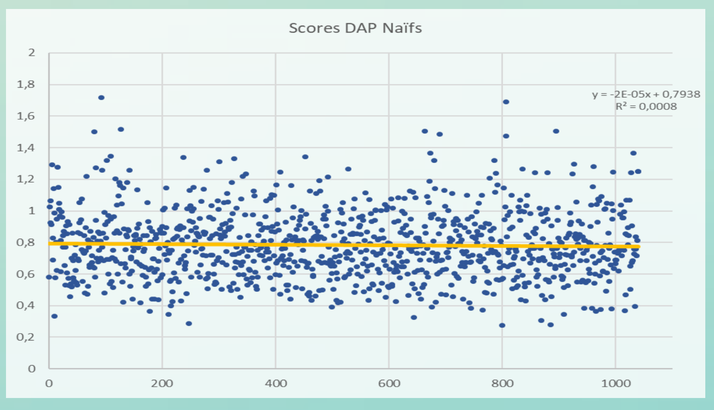

Pas d'effet DAP (p = 0,37)

Pseudo-Mots > Mots

Naïfs vs Experts

• Effet d'apprentissage

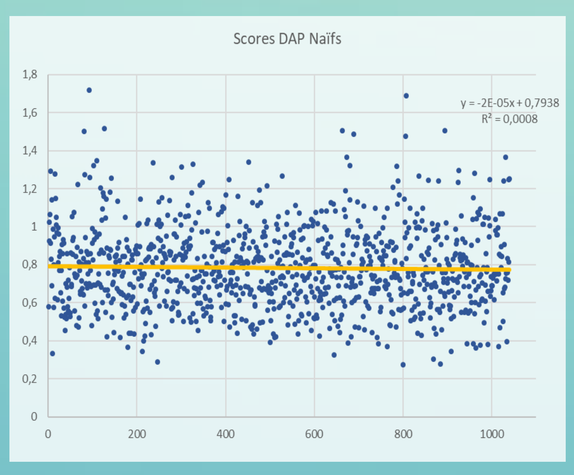

Pas d'effet DAP Naïfs (p = 0,37)

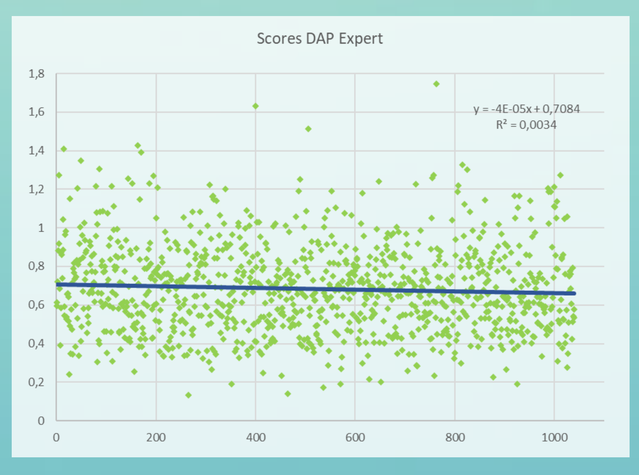

Pas d'effet DAP Experts (p = 0,06)

Pas d'effet d'apprentissage pour les deux groupes d'auditeurs

• Effet d'expertise auditive clinique

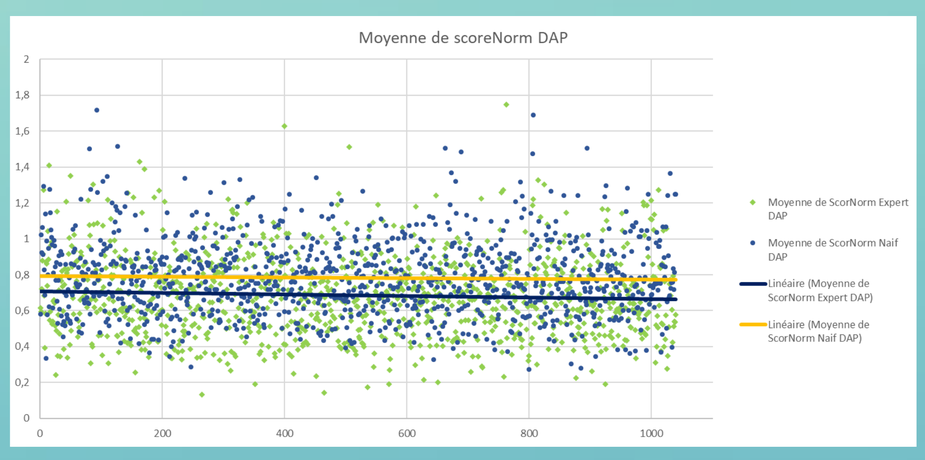

Naïfs vs Experts
Différence significative (p < 0,001)
mais faible
0,1 trait d'écart par phonème
(Cohen's d : 0,102)

Différence non préjudiciable à l'évaluation

Experts sont de meilleurs décodeurs par rapport aux Naïfs

Grant n°2014-135 INCA « Sciences humaines et sociales, Epidémiologie et Santé publique ». V. Woisard, Hôpitaux de Toulouse

Development of a novel anti-cancer strategy for Adrenocortical Carcinoma by nanovectorization of microRNAs via Lipidots

Soha Reda El Sayed[1], Adrien Nougarede[2], Josiane Denis[1], Laurent Guyon[1], Fabrice Navarro[2] and Nadia Cherradi[1*]

[1]Université Grenoble Alpes, INSERM, CEA, IRIG, Laboratoire Biologie du Cancer et de l'Infection, UMR_S 1036, Grenoble, FRANCE
[2] Université Grenoble Alpes, CEA, LETI-DTBS, Grenoble, FRANCE

01 Introduction

Adrenocortical cancer (ACC) is a rare endocrine malignancy of the adrenal gland. It is associated with poor prognosis and unmet clinical needs. Analysis of ACC microRNA landscape revealed an aberrant microRNA expression in both tumor and patient serum [1].

MicroRNAs (miRs) are small non-coding RNAs of about twenty nucleotides that repress gene expression at the post-transcriptional level. We have demonstrated that overexpression of two miRs, miR-483-5p and miR-139-5p is involved in ACC aggressiveness [2].

Journée jeunes chercheurs- Ligue contre le cancer 2020

02 Background

Targeting dysregulated miRs has been shown to be a relevant anti-cancer strategy. However, therapeutic miRs pose clearance, accessibility and targeting issues. Organic (liposomes, polymers…) or inorganic (gold nanoparticles, silica..) nanomaterials are used to vectorize nucleic acids.

Lipidots: Lipid nanoparticles (LNP) for nucleic acid delivery

FDA APPROVED COMPONENTS

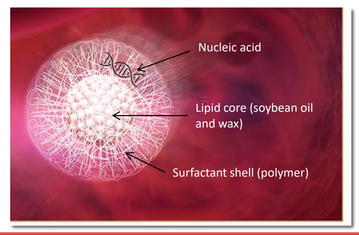

- Tropism to adrenals [3]

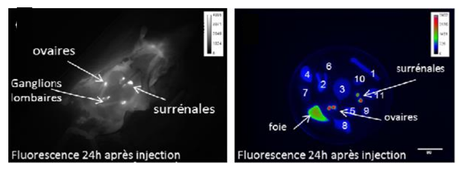

03 Objectives

- Validate miR-139-5p and miR-483-5p as oncomiRs in ACC
- Develop an experimental approach for ACC therapy by systemically injecting miR inhibitor-lipidots complexes into tumor bearing mice

04 Materials & Methods

In vitro (NCI H295R cells) → **In vitro (miR inhib – Lipidots)** → **In vivo (ACC mouse model)**

- NCI H295R cells were transiently transfected with 10nM of miR-139-5p/miR-483-5p inhibitors for a total of 72 hours.
- Gene expression and signaling pathway alterations in transfected cells were analyzed by antibody arrays, western blot and PCR arrays.
- miR inhibitors were complexed with DiI-labeled lipidots at N/P=16 then administered to NCI H295R cells in culture.
- Internalization and cargo release were assessed by microscopy and quantitative PCR.
- Migration assays were performed using Boyden chambers

05 Results

05.1. miR expression is significantly downregulated in NCI H295R transfected with miR inhibitors

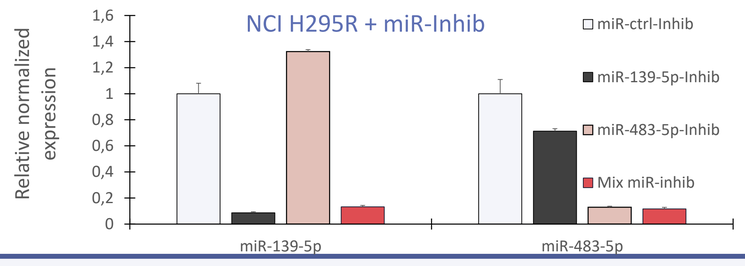

05.2. miR-483-5p and miR-139-5p inhibition represses oncogenic proteins

- Oncology antibody array

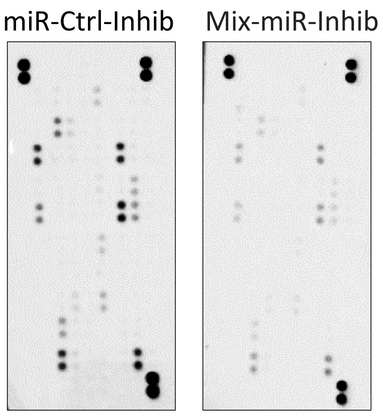

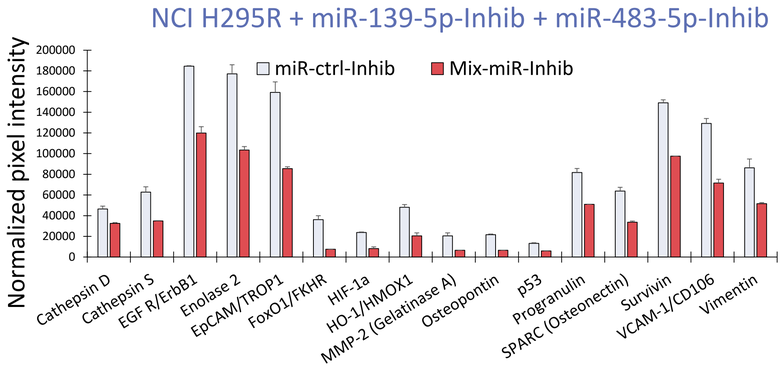

05.3. miR-483-5p and miR-139-5p inhibition represses expression of genes involved in cell invasion and migration

- Western blot

- EMT PCR array

05.4. Lipidots are efficiently internalized in NCI H295R cells when complexated with miR-inhibitors

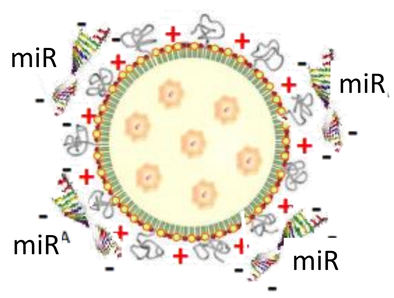

- miR-inhib-LNP-DiI

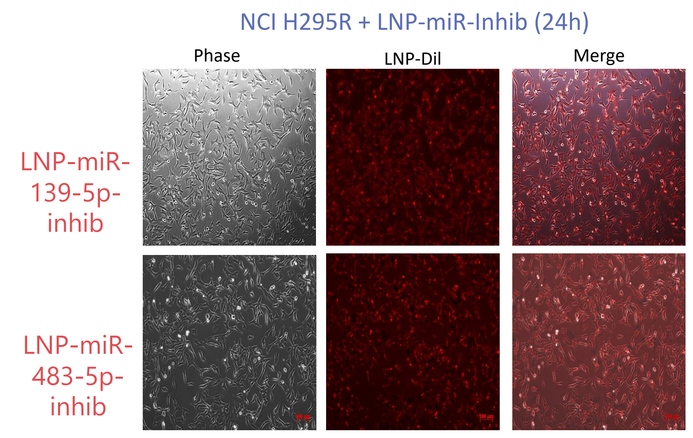

05.5. Lipidots efficiently release their cargo in NCI H295R cells

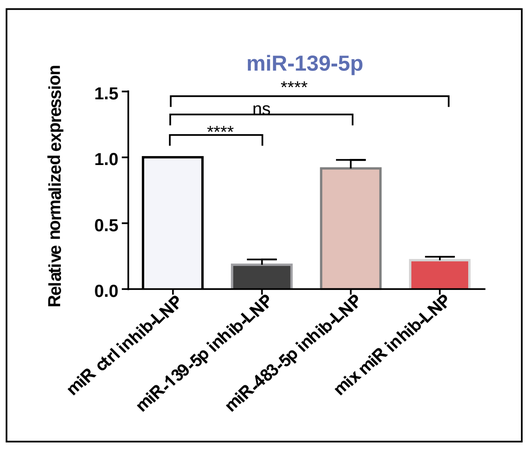

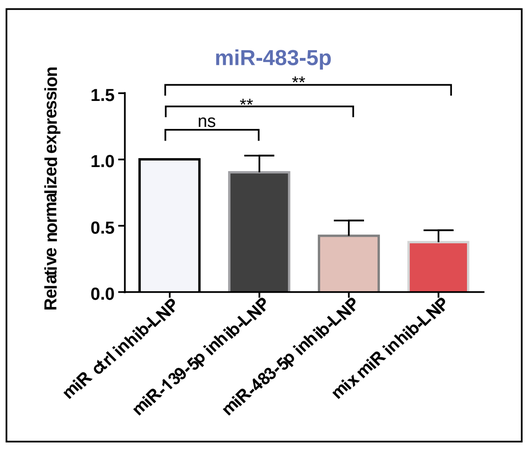

05.6. Delivering miRNA inhibitor-Lipidots complexes reduced NCI H295R migration

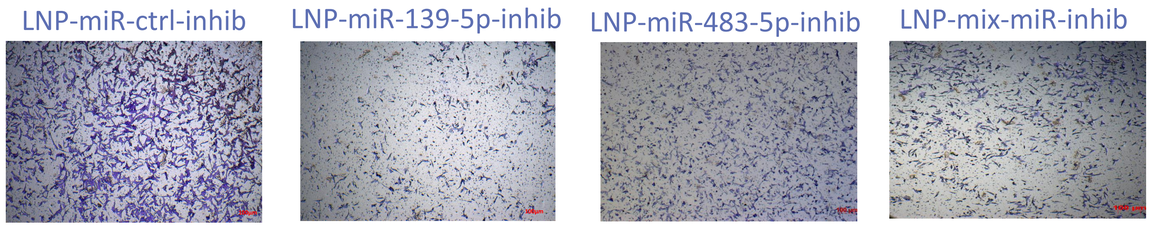

06 Conclusion

- Inhibiting miR-139-5p and miR-483-5p downregulates expression of oncogenes and genes of the Epithelio-Mesenchymal Transition in ACC
- miR-139-5p and miR-483-5p are oncomiRs in ACC and potentially contribute to tumor progression. Therefore, targeting these miRs is a promising therapeutic strategy for ACC
- Lipidots are successfully taken up by ACC cells in culture with no observed cytotoxicity
- Lipidots-delivered miR inhibitors repress expression of the corresponding miR in ACC cells. Evaluation of their anti-tumor efficacy *in vivo* will be started shortly.

Soha.redaelsayed@cea.fr

References:
[1] Assie et al, Nature Genetics, 2014
[2] Agosta et al, International Journal of Cancer, 2018
[3] Merian et al, The Journal of Nuclear Medecine, 2013

Rôle de la désensibilisation de CXCR4 dans la spécification lympho-myéloïde des progéniteurs hématopoïétiques multipotents

V. Rondeau[1], A. Bonaud[1], J. Nguyen[1], Z. Abou-Nader[1], J. Lemos[1], M. Delord[1], D. Haferssas[1], C. Kappel[1], L. Vogg[1], D. McDermott[2], P.M. Murphy[2], M. Aurrand-Lions[3], S. Mancini[3], A. Anginot[1], M. Espéli[1] et K. Balabanian[1]

[1]Université de Paris, Institut de Recherche Saint-Louis, EMiLy, INSERM U1160, 75010, Paris, France.
[2]Laboratoire d'Immunologie Moléculaire, Section Signalisation Moléculaire, Institut National des Maladies Allergiques et Infectieuses, NIH, Bethesda, MD, 20892
[3]CRCM, Inserm U1068, CNRS UMR7258, Aix Marseille Univ U105 - Institut Paoli-Calmettes, 13273, Marseille, France.

Introduction Les cellules souches et progéniteurs hématopoïétiques (CSPH) résident dans la moelle osseuse (MO) entourés par les niches endostéales et (péri)-vasculaires et sont à l'origine des cellules immunes circulantes. Les niches médullaires jouent un rôle dans la spécification et l'engagement myéloïde *versus* lymphoïde des CSPH. Dans la MO, le couple formé par la chimiokine CXCL12 et l'un de ses récepteurs, CXCR4, exerce un rôle clé dans la régulation de la rétention et la quiescence des CSPH. Ces processus sont dérégulés dans le Syndrome WHIM (SW), une maladie immuno-hématologique rare liée à des mutations autosomiques dominantes du gène codant CXCR4, qui altèrent la désensibilisation du récepteur et conduisent à un gain de fonction en réponse à CXCL12. Cliniquement, le SW se caractérise notamment par une profonde lymphopénie circulante dont les mécanismes restent à déterminer. Grâce à un modèle murin du SW nous avons révélé un rôle-clé de la désensibilisation de CXCR4 dans la différenciation lymphoïde des CSPH et identifié les progéniteurs multipotents (MPP) comme étant le stade défectueux. La divergence entre les lignages lymphoïde et myeloïde se produit précisément au stade MPP au sein duquel existe une hétérogénéité : les MPP2/3 sont biaisés myéloïde et les MPP4 sont orientés lymphoïde. L'ensemble de ces données nous a incité à analyser l'impact de la désensibilisation de CXCR4 sur la diversité moléculaire et fonctionnelle du compartiment MPP.

I. Modélisation du SW

Stratégie de knock-in

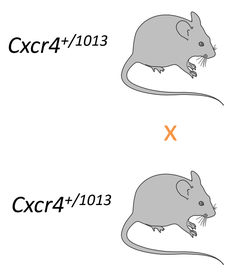

25% *Cxcr4*$^{+/+}$ (+/+)
50% *Cxcr4*$^{+/1013}$ (+/1013)
25% *Cxcr4*$^{1013/1013}$ (1013/1013)

Hypersensibilité à Cxcl12

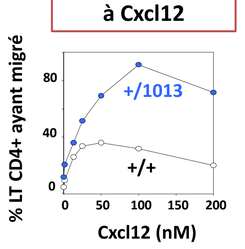

Lymphopénie

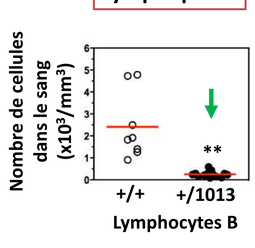

Balabanian *et al.*, Blood, 2012

Stade MPP défectueux dans la MO des souris mutantes

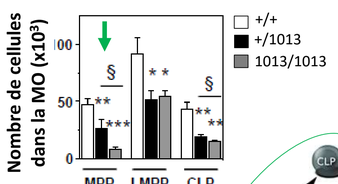

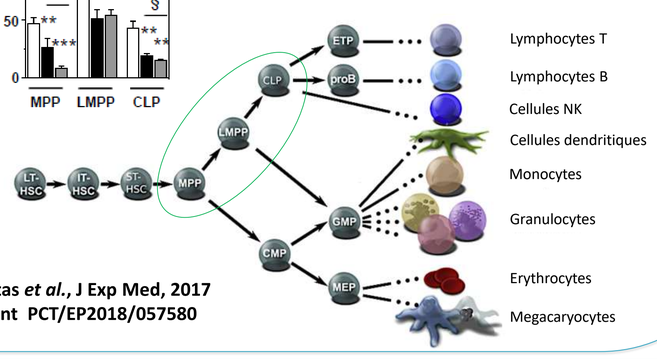

Freitas *et al.*, J Exp Med, 2017
Patent PCT/EP2018/057580

II. La désensibilisation de Cxcr4 est requise au maintien des progéniteurs lymphoïdes chez l'Homme et la souris

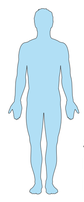

Aspirâts de MO :
Donneurs sains (DS)
Patients WHIM (SW)

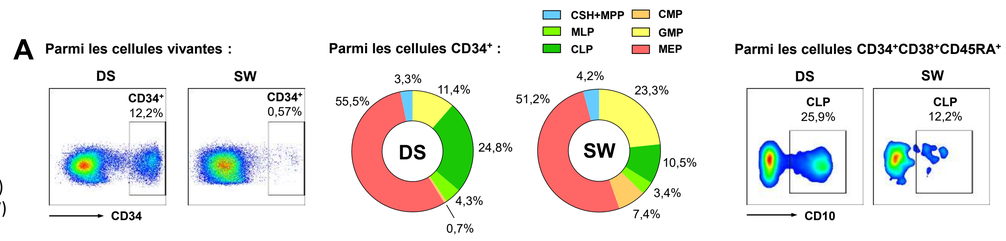

Biais myéloïde du compartiment CSPH dans la MO des patients

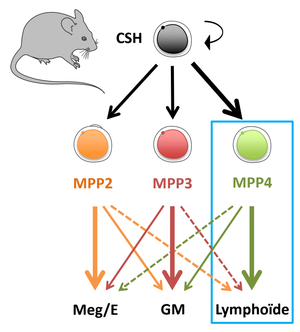

Pietras *et al.*, Cell Stem Cell, 2015

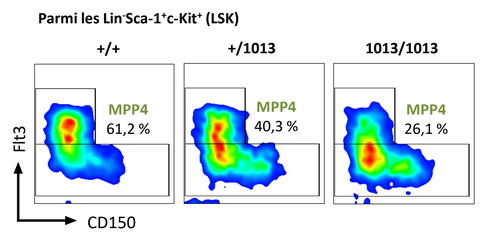

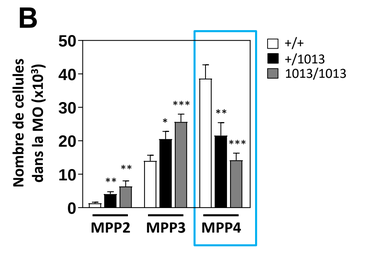

Rondeau *et al.*, en préparation

Biais myéloïde du compartiment MPP dans la MO des souris mutantes

*(A) Pourcentage de cellules CD34⁺ et de CLP au sein d'aspirâts de MO (gauche et droite) et diagrammes circulaires représentant la contribution de chacun des progéniteurs indiqués au contingent de cellules CD34⁺ (centre). Les données ont été obtenues par cytométrie en flux (CF). **(B)** Nombres absolus de MPP2, 3 et 4 dans la MO déterminés par CF.*

III. La désensibilisation de Cxcr4 régule intrinsèquement l'identité moléculaire des MPP4

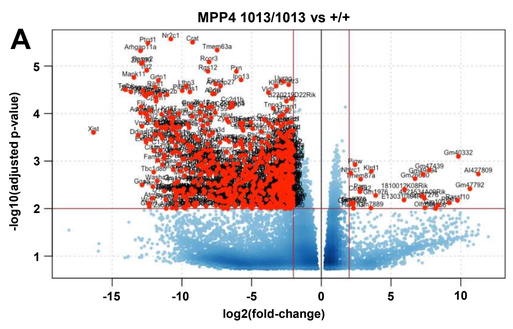

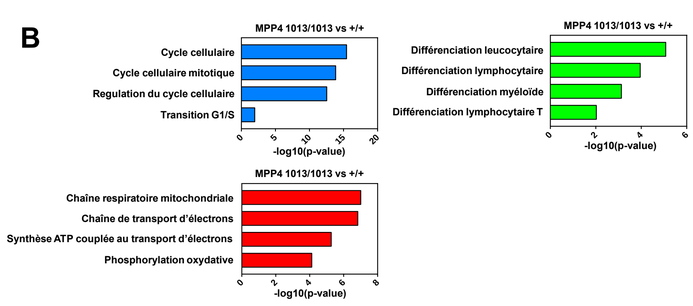

Signatures de l'expression de gènes associées à des dérégulations de la spécification lympho-myéloïde, du métabolisme relié à la phosphorylation oxydative et du cycle cellulaire dans les MPP4 mutants

*Les données transcriptomiques ont été obtenues par des analyses RNAseq. **(A)** Volcano plot représentant l'expression différentielle des gènes entre les MPP4 +/+ et 1013/1013. **(B)** Processus biologiques impactés dans les MPP4 1013/1013 identifiés grâce à des analyses par Gene Ontology (GO).*

IV. La désensibilisation de Cxcr4 contrôle la différenciation lympho-myéloïde des MPP4

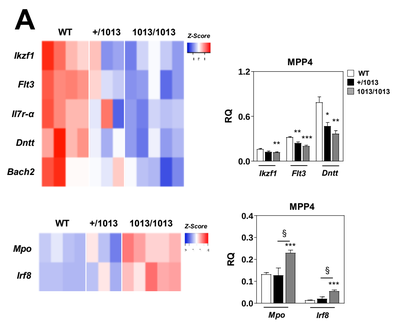

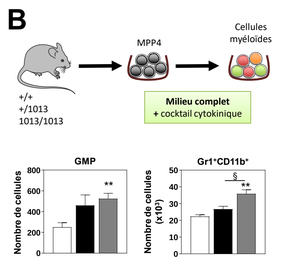

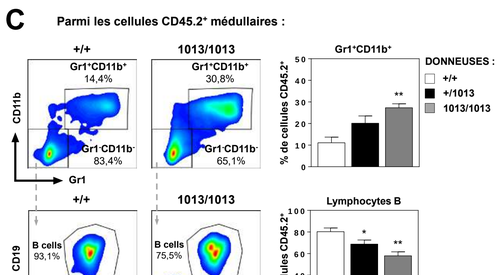

Reprogrammation myéloïde des MPP4 mutants

*(A) Expression transcriptionnelle des gènes clés de la spécification lymphoïde versus myéloïde déterminée par q-PCR multiplexée (Biomark). **(B)** 500 MPP4 +/+ ou mutants ont été mis en culture en milieu liquide supplémenté en cytokines afin d'étudier leur différenciation in vitro. Les nombres de GMPs et de cellules myéloïdes ont été déterminés par CF après 4 et 7 jours de différenciation respectivement. **(C)** Proportion de cellules myéloïdes (Gr1⁺CD11b⁺) et de lymphocytes B (CD19⁺B220⁺) générés à partir des MPP4 +/+ ou mutants CD45.2⁺ 14 jours après leur injection à des souris receveuses +/+ CD45.1⁺ irradiées sous-létalement. Les données ont été obtenues par CF.*

V. La désensibilisation de Cxcr4 régule le métabolisme mitochondrial des MPP4

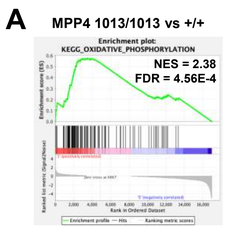

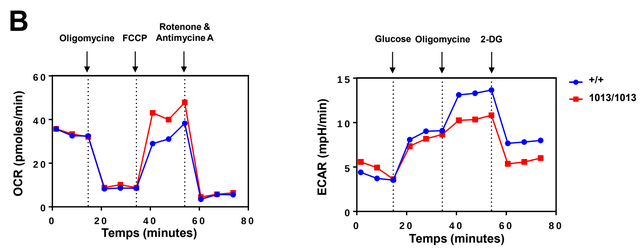

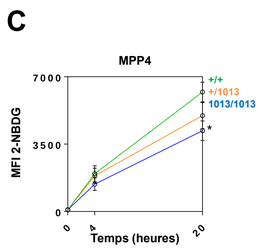

↑ phosphorylation oxydative | **↓ glycolyse**

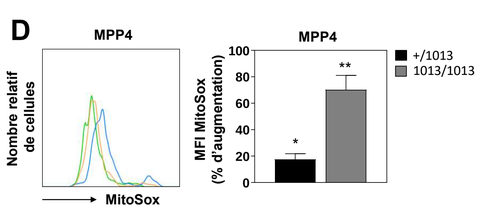

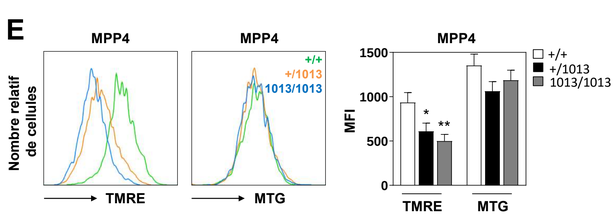

↑ ROS | **Altération du potentiel de membrane mitochondrial**

*(A) Gene Set Enrichment Analysis (GSEA) pour la phosphorylation oxydative réalisée à partir des données du RNAseq des MPP4 +/+ et 1013/1013. **(B)** Taux de consommation de l'oxygène (OCR) et taux d'acidification extracellulaire (ECAR) déterminés grâce à des analyses Seahorse. **(C)** Test in vitro de capture de glucose réalisé grâce à un analogue non métabolisable (2-NBDG). Les données ont été obtenues par CF. **(D)** Détection des espèces réactives de l'oxygène (ROS) par CF réalisée grâce à des marquages au MitoSox. Les résultats sont présentés en pourcentage d'augmentation de l'intensité moyenne de fluorescence (MFI) en comparaison aux MPP4 +/+. **(E)** Mesures de la masse mitochondriale (MTG) et du potentiel de membrane mitochondrial (TMRE) réalisées par CF. Les résultats sont représentés en MFI.*

VI. L'inhibition de Cxcr4 *in vivo* normalise le compartiment de MPPs et corrige la lymphopénie chez la souris mutante

Traitement chronique avec un antagoniste de Cxcr4 (AMD3100)
Injection quotidienne de 5mg/kg pendant 3 semaines.

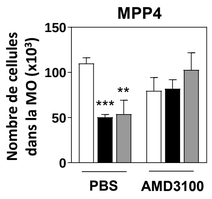

Normalisation du nombre de MPP4

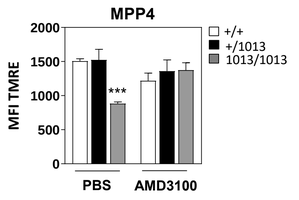

Restauration du potentiel de membrane mitochondrial

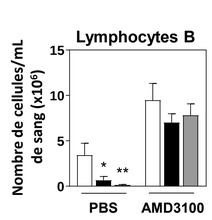

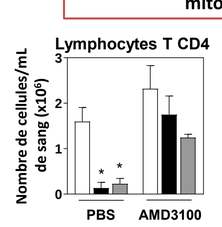

Correction de la lymphopénie

Les souris ont reçu une dose quotidienne de 5mg/kg d'AMD3100 par injection intra-péritonéale pendant 3 semaines. Le nombre absolu de MPP4, la mesure du potentiel de membrane mitochondrial et le nombre de lymphocytes B et T CD4 circulants ont été déterminés par CF à la fin du traitement.

L'analyse de prélèvements médullaires de patients atteints du SW rapporte une diminution de la fréquence des progéniteurs lymphoïdes et une augmentation de celle des progéniteurs myéloïdes. Dans la MO du modèle murin du SW, nous avons observé une diminution du nombre de MPP4, tandis que ceux des MPP2/3 sont augmentés. Ce biais myéloïde du compartiment MPP est associé à une reprogrammation métabolique et myéloïde des MPP4 porteurs de la mutation de *CXCR4*, comme le rapportent nos analyses par RNAseq combinées à des études fonctionnelles appropriées. Enfin, l'inhibition de Cxcr4 *in vivo* permet chez les souris mutantes la normalisation du compartiment MPP, la restauration des propriétés métaboliques des MPP4 et la correction de la lymphopénie.
Dans leur ensemble, ces données suggèrent que **l'absence de désensibilisation de Cxcr4 altère les propriétés métaboliques des MPP4 ce qui engendre un défaut de spécification lymphoïde de ces cellules.** Nos résultats supportent ainsi **un rôle majeur de la désensibilisation de CXCR4 dans le processus de lympho-hématopoïèse**, notamment par la capacité de ce processus à **réguler le potentiel lymphoïde** qui caractérise les MPP4.

INSTITUT DE RECHERCHE SAINT-LOUIS Hématologie | Immunologie | Oncologie Département de l'UFR Médecine · LA LIGUE CONTRE LE CANCER · Inserm La science pour la santé From science to health · AGENCE NATIONALE DE LA RECHERCHE ANR · FRM FONDATION RECHERCHE MÉDICALE · InsermTransfert · sfh Société Française d'Hématologie · abEx LERMIT Laboratoire d'Excellence en Recherche sur le Médicament et l'Innovation Thérapeutique · INSTITUT NATIONAL DU CANCER · ONCORNET · MARIE CURIE ACTIONS · FONDATION ARC POUR LA RECHERCHE SUR LE CANCER · PRESTIGE · îledeFrance

A role for Perlecan in inter-organ signaling linked to BMPs ?

Smolen P., Bonche R., Pizette S., Thérond P.
Université Côte d'Azur, CNRS 7277, Inserm 1091, Institut Biologie Valrose, Nice, France
Prune.SMOLEN@univ-cotedazur.fr

Introduction

Basement membrane

Basement membrane (BM)

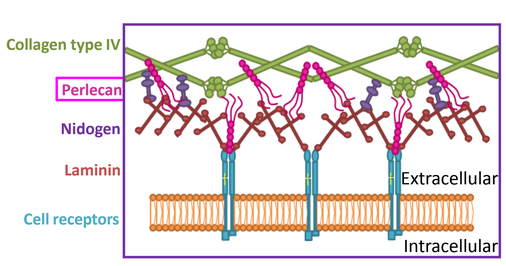

- Specialized extracellular matrix
- Surrounds organs and lines the basal side of epithelia
- Mechanical support
- Signalling plateform

Perlecan (Pcan) isoforms

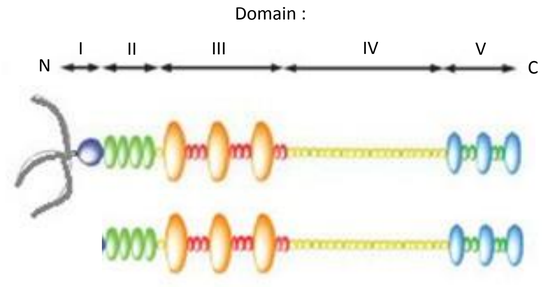

- Main heparan sulfate (HS) proteoglycan
- 5 domains
- Domain I carry HS chain
- In *Drosophila* : 2 families of isoforms with domain I and without domain I (FlyBase)

Control of the developmental timing

A Ecdysone

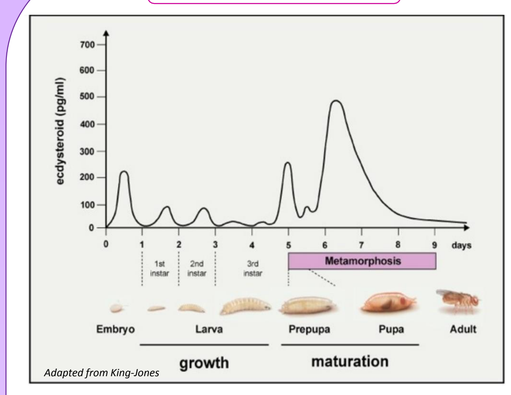

B Ring Gland

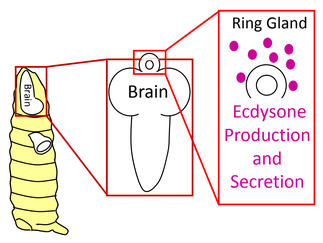

C BMP

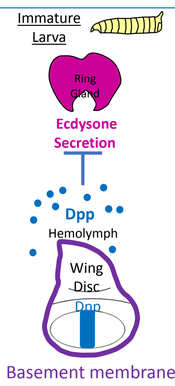

The developmental progression of *Drosophila* is under the control of the steroid hormone ecdysone (**A**) produced by a specific gland in the bain, the ring gland (**B**). Growth occurs exclusively during larval stages and halts at the end of the 3rd instar larval stage that is induced by a large titer of ecdysone, causing the larvae to pupariate and undergo metamorphosis. The entire life cycle of *Drosophila* takes approximately 10 days at 25°C, and metamorphosis occurs after 5 days, that is, 120h after egg laying (hAEL) (**A**).
One of the signals controlling the timing of the metamorphosis is BMP2/4 (Dpp). Dpp is mainly secreted by the wing imaginal disc (the precursor of the adult wing), and diffuses over a long distance via the hemolymph (blood equivalent) to the « ring gland » (RG) where it activates its signaling pathway to block the production of ecdysone (**C**) (**Setiawan, et al, 2018**)

Working hypothesis : Perlecan without domain I can prevent the diffusion of Dpp thus leading to metamorphosis

How is Dpp secretion to the hemolymph stoped to allow metamorphosis?

When the larvae are mature and their organs have reached their final size, Dpp pathway in the RG is no longer activated because Dpp cease to be secreted into the hemolymph, although Dpp is still produced by the wing disc.

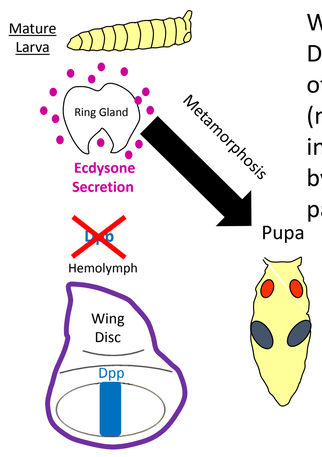

We found that in the mature larva, Dpp induces the late transcription of Pcan isoforms without domain I (not shown) in the wing disc which inhibit the Dpp pathway, as seen by the hyperactivation of the pathway in Pcan LOF (D).

D

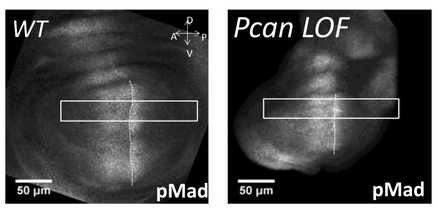

Immunofluorescence for pMad, a reporter of Dpp, in the wing disc

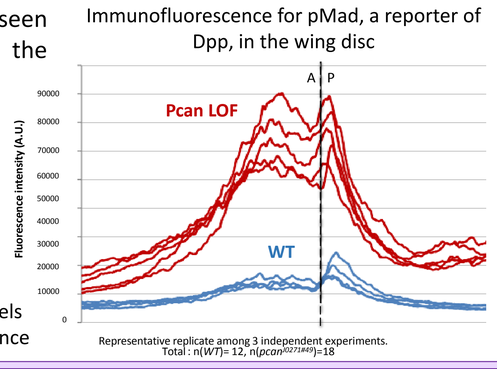

Representative replicate among 3 independent experiments.
Total : n(*WT*)= 12, n(*pcan*$^{\Delta 271\#49}$)=18

Analysis of pMad levels by immunofluorescence

So we propose that :
The increase in the production of Dpp during the larval growth period leads to the expression of Pcan without domain I enriching the BM (E, F). Pcan without domain I will then bind Dpp and sequester it, decreasing its diffusion into the hemolymph and thus its activity at the Ring Gland level (F). This decrease will allow the metamorphosis (G).

E Immature Larva

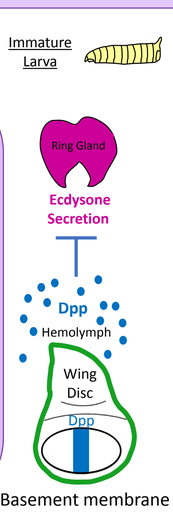

Basement membrane enriched with Perlecan with domain I

F Mature Larva

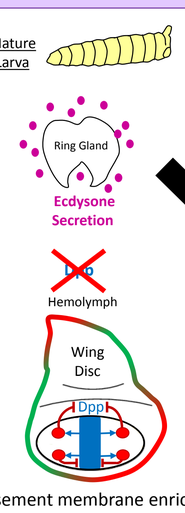

Basement membrane enriched with Perlecan with domain I and withtout domain I

G

(Ma et al., 2017)
(Setiawan et al., 2018)

Results

Characterization of Pcan loss-of-function (LOF)

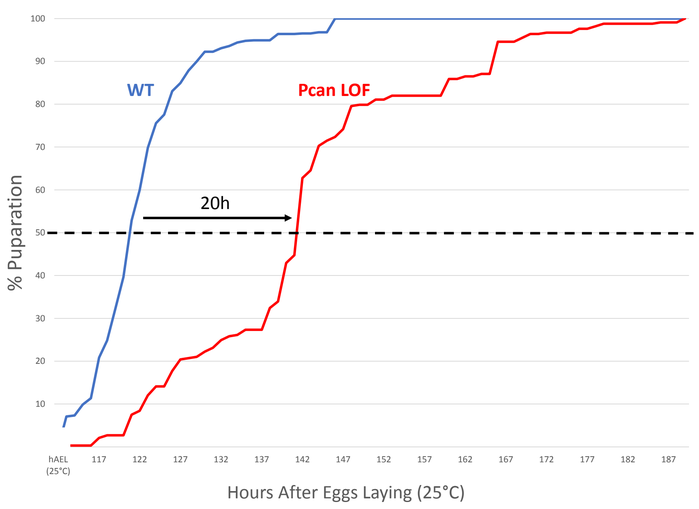

Pcan loss-of-function mutants have a developmental delay.

▬ ▬ : 50% of the larvae are in the state of pupae

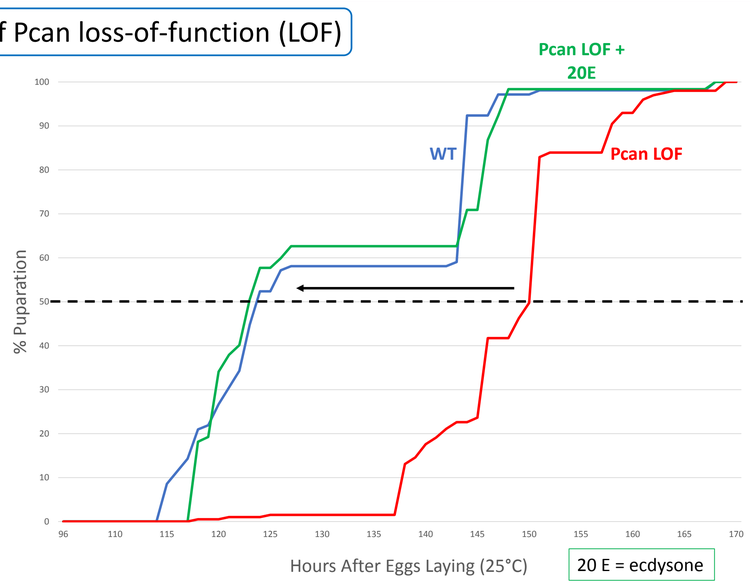

20 E = ecdysone

Addition of ecdysone rescues the developmental delay of perlecan loss-of-function mutants, indicating that ecdysone signalling is not affected.

Dpp signaling pathway in the RG

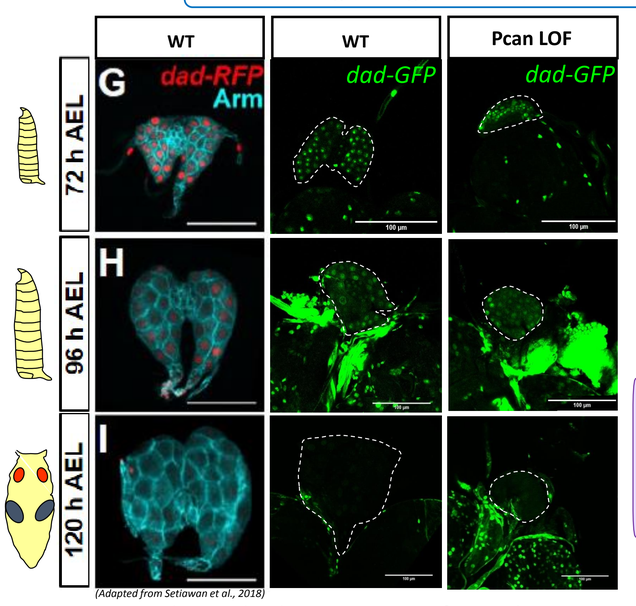

Dad-GFP and Dad-RFP are reporters of Dpp pathway activity

We expected a persistence of Dpp signaling in the RG in the Pcan loss-of-function mutants BUT Dpp signaling pathway still decreases in the RG prior to metamorphosis.

Dpp does not seem to be directly involved in the developmental delay of Pcan loss-of-function mutants.

Arm = armadillo = cellular cortex

Results

Some of the main inputs that can control the developmental timing

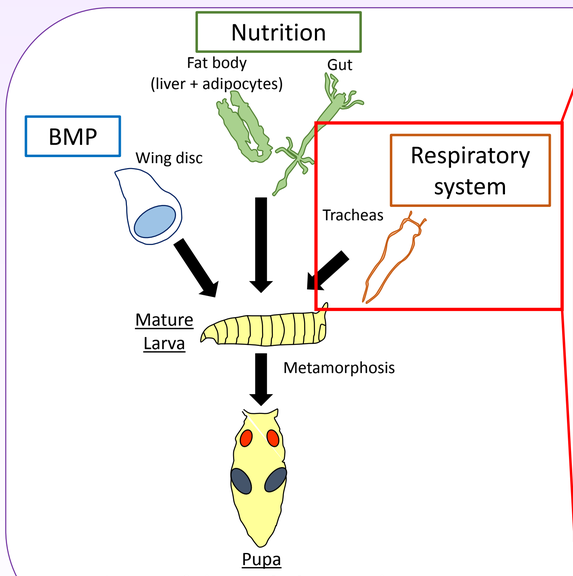

Pcan LOF in the respiratory symtem

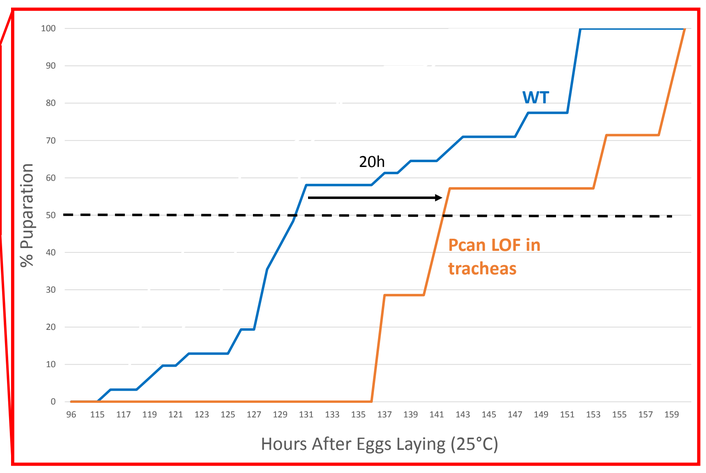

The presence of Pcan in the respiratory system seems important for a normal developmental timing.

Conclusions and Perspectives

- Dpp does not seem to be directly involved in the developmental delay of Pcan loss-of-function mutants
- The presence of Pcan in the respiratory system is important for a normal developmental timing
- The presence of Pcan in the wing disc, fat body and gut is not important for a normal developmental timing (not shown)

- Are the larvae in hypoxia ?
- Is the morphology of the trachea affected ?
- Which isoform of Pcan is important to control the developmental timing ?
- It has been shown that the oxygen level is important for proliferation and survival of cancer cells. Could Perlecan therefore be involved in this process ?

Mechanistic study of ZEB1 and ZEB2 antagonistic roles in melanoma

Yaqi Tang, Maxime Grimont, Roxane Pommier, Stéphane Dalle, Julie Caramel.
Cancer Cell Plasticity in Melanoma team, Cancer Research Center of Lyon.
Contact mail: Yaqi.TANG@lyon.unicancer.fr

ZEB family: ZEB1 and ZEB2

Zinc finger E-box binding homeobox transcription factors

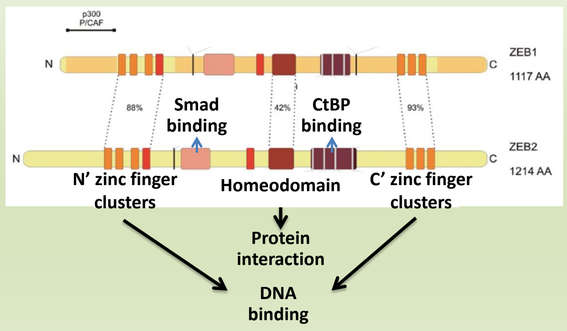

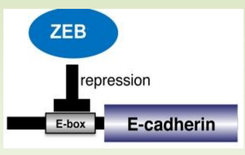

Target genes:
- **Epithelial markers: E-cadherin…**
- **Mesenchymal: vimentin…**

Antagonistic expression and function of ZEB1/2 in melanoma

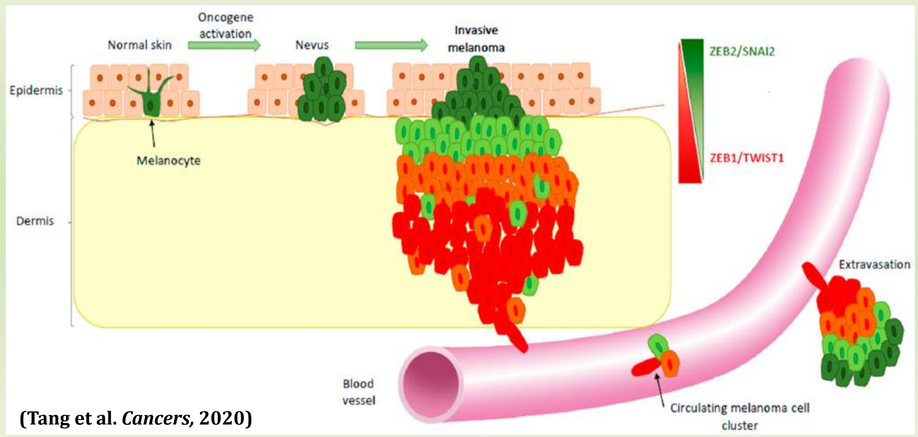

(Tang et al. *Cancers*, 2020)

Phenotype switching and intermediate phenotypes

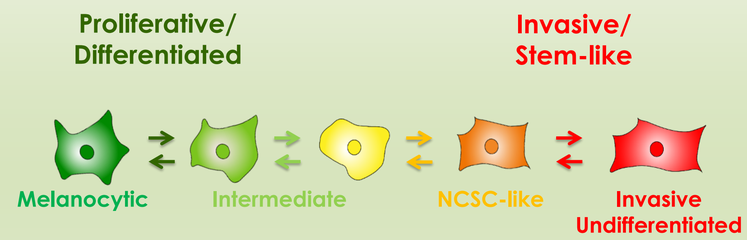

Objectives

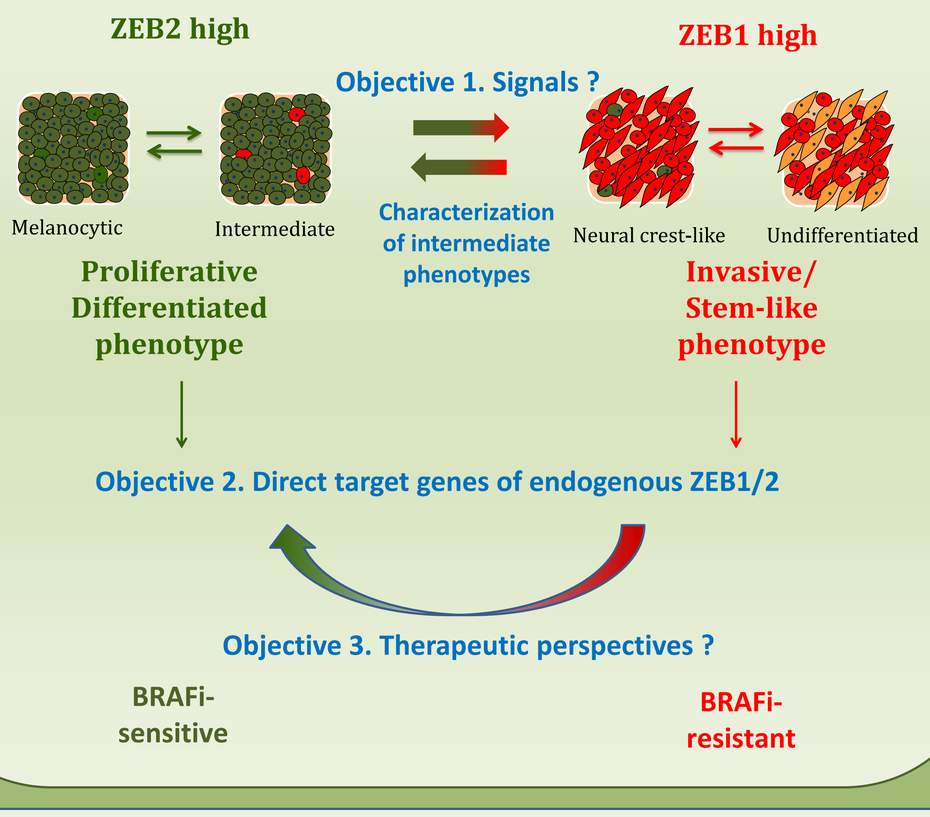

Cellular models

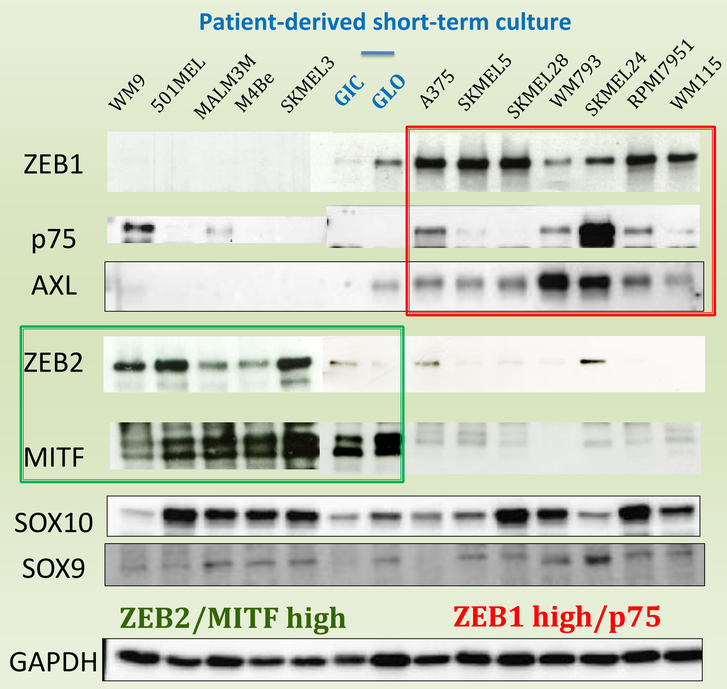

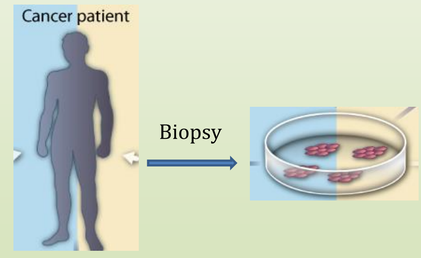

Advantages of melanoma short-term culture:
- Closer to physiological conditions
- Diaplay an intermediate expression pattern to switch ZEB1/ZEB2 expression

Result 1. TNFα and TGFβ1 induce phenotype-switching along the intermediate phenotypes

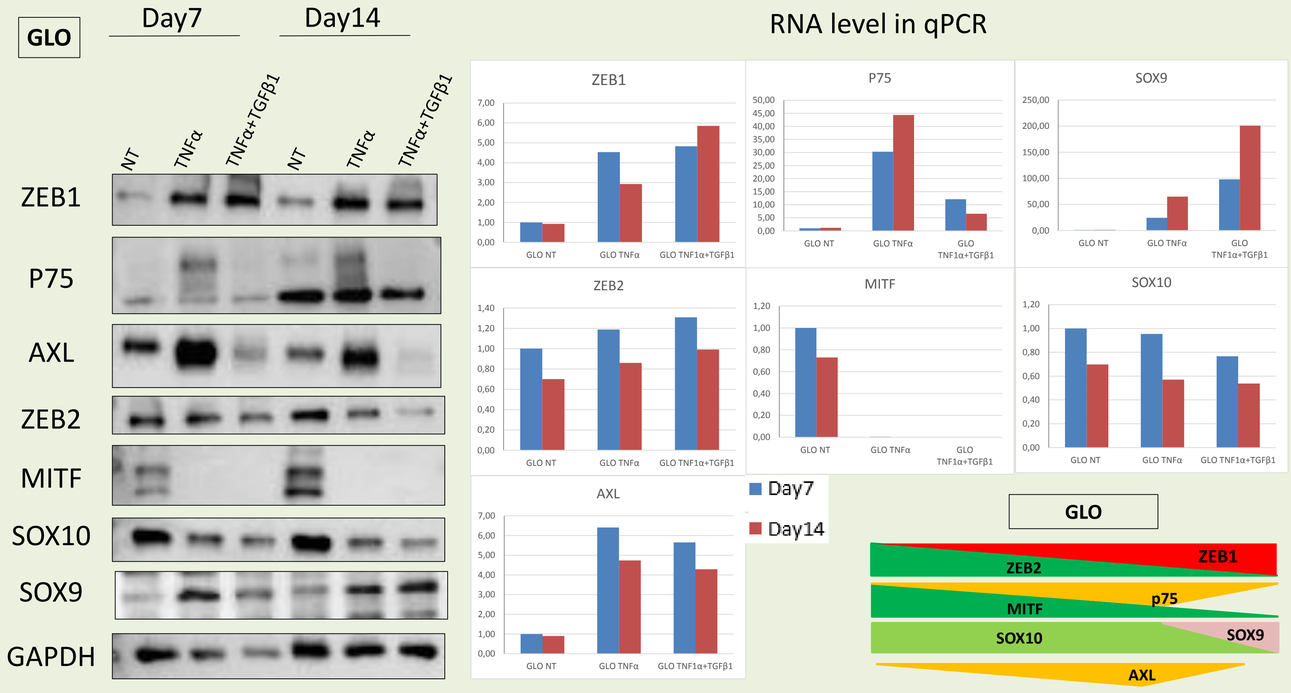

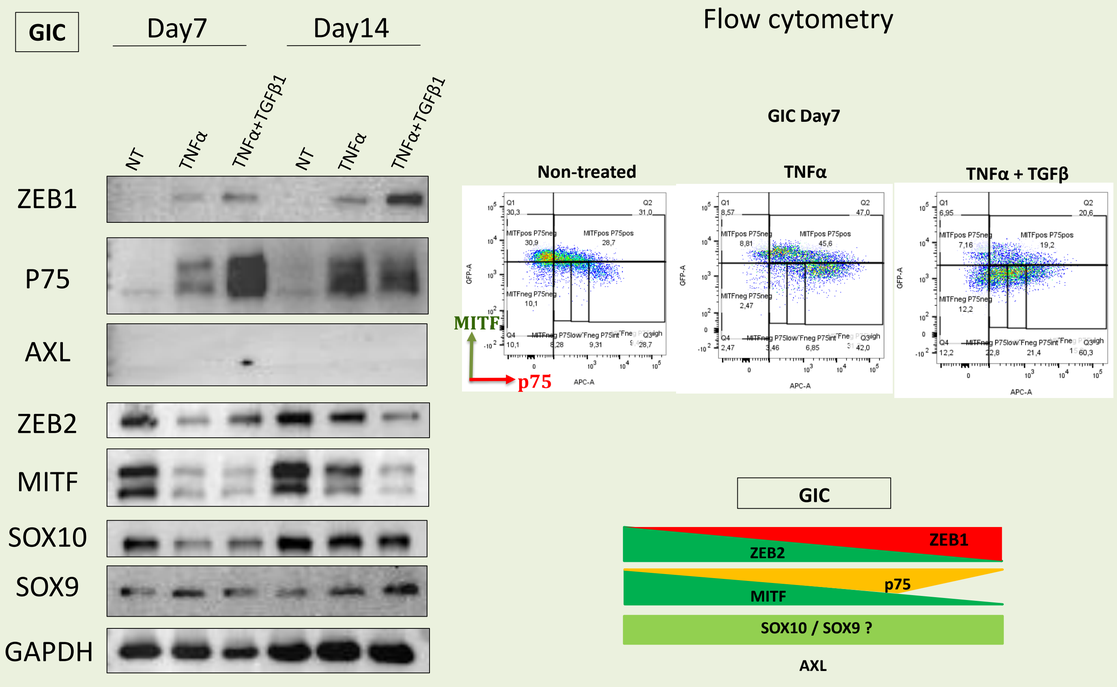

Result 2. Determination of ZEB1 direct target genes by ChIP-seq

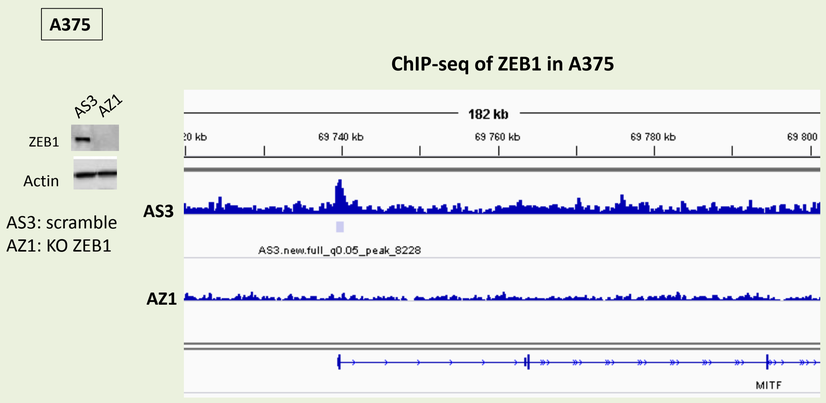

8800 specific peaks
4700 in promoters

Major cellular pathways:
- AIGNER_ZEB1_TARGETS
- WANG_TUMOR_INVASIVENESS_UP
- WU_CELL_MIGRATION
- ONDER_CDH1_TARGETS_2_DN
- PLASARI_TGFB1_TARGETS_10HR_UP
- COULOUARN_TEMPORAL_TGFB1_SIGNATURE_UP
- CHARAFE_BREAST_CANCER_LUMINAL_VS_BASAL_DN
- CHARAFE_BREAST_CANCER_BASAL_VS_MESENCHYMAL_UP
- REACTOME_P75_NTR_RECEPTOR_MEDIATED_SIGNALLING

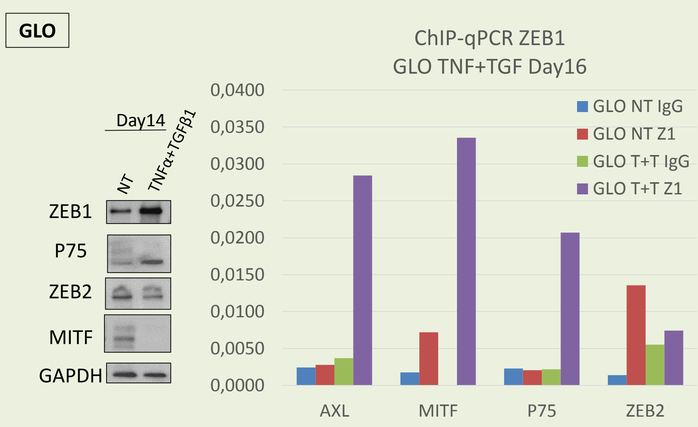

Perspectives:
- ✓ ChIP-seq endogenous ZEB1/ZEB2 in GLO/GIC under TNFα and TGFβ1, in neural crest-like and in undifferentiated phenotypes
- ✓ RNA-seq
- ✓ Intra-tumor heterogeneity
  FACS -> Single cell RNA-seq

Result 3. HDACi represses ZEB1 expression

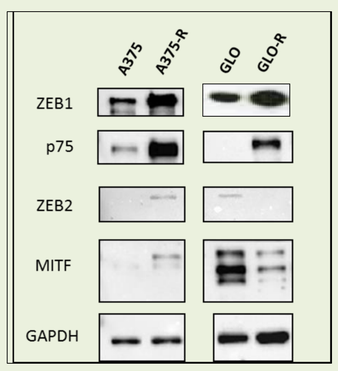

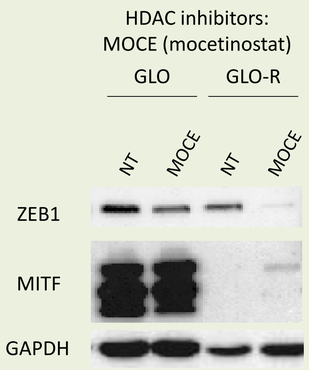

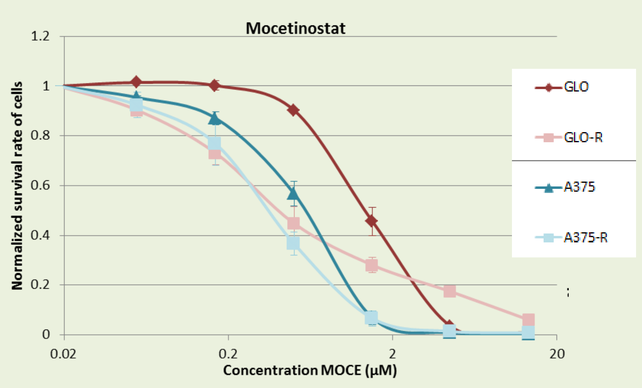

Conclusion

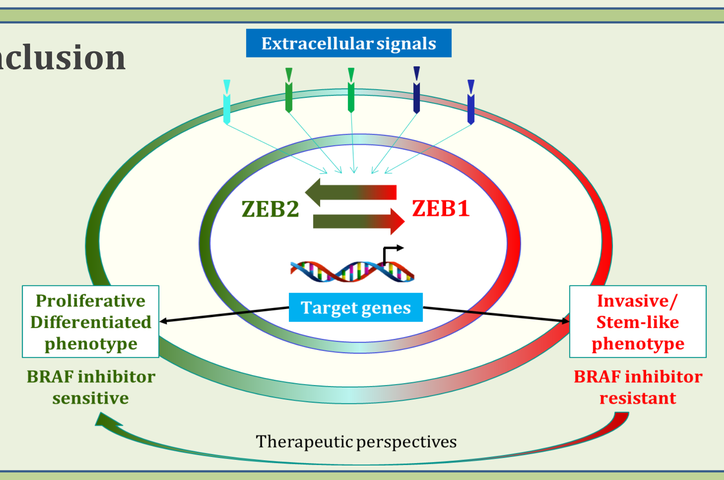

The role of ZNRF3 and TP53 inactivation in adrenocortical tumorigenesis

James WILMOUTH Jr[1], Julie OLABE[1], Kaitlin J. BASHAM[2], Laly PUCHEU[1], Florence ROUCHER-BOULEZ[1], Cecily LUCAS-RODRIGUES[1], Anne-Marie LEFRANÇOIS-MARTINEZ[1], Antoine MARTINEZ[1], Gary HAMMER[2], & Pierre VAL[1*]

Email: james.wilmouth@uca.fr

[1]Université Clermont Auvergne, GReD, CNRS UMR 6293, INSERM U1103, 28, place Henri Dunant, BP38, F63001 Clermont-Ferrand, France

[2]Endocrine Oncology Program, University of Michigan Rogel Cancer Center, Ann Arbor, MI 48109

INTRODUCTION

Adrenocortical carcinoma (ACC) is an infrequent and aggressive cancer that originates from steroidogenic cells within the adrenal cortex. Half of patients present with metastasis at initial diagnosis, lowering the 5 year survival rate dramatically. Recent genomic analysis identified the most common alteration in ACC as inactivation of the transmembrane E3 ubiquitin-ligase Zinc and Ring Finger 3 (Znrf3), a potent tumor suppressor responsible for regulating the WNT/B-catenin pathway. In order to study the role of Znrf3 inactivation in the adrenal cortex, we generated a steroidogenic factor-1 (Sf-1) Cre mediated Znrf3 knockout mouse model. The resulting mice developed hyperplasia associated with moderate increase in WNT/B-catenin signaling by 6 weeks; however, this was followed by regression characterized by the induction of senescence and immune recruitment (Figure 1a top). In an attempt to surpass this senescent phenotype, we developed a mouse model derived from the most aggressive subgroup of ACC, composed of p53 & Znrf3 inactivation (Figure 1a bottom). TP53 is involved in p21-induced senescence, therefore we hypothesize that p53 ablation in the context of Znrf3 inactivation will surpass the senescent phenotype and allow tumorigenesis to proceed.

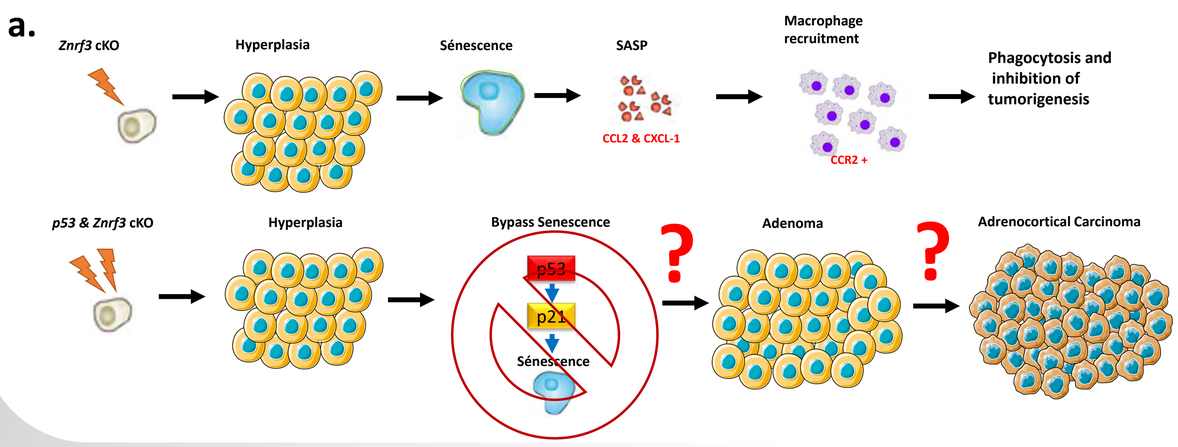

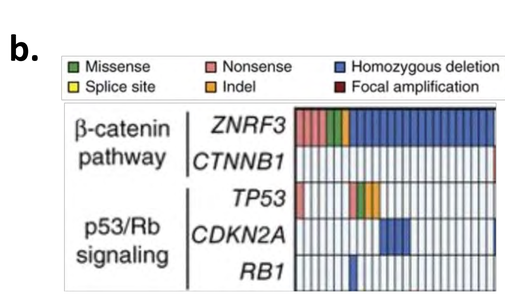

Figure 1 | Znrf3 inactivation in young mouse adrenals
(a) Znrf3 knockout (KO) mice mediated by steroidogenic factor 1(Sf-1) Cre result in initial hyperplasia at 6 weeks. These hyperplastic cells exhibit senescent associated markers p21, p16, & B-galactosidase. The resulting senescent associated secretory phenotype releases cytokines and chemokines responsible for the recruitment of immune cells, and more specifically macrophages. Macrophages are recruited and phagocytose steroidogenic Znrf3 KO cells resulting in regression of the initial hyperplasia. A key characteristic of this process of the fusion of these macrophages, creating large multinucleated cells with a foamy appearance. We hypothesize that combined p53 & Znrf3 inactivation will surpass the senescent phenotype and result in aggressive tumorigenesis. (b) Mutational status of patients in the most aggressive subtype of adrenocortical carcinoma (ACC), defined by alterations in WNT/β-catenin signaling and p53/RB signaling. Patients with Znrf3 homozygous deletions overlap with p53 alterations, suggesting that combined inactivation of both genes could create an ACC mouse model recapitulating patient characteristics. Figure courtesy of *Assié, G., Letouzé, E., Fassnacht, M. et al. Integrated genomic characterization of adrenocortical carcinoma. Nat Genet* ***46,*** *607–612 (2014). https://doi.org/10.1038/ng.2953*

RESULTS

II. Does combined p53 & Znrf3 inactivation alter early immune recruitment & senescent phenotype seen in Znrf3 cKOs?

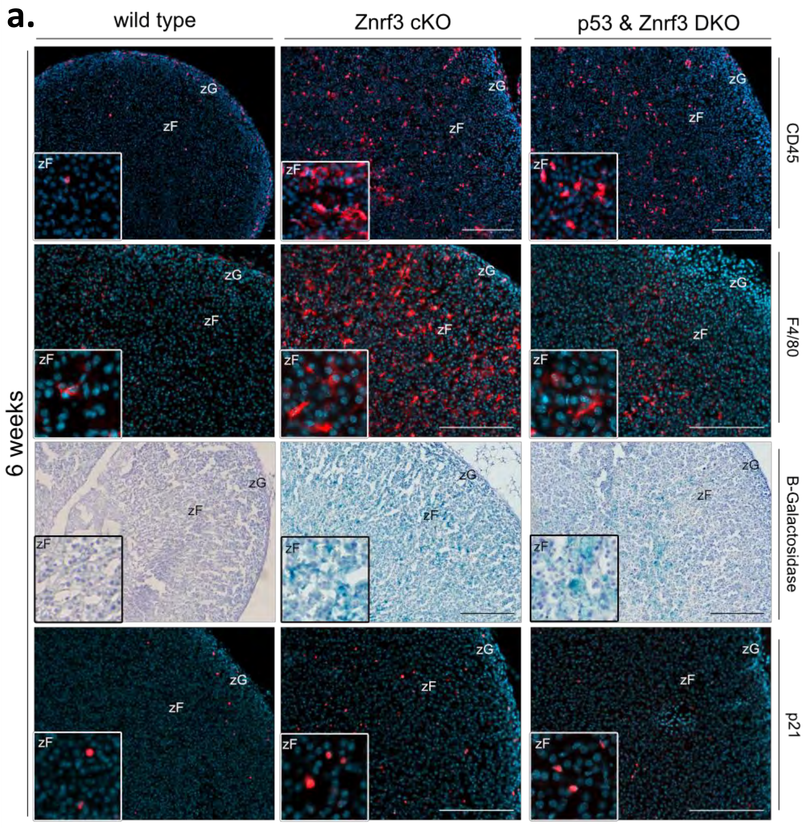

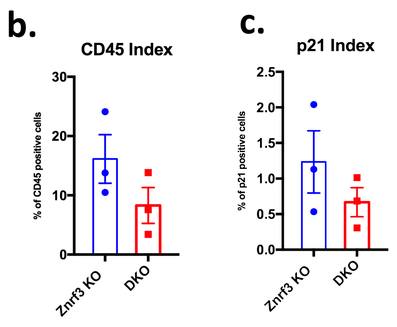

Figure 2 | DKO adrenals exhibit blunted immune recruitment and senescent phenotype compared to Znrf3 cKO adrenals
(a) Immunohistochemistry of immune cell (CD45 & F4/80) and senescent markers (β-Galactosidase & p21) on 6 week old wild-type, Znrf3 cKO, & combined p53 and Znrf3 cKOs (DKO) adrenals. DKOs maintain immune cell recruitment (CD45 & F4/80) and senescence associated markers (β-Galactosidase & p21) characteristic of the Znrf3 cKO phenotype, however the DKOs phenotype is blunted in comparison to Znrf3 cKOs alone. Insets of images include a location of where they preside: zona Glomerulosa (zG) & zona Fasciculata (zF). DAPI is represented in blue and respective markers are shown in red. Scale bars represent 200µm. (b) Calculated CD45 Index (% of positive CD45 cells/ total number of cells in the cortex) comparing Znrf3 cKOs to DKOs, confirming the trend shown via IHC. (c) Calculated p21 Index (% of positive p21 cells/ total number of cells in the cortex) comparing Znrf3 cKOs to DKOs, confirming the trend shown via IHC. *Indexes were calculated with the QuPath software.

III. Do aggressive tumors arise in DKOs at later time points?

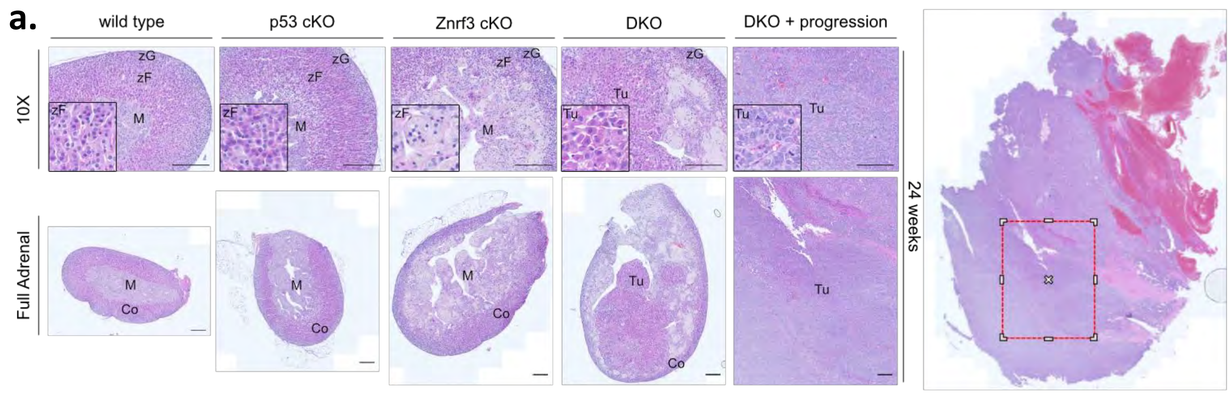

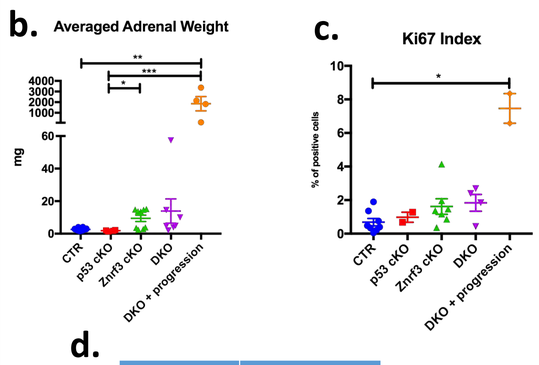

d.

	Rate of Metastasis	
Control	0%	n=16
p53 KO	0%	n=4
Znrf3 KO	0%	n=9
DKO	36%	n=11

Figure 3 | Subset of DKO adrenals result in aggressive tumorigenesis and metastasis
(a) Haematoxylin & Eosin staining across wild-type, p53 cKO, Znrf3 cKO, & DKO adrenals at 24 weeks of age. At this time point, DKOs can be separated into two groups: DKOs & DKOs with progression. Interestingly, DKOs without progression have a similar appearance to Znrf3 cKO adrenals due to the presence of fused macrophages. The red crop is the size of the 'Full Adrenal' crops, emphasizing the size difference of aggressive tumors. Insets of images include a location of where they preside: cortex (Co), medulla (M), zona Glomerulosa (zG), zona Fasciculata (zF), & Tumor (Tu). Scale bars represent 200µm. (b) Averaged adrenal weight across the different genotypes. Statistics were calculated by nonparametric Kruskal Wallis test with multiple comparisons. (c) Calculated Ki67 Index from immunohistochemistry (% of positive Ki67 cells/ total number of cells in the cortex) across the different genotypes. Statistics were calculated by nonparametric Kruskal Wallis test with multiple comparisons. (d) Rate of metastasis across the different genotypes. Notably, these metastases are located in sites commonly found in patients with ACC (lungs, liver, and peritoneal). *Indexes were calculated with the QuPath software.

IV. How is immune infiltration involved in tumorigenesis?

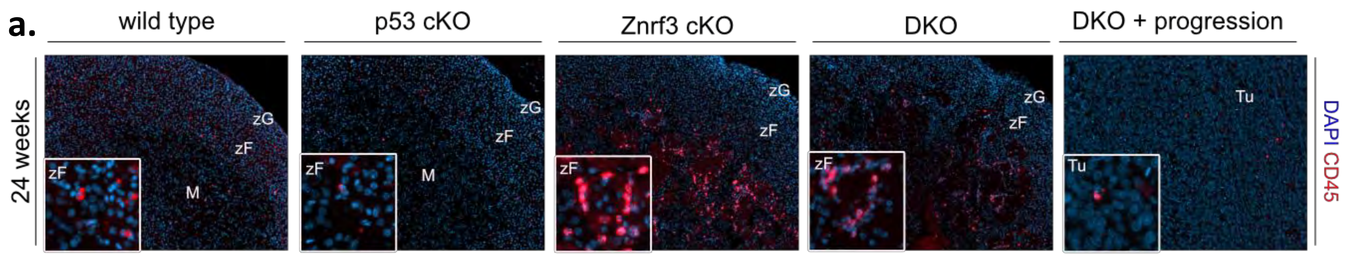

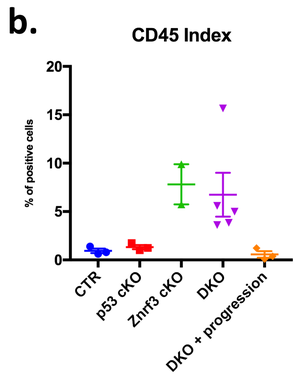

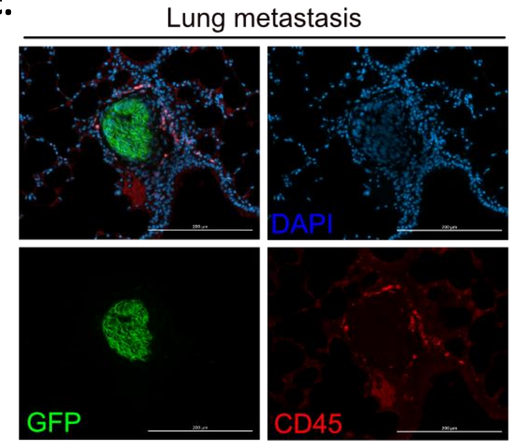

Figure 4 | Aggressive tumors correspond with immune cell exclusion, a characteristic potentially maintained at distant metastatic locations
(a) Immunohistochemistry analysis of immune cell marker CD45 across the different genotypes at 24 weeks of age, showing how progressed tumors are associated with immune cell exclusion. DAPI is represented in blue and CD45 is represented in red. Insets of images include a location of where they preside: zona Glomerulosa (zG), zona Fasciculata (zF), medulla (M), & tumor (Tu). Scale bars represent 200µm. (b) Calculated CD45 Index (% of positive CD45 cells/ total number of cells in the cortex) across the different genotypes confirming IHC. (c) Immunohistochemistry of distant lung metastasis from a DKO mouse at 24 weeks of age. By using the mTmG reporter in our mouse breeding, we are able to easily identify tumor cells via GFP. This image illustrates immune cell exclusion at distant locations. DAPI is represented in blue, CD45 in red, & GFP in green. Scale bars represent 200µm. *Indexes were calculated with the QuPath software.

CONCLUSION - PERSPECTIVES

Inactivation of p53 & Znrf3 in the mouse adrenal cortex does not completely surpass the immune recruitment and senescent phenotype caused by Znrf3 inactivation alone, however these DKOs eventually form aggressive carcinomas that metastasize to the lungs, liver, and peritoneal. Interestingly, these aggressive tumors are associated with immune cell exclusion at primary and potentially secondary locations.

Investigate whether immune cell exclusion is required for tumor progression, and how steroid secretion plays a role in this process.

Utilize metastatic model to capture and characterize circulating tumor cells.

We acknowledge La Ligue Nationale Contre le Cancer for the funding sources that supported this work.